

THE FORMATION OF THE PANGUNA PORPHYRY COPPER DEPOSIT,
BOUGAINVILLE, PAPUA NEW GUINEA.

with an appendix on the
Frieda porphyry copper prospect, New Guinea.

by

C. J. EASTOE, B.Sc.(Hons.)

Submitted in partial fulfilment of the requirements
for the Degree of Doctor of Philosophy.

UNIVERSITY OF TASMANIA

HOBART

1979

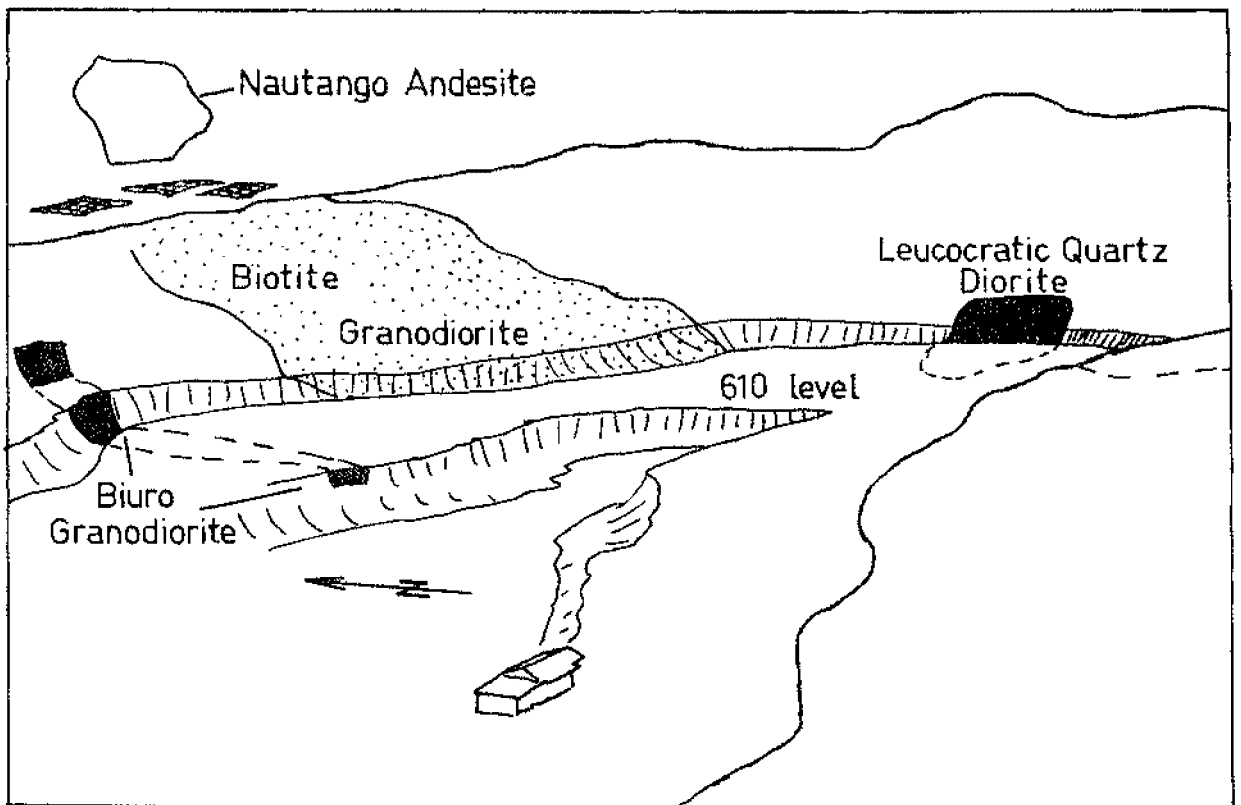
This thesis contains no material which has been accepted for the award of any other degree or diploma in any university and, to the best of my knowledge and belief, contains no copy or paraphrase of material previously published or written by another person, except where due reference is made in the text of this thesis.



C. J. EASTOE

University of Tasmania,

January, 1979.



Frontispiece: The open pit at Panguna in November 1974.

ABSTRACT

Various hydrothermal processes have been suggested as important in the formation of porphyry coppers, e.g. orthomagmatic evolution of salt-rich liquid, condensation of salt-rich liquid from magmatic vapour, convection of groundwater driven by magmatic heat, boiling of groundwater. A fluid inclusion study based on detailed two-dimensional sampling indicates that all of these processes appear to have contributed to the evolution of the Panguna deposit, but suggests that copper was deposited mainly by salt-rich liquid expelled direct from the magma.

The deposit formed at the southern contact of the Kaverong Quartz Diorite with the Panguna Andesite. Three smaller porphyritic stocks, the Biotite Granodiorite, the Leucocratic Quartz Diorite and the Biuro Granodiorite, were emplaced in the deposit during mineralisation, which comprised three phases of hydrothermal activity. The first, phase A, took place when the southern part of the Kaverong Quartz Diorite was at temperatures over 700°C. The Panguna Andesite was pervasively altered to an amphibole-magnetite-plagioclase assemblage, upon which was superimposed copper mineralisation and associated K-silicate alteration. The limit of copper deposition and quartz veining to the southwest coincides closely with a zone in which salt-rich liquid was cooled and diluted. A pyritic halo parallels this zone. The system cooled below 400°C before undergoing renewed mineralisation at temperatures over 400°C in two approximately concurrent but separate phases B and C. These phases were accompanied by the intrusion of porphyritic stocks. Phase B formed a well-defined cell bounded by a pyritic halo and centred on the Leucocratic Quartz Diorite. Phase C was expressed as veining of the Biotite Granodiorite, the Biuro Granodiorite and the area between them.

Copper mineralisation took place at a pressure near 300 bars and at temperatures between 350°C and 700°C or higher. Cu,Fe sulphides, quartz, anhydrite and hematite in veins, and potassium silicate alteration were formed from boiling salt-rich liquid, of density 1.2 - 1.5 g/cm³, mostly of magmatic origin. The composition of these liquids (which nucleated both KCl and NaCl in fluid inclusions) in terms of the system NaCl-KCl-H₂O varied between 76% salts (60% NaCl, 16% KCl) and 46% salts (30% NaCl, 16% KCl) by weight. Other liquids, apparently more dilute, nucleated only NaCl. The salt-rich liquids also contained Fe, Ca and S, and minor quantities of Mg, Cu, Mn and Zn. A Cu concentration of 1900 ppm has been estimated in one liquid. The atomic K/Na ratios of salt-rich liquids from three principal phases of vein mineralisation and from quartz phenocrysts conformed to a single trend, increasing from 0.17 to 0.46 as the NaCl content decreased.

Groundwater, mainly of less than 5% salinity, inundated the orebody between phase A and phases B and C, and again after phases B and C, at temperatures below 400°C. Groundwater deposited quartz-pyrite and probably pyrite-clay and sphalerite-pyrite veins at temperatures near 300°C and caused local phyllic alteration. Given a hydrostatic pressure regime in the groundwater system, the depth of formation was near 3 km.

Fluids of groundwater composition, trapped as inclusions at or above their critical points, seem to bound the regions in which two fluids coexisted during phases A and B, and possibly C. The evolution of fluid compositions and phase properties across the two-phase region is consistent with the predicted evolution of boiling salt-rich liquid expelled unsaturated from the magma, cooled to saturation and supersaturation by 500°C, then cooled and diluted by mixing with salt-rich liquid formed by the concentration of groundwater (as high as 45% salts)

by boiling. The salt-rich liquids were unsaturated near 430°C , and at lower temperatures the liquid and gas compositions converged to the critical composition at the boundary. Pressures fell sharply from lithostatic between the magma and the zone of supersaturated liquids of the ore-zone, and were hydrostatic in the lower-temperature unsaturated fluids. In the zone of supersaturation, pressures may have been lower than in the groundwater. Salt-rich liquid was pumped into the ore-zone by the lithostatic-hydrostatic pressure difference, then descended through the ore-zone because of its density.

The transport of Fe and possibly Cu in the vapour is insignificant under porphyry copper conditions, but Zn and Mo may undergo significant vapour transport. This may explain the separation of Zn and Mo from Fe and Cu in porphyry copper systems.

The absence of major sericite alteration (as opposed to the K-feldspar commonly associated with the salt-rich liquid) suggests that boiling removed excess HCl formed during the alteration of plagioclase and amphibole to biotite. The sulphate in anhydrite deposited by salt-rich liquid probably originated from the decomposition of SO_2 . This mechanism does not account for increased sulphide deposition below 500°C because the liquid maintained a constant $\text{SO}_2:\text{H}_2\text{S}$ ratio but the reduction of SO_2 by Fe^{2+} may have become important at lower temperatures. The high oxidation state of magmatic fluids during copper mineralisation was due to the loss of H_2 from the magma in those early-evolved volatiles that formed the amphibole-bearing assemblage.

Chalcopyrites have a $\delta^{34}\text{S}$ range of -1.6 to 1.5‰, pyrites +0.5 to 3.1‰ and anhydrites +7.6 to 16.0‰. The salt-rich liquid that deposited anhydrite and chalcopyrite had $\delta^{34}\text{S} = +1\%$. The complexity of the hydrothermal processes indicates that there was not a simple relationship between these values and the $\delta^{34}\text{S}$ values of sulphur in the magma.

TABLE OF CONTENTS

	page
<u>ABSTRACT</u>	i
<u>TABLE OF CONTENTS</u>	iv
<u>LIST OF FIGURES</u>	xi
<u>LIST OF TABLES</u>	xiv
<u>INTRODUCTION</u>	1
NOTATION	2
ACKNOWLEDGEMENTS	3
<u>CHAPTER ONE: REVIEW</u>	6
CLASSIFICATION	6
Ore localisation.	6
Morphology and environment.	6
Relative metal abundances.	8
Composition of intrusive rocks.	9
Classifications based on multiple criteria.	9
Summary.	10
CLASSIFICATION OF PORPHYRY COPPER DEPOSITS OF THE SOUTHWEST PACIFIC	10
GENETIC ASPECTS: THE ROLE OF FLUIDS IN PORPHYRY COPPER FORMATION	12
Models of fluid interaction.	15
SELECTED STUDIES OF PORPHYRY COPPER FLUIDS	17
Bingham, Utah.	17
Sar Cheshmeh, Iran.	18
Hydrogen and oxygen isotopes at Panguna.	19
<u>CHAPTER TWO: GEOLOGY</u>	21
STRATIGRAPHY	21
The Kieta Volcanics.	21
The Buka Formation.	21
The Keriaka Limestone.	21
Unnamed Volcanics.	21
The Bougainville Group.	21
The Sohano Limestone.	22
Quaternary Alluvium.	22
Dioritic Intrusives.	22

	page
STRUCTURE	22
MINERALISATION	23
GEOLOGY OF THE PANGUNA AREA	23
Panguna Andesite.	23
Kaverong Quartz Diorite.	24
Marginal phases of the Kaverong Quartz Diorite.	24
The order of intrusion.	26
Alteration.	27
Mineralisation.	29
Structure.	30
Comment.	30
<u>CHAPTER THREE: THE VEIN SYSTEM</u>	31
(i) AMPHIBOLE-MAGNETITE-QUARTZ VEINS	33
(ii) PART 1: QUARTZ-Cu,Fe SULPHIDE VEINS - OCCURRENCE AND MINERALOGY	33
Copper-iron sulphides.	34
Iron oxides.	35
Rutile.	35
Molybdenite.	36
Other ore minerals.	36
Gangue minerals.	36
(ii) PART 2: ALTERATION ASSOCIATED WITH QUARTZ-Cu,Fe SULPHIDE VEINS	37
Biotite.	38
Sericite.	38
Albite.	38
K-feldspar.	38
Chlorite.	39
Epidote.	40
Anhydrite.	40
Opaque minerals in alteration assemblages.	40
Summary.	40
(iii) ANHYDRITE VEINS	41
(iv) QUARTZ-PYRITE VEINS	41
(v) THICK, MASSIVE PYRITE VEIN	43
(vi) PYRITE ± BLEACHED SELVAGE	43
(vii) DISCONTINUOUS SULPHIDE VEINLETS	43
(viii) CHABAZITE-BEARING VEINS	44

	page
(ix) SPHALERITE-PYRITE VEINS	44
(x) PYRITE-CLAY VEINS	45
(xi) GYPSUM VEINLETS	45
(xii) BARREN QUARTZ VEINLETS	46
(xiii) CALCITE	46
(xiv) VIVIANITE VEINLETS	46
SUMMARY OF OBSERVATIONS ON VEIN ORDER	47
 <u>CHAPTER FOUR: FLUID AND SOLID INCLUSION STUDIES</u>	 48
GENERAL	48
EQUIPMENT	48
TREATMENT OF DATA	49
CLASSIFICATION AND DESCRIPTION OF INCLUSIONS	52
Solid inclusions.	52
Fluid inclusions.	54
Type I inclusions.	55
Type II inclusions.	55
Type III inclusions.	56
Hematite.	59
Boiling.	59
 <u>CHAPTER FIVE: FLUID INCLUSIONS IN QUARTZ-Cu,Fe SULPHIDE VEINS</u>	 61
TYPE I INCLUSIONS	61
Pressure corrections.	64
TYPE II INCLUSIONS	64
DENSITY AND COMPOSITION OF TYPE III INCLUSIONS BY VOLUME MEASUREMENT	65
COMPOSITION OF TYPE III INCLUSIONS BY MICROTHERMOMETRY	68
TEMPERATURES FROM TYPE III INCLUSIONS	73
The behaviour of the inclusions.	73
Solution of silica.	75
Supersaturation.	76
Interpretation of T_h data.	76
Upper temperature limit.	77
Lower temperature limit.	77
Temperature estimates independent of the fluid inclusion data.	78
LEACHING STUDIES OF VEIN QUARTZ	80
SUMMARY	83

<u>CHAPTER SIX: FLUID INCLUSION STUDIES IN HOSTS OTHER THAN</u>	
<u>QUARTZ-Cu,Fe SULPHIDE VEINS</u>	85
QUARTZ PHENOCRYSTS	85
AMPHIBOLE-MAGNETITE-QUARTZ VEINS	88
QUARTZ-PYRITE VEINS	89
Salinity.	91
Temperatures.	92
Relationship with type I inclusions from quartz-Cu,Fe sulphide veins.	92
PYRITE \pm BLEACHED SELVAGE	93
SPHALERITE-PYRITE VEINS	94
QUARTZ HEALING BRECCIATED SPHALERITE	94
<u>CHAPTER SEVEN: PRESSURE ESTIMATES</u>	95
QP ASSOCIATION	95
TYPE II INCLUSIONS	95
TYPE III INCLUSIONS	96
SUMMARY	97
<u>CHAPTER EIGHT: THE HISTORY OF THE DEPOSIT</u>	98
PHASE C	99
PHASE B	99
RELATIONSHIP OF B AND C	100
PHASE A	100
CONDITIONS DURING PHASE B	102
EVENTS PRIOR TO PHASE A	103
SUMMARY	104
<u>CHAPTER NINE: FLUID SYSTEMS AND PORPHYRY COPPER FORMATION</u>	106
THE WATER IN TYPE I INCLUSIONS	106
THE ORTHOMAGMATIC MODEL AND THE VAPOUR-PLUME MODEL	108
Quantities of salt-rich liquid.	108
K/Na ratios.	110
FLUID EVOLUTION ACROSS THE TWO-PHASE REGION	111
Predictions.	111
Comparison of predictions and observation.	114
The hydrothermal system at Sar Cheshmeh.	116
CONDITIONS IMPOSED BY THE REAL SYSTEM	117
The presence of KCl.	117
The role of groundwater.	118

	page
THE RELATIONSHIP OF FLUID DISTRIBUTION WITH METAL AND ALTERATION ZONING	119
TEMPERATURES AND PRESSURES IN THE TWO-PHASE REGION	121
Temperatures.	121
Pressures.	121
K/Na RATIOS IN THE SALT-RICH LIQUIDS	122
K/Na fractionation during boiling.	122
The precipitation of halite.	123
K/Na fractionation due to differential diffusion.	123
Mixing of two liquids.	123
Rock-fluid interaction.	125
Summary, implications and comparison with other deposits.	126
ADDING THE VERTICAL DIMENSION	128
Vertical and horizontal flow.	128
The top of the system.	130
The system below the exposed ore-zone.	131
Summary.	132
COMPARISON OF PANGUNA WITH PREVIOUSLY-SUGGESTED FLUID MODELS	133
<u>CHAPTER TEN: CHEMICAL CONSIDERATIONS</u>	134
THE BUFFERING OF K/Na IN SALT-RICH LIQUIDS	136
THE FUGACITIES OF OXYGEN AND SULPHUR DURING COPPER MINERALISATION	139
Oxygen fugacity.	139
Sulphur fugacity.	141
THE CHEMISTRY OF THE VAPOUR PHASE.	143
State of water.	143
Fugacity of HCl.	143
Fugacity of NaCl.	144
Sulphur species.	145
BASE METAL TRANSPORT IN THE VAPOUR	148
Enhanced volatility in salt mixtures.	148
Chloride volatility versus hydroxide volatility.	149
IRON SPECIES	150
Ferrous species.	150
Ferric species.	153
COPPER SPECIES	154
The polymers of CuCl.	155
Na-bearing species.	156

	page
Fe-bearing species.	157
Summary.	158
ZINC SPECIES	159
Na-bearing species.	159
Fe-bearing species.	160
ZnCl ₂ .	160
MOLYBDENUM SPECIES	161
DISCUSSION OF VAPOUR CHEMISTRY	163
THE ACIDITY OF THE SALT-RICH LIQUID	165
SULPHIDE AND SULPHATE DEPOSITION	169
METAL ZONING	170
THE OXIDATION STATE OF MAGMATIC FLUIDS	171
<u>CHAPTER ELEVEN: SULPHUR ISOTOPE STUDY</u>	174
INTRODUCTION	174
THERMOMETRY	176
Sphalerite-pyrite veins.	176
Anhydrite-chalcopryrite.	177
VARIATION OF $\delta^{34}\text{S}$ IN TIME AND SPACE	178
Pyrite.	178
Chalcopryrite.	178
FURTHER EXAMINATION OF ANHYDRITE-CHALCOPRYRITE FRACTIONATION	179
$\delta^{34}\text{S}$ IN THE SULPHIDES, SULPHATES & FLUIDS AS A FUNCTION OF f_{O_2}	180
COMPARISON WITH OTHER DEPOSITS	182
THE ISOTOPIC COMPOSITION OF MAGMATIC SULPHUR	184
Comments.	187
<u>CONCLUSIONS</u>	188
<u>REFERENCES</u>	195
<u>APPENDIX 1: LIST OF SPECIMENS FROM PANGUNA</u>	205
<u>APPENDIX 2: FLUID INCLUSION DATA FROM PANGUNA</u>	210
<u>APPENDIX 3: A RECONNAISSANCE FLUID INCLUSION AND SULPHUR ISOTOPE STUDY OF THE FRIEDA PORPHYRY COPPER PROSPECT, PAPUA NEW GUINEA</u>	239
INTRODUCTION	239
Scope of the study.	239
Acknowledgements.	240
A note on geographic nomenclature.	240

	x
	page
REGIONAL GEOLOGY	240
The Salumei Formation.	240
The Wogamush Beds.	241
The April Ultramafics.	241
The Frieda Complex.	241
Structure.	241
INTRUSIVE ROCKS	242
ALTERATION	243
Potassic alteration.	243
Phyllic alteration.	243
Propylitic alteration.	244
Other notes.	244
MINERALISATION	244
FLUID INCLUSION STUDIES IN QUARTZ VEINS	247
Type I inclusions.	247
Type III inclusions.	248
FLUID INCLUSION STUDIES IN ANHYDRITE VEINS	250
SULPHUR ISOTOPES	252
CONCLUSIONS	253

LIST OF FIGURES

Figure		after page
0-1	Locality map.	1
2-1	Geology of Bougainville and Buka.	21
2-2	Geology of the Panguna area.	23
2-3	Geology of the orebody, Panguna.	24
2-4	Alteration in the Panguna deposit.	29
3-1	Density of quartz veining.	31
3-2	Amphibole-magnetite-quartz vein.	33
3-3	Type (ii) veins in the Leucocratic Quartz Diorite.	33
3-4	Chalcopyrite and sphalerite replacing pyrite.	34
3-5	Intergrowth and eutectoid exsolution of chalcopyrite and bornite.	34
3-6	Intergrowth and eutectoid exsolution of bornite and digenite.	34
3-7	Bornite and sphalerite occurrences in quartz-Cu,Fe sulphide veins.	35
3-8	Molybdenite occurrences.	35
3-9	Magnetite replaced by chalcopyrite and hematite.	36
3-10	Molybdenite-chalcopyrite intergrowth.	36
3-11	Chalcopyrite and sphalerite replacing pyrite.	36
3-12	Occurrences of sericite and albite in alteration assemblages of quartz-Cu,Fe sulphide veins.	40
3-13	Occurrences of anhydrite veins, chabazite-bearing veins, pyrite-clay veins and sphalerite-pyrite veins.	40
3-14	Occurrences of thin pyrite veins.	43
3-15	Occurrences of discontinuous sulphide veinlets.	43
3-16	Sphalerite, chalcopyrite and tennantite replacing pyrite.	44
3-17	Pyrite containing radiating blades of hematite.	44
4-1	Calibration curve for Chaixmeca apparatus.	49
4-2	Effects of perturbation of fluid inclusions.	51
4-3	Solid inclusions in 103019.	52
4-4	Photomicrographs of fluid inclusions.	54
4-5	Photomicrographs of fluid inclusions.	54
4-6	Opened fluid inclusions, and analyses.	57
4-7	Semiquantitative spectra of daughter salts.	57
4-8	Decrepitation products of a type III inclusion, and analyses.	57

Figure		after page
5-1	T_h and T_f data for type I inclusions from quartz-Cu,Fe sulphide veins.	62
5-2	Map of T_h distribution for type I inclusions from quartz-Cu,Fe sulphide veins.	62
5-3	Map of T_f distribution for type I inclusions from quartz-Cu,Fe sulphide veins.	62
5-4	T_h histogram for type II inclusions from quartz-Cu,Fe sulphide veins.	65
5-5	Calculation of the volume of a negative quartz crystal.	65
5-6	$T_s\text{NaCl}$ histograms for three discrete planes of type III inclusions.	69
5-7	Data for type III inclusions from quartz-Cu,Fe sulphide histograms.	69
5-8	Map of T_h and $T_s\text{NaCl}$ data from type III inclusions.	69
5-9	Sample localities of specimens used in the fluid inclusion study.	69
5-10	$T_s\text{NaCl}$ and $T_s\text{KCl}$ data for type III inclusions from quartz-Cu,Fe sulphide veins.	69
5-11	The ternary diagram $\text{NaCl-KCl-H}_2\text{O}$.	69
5-12	A portion of the ternary diagram $\text{NaCl-KCl-H}_2\text{O}$ with microthermometric data from Panguna superimposed.	69
5-13	$T_s\text{salt A}$ vs. $T_s\text{NaCl}$ for type III inclusions.	72
5-14	A metastability effect in type III inclusions.	72
5-15	T_h data greater than 580°C for three specimens.	72
6-1	Photomicrographs of inclusions from phenocrysts and from an amphibole-bearing vein.	85
6-2	Data from type III inclusions in quartz phenocrysts.	86
6-3	Fluid inclusion data from type I and III inclusions from quartz in an amphibole-bearing vein.	89
6-4	The distribution of QP association fluids.	89
6-5	T_h data vs. T_f data for type I inclusions from quartz-pyrite veins.	92
6-6	Histograms of T_h data for type I inclusions from quartz-pyrite veins.	92
6-7	T_h histogram and T_h vs. T_f for two specimens associated with sphalerite-pyrite veins.	94
7-1	Vapour pressures in the system $\text{NaCl-KCl-H}_2\text{O}$.	96
8-1	Map of phase A fluid distribution.	100
8-2	Four proposed stages in the evolution of the Panguna deposit.	102

Figure		after page
9-1	Isobars of the two-phase region in the system NaCl-H ₂ O.	110
9-2	A selection of histograms of fluid inclusion data.	114
9-3	Distribution of phase-behaviour of salt-water liquids.	114
9-4	Variation of vapour pressures as a function of temperature.	121
9-5	T _S KCl vs. T _S NaCl for other porphyry coppers.	127
9-6	Diagrammatic vertical section of a porphyry copper deposit.	133
10-1	Compositions of plagioclase phenocrysts.	137
10-2	log f _{S₂} - log f _{O₂} plots at 700, 800 and 850 K.	140
10-3	A log f _{S₂} - log f _{O₂} path as a function of temperature.	142
10-4	Fugacities of H ₂ O, SO ₂ , H ₂ S and S ₂ .	147
11-1	Specimen locality map for sulphur isotope study.	178
11-2	Distribution of $\delta^{34}\text{S}$ of pyrite at Panguna.	178
11-3	$\delta^{34}\text{S}$ of anhydrite and chalcopyrite as a function of $\Delta(\text{anhydrite-chalcopyrite})$.	179
A-1	Locality maps, Frieda.	239
A-2	Geological map and section of the Frieda Intrusive Complex.	239
A-3	Geology of the Koki Creek area.	242
A-4	Specimen localities, Koki Creek area.	242
A-5	Geology of Ok Flimtem and Ok Emtem areas.	242
A-6	Specimen localities, Ok Flimtem and Ok Emtem areas.	242
A-7	Histograms of Frieda fluid inclusion data.	248
A-8	T _h vs. T _S NaCl for type III inclusions.	248
A-9	T _f vs. T _h for type I inclusions.	248
A-10	Photomicrographs of fluid inclusions.	248
A-11	$\delta^{34}\text{S}$ vs. Δ for anhydrite-sulphide pairs.	248

LIST OF TABLES

Table		after page
2-1	Stratigraphy of Bougainville and Buka.	21
2-2	Stratigraphy of the Panguna area.	23
3-1	Vein classification.	31
3-2	Silicate alteration adjacent to quartz-Cu,Fe sulphide veins.	37
4-1	X-ray counts on decrepitation products.	57
5-1	Pressure corrections for type I inclusions.	64
5-2	Density determinations on type III inclusions.	66
5-3	Compositions of type III inclusions, from volume measurements.	66
5-4	Leaching studies of vein quartz.	81
6-1	Analyses of a solid inclusion from a quartz phenocryst.	86
8-1	The sequence at Panguna.	105
9-1	Distribution of NaCl between vapour and liquid.	108
10-1	Fugacities of S ₂ and SO ₂ .	142
10-2	Fugacity of water.	143
10-3	Fugacity of HCl.	143
10-4	Dimerisation of NaCl.	143
10-5	Sulphur species equilibria.	146
10-6	Molybdenum species equilibria.	162
11-1	$\delta^{34}\text{S}$, Δ and temperatures for pyrite-sphalerite veins.	177
11-2	$\delta^{34}\text{S}$, Δ and temperatures for anhydrite-chalcopyrite pairs.	177
11-3	Sulphide $\delta^{34}\text{S}$ values, classified by vein-type.	178
11-4	^{34}S fractionation among sulphur species.	181
11-5	Sulphur isotope data from selected deposits.	183
A-1	Fluid inclusion data, Frieda.	255
A-2	Sulphur isotope data, Frieda.	255
A-3	List of specimens from Frieda.	255

INTRODUCTION

The Panguna porphyry copper deposit is situated in the Crown Prince Range on the island of Bougainville, northernmost of the large islands of the Solomons group (fig. 0-1). Politically, Bougainville is part of the North Solomons Province of Papua New Guinea.

The deposit is a large one by world standards, with pre-mining reserves estimated at 900 million tons of 0.48% Cu (with an economic cut-off at 0.3%) and ^{0.}36 dwt/ton Au (Espie, 1971). The presence of copper mineralisation in the area had been known since the 1930's, when small gold mines operated on some of the richer veins at Panguna (= Pumpkuna, Thompson, 1962) and at nearby Kupei. Exploration of the area by the C.R.A. group in the early 1960's established the existence of a large, low-grade orebody at Panguna and mining began in 1972. Exploitation has involved major engineering problems in a terrain of steep slopes, high rainfall, high seismicity, and active vulcanism.

The fluid inclusion study was designed to examine spatial and temporal variations in temperature, pressure and fluid chemistry in the various types and generations of quartz veins. The samples were collected during a reconnaissance by Dr. M. Solomon (University of Tasmania) in January, 1974 and in October-November 1974 by the author. During the latter period, the open pit included the southeastern half of the area enclosed by the outer 0.3% Cu contour (see fig. 2-3) and took in all the main intrusions. Samples were taken between 595 and 775 m above sea level in the open pit, and from outcrop and diamond drill core up to 1.5 km beyond the pit limits.

This study differs from previous studies of fluid inclusions in porphyry coppers in that considerable effort was made to obtain and study

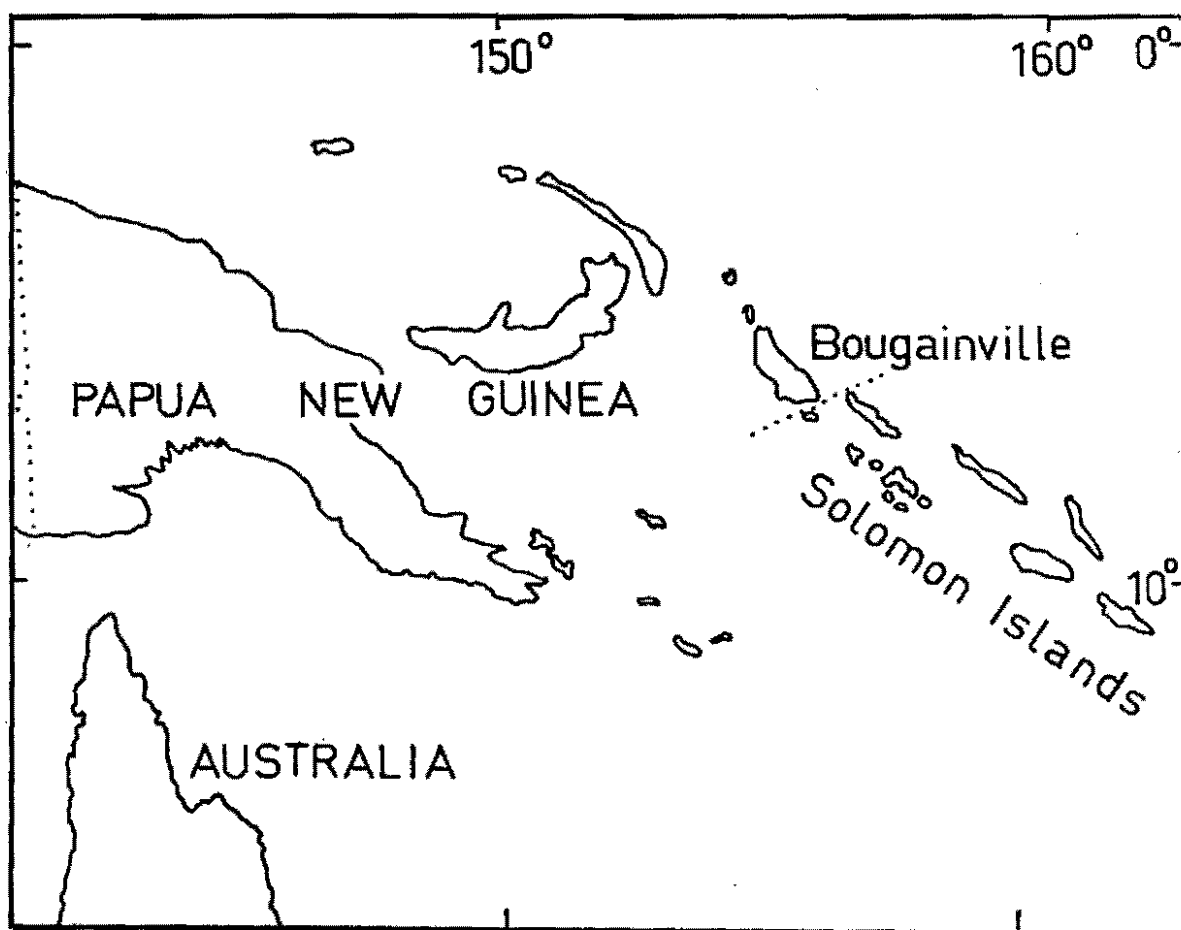


Fig. C-1 Locality map.

vein samples covering the complete horizontal section exposed in and around the open pit. Because the general geology has already been described (Macnamara, 1968; Fountain, 1972, 1973; Knight *et al.*, 1973; Baumer & Fraser, 1975; Baldwin *et al.*, 1978), the deposit is particularly well suited for such a study. In addition, specialised work has been done in the following fields: geochronology (Page & McDougall, 1972); ore mineralogy (Lawrence & Savage, 1975); host-rock geochemistry (Fountain, 1972, 1973; Ford, 1976, 1978); igneous petrology (Mason & McDonald, 1978); O and H isotopes (Ford, 1976; Ford & Green, 1977); S-isotopes (Ayres *et al.*, in press). The deposit is young (3 to 5 m.y., Page & McDougall, 1972) and lacks significant metamorphism and deformation.

NOTATION

In the fluid inclusion work (Chapter 4 ff.) the following symbols are used:

T	temperature
P	pressure
ρ	density
T _h	temperature (measured during heating) of homogenisation of two fluid phases, i.e. disappearance of a bubble, of the liquid phase rimming a bubble, or of the distinction between liquid and gas, whichever is applicable. Daughter minerals may persist to higher temperatures.
T _{s salt i}	temperature (measured during heating) of disappearance of salt i. Salt A refers to an unidentified salt other than halite or sylvite.
T _f	temperature (measured during warming) of fusion of ice.
T _c	critical temperature
P _c	critical pressure
% eq. NaCl	equivalent weight percentage of NaCl (corresponding to a T _f or T _c reading).

In Chapters 10 and 11, the following symbols are used in the discussion of chemical aspects of the study.

a	activity
D	bond dissociation energy of a diatomic molecule
\bar{D}	average bond dissociation energy of a polyatomic molecule
f	fugacity
G	Gibbs free energy
H	enthalpy
HM	the hematite-magnetite buffer, or the value of $\log f_{O_2}$ fixed by this buffer.
k_i	the equilibrium constant of the i^{th} reaction
m	molality
P	pressure
r	ionic radius
R	gas constant
S	entropy
T	temperature (absolute)
U	potential energy
ΔV_s	partial molal volume change of solid phases
x	mole fraction
γ	activity or fugacity coefficient.

Specimens used in the study are housed in the University of Tasmania Geology Department collection, and are referred to by their catalogue numbers (e.g. 102594, 103047).

ACKNOWLEDGEMENTS

The study was suggested by Dr. M. Solomon and carried out under his supervision at the University of Tasmania. The author has much pleasure in expressing his thanks to Dr. Solomon for his guidance and constructive criticism during the course of the work. Other members of the academic and technical staff at the University - particularly Prof. D.H. Green, Drs. W. Parkinson, J.C. van Moort and Mr. R.J. Ford of Geology and Prof. H. Bloom and Dr. L.A. Dunn of Chemistry - are thanked

for their assistance. The author also thanks his fellow students D.J. Patterson, A. Bush, M. Ahmad, G.R. Green, H.A. Davey, D.J. Ellis and particularly J.L. Walshe and P.L.F. Collins of Geology, and J.D. Williams of Chemistry for discussion and assistance of many varieties.

It is also a pleasure to acknowledge the assistance of the staff of the Centre de Recherches Pétrographiques et Géochimiques of the C.N.R.S. in Nancy, France. The fluid inclusion work done there benefited greatly from the experience of MM. B. Poty, A. Weisbrod, M. Pagel, M. Denis, J. Leroy, B. Charoy, H. Etminan, A. Rouiller and L. Jachimovicz and Mme. M. Seguin among others. The leach analyses were performed under the guidance of M. Denis and B. Charoy.

During an extended visit to Panguna, Bougainville Copper Ltd. generously provided accommodation and the use of company facilities. Mr. J. Baldwin and his geological staff assisted in acquainting the author with the geology of the mine.

The sulphur isotope study was performed at the C.S.I.R.O. Minerals Research Laboratories, North Ryde, N.S.W., under the guidance of Messrs. J.W. Smith and M.S. Burns. Dr. P.J. Eadington of the same institution kindly determined some of the higher fluid inclusion temperatures beyond the reach of the University's apparatus.

Others to whom the author wishes to express his appreciation for valuable comment and discussion include Drs. R. Fournier, R.W.T. Wilkins, D.C. Green, J.H. Ford, I.D. Ryabchikov, J.J. Hemley, P.B. Barton, V.J. Wall, W. Nesbitt, L.B. Gustafson and above all Dr. E. Roedder, who spent much time making suggestions as to how the study and its presentation could be improved. Mr. J. McKeon is thanked for his help with the proof-reading.

The study has been financed by an Australian Government Post-Graduate Research Award, and research moneys of the University of Tasmania. The author was in receipt of a Rotary Foundation Fellowship during the period spent in France.

CHAPTER ONE: REVIEW

The literature on porphyry copper deposits includes several generalised discussions on the classification and on the genesis of this type of ore deposit. It is the purpose of this section to review these aspects, as a background for the Panguna study.

CLASSIFICATION

Since the recognition of the class of large, low-grade copper deposits associated with intrusive rocks (porphyry copper deposits) the process of classification has moved in directions both synthetic and analytic.

It is recognised that a class of large, low-grade molybdenum deposits, the porphyry molybdenums, shares much in common with porphyry coppers, e.g. association with intrusive rocks and with similar types of hydrothermal alteration (Woodcock & Hollister, 1978). The term porphyry deposits is now in use (e.g. in Sutherland Brown, 1976a) for porphyry coppers and molybdenums. Analytic classifications of porphyry deposits have been attempted on the basis of ore-localisation, morphology and environment, relative metal abundances and the composition of the associated intrusive rocks as criteria.

Ore localisation. Titley (1972) suggested a classification of porphyry coppers into "intrusion" and "wallrock" types, with the mineralisation respectively in intrusion and in wallrock.

Morphology and environment. Sutherland Brown (1976b) attempted a morphological classification of the British Columbian deposits into three types. These emerge from a consideration of symmetry (judged

subjectively) and age as functions of depth of formation (also judged subjectively). The resulting clusters are correlated with deposit types which differ most importantly in their geological environment. This is implicit in Sutherland Brown's choice of environmental names - volcanic and plutonic - for two of the classes. It seems more appropriate to continue the environmental approach to all classes and to rename the third category ("phallic" in Sutherland Brown's scheme) "stock-associated". Briefly, the three classes are as follows:

1. Stock-associated. The deposit is located about a small stock penetrating high into the crust, and has cylindrical symmetry. Radial dyke swarms and diverse breccias are common associates. The stocks generally intrude unrelated country rock, and the depth of the deposit is thought to be about 3 km. This is essentially the type of deposit described by Lowell & Guilbert (1970).

James (1971) presented a diagram of ore distribution around stock-associated deposits. It is based on four examples: Bingham, Chino and Ray (U.S.A.) and El Teniente (Chile). Each of these is a different section of a single type of system in which the ore is localised in an inverted cup cutting the stock rather than capping it, and irregularly draping lower portions of the stock with ragged skirts of primary ore. Stockworks above such deposits, and favourable strata below, may also carry ore. So stock-associated deposits which do not have a barren centre at exposed levels might be annular at depth, and much ore may have been eroded from deposits with exposed annular ore-zones.

2. Volcanic. The deposit is associated with irregular, usually elongate dyke-like intrusions penetrating a coeval volcanic edifice (at 1-2 km depth). The orogenic setting is commonly marine; the hydrostatic pressure of seawater may be an important factor in the formation of volcanic-type deposits. Two kilometres of seawater exerts a pressure of about 225 bars.

3. Plutonic. The orebody is developed in medium-sized plutons which show mineral zonation, and which may intrude a coeval volcanic pile at a depth of about 5 km. The host rocks of the pluton exhibit a schistose fabric parallel to the contact and are metamorphosed to the amphibolite facies. Breccias are rare. Mineralisation may be centrally or eccentrically located, but is never peripheral.

Sillitoe (1973) has compiled observations on the vertical extensions of porphyry copper deposits. An economic orebody generally exposes about 1 km of the vertical extent of the whole hydrothermal system which Sillitoe considers may extend over 5 km or more. The bottoms are characterised by mineralisation or alteration lying within batholiths. The centres are associated with small intrusions penetrating volcanic edifices. The tops are expressed as argillic and propylitic alteration associated with the development of large masses of native sulphur, gypsum and pyrite or marcasite. A polymetallic vein deposit may be the high-level expression of a porphyry copper system in one South American case. These considerations may, in fact, unite Sutherland Brown's three classes into a single scheme, at least in the continental setting.

Seraphim and Hollister (1976) classify the structural settings of porphyry deposits into groups corresponding to Sutherland Brown's first two types, and add stockworks, breccias and also deposits where the stratigraphy of the country rock complicates the ore-distribution (e.g. skarns).

Relative metal abundances. Kesler (1973) showed that island-arc and continental porphyry copper deposits differ in their relative Cu, Au and Mo contents, the former being high in Au and low in Mo, and the latter high in Mo and low in Au.

Composition of intrusive rocks. Hollister (1975) classified porphyry coppers into two categories: a calc-alkalic type, quartz-rich with a high silica-to-alkalis ratio and a diorite type, quartz-poor, with a low silica-to-alkalis ratio. This criterion differs slightly from those used in other articles, e.g. the British Columbian deposits have been divided into alkalic (syenitic) and calc-alkalic clans (Ney & Hollister, 1976). Hollister (1975) pointed out that his diorite type includes deposits associated with silica-deficient calc-alkalic intrusions difficult to distinguish from intrusions of alkalic affinity.

Classifications based on multiple criteria. Hollister (1975) compared and contrasted his diorite type of porphyry copper with the type described by Lowell & Guilbert (1970). Hollister equated the Lowell & Guilbert type with his calc-alkalic type, whereas Lowell & Guilbert had considered mainly morphology and mineralogy as criteria in establishing their type deposit. According to Hollister, the Lowell & Guilbert type characteristically has quartz and orthoclase in fractures, but only minor albite; magnetite is minor, molybdenite is common and gold is rare; well-developed phyllic alteration occurs between potassic alteration in the core and peripheral propylitic alteration. In the diorite type, quartz and orthoclase are erratic in fractures but albite is common; magnetite is common, molybdenite rare and gold "important"; phyllic alteration is only poorly developed, if at all, between potassic and propylitic zones.

Ney & Hollister (1976) examined the relationship between relative metal abundances and intrusive-rock composition for deposits of the British Columbian province, and found that high Mo, low Au deposits are never associated with alkalic rocks, and that old alkalic deposits (170-205 m.y.) have low Mo and high Au.

Woodcock & Hollister (1978) considered the differences between porphyry coppers and porphyry molybdenums. Porphyry molybdenums are distinguished by the presence of fluorine-bearing minerals, and by higher W:Mo ratios than porphyry coppers. They may be of stock-associated or plutonic type, and a thick, sialic crustal environment appears to be a necessary condition for significant molybdenum mineralisation in the North American Cordillera. Common features in porphyry molybdenums and coppers include the presence of a pyritic halo and late polymetallic veining, and the peaking of the copper halo just outside the Mo halo in deposits where both are visible.

Summary. The most comprehensive classification schemes to date are those of Sutherland Brown (1976b) and Hollister (1975). Neither accounts for the whole spectrum of phenomena. Sutherland Brown's does not consider the compositional variety that may occur within a given environment, while Hollister's may not encompass deposits from the volcanic and plutonic settings of Sutherland Brown's classification.

CLASSIFICATION OF THE PORPHYRY COPPER DEPOSITS OF THE SOUTHWEST PACIFIC

The classification schemes discussed above are based mainly on studies of deposits in the North American Cordillera. The Panguna deposit is part of a porphyry copper province in the southwest Pacific. There is now considerable information on the province as a whole, so that the classification schemes can be tried out on an independent set of data.

The province stretches from the Philippines through Indonesia and New Guinea to the Solomon Islands, the New Hebrides and Fiji, and also extends along the entire east coast of Australia and into the North Island of New Zealand. In Australia, the deposits are of Palaeozoic and

Mesozoic ages (Horton, 1978). The lower Tertiary is represented in Sabah (Kosaka & Wakita, 1978), and the Miocene to Pleistocene in New Guinea and the Solomon Islands (Page & McDougall, 1972). The Cordilleran and southwest Pacific provinces have been subjected to continual phases of mineralisation over hundreds of millions of years. The superimposition of these in North America contrasts with the spatial separation of deposits of different ages in the southwest Pacific, and this contrast reflects the difference in tectonic phenomena in general between the eastern and western shores of the Pacific.

Complexity of intrusion and alteration history is the rule in southwest Pacific porphyry copper deposits, and telescoping of alteration and metal zoning is characteristic (Titley, 1975). The complexity of the intrusions makes classification of their morphology difficult in many cases. Panguna and Ok Tedi (Bamford, 1972) have some of the features of stock-associated porphyry deposits and, true to Sutherland Brown's (1976b) environmental criterion for this category, occur in country rock unrelated to the plutons. Other deposits occur within larger plutons (e.g. Yandera, Titley *et al.*, 1978) while Frieda may lie high within a coeval volcanic edifice (Hall & Simpson, 1975).

Titley (1978) has treated new assay data from this province in the same way and found that the deposits differ from the island arc deposits (mainly Caribbean) examined by Kesler, but in an exaggerated relative Au enrichment. Mo is low relative to the other metals with the exceptions of Sipalay (Philippines) and Yandera (New Guinea). Economic porphyry molybdenums are apparently absent.

The deposits are associated with calc-alkaline intrusive rocks, and Gustafson (1978) considers that none of alkalic affinity are present. Hollister (1975), however, regards some of the Philippine deposits as

belonging to his diorite type. The Panguna deposit (see subsequent chapters) seems to sit astride Hollister's division of porphyry coppers into Lowell & Guilbert and diorite types. The deposit is quartz-rich and associated with quartz diorites and granodiorites (characteristics of the Lowell & Guilbert type), yet it lacks significant phyllic alteration between the potassic and propylitic zones, has plentiful magnetite, is low in Mo and high in Au (characteristics of the diorite type). This suggests that Hollister's criterion of silica-to-alkali ratios is but one of several independent factors, and does not on its own govern all of the variety in porphyry deposits. The relative amounts of K and Na may be another important factor; the deposits of the southwest Pacific province are characteristically associated with intrusive rocks low in K (Gustafson, 1978).

GENETIC ASPECTS: THE ROLE OF FLUIDS IN PORPHYRY COPPER FORMATION

A recent synthesis by Gustafson & Hunt (1975) recognises three elements in the formation of porphyry copper deposits:

- "1. Relatively shallow emplacement of a usually complex series of porphyritic stocks and dikes in and above the cupola zone of an underlying batholithic body,
 - "2. Metasomatic introduction of copper and other metals, sulfur, alkalis, and hydrogen ions from the solidifying melt into both the porphyries and the country rock, usually during only part of the intrusive process, and
 - "3. The interaction of groundwater with the cooling, mineralized center."
- The formation of each deposit is seen as a variation on this theme, and the uniqueness of each stems from differences in the degree of development of these elements. For example, late (groundwater) effects may be minimal, or may completely mask earlier features. This, in turn, may

depend on the depth of formation and the availability of groundwater.

The differences in environment emerging from Sutherland Brown's (1976b) classification are likely to affect the character of porphyry copper deposits through their influence on fluid phenomena. Problems concerning relative metal abundances may be resolved by a consideration of fluid phenomena, for example the occurrence of distinct porphyry copper and porphyry molybdenum deposits. Thick sialic crust may well be required as a source for molybdenum in porphyry molybdenums, but this does not explain the virtual absence of copper from some of these deposits. Attempts to correlate metal abundances with intrusive rock compositions lead only to weak generalisations. It seems more promising to look to variations in the physics and chemistry of the mineralising fluids to explain metal abundances. These matters will be dealt with in subsequent sections.

Studies of fluid inclusions and of oxygen and hydrogen isotopes have been brought to bear on problems related to fluids in porphyry copper deposits.

Nash (1976) summarised the findings of fluid-inclusion studies on porphyry coppers, mainly examples from the Americas. In the economic Cu zone, four types of fluid inclusions have been reported:

- I. Low to moderate salinity inclusions with small bubbles (say, <50% of cavity volume) and no halite as a daughter salt at room temperature;
- II. Gas-rich inclusions with large bubbles (say, >50% of the cavity volume) sometimes with daughter salts;
- III. Halite-bearing, with small bubbles and commonly a rich variety of other daughter salts;
- IV. CO₂-rich, in which liquid CO₂ is present.

Type I inclusions have been found in all deposits in which fluid inclusions have been examined. Type III occur in most, and type II in a slightly smaller number, while type IV have been reported in relatively few. Types II and III are characteristically closely associated, although this is not universally so. This is usually taken to mean that the salt-rich liquid was boiling. In some cases, types I and II are closely associated, so that liquids of lower salinity may also have boiled in these deposits. Type IV inclusions can be CO₂-rich versions of any of the other three types, which may in fact contain considerable quantities of CO₂ without forming liquid CO₂. The amount of CO₂ differs greatly from deposit to deposit, and this suggests that CO₂ is not instrumental in the formation of porphyry coppers. In general, there is an association between type III inclusions, copper mineralisation and potassic alteration. Those deposits in which no type III inclusions occur may have suffered almost total masking of early effects during the superposition of groundwater-associated effects. The supposed absence of certain fluids in some deposits should be treated with caution; it is negative evidence, to be weighed against the thoroughness of the particular study. Sufficient detail in fluid inclusion studies is important in order that valid conclusions may be drawn about fluid abundances. Few previous studies of porphyry coppers have been detailed enough; some of the more informative studies will be discussed below.

The usual interpretation of isotopic studies of hydrous phyllosilicates in alteration assemblages is that waters of two different origins were involved in the formation of porphyry coppers. In most cases (summarised by Taylor, 1974) the waters are magmatic and meteoric. The magmatic waters are associated with potassic alteration and the meteoric waters with propylitic and phyllic alteration. One case,

Valley Copper in British Columbia, had seawater in place of meteoric water (Osatenko & Jones, 1976) and Sutherland Brown (1976b) has suggested that this may be true of a whole class of porphyry deposits. The predominance of isotopic studies on continental stock-associated porphyry deposits (particularly in the southwest U.S.A.) may be giving the impression that meteoric water is involved in the formation of a larger proportion of porphyry copper deposits than is actually the case.

Models of fluid interaction. The studies summarised above suggest that two systems of fluid are involved, one magmatic and the other the ambient fluid in the country rock, and that one system or both may be boiling. The literature contains a variety of ideas about how the fluids interact and deposit copper. Henley & McNabb (1978) grouped them into four types:

1. The circulation of ambient waters is powered by heat from the intrusion, and copper is leached from the country rocks by the convecting waters. Cathles (1977), Norton & Knight (1977) and Norton (1978) have quantified this model for various cases of pluton size and depth, and of wallrock permeability. Cathles computed flow-lines and heat and fluid fluxes to show the evolution in time of geothermal systems about cooling intrusions. In general, most of the geothermal activity is over in 20000 - 30000 years. In applying this to porphyry coppers, Cathles has investigated copper precipitation over the temperature interval 350°C to 250°C, so chosen because it corresponds with the large decrease in copper and iron solubilities found by Crerar & Barnes (1976). He recognises that this approach does not succeed, because the type of cooling inherent in the model will cause isothermal surfaces to retreat inwards. This could not generate the distinct ore-shells seen in many deposits. Rather, he is forced to appeal to salinity gradients or to some other chemical change.

2. (a variant of 1) The ambient waters, circulating as in 1, boil near the pluton. This mechanism finds little favour at present, but could reconcile the high salinities of fluid inclusions with the lower salinities of ambient waters. The possibility of boiling is dealt with in Cathles' (1977) calculations.
3. Boiling salt-rich liquid is exsolved by the crystallising pluton, and may spread, boiling, into the country rock, depositing copper as it cools. This is the orthomagmatic model, as proposed by Rose (1970), among others.
4. (a variant of 3, due to Henley & McNabb, 1978) In exsolving fluids, the crystallising pluton gives rise to large quantities of vapour bearing a few percent NaCl. The vapour forms a plume above the pluton, eventually mixing with groundwater. On cooling to 600°C, at which temperature the solubility of NaCl in the vapour is at its minimum in the relevant pressure range (Sourirajan & Kennedy, 1962), the vapour must condense out some salt-rich liquid. This would create a region containing two fluid phases, indistinguishable (superficially at least) from the two-phase region generated by mechanism 3. The salt-rich liquid could deposit magma-derived copper, provided the concentrations of copper and other components in the vapour were sufficient.

Ostensibly, each of these processes is perfectly feasible, and all probably occur to some degree. All may bring about some transport of copper, so that the question is one of dominant processes rather than right and wrong alternatives, and of identifying which features of a deposit might correspond to each process.

SELECTED STUDIES OF PORPHYRY COPPER FLUIDS

Bingham, Utah. The Bingham Cu-Mo deposit is located largely in a composite stock, the oldest part of which is an equigranular quartz monzonite. The quartz monzonite intrudes sediments and is in turn intruded by three subsequent porphyritic phases. The distribution of alteration types (potassic and sericitic) is apparently not related to the age of the intrusions, and mineralisation (associated with quartz veins) likewise affects all phases (Moore & Nash, 1974).

Roedder (1971) published a reconnaissance study of fluid inclusions from Bingham, concentrating particularly on the compositions and temperatures of formation of a limited number of samples. In the Cu-Mo core of the deposit there are salt-rich and gas inclusions giving homogenisation temperatures of 400 - 725°C. The salt-rich inclusions contained more than 60% salts by weight in some cases. Volumetric and microthermometric estimates agree at about 40% NaCl and 12% KCl in some of the salt-rich liquids. Some were boiling, and the vapour was CO₂-rich steam. Lead-zinc deposits (veins in limestone) contained fluid inclusions of low salinity. Some of those fluids were boiling. They gave temperatures of 294 - 330°C. Some inclusions contain a liquid identified as H₂S. Volumetric measurements indicated densities up to 1.3 g/cm³ for the salt-rich liquids, 0.1 - 0.3 g/cm³ for the vapours and 0.75 - 0.95 g/cm³ for fluids from the peripheral deposits.

Moore & Nash (1974) studied the distribution of inclusions in a large number of petrographic samples, also taking account of moderate salinity inclusions (type I - Nash, 1976). Only 10 specimens were heated, and compositions of 16 - 22 wt. % KCl and 28 - 36% NaCl were found. The distribution of fluid inclusion types "shows little obvious relation to the age of the host or type of silicate alteration." Salt-rich inclusions, however, correspond broadly with biotite alteration and

copper mineralisation. The authors suggest that there were two hydrothermal peaks during the history of the deposit, one at $600 \pm 50^{\circ}\text{C}$; the other at $400 \pm 50^{\circ}\text{C}$, and that pressures may have varied from 800 bars under initial lithostatic conditions to 180 bars under subsequent hydrostatic conditions. They regard the high temperatures as evidence of continuity between magmatic and hydrothermal conditions.

Sar Cheshmeh, Iran. The porphyry copper of Sar Cheshmeh is of considerable interest because of the detail in which it has been studied. Waterman & Hamilton (1975) have presented an account of the geology, and Etminan (1977) has amplified this account and given a detailed treatment of the relationships between fluids, alteration and mineralisation.

The country-rock andesite has been intruded by an elliptical granodiorite porphyry stock about which are developed concentric haloes of potassic, phyllic and propylitic alteration assemblages in order outwards. This is the classic zonation of Lowell & Guilbert (1970). The distributions of Cu and Mo are likewise classically annular, if asymmetric, the highest grades corresponding approximately with the contact of the granodiorite porphyry. Inside and outside the annuli, grades are lower, but Cu grades are sub-economic only in subsequent intrusions. The largest of these is an intrusive breccia which clearly intersects the mineralisation pattern and is characterised by the alteration of plagioclase to sericite. Four more sets of dykes were emplaced, and these are altered and mineralised to different degrees, the last set being essentially fresh and barren.

Mineralisation is associated with quartz veins, of which there are four main generations. One is associated with the main phase of mineralisation, another is later, and two are found only in the propylitic zone. In the main mineralisation phase, boiling salt-rich liquid is associated

with potassic alteration. Salt-rich liquid gives way to boiling liquid of lower salinity (unsaturated at room temperature) at about 380°C in veins transitional between potassic and phyllic alteration. Similar fluids were present at $240 - 315^{\circ}\text{C}$ in the phyllic and propylitic zones. CO_2 is abundant, and is commonly observed as a rim of liquid in gas-rich inclusions. Fluid-inclusion studies on quartz phenocrysts from the intrusive breccia and from one of the later sets of dykes have shown that boiling salt-rich liquids were also associated with these intrusions. The intensity of mineralisation seems to be related to the abundance of gas-rich inclusions, and Etminan suggests that this is an indication of the amount of boiling that took place.

Hydrogen and oxygen isotopes at Panguna. Ford & Green (1977) published an isotopic study of whole rocks, individual phyllosilicates and quartz from the open pit and the surrounding area at Panguna. The usual type of porphyry copper isotope study, a comparison of the waters which were in equilibrium with hydrous minerals and waters of magmatic, meteoric and oceanic origins, is hampered at Panguna by the overlap in the δD values of present-day meteoric water on Bougainville and magmatic water. It was assumed that Pliocene meteoric water differed little from present-day water. Thus, unambiguous interpretations of the data were not possible. Although $\delta^{18}\text{O}$ and δD of biotites from Panguna are similar to those of other porphyry copper deposits, the waters involved could have been derived from groundwater or from a magma. Likewise, the sericite-bearing assemblages could have formed in equilibrium with magmatic water at 500°C or meteoric water at 300°C , or both (i.e. two separate generations of sericite may be present). There is no isotopic evidence for the presence of seawater or connate water. The $\delta^{18}\text{O}$ values of vein quartz increase away from the intrusive centres, consistent with

declining temperature. Whole-rock isotopic data help to resolve the ambiguity of the biotite data by indicating that there is insufficient ^{18}O depletion in the propylitic zone to match a purely meteoric-hydrothermal model. Nonetheless, the data for the propylitic zone are consistent with the presence there of meteoric water. So an inner magmatic-hydrothermal system flanked by a meteoric-hydrothermal one is proposed by Ford & Green.

CHAPTER TWO: GEOLOGY

The islands of Bougainville and Buka consist of a complex pile of volcanic rocks and sediments, the stratigraphy of which was established by Blake & Miezeitis (1967, and Table 2-1). The geological map (fig. 2-1) is adapted from their work, as is the following description of the geology.

STRATIGRAPHY

The Kieta Volcanics: the oldest exposed formation, comprising lavas (mostly andesite, but with some basalt and trachyandesite), pyroclastics (agglomerates, crystal tuffs and lithic tuffs) and widespread sedimentary rocks (poorly sorted sandstone, siltstone and conglomerate). The latter are thought to be the products of erosion of old volcanoes to give fan deposits. The sediments are apparently non-fossiliferous except for limestone pebbles in a single conglomerate unit. Foraminifera from the pebbles indicate a maximum age of lower Miocene.

The Buka Formation: sandstone, siltstone and agglomerate, limited to Buka and nearby small islands. The Buka Formation and the Kieta Volcanics are thought to be of similar age.

The Keriaka Limestone: an uplifted reef formation overlying the Kieta Volcanics in central Bougainville. A fauna of foraminifera indicates an age of lower Miocene (Tertiary "e" stage).

Unnamed Volcanics: andesitic, dacitic and basaltic lavas and pyroclastics of uncertain age, in central Bougainville.

The Bougainville Group: andesitic and dacitic lavas, pyroclastics and sediments derived from nine recognisable volcanic centres along the

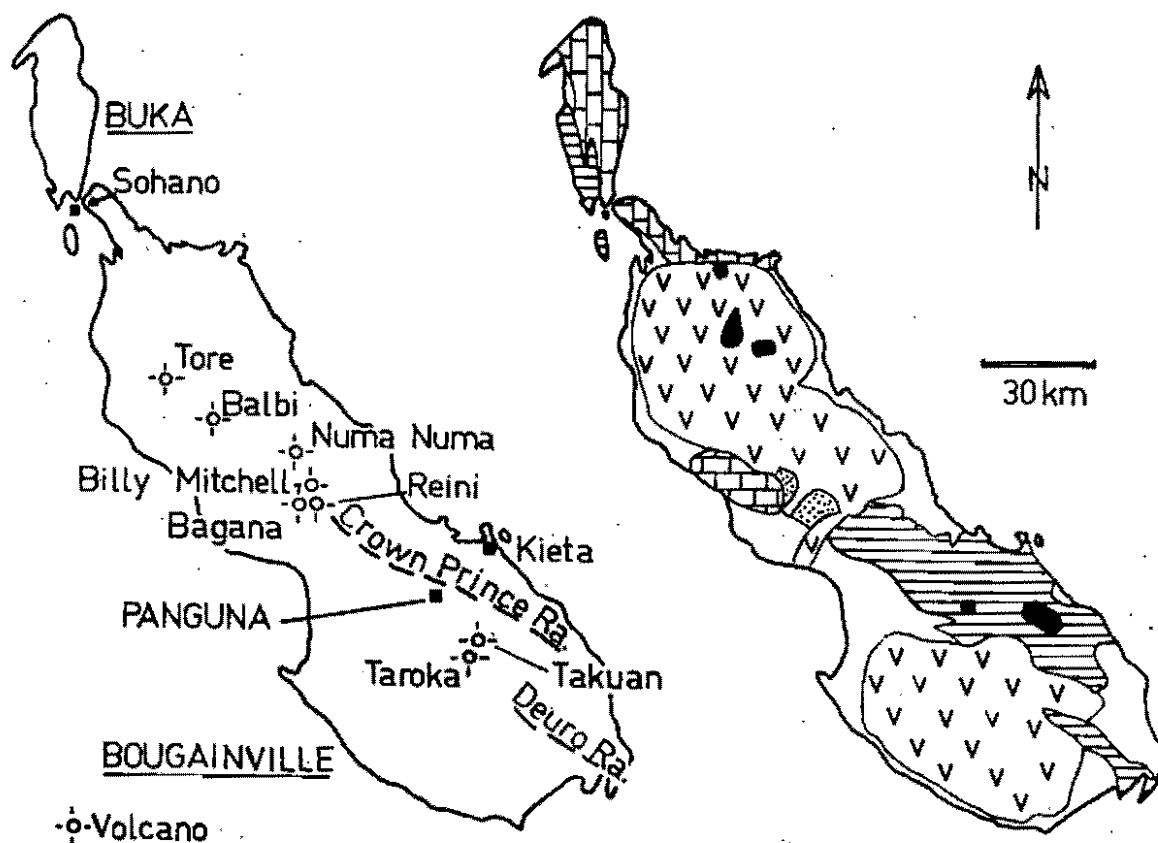









Fig. 2-1 Geology of Bougainville and Buka, after Blake & Mieztis (1967).

Table 2-1
STRATIGRAPHY OF BOUGAINVILLE AND BUKA

Age	Unit	
Quaternary	Alluvium	
Pleistocene	Sohano Limestone	
Pliocene (?) to Recent	Bougainville Group	
Miocene (?) to Pliocene (?)	Unnamed volcanics	
Lower Miocene "e" stage	Keriaka Limestone	
Oligocene (?) - Pleistocene (?)	Diorite intrusives	
Oligocene (?) to lower Miocene (?)	Buka Formation (Buka Is.) Kieta Volcanics (Bougainville Is.)	

(after Blake & Mieztis, 1967).

axis of Bougainville, and from other unspecified centres in the north of the island. Activity has continued since the Pliocene. Of the centres, Bagana is very active at present, and Balbi and the Loloru crater of the Taroka complex are considered dormant.

The Sohano Limestone: an uplifted reef formation on Buka, Sohano Island and the north coast of Bougainville. The upper part contains Pleistocene foraminifera, but the lower part may be considerably older.

Quaternary Alluvium: occurs in broad expanses on the west coast of Bougainville and in river deltas elsewhere. In addition, volcanic ash of Quaternary age thinly covers much of Bougainville and Buka.

Dioritic Intrusives: numerous intrusive bodies intersect the Bougainville Group, the unnamed volcanics and the Kieta Volcanics. The plutons of the Crown Prince Range (southeastern Bougainville) consist largely of diorite, quartz-diorite and granodiorite, and those of northern Bougainville consist of the former rock-types as well as gabbro, syenogabbro, syenite and monzonite (Ford, 1976). Page & McDougall (1972) have published K-Ar dates of 4 to 5 m.y. for the main Panguna intrusion, and Webb (reported in Blake & Mieziitis, 1967) dated one specimen from the Isinaï intrusive of the southern Crown Prince Range at 5 m.y. Hornfelsed volcanics and sediments are found as contact metamorphic aureoles around most of the intrusions.

STRUCTURE

There is little evidence for folding; most dips are less than 15° . These appear to be largely due to original attitudes in the case of volcanic units and the result of tectonic warping in the cases of the Keriaka Limestone (dip about 3°) and the Sohano Limestone (dip less than 1°).

The detail of faulting is poorly known, but three major lineament directions have been recognised: NW (the axis of Bougainville), NNW (the axis of Buka) and W-WSW.

MINERALISATION

Gold, copper and pyrite mineralisation, of minor importance save in the Panguna area, is associated with several of the dioritic intrusions.

GEOLOGY OF THE PANGUNA AREA

The stratigraphy of the Panguna area is given in Table 2-2 (slightly modified, after Macnamara, 1968). Macnamara's nomenclature of the intrusions is used here, along with a few terms in current use by mine geologists (Baldwin *et al.*, 1978). Fig. 2-2 is the geological map of the Panguna and Kupei areas (after Macnamara, 1968).

Copper mineralisation at Panguna occurs at or near the southern contact of the Kaverong Quartz Diorite with the Panguna Andesite. Only pyritic mineralisation is found in the other local units of the Kieta Volcanics. The pyrite in the Binivan Andesite Breccia is considered to be deuteric by Macnamara (1968).

The following descriptions of the rock-types in the area of copper mineralisation have been adapted from Fountain (1972) unless otherwise stated.

Panguna Andesite. There are two textural types: a predominant, massive variety with abundant xenoliths, and a subordinate, finer-grained, banded type with relict pyroclastic structures. Contact metamorphism (or hydrothermal alteration in the opinion of Ford, 1976) has given rise to a hornblende-plagioclase-magnetite assemblage within about

Table 2-2

STRATIGRAPHY OF THE PANGUNA AREA

Age	Rock Units	
Quaternary	River gravels	0-50 ft.
	Volcanic Ash	0-100 ft.
	Boulder Terraces	50 ft.
<hr/>		
Pliocene (?)	<u>Intrusive rocks</u>	
	Nautango Andesite	
	Karoona Porphyry and other porphyry dykes	
	Biuro Granodiorite	
	Kaverong Quartz Diorite	
	- marginal phases:	
	1. Leucocratic Quartz Diorite	
	2. Biotite Diorite	
	3. Biotite Granodiorite	
<hr/>		
Miocene	Pakia Gap Tuff	(+ 600 ft.)
<hr/>		
Unconformity		
<hr/>		
Oligocene (?) - lower Miocene	Kieta Volcanics Formation	{ Undifferentiated welded tuffs & agglomerates Binivan Andesite Breccia Member (+1000 ft.) Panguna Andesite Member (+3000 ft.) Pinei Agglomerate Member (+1500 ft.) Nairovi Siltstone Member (+1500 ft.)

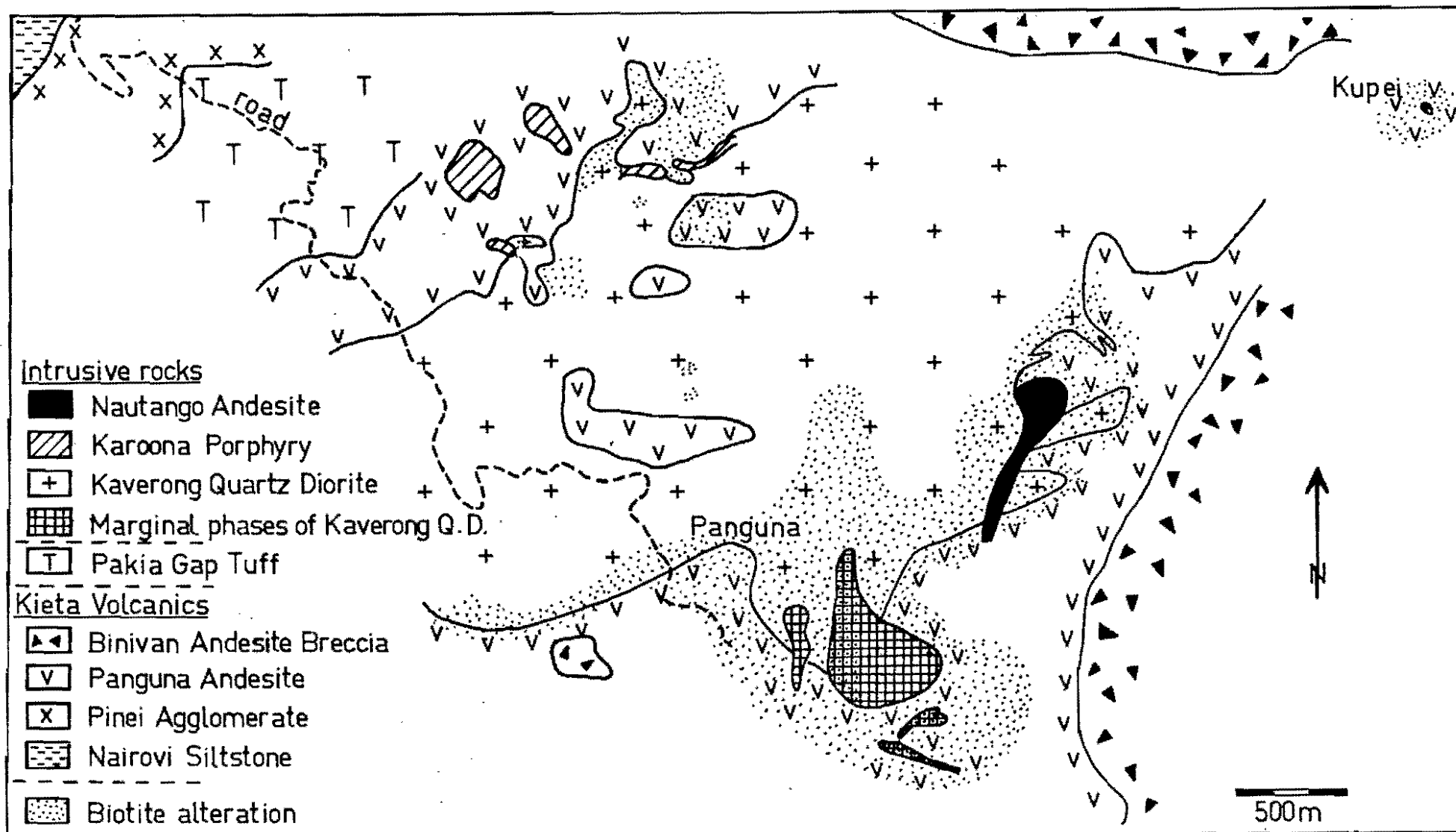


Fig. 2-2 Geology of the Panguna area, after Macnamara (1968).

600 m of the Kaverong Quartz Diorite contact. Beyond 600 m, epidote-chlorite-albite-K feldspar-calcite-pyrite becomes the dominant assemblage, and beyond 1300 m, grains of fresh igneous hornblende and pyroxene appear. Later hydrothermal alteration associated with the copper mineralisation has superimposed potassic and argillic assemblages on to this zonation.

Kaverong Quartz Diorite is the predominant rock-type of the Panguna intrusive complex. Equigranular and porphyritic phases have been distinguished. Where fresh, the equigranular phase consists of hornblende, zoned andesine and interstitial quartz and alkali feldspar. The fresh porphyritic phase contains phenocrysts of zoned andesine and hornblende in a groundmass of quartz and alkali feldspar. Hydrothermal alteration has superimposed propylitic (chlorite-epidote-pyrite and minor calcite, sericite and albite) and potassic (biotite-plagioclase-quartz-magnetite-sulphides and minor chlorite) assemblages. The biotite-bearing assemblage occurs along the southern margin and in small areas elsewhere; it is the Biotite Diorite rock-type of Macnamara's (1968) classification.

Marginal Phases of the Kaverong Quartz Diorite. Numerous stocks and dykes of altered quartz-plagioclase-hornblende porphyry intrude the Panguna Andesite and the Kaverong Quartz Diorite (fig. 2-3). The three main types, the Biotite Granodiorite, the Leucocratic Quartz Diorite and the Biuro Granodiorite, differ only subtly from one another and from the Kaverong Quartz Diorite according to original composition. Distinctions are more evident when based on alteration style and relationship to copper mineralisation. The Leucocratic Quartz Diorite typically contains quartz, andesine (replaced by albite and sericite), chlorite, epidote and minor calcite, magnetite and hematite. It is richly

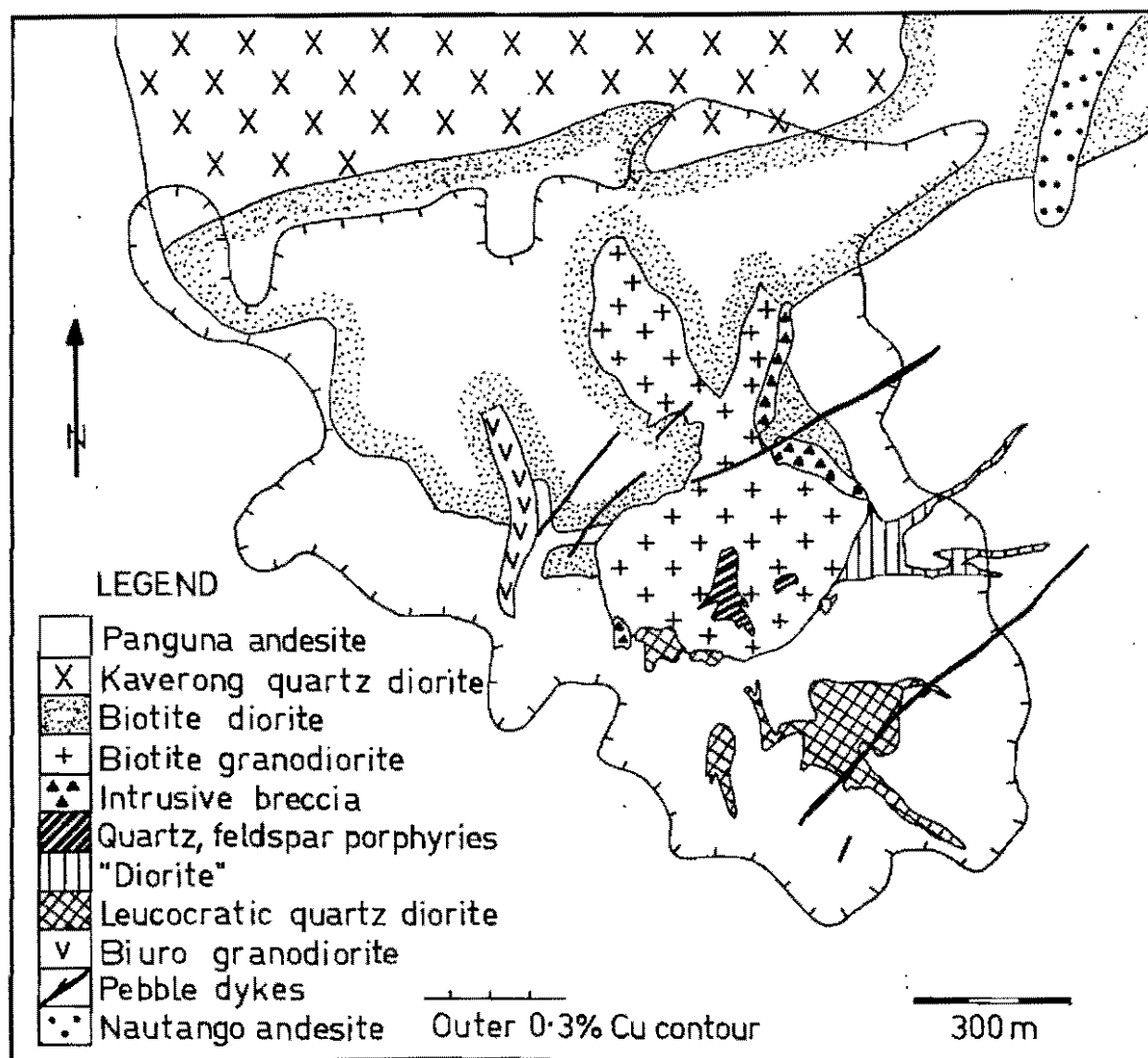


Fig. 2-3 Geology of the orebody, Panguna, after BCL geological maps.

mineralised (more than 1% Cu). The Biotite Granodiorite contains three assemblages: 1 - biotite, plagioclase, quartz, sulphides; 2 - chlorite, sericite, quartz, sulphides; 3 - quartz, sericite, clay, sulphides. Copper grades are low, but never less than 0.1%. The Biuro Granodiorite is distinguished by low grades of both alteration and mineralisation. Unaltered hornblende is present, and the copper grade is less than 0.05%.

Smaller stocks and dykes in the vicinity of the mine have been classified as follows:

- (a) Feldspar and quartz-feldspar porphyries, a group (possibly comprising more than one generation) of dykes marginal to the Kaverong Quartz Diorite. These contain phenocrysts of plagioclase and quartz in a fine grey groundmass.
- (b) The diorite, a set of dykes east of the Biotite Granodiorite. They are not described in the literature but are recognised by mine geologists. A single specimen described for this study contained 60-70% of ragged plagioclase phenocrysts set in a fine, recrystallised quartz-alkali feldspar groundmass. The phenocrysts are turbid because of the development of fine-grained alteration products, the coarsest grains of which appear to be sericite. Coarse epidote and chlorite replace plagioclase sporadically. Recent mapping by mine geologists interprets part of the area of Diorite (fig. 2-3) as Biotite Diorite.
- (c) Intrusive Breccias and Collapse Breccias occur at the margins of the Biorite Granodiorite and include fragments of Biotite Granodiorite, Biorite Diorite and Panguna Andesite. Baumer & Fraser (1975) report that the matrix is usually chloritic and in some cases carries disseminated sulphides. Locally, the matrix consists of coarse pink sanidine, coarse green biotite, quartz and chalcopyrite (e.g. 103009), or actinolite

and coarse crystals of apatite (Baldwin *et al.*, 1978).

(d) Pebble Dykes, a set of steeply-dipping, NNE-NE fractures filled with tabular bodies composed of rounded cobbles of the enclosing rocks in an unmineralised matrix of cominuted rock fragments, clay and calcite. Some extend more than 500 m along strike, pinching and swelling up to 10 m in width. At depth the pebble dykes become more numerous and more continuous in plan.

(e) Nautango Andesite, a barren stock, elongate in plan, of fresh hornblende andesite. It crops out NE of the deposit and may be a sub-volcanic plug. It is 1.6 m.y. old (Page & McDougall, 1972).

The Order of Intrusion. The establishment of the order of emplacement of the marginal phases of the Kaverong Quartz Diorite is fundamental to an understanding of the Panguna deposit because of the different relationships between mineralisation and the various intrusions. Two different orders have been proposed in the literature (oldest first):

Fountain (1972)	Baumer & Fraser (1975)
1. Leucocratic Quartz Diorite (Stage I Porphyry)	1. Biotite Granodiorite
2. Biotite Granodiorite (Stage II Porphyry)	2. Leucocratic Quartz Diorite
3. Biuro Granodiorite (Stage III Porphyry)	3. Biuro Granodiorite

Fountain justified his version with the observations that a dyke of Biotite Granodiorite, apparently detached from the main stock, cuts the Leucocratic Quartz Diorite, and that the Biuro Granodiorite cuts all mineralisation and alteration patterns in its vicinity. Ford (1976) supported Fountain's view, and stated that the geochemical variation in

the intrusive suite at Panguna is consistent with it. Baumer & Fraser, in support of their hypothesis, cited a body of Leucocratic Quartz Diorite which cuts the Biotite Granodiorite. All of these propositions are open to question. The intersection of one intrusion by another is evidently difficult to observe with certainty at Panguna; the examples quoted here both depend on the identification of the rock-types in small stocks with those in the large Leucocratic Quartz Diorite and Biotite Granodiorite stocks. Given the similarity of the initial textures and compositions of these rocks (so that the identifications are based largely on alteration types which are not necessarily unique in time and space) such arguments cannot be regarded as conclusive. Ford's geochemical data seem consistent with any hypothesis by which the Leucocratic Quartz Diorite, the Biotite Granodiorite and the Biuro Granodiorite were emplaced in a group some time after the emplacement of the Kaverong Quartz Diorite. The data do not seem sufficient to place the three marginal phases in order.

Alteration. Fountain (1972) described the following five main types of alteration at Panguna.

(i) Biotite alteration, in which secondary biotite replaces earlier mafic minerals. K-feldspar may also be present. Biotite alteration is pervasive in parts of the Kaverong Quartz Diorite and the Biotite Granodiorite, and the biotite occurs interleaved with chlorite in these rock types. Elsewhere, biotite alteration is a wallrock effect only.

(ii) Chlorite-epidote alteration, which is attributed to thermal metamorphism as well as to hydrothermal alteration in the Panguna Andesite (see above). It is also found in the Kaverong Quartz Diorite, where it is pervasive near the orebody, and pervasively disseminated in the Leucocratic Quartz Diorite.

(iii) Chlorite-sericite alteration, occurring only in the Biotite Granodiorite. Chlorite replaces biotite, sericite replaces plagioclase and groundmass alkali feldspar remains unaffected. Fountain suggested that the chlorite selvages of certain pyrite veins in the Panguna Andesite might be equivalent to this alteration type.

(iv) Sericite-clay alteration, again only in the Biotite Granodiorite. Plagioclase is replaced by kaolinite and sericite.

(v) Clay-calcite, limited to faults post-dating the Biuro Granodiorite and to the matrix of the pebble dykes. It is most intense near the Biuro Granodiorite.

These types correspond broadly with the classical nomenclature of porphyry copper alteration zones as follows: (i) with potassic, (ii) with propylitic, (iii) with phyllic and (iv) and (v) with argillic. Fountain related their distribution to the temperature distribution at the time of emplacement of the Biotite Granodiorite.

Baumer & Fraser (1975) classified the alteration zones according to the four classical types and suggested a more sophisticated scheme of multiple overprinting. They noted the asymmetry of the zones with respect to the copper mineralisation, but recognised a general conformity with the Lowell & Guilbert (1970) model. Their tentative alteration sequence is:

(i) regional propylitisation, intense at the orebody margins and decreasing inwards;

(ii) weak, pervasive potassic alteration with disseminated ore, centred on the western part of the orebody and best shown in the Biotite Diorite and Biotite Granodiorite. Near the Leucocratic Quartz Diorite it is a contact phenomenon.

(iii) a fracture-controlled potassic alteration associated with the main ore-mineralisation phase. This grades into

(iv) fracture-controlled argillic alteration.

Some argillic alteration belongs to an earlier phase which occurred before copper mineralisation.

Ford & Green have recognised the amphibole-plagioclase-magnetite assemblage pre-dating copper mineralisation as an early hydrothermal alteration style. Baldwin *et al.* (1978) added a late amphibole alteration - actinolite and apatite in the spaces of a collapse breccia northeast of the Biotite Granodiorite - to the list of alteration assemblages.

Fountain grouped the alteration assemblages into two sequences, a regressive sequence (grade of alteration decreasing) from biotite to chlorite-epidote to fresh rock, and a progressive sequence (grade increasing) from biotite to sericite-chlorite to sericite-clay.

Fountain's and Baumer & Fraser's work on alteration are combined in fig. 2-4.

Mineralisation. Primary sulphides, mainly chalcopyrite, pyrite and bornite, occur in veins, in breccia fillings and as disseminations. Baumer & Fraser (1975) estimated that 80% of the mineralisation occurs as veins or as wallrock disseminations around veins; most of the rest is disseminated sulphide associated with pervasive alteration. It is likely that even the disseminated sulphide and the pervasive alteration are associated with the deposition of veins in a fluid-rich system, and on this basis the history of veining can be treated as the history of mineralisation.

It has been evident to previous workers that the vein system is complex, yet little headway has been made towards establishing a sequence. Ten types were distinguished by Baumer & Fraser (1975) on the basis of composition and habit, but it was reported that the age relationships had been resolved only in very small areas. Fountain (1972) proposed four stages of vein formation. The stages are distinguished

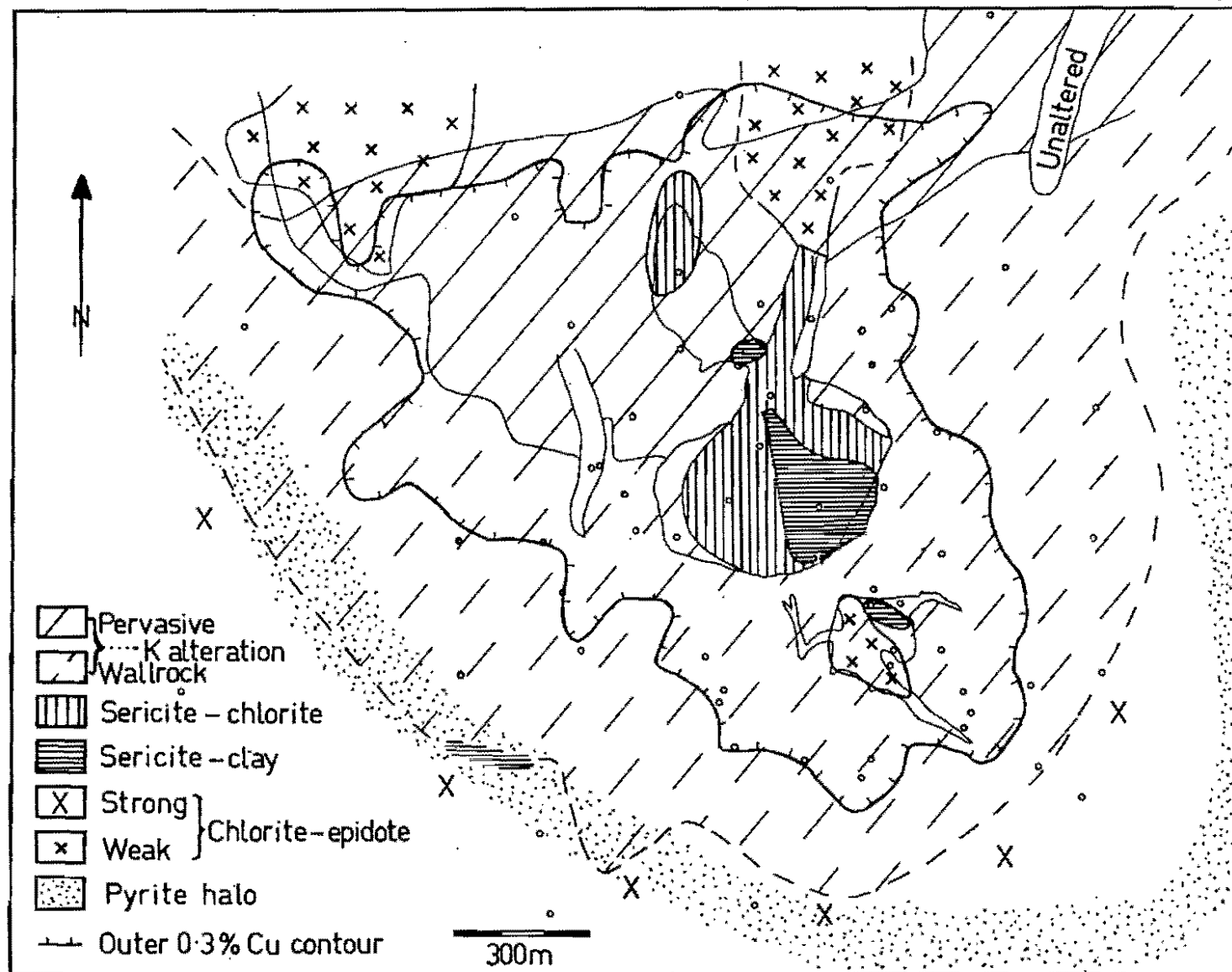


Fig. 2-4 Alteration in the Panguna deposit, after Fountain (1972) and Baumer & Fraser (1975). Geological boundaries and outer 0.3% Cu contour as in fig. 2-3. Sample locations (small circles) as in fig. 5-9.

according to the intersection relationships of veins and intrusions and are therefore subject to the same criticism levelled at interpretations of the intrusive history.

Secondary enrichment and oxidation of hypogene sulphides are of minor importance at Panguna because erosion is very rapid. Baumer & Fraser (1975) stated that it is developed only under ridges and that water-courses cut into the hypogene zone. Covellite and chalcocite coat chalcopyrite and bornite in the supergene zone. Chrysocolla, diopside, cuprite, malachite, chalcotrichite and native copper are the chief products of oxidation. They are spectacularly developed in the higher parts of the Intrusive Breccias, where dense fracturing and high copper grades coincide.

Supergene processes may also have been responsible for the gypsum veinlets that replace anhydrite.

Structure. Abundant fractures are the predominant structural feature at Panguna. Fig. 5 of Baumer & Fraser (1975) is a map of fracture density and orientation. Except for some modification near the intrusions, fracturing conforms basically to the pattern of faulting, i.e. three steeply-dipping sets oriented WNW, N-NW and NE and another SE set dipping 50-60°. The faulting is related to the large-scale structures of Bougainville. Baldwin *et al.* (1978) have divided the deposit into four domains based on the orientation of faults.

Comment. While many aspects of the geology of the Panguna deposit are now well-known, the detailed history of the deposit remains unclear. In this study, an attempt has been made to rectify this situation (see Chapter 8) starting with data on the vein system as primary material and using it to gain information on the intrusive and alteration histories.

CHAPTER THREE: THE VEIN SYSTEM

The principal vein types, classified according to their composition, are listed in Table 3-1 with detailed mineralogy. It seems clear (Fountain, 1972; Ford, 1976) that the sequence amphibole-magnetite-quartz (group Va of Table 3-1), then Cu, Fe mineralisation (group Vb), then pyrite-clay (group Vc), then gypsum (group Vd) applies to the whole deposit. However, there remains considerable uncertainty about the order within group Vb. Despite the excellent exposure in the faces of the open pit, it was difficult to find satisfactory evidence of the order of formation of the various types of veins. It is evident in the field that there are several generations of quartz - Cu,Fe sulphide veins [type (ii) of Table 3-1], and that the number of generations varies from place to place in the orebody. Evidently, the history of the deposit is complex, and differs from one area to another. Other vein-types are relatively uncommon, or limited to certain areas, or both, so that few intersections are found. Many of these are unclear, and most clear relationships may be of local significance only (because similar veins may have been generated at other times in other areas). No clear inter-vein relationships were found for types (xii) to (xiv) of Table 3-1. Therefore these have not been classified in terms of the groups Va - Vd. The evidence gathered for the other types is discussed below and summarised at the end of the chapter.

The density of quartz veining [most quartz veins are type (ii), and others mainly type (iv)] was measured at many of the sample locations in the pit. The number of vein intersections per metre was counted along a horizontal line through the sample point in the face. The distribution map (fig. 3-1) has been divided into regions of greater and lesser vein density at the 2 veins/m contour in order to emphasise these features:

Table 3-1

CLASSIFICATION OF VEINS AT PANGUNA

Group	Type	Ore Mineralogy	Gangue Mineralogy
Va	(i) Amphibole-Quartz	mt	qtz, hbl, plag, sphene
Vb	(ii) Quartz-Cu,Fe sulphide (iia) massive with disseminated sulphide (iib) with a central parting	(iia and b) ccp, bn, py, hm, mt, mbd, rut. (sp, gn, dig, ten, brav, stan, po, CdS)	qtz (Kf, bt, anh)
	(iii) Anhydrite	ccp, bn	anh (qtz)
	(iv) Quartz-pyrite (some with QP fluid association)	py (ccp, sp, mcs)	qtz, (chlorite)
	(v) Thick, massive pyrite	py (ccp)	
	(vi) Pyrite ± bleached selvage	py (ccp)	qtz
	(vii) Discontinuous sulfide	py, ccp, mbd	(qtz)
Vb?	(viii) Chabazite-bearing	mbd, py	qtz, chabazite
Vc	(ix) Sphalerite-pyrite	sp, py, ccp, gn, ten (hm)	carbonate, (qtz)
	(x) Pyrite-clay	py	kaolinite
Vd	(xi) Gypsum		gypsum
?	(xii) Barren quartz (xiii) Calcite (xiv) Vivianite	py	qtz calcite vivianite

Explanation: Groups Va to Vd are listed in order from oldest to youngest. This order is applicable to the whole deposit. Within groups Vb and Vc, no general sequence applies to the whole deposit and the vein types are listed in the order in which they are discussed in the text. For groups Vb and Vc ordering of local significance is discussed in the text.

Mineral name abbreviations: anh = anhydrite; bn = bornite; brav = bravoite; bt = biotite; ccp = chalcopyrite; CdS = either greenockite or hawleyite; dig = digenite; gn = galena; hbl = hornblende; hm = hematite; Kf = K feldspar; mbd = molybdenite; mcs = marcasite; mt = magnetite; plag = plagioclase; po = pyrrhotite; py = pyrite; qtz = quartz; rut = rutile; sp = sphalerite; stan = stannite; ten = tennantite.

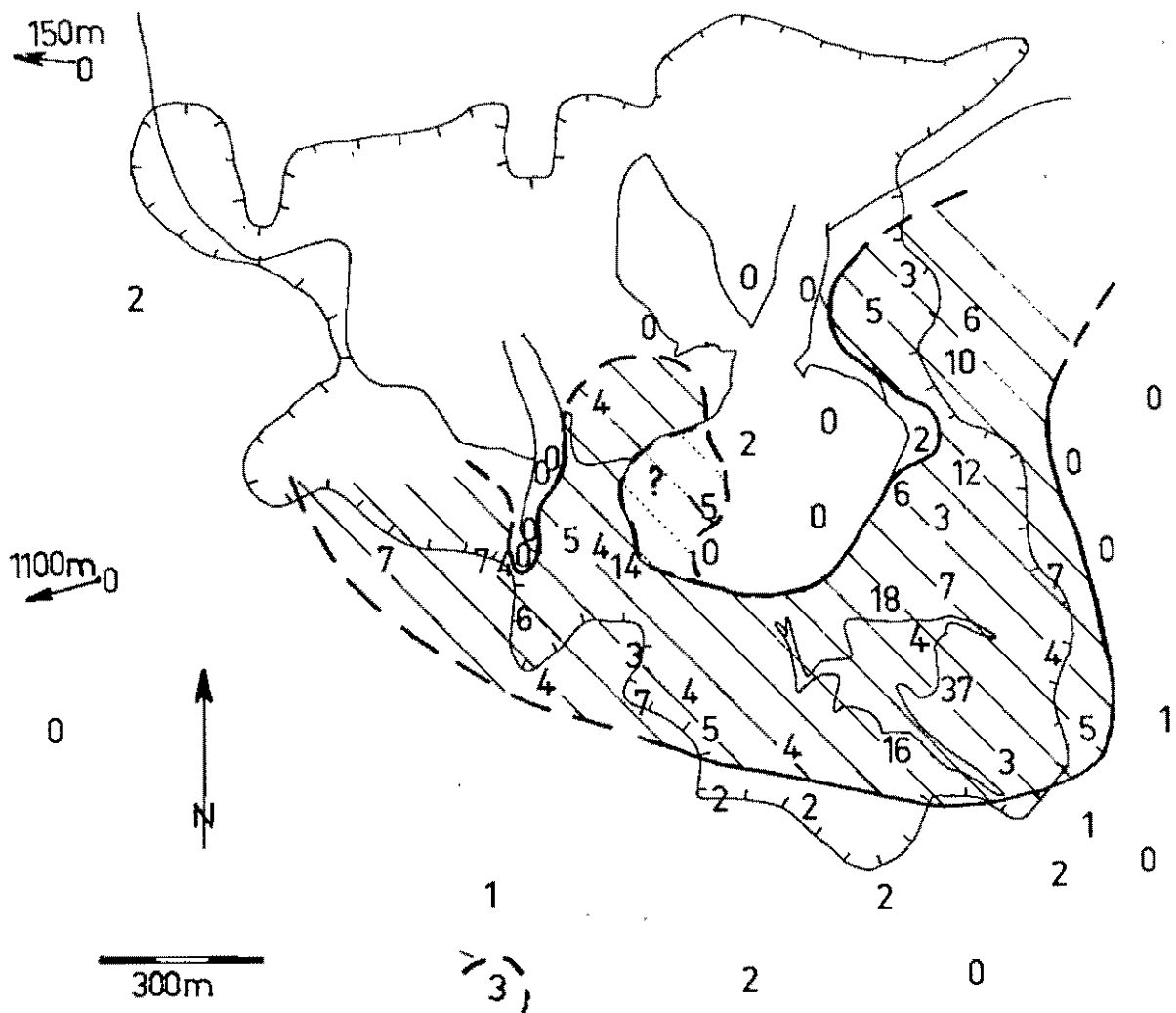


Fig. 3-1 Density of quartz veining. The numbers are the number of quartz veins per metre (measured for a horizontal line on the pit face). The outlined, hatched area denotes more than 2 veins/m. Geological contacts and outer 0.3% Cu contour as in fig. 2-3.

- (1) the correspondence of decreasing vein density and decreasing copper grade south and east of the deposit;
- (2) the sparseness of veining within the Biotite Granodiorite and the Biuro Granodiorite. Vein densities in the Kaverong Quartz Diorite could not be compared with the other measurements. Although the inspection of diamond drill holes suggested a very low veining density, account must be taken of the steep dips of most of the veins in the deposit (Baumer & Fraser, 1975) so that counts along the steeply-plunging lines of the drill-holes would not be comparable with horizontal linear integration.

Even those measurements made in the open pit are subject to difficulties because the orientation of the pit face varies with respect to the preferred attitude of the veins (of which there may also be several sets, each with its own attitude). The volume of quartz veining, perhaps a more useful parameter, cannot strictly be related to the data in fig. 3-1 because no account has been taken of the widths of the veins.

The following sections are descriptions of the various vein-types, considered in the order of Table 3-1. Observations on wallrock alteration are included with the descriptions. Most attention has been given to alteration associated with the quartz-Cu, Fe sulphide veins, but a few specimens of the other vein types were also examined. No attempt has been made to duplicate the extensive studies of Fountain (1972), Baumer & Fraser (1975) and Ford (1976) who have contributed to the present understanding of the large-scale distribution of alteration types. On the smaller scale of individual vein selvages, the possibilities of superposition of various phases of veining and alteration are many, so that in order to understand fully the relationships between

fluid properties and wallrock alteration, the selvages of representative veins from the fluid inclusion sample set must be examined.

(i) AMPHIBOLE-MAGNETITE-QUARTZ VEINS

The single example (103049) studied in detail here has no sharp boundaries, but is distinguished from its host Panguna Andesite (here largely an amphibole-plagioclase-magnetite assemblage with biotite replacing some of the amphibole) by a central concentration of relatively coarse-grained amphibole with lesser amounts of plagioclase, magnetite, quartz and sphene (fig. 3-2). This is set in a felsic margin of plagioclase with minor sphene, magnetite and apatite. In the same sample, there is a narrow vein of amphibole and magnetite only. This vein apparently pre-dates the alteration-product amphibole in the wall-rock.

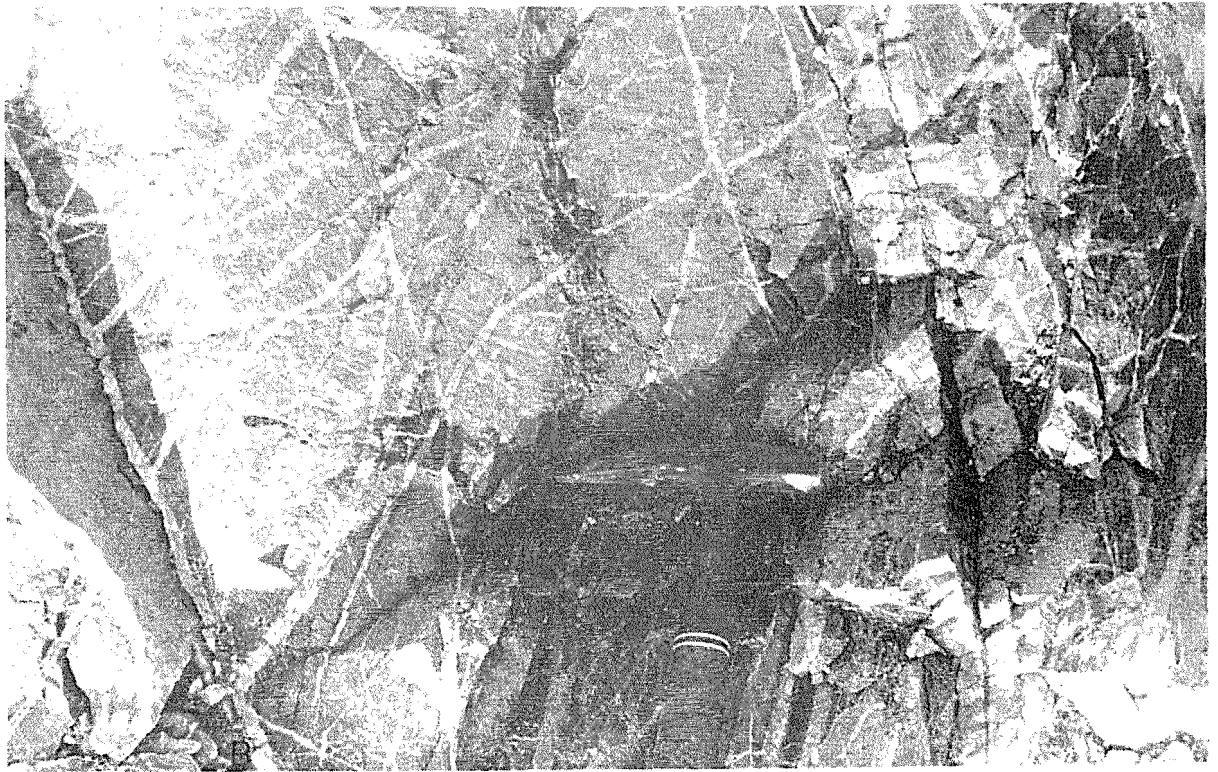
(ii) PART 1: QUARTZ-Cu,Fe SULPHIDE VEINS - OCCURRENCE AND MINERALOGY

This broad class of veins furnished most of the material studied. The veins range in thickness between 0.1 and 25 cm and vary in habit. Some consist of massive quartz with disseminated sulphides (type iia), others have a central parting which may be empty, or contain massive Cu,Fe sulphides or detached grains of sugary quartz (type iib). Thick veins may exhibit a combination of habits. Similar material occurs in the matrix of certain breccias (e.g. 103009, 103023) and lining vugs in the intrusive rocks (Fountain, 1972).

Type (ii) veins cut type (i) veins, and certain type (ii) veins are cut by types (iv), (vi), (vii), (ix) and (x). In the open pit, type (ii) veins cut all rock units except pebble dykes. Near the

Fig. 3-3 Quartz-Cu,Fe sulphide veins (type ii) in the Leucocratic Quartz Diorite. A type (iib) vein (AB) with a central seam of chalcopyrite cuts a network of type (iia) veins with disseminated chalcopyrite.

Fig. 3-2 Photomicrograph of an amphibole-magnetite-quartz vein (103049), plane polarised light. a = amphibole, s = sphene, black = magnetite, white = quartz and plagioclase. The black circle is a bubble in the Canada Balsam.



Leucocratic Quartz Diorite contact a group of type (iia) veins parallel to the contact appears to be contemporaneous with silicate melt. These veins are sharply defined in the country rock (Panguna Andesite), but in the stock, within 1 m of the contact, lose their definition and merge with the intrusive rock. Another set of veins, type (iib), clearly cuts these and other type (iia) veins and the stock (fig. 3-3).

Lawrence & Savage (1975), in their discussion of the hypogene ore mineralogy at Panguna, did not distinguish the various types of veins but most of their descriptions appear to apply to type (ii) veins or to mineralised wallrock of the same generation; their work is referred to in this section on that assumption.

Copper-iron sulphides. Chalcopyrite and pyrite are the predominant sulphides in type (ii) veins and in the deposit as a whole, but are not the only Cu,Fe sulphides present. The assemblages of type (ii) veins make up a compositional series from bornite-digenite to bornite-chalcopyrite to chalcopyrite alone, to chalcopyrite-pyrite. Pyrrhotite is present as inclusions in pyrite and chalcopyrite in 103029. Lawrence & Savage also report an assemblage bearing hypogene chalcocite with bornite, chalcopyrite, digenite and pyrite. Two or more of the assemblages above may occur in the same specimen, but showing a replacement texture (e.g. chalcopyrite replacing pyrite in many veins) or occurring separately (as in 102619, where the pyrite and bornite are in different grains). Otherwise, pyrite and bornite were not seen together in this study. In the chalcocite-bearing specimen mentioned above, the pyrite is clearly replaced by the other sulphides (see Lawrence & Savage's fig. 5). In the specimens used in this study, chalcopyrite has commonly been observed replacing pyrite (fig. 3-4); textures indicating other relationships are doubtful at best. Chalcopyrite and bornite occur as intergrowths and as exsolutions (some eutectoid)

Fig. 3-4 Photomicrograph of chalcopyrite (medium grey) and sphalerite (dark grey) replacing skeletal pyrite (light grey) in specimen 103034. Black areas are surface imperfections. Plane - polarised reflected light.

Fig. 3-5 Photomicrograph of chalcopyrite (light grey) and bornite (dark grey) in 103047, showing intergrowth and eutectoid exsolution texture. Black areas are surface imperfections. Plane-polarised, reflected light.

Fig. 3-6 Photomicrograph of bornite (dark grey) and digenite (light grey) showing intergrowth and eutectoid exsolution texture, and veined by tennantite (ten) in 102594. Black areas are surface imperfections. Plane-polarised, reflected light.

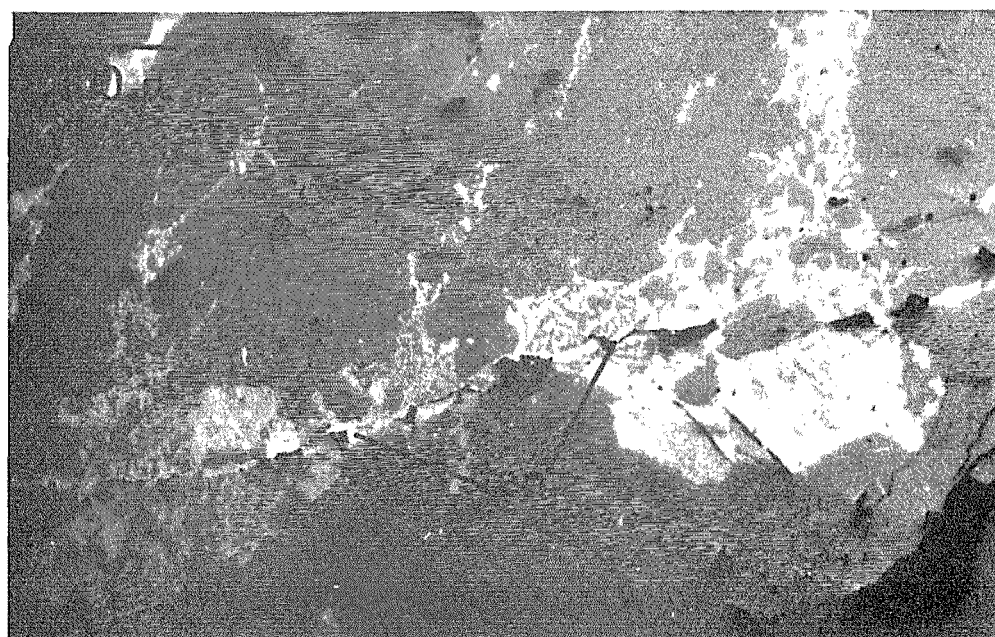
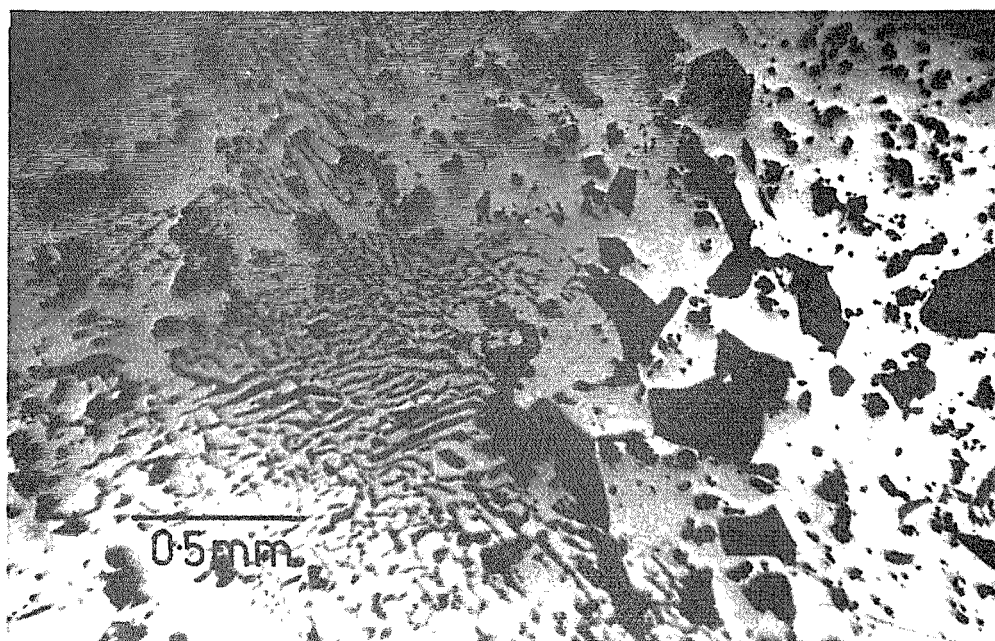
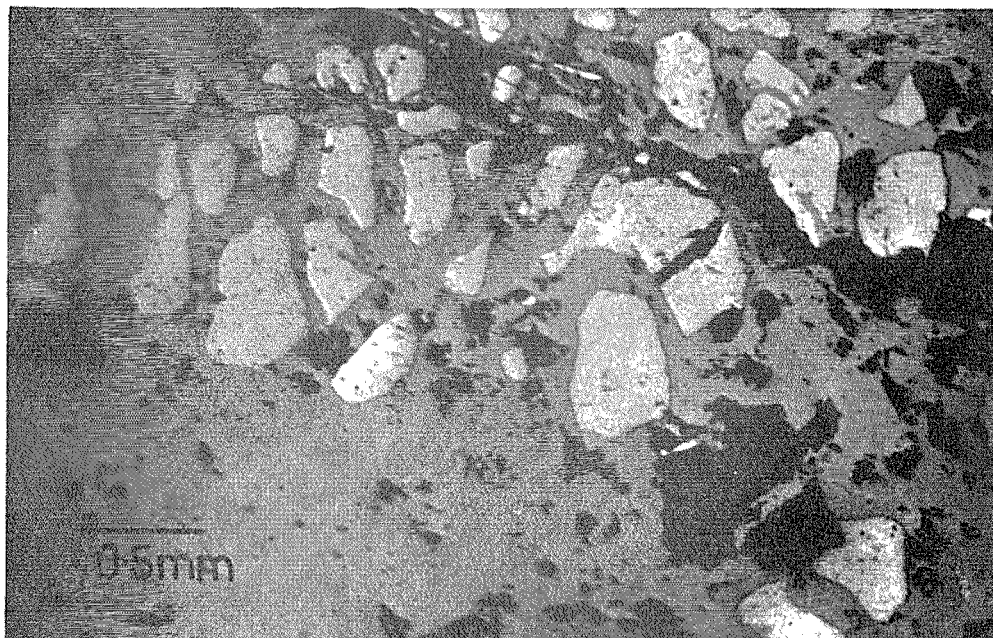


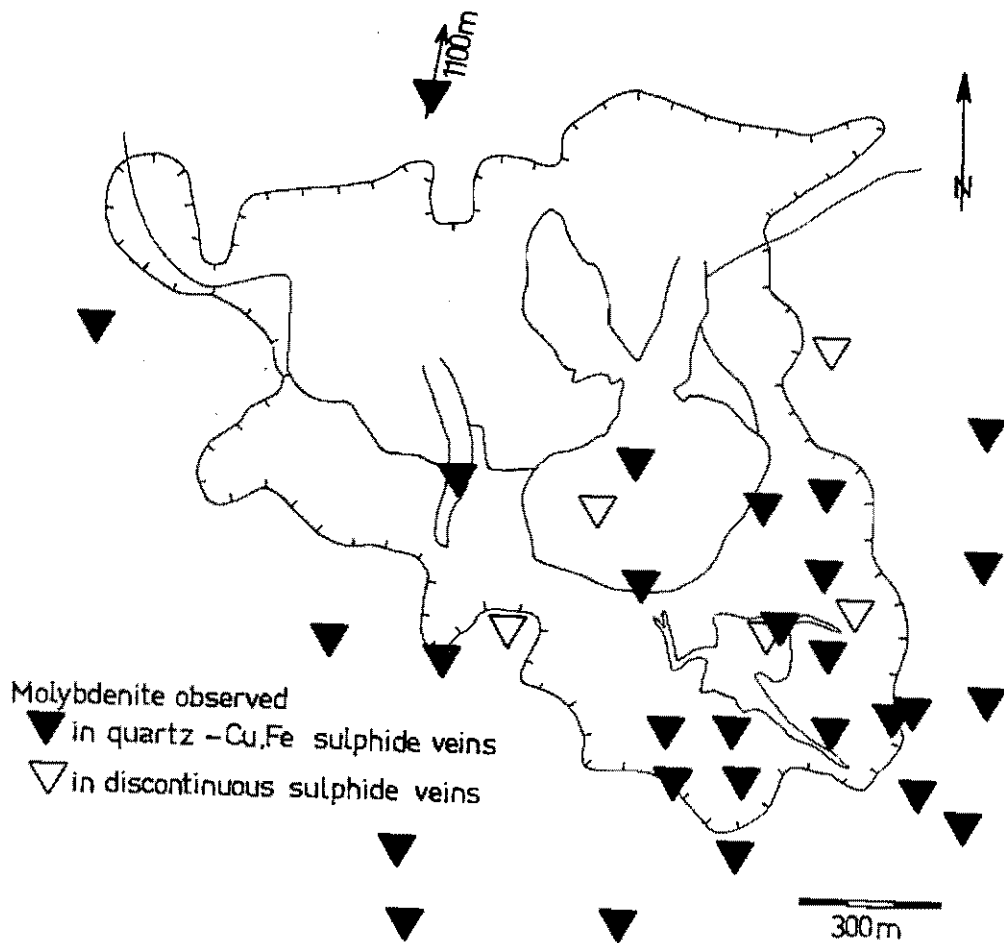
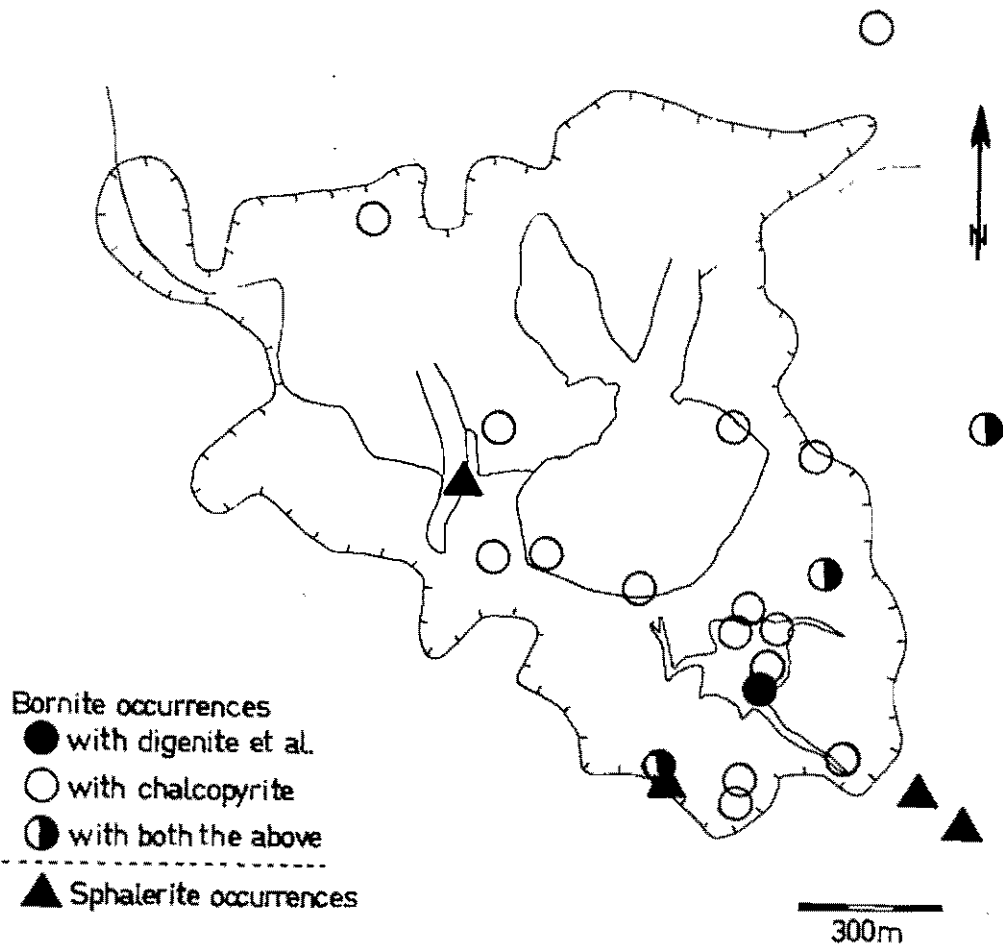
(fig. 3-5), as do bornite and digenite (fig. 3-6) and bornite and covellite. The distribution of bornite, based on microscopic observations, is shown in fig. 3-7. At hand-specimen scale, only two bornite occurrences were evident: 102594, a broad, complex vein near the Leucocratic Quartz Diorite, and 103023, a breccia filling from the area between the Biotite Granodiorite and the Biuro Granodiorite. As association of bornite with the Leucocratic Quartz Diorite is strongly suggested by the microscopic work; apart from this, there seems to be no system to the distribution of Cu,Fe sulphides.

Iron oxides. Both hematite and magnetite are widespread in type (ii) veins or their selvages. Magnetite, although abundant in wallrock adjacent to these veins, is found as a hydrothermal fracture-filling in relatively few type (ii) veins. Wallrock magnetite commonly appears to be of earlier origin (igneous, or a product of the amphibole-magnetite alteration) than these veins, and it is frequently replaced by patchy hematite. In 103008, however, magnetite in the wallrock is intergrown with chalcopyrite (fig. 3-9). Hematite, conversely, is not abundant, but it is present in a majority of specimens in the form of minute solid inclusions, or as a daughter mineral in fluid inclusions in the quartz (see Chapter 4). It is commonly not visible in polished sections of these specimens, but in 103007 and 103014, specular hematite is visible in the polished section, intergrown with chalcopyrite in 103007. Lawrence & Savage (1975) also report intergrowths with bornite, molybdenite and pyrite.

Rutile occurs abundantly in at least three modes: included in vein quartz, intergrown with other ore minerals and intergrown with secondary chlorite. Lawrence & Savage considered it to be of hydrothermal origin, and suggested that it formed by direct precipitation or as a result of

Fig. 3-7 Map of bornite and sphalerite occurrences in quartz-Cu,Fe sulphide veins. Geological contacts and outer 0.3% Cu contour as in fig. 2-3.

Fig. 3-8 Map of molybdenite occurrences. Geological contacts and outer 0.3% Cu contour as in fig. 2-3.



the chloritization of titaniferous biotite (Panguna biotites contain up to 4.2% TiO_2 according to Ford, 1976). Rutile may also have formed by the alteration of sphene from the earlier alteration assemblage consisting principally of amphibole, magnetite and plagioclase.

Molybdenite is frequently observed, but in small quantities. It is most abundant in the Leucocratic Quartz Diorite. Fig. 3-8 shows all sample sites at which molybdenite was seen in quartz-Cu,Fe sulphide veins (but not necessarily in the samples taken for this study); it is common around the Leucocratic Quartz Diorite. It occurs intergrown with chalcopyrite (fig. 3-10) and also with bornite, hematite, chalcocite, rutile and pyrite (Lawrence & Savage, 1975).

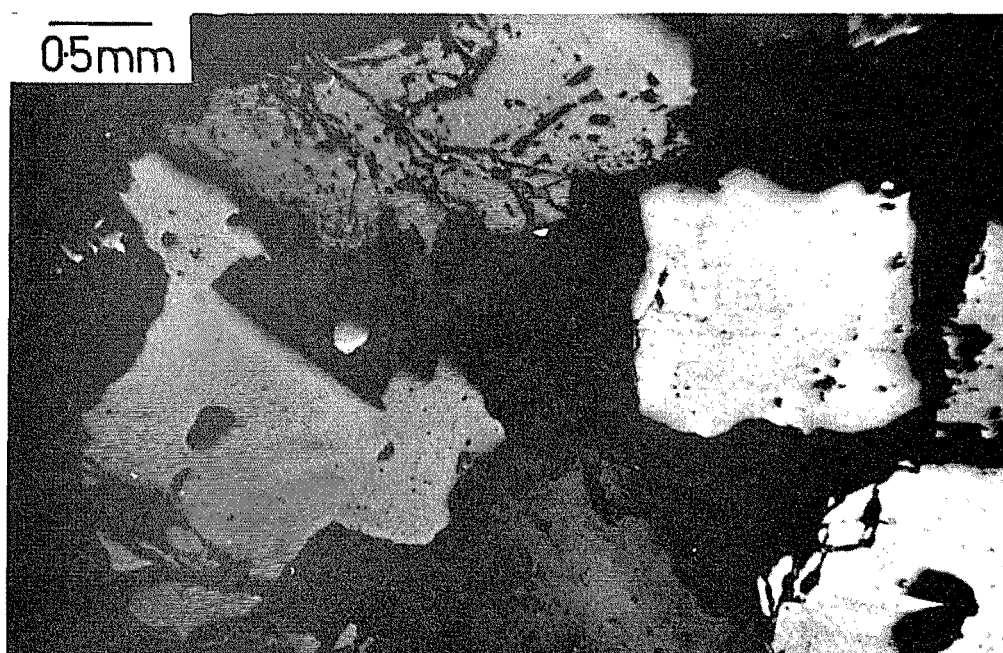
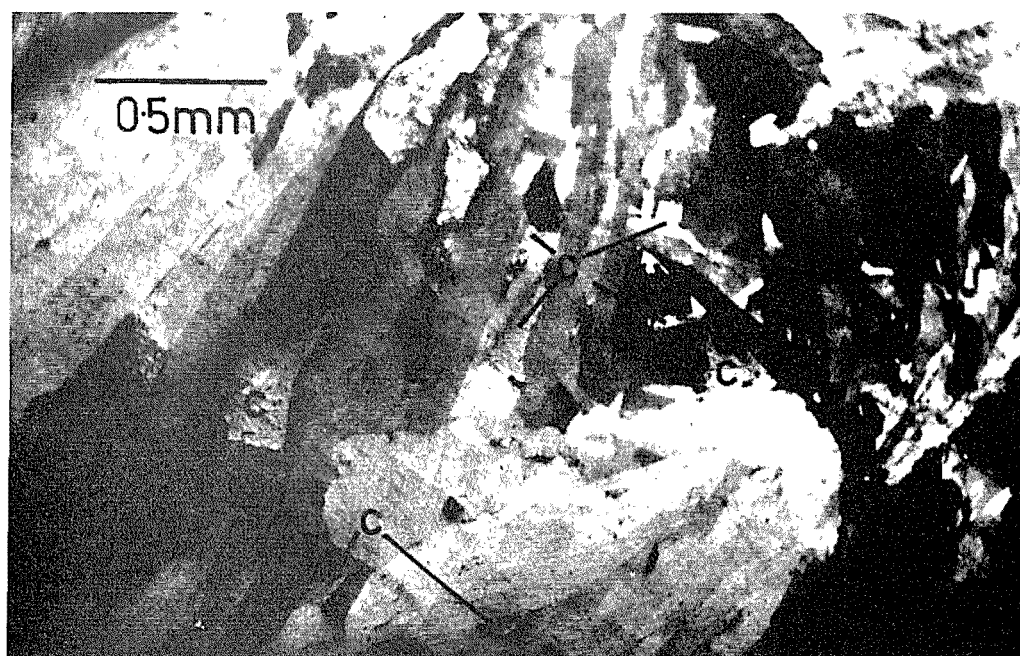
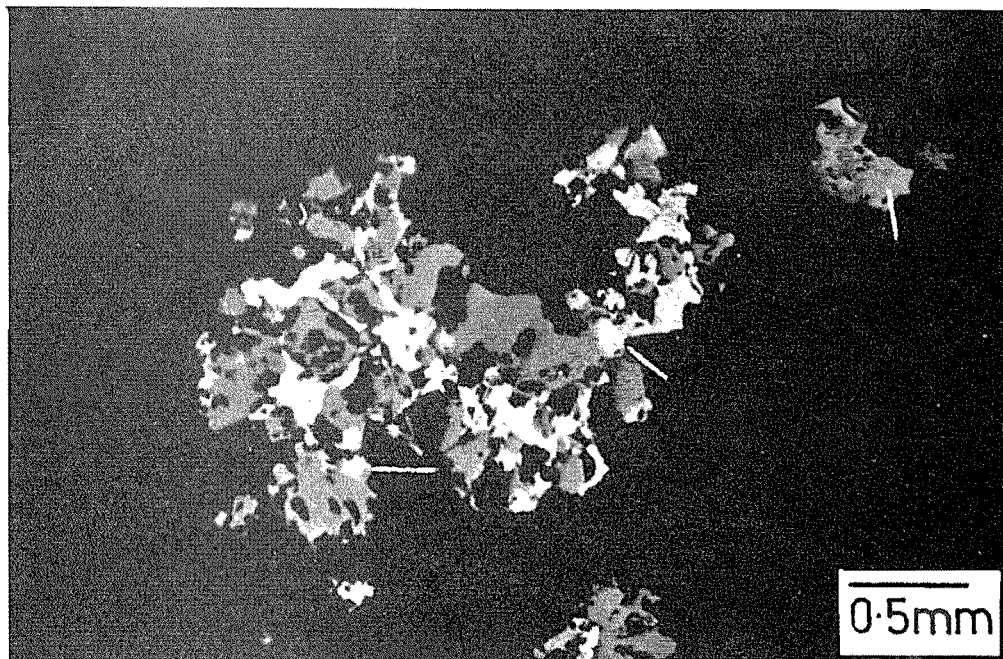
Other ore minerals. Sphalerite occurs intergrown with chalcopyrite in four specimens (103014, 103034, 103035, 103037 ; see fig. 3-7). Lawrence & Savage report it intergrown also with hematite. Bornite is associated with a variety of sulphides and sulphosalts. Veins and patches of tennantite and small inclusions of Zn-bearing stannite, bravoite and galena occur in 102594, galena, sphalerite and greenockite in 103019. The minerals were identified by electron microprobe and the CdS polymorph by reference to fluid inclusion temperatures (Chapter 5) and the data of Tauson & Chernyshev (1977). Lawrence & Savage also noted native bismuth and wittichenite in bornite. Gold (or electrum with 10 to 16% Ag), observed as inclusions in chalcopyrite by Lawrence & Savage, was not seen in specimens used in this study.

Gangue minerals. Quartz is by far the most important gangue mineral. Sanidine is found as a fracture filling in few cases (e.g. 102998) and in the Intrusive Breccia matrix (103009) with biotite. The occurrence of anhydrite is discussed below. Calcite occurs in 102998, but it is not certain whether it is of primary or secondary origin.

Fig. 3-9 Photomicrograph of opaque grains in a vein selvage (dark background). Magnetite (darker grey) is replaced by chalcopyrite (lighter grey) and hematite (lighter grey indicated by white lines). Specimen 103008. Plane-polarised, reflected light.

Fig. 3-10 Photomicrograph of a molybdenite-chalcopyrite (c) intergrowth in 102661. Reflected light, nicols half-crossed.

Fig. 3-11 Photomicrograph of specimen 103014. Pyrite (lightest grey) is replaced by chalcopyrite (medium grey) and sphalerite (darkest grey). Black areas are quartz and secondary covellite. Plane-polarised, reflected light.



Other minerals from the wallrock alteration assemblages also occur as vein minerals, but their occurrence is better treated in the context of alteration.

(ii) PART 2: ALTERATION ASSOCIATED WITH QUARTZ-Cu,Fe SULPHIDE VEINS

As well as forming selvages to the veins, the typical alteration-product silicates are found intergrown with, and as inclusions in, vein quartz. The examination of these is a valuable supplement to the study of the selvages, where mineral relationships are more difficult to interpret. A mineral represented by inclusions in quartz may even be absent from the selvage because of later superimposed events.

Fountain (1972) noted that all potassic alteration in the Panguna Andesite was wallrock alteration rather than pervasive alteration, although the 2 cm or less width of selvage in the thin sections used in this study was insufficient to expose the edge of potassic alteration (i.e. the appearance of amphibole). As revealed in thin section, the selvages are structured and inner and outer bands of different mineralogy can commonly be recognised. The observations for 30 quartz-Cu,Fe sulphide veins are summarised in Table 3-2. The distribution of albite and sericite as alteration products is shown in fig. 3-12.

The interpretation of certain specimens is difficult. For instance, in 103022 the thin (<1 mm) inner selvage rich in K-feldspar contains also sericite and chlorite. These may be replacing the K-feldspar. The quartz adjacent to the vein wall contains inclusions of biotite which no longer occurs in the immediate selvage, but which reappears, mostly replaced by chlorite, at about 8 mm from the vein wall. Two assemblages (at least) are therefore apparently associated with a single vein, and it is not clear whether one gradually-changing fluid or two or more distinct fluids were involved.

Table 3-2

SILICATE ALTERATION ASSOCIATED WITH QUARTZ-Cu-Fe SULPHIDE VEINS

Number	Rock Type	In Quartz	Inner Selvage	Outer Selvage
102609	PA	Biotite inclusions.	Chlorite + epidote (replacing biotite).	Biotite (including biotite veins).
102612	lqD	Biotite inclusions; quartz replaces plagioclase.	K-feldspar (minor); vein quartz replaces wallrock plagioclase.	Chlorite-biotite intergrowths (some chlorite may replace biotite). Sericite replaces plagioclase and some chlorite.
102619	lqD	Epidote at centre.	Chlorite (replacing primary biotite) + epidote.	Biotite (a little secondary, primary biotite replaced by chlorite).
102626	PA	Biotite inclusions; biotite replacing K-feldspar crystal; chlorite + sericite at centre.	Biotite (replaced by chlorite).	
102661	PA		K-feldspar + biotite.	Biotite.
102675	bc	Biotite inclusions.	Anhydrite (+ biotite?) replaced throughout by chlorite + calcite + epidote.	
102990	KqD	K-feldspar; calcite (secondary?).	K-feldspar + sericite.	
102999	PA	Biotite & chlorite inclusions	Albite + chlorite + epidote.	Biotite.
103000	bc	Biotite inclusions at margin Chlorite + epidote intergrowths at centre.	Chlorite (replacing biotite). Very thin.	Biotite (with scattered epidote crystals & chlorite replacing biotite).
103001	bc	Calcite (secondary?).	K-feldspar (replaced by calcite).	Biotite (green & brown) replaced by chlorite.
103003	PA	Biotite inclusions. K-feldspar crystal enclosed. Calcite, chlorite & epidote vein the quartz.	Albite + K-feldspar	Biotite.
103006	IB	Chlorite + sericite + K-feldspar intergrowths.	K-feldspar + sericite (one side) K-feldspar + chlorite (other side).	Biotite + K-feldspar.
103007	PA	Biotite inclusions; chlorite at centre of vein.	Very thin chlorite selvage (replacing biotite & K-feldspar).	Biotite + K-feldspar, then biotite. Chlorite replacing & replaced by biotite.
103008	PA	Epidote inclusions; albite + K-feldspar + chlorite intergrowths.	Chlorite + albite + K-feldspar + sericite.	Chlorite - epidote clots.
103009	IB		Brassic matrix; quartz + K-feldspar + biotite.	
103010	IB	Biotite inclusions near margin. Also some sericite inclusions.	Sericite + chlorite (replacing K-feldspar + biotite?).	Sericite + chlorite + calcite (replacing biotite).
103011	bc	Sericite at centre.	Sericite + chlorite.	Biotite (minor, at > 1 cm from vein).
103012	PA	Biotite inclusions.	K-feldspar + sericite + chlorite.	Biotite, green & brown, replaced by chlorite.
103014	BIG	Sericite intergrowths.	K-feldspar + sericite.	?
103015	bc	Biotite & sericite inclusions at margin. Chlorite in later quartz generation.	K-feldspar + biotite (replaced by sericite + chlorite).	Biotite.
103021	qfp	K-feldspar & sericite enclosed.	Quartz + sericite.	Quartz + sericite + chlorite.
103022	bc	Biotite & K-feldspar inclusions	K-feldspar (? replaced by chlorite + sericite).	Chlorite + sericite out to 8 cm, where there are clots of biotite.
103024	PA	Sericite inclusions.	Albite + sericite + sericite replaces chlorite.	
103025	PA	Biotite inclusions.	Albite + chlorite (very thin).	Biotite.
103026	PA		Albite + chlorite + biotite + K-feldspar.	Biotite.
103028	PA		Albite + sericite + chlorite.	
103029	PA		Albite + chlorite + epidote.	Biotite & chlorite; a little sericite.
103031	PA	Chlorite with overgrowths of quartz.	?	?
103033	PA	Biotite inclusions. K-feldspar between quartz crystals.	Chlorite + calcite replacing biotite + K-feldspar.	?
103035	PA	Biotite, chlorite & sericite inclusions at margin.	Chlorite & epidote.	Chlorite, epidote + ?sericite.

Abbreviations: bc - Biotite Diorite; BIG - Biotite Granodiorite; IB - Intrusive Breccia; KqD - Kaverong Quartz Diorite; lqD - Leucocratic Quartz Diorite; PA - Panguna Andesite; qfp - Quartz Feldspar Porphyry.

The following are observations which have been made for individual mineral species.

Biotite. Brown and rarely green (103001) varieties occur. Inclusions enclosed by vein quartz near the vein wall are very common, and indicate that the fluids that deposited early quartz were in equilibrium with biotite. In 102609, 102612, 102999, 103003, 103007, 103010, 103012, 103022, 103025 and 103035, the alteration products immediately adjacent to the biotite-bearing quartz contain only vestigial biotite (replaced by other minerals) or none at all. Biotite is commonly present in the outer selvage in such cases.

Sericite. This mineral occurs in 16 of the 30 sections. In the Biotite Granodiorite and the Leucocratic Quartz Diorite, its distribution corresponds with earlier workers' sericite-bearing alteration zones (cf. figs. 2-4 and 3-13). Sericite is also found in specimens from the south-western edge of the deposit, where it may represent a narrow zone of transition from potassic to propylitic alteration. Sanidine and sericite formed together in 102998, and probably also in 103006, 103008, 103012 and 103014. Sericite and albite were formed in equilibrium in 103024, 103028 and probably in 103008. Sericite and quartz are the only alteration products in the selvage of 103021.

Albite. The first occurrences of albite ($Ab_{75}-Ab_{100}$) in vein selvages occur on the orebody side of the potassic-propylitic boundary (as shown by Fountain, 1972). In 103003, 103025 and 103026, the albite is found in the inner selvage and the (?) outer selvage consists of intensely biotitised rock. In 103028 and 102999 albite is more intensely developed, with chlorite. A chequerboard twin-pattern is characteristic.

K-feldspar. Most veins which have only potassic alteration assemblages in their selvages are rimmed by K-feldspar which is succeeded outwards by biotite. The optical properties, particularly the low 2V,

correspond with those of sanidine. Red solid inclusions, presumably hematite, are in some cases present and linear, oriented gas-rich inclusions are abundant. Sanidine, with quartz and opaque minerals, forms discontinuous veinlets in 102998 (cf. Gustafson & Hunt, 1975, vein-type A which they suggest formed in almost-crystallised rock). K-feldspar has also been detected by electron microprobe analyses beside veins from the southwestern edge of the deposit. It is associated with albite in these, but individual grains cannot be distinguished optically. The relationship of the two phases is uncertain.

- Chlorite. This mineral has a large number of modes of occurrence:
- with the central quartz of certain veins (e.g. 102636, 103000, 103015, 103031), commonly with epidote.
 - veining quartz (103003), with calcite and epidote.
 - included in quartz (103035).
 - as a thin inner selvage replacing a potassic assemblage, with albite (103028, 103029) or alone (103000) or with epidote (102609, 102619).
 - replacing clots of epidote crystals (103007).
 - in a thick selvage of propylitic mineralogy (103035) or with albite and sericite (103028).
 - in outer selvages containing biotite, either replacing the biotite or interleaved with it.

Many of these modes suggest that the chlorite is later than the quartz-Cu,Fe sulphide - potassic alteration event, but this is not so in 103028, 103029 and 103035, and possibly 102999, 103008, 103025 and 103026. The optical properties of chlorites vary widely, but no systematic study has been carried out. The chlorite in 102999 is notably different from others at Panguna in exhibiting strong zonation of anomalous interference colours, which vary from blue-grey to brown and bright violet.

Epidote occurs only as mentioned in the paragraph on chlorite.

Anhydrite is found as an alteration product only in the north-western part of the deposit, where unsheathed anhydrite also survives as a vein mineral. Although anhydrite was certainly deposited in most of the rest of the orebody, there is apparently no textural evidence of leaching and replacement of anhydrite in the alteration assemblages there.

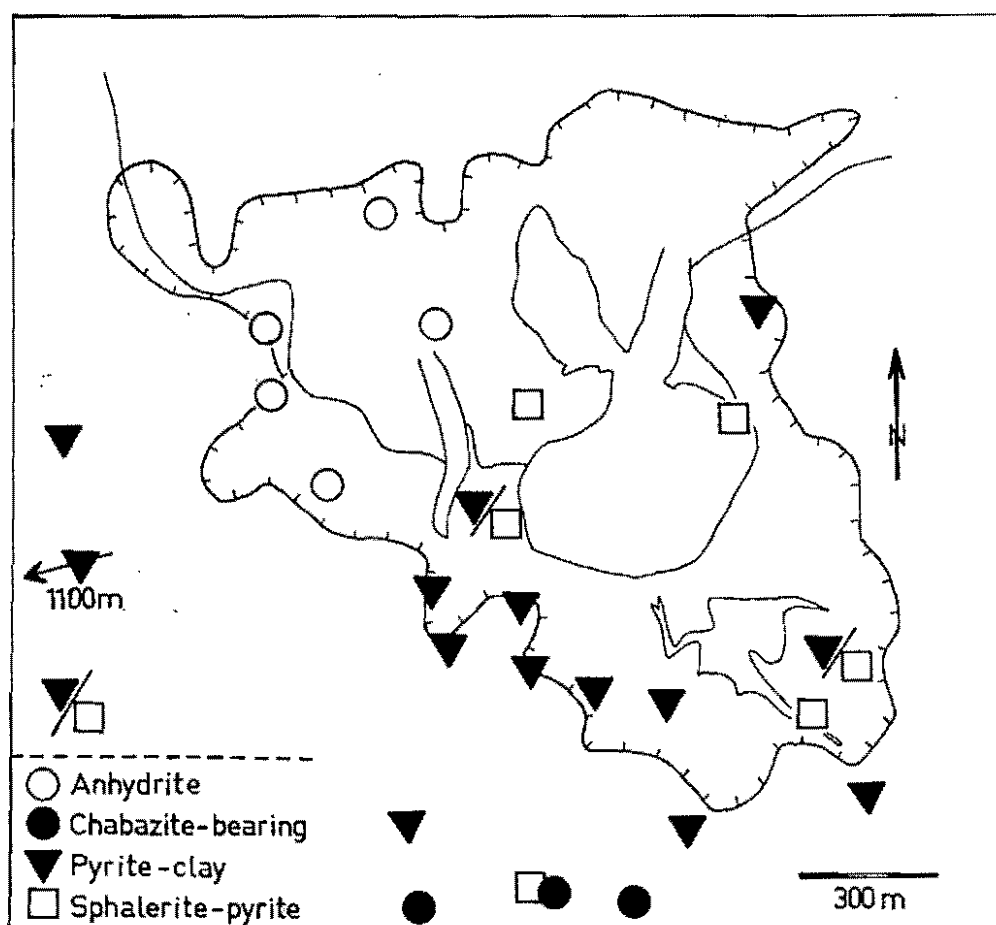
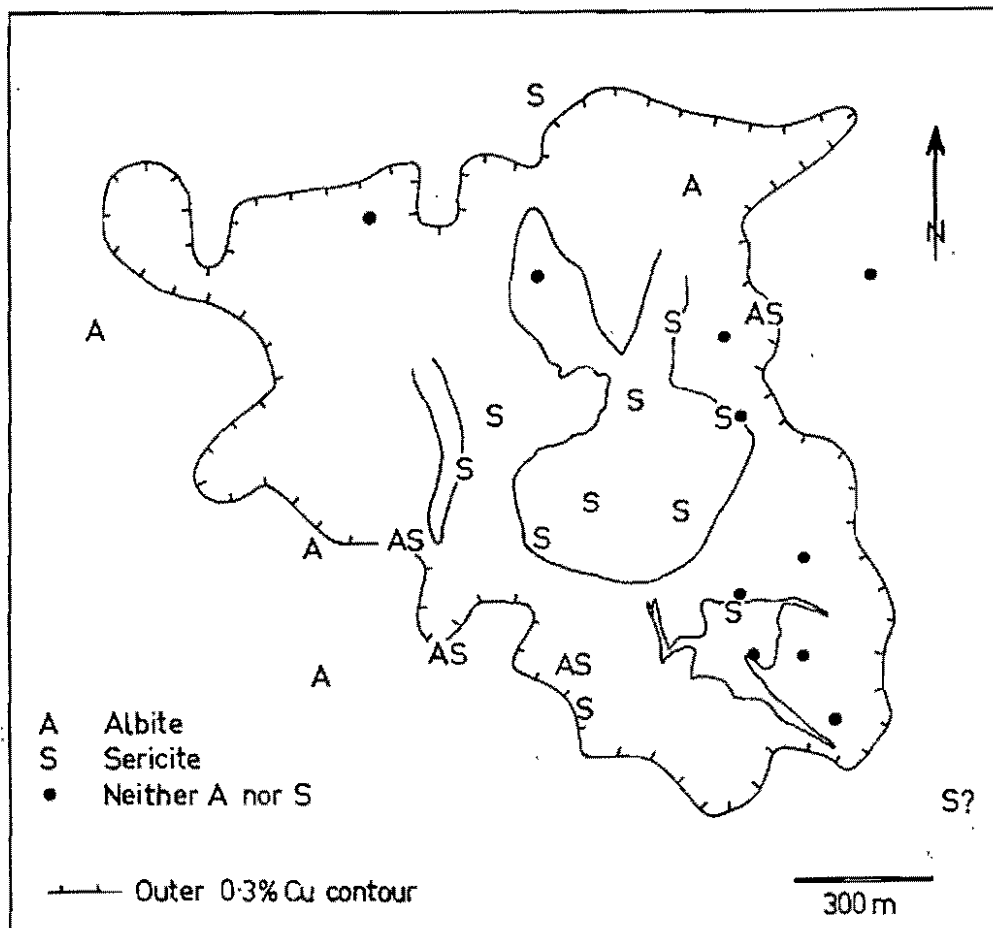
Opaque minerals in alteration assemblages. Magnetite, presumably predating quartz-Cu,Fe sulphide mineralisation, is commonly rimmed by fine-grained hematite near the veins, but it is difficult to tell whether this hematite is of supergene or hypogene origin. Near the vein in 103028, magnetite is extensively replaced by relatively coarse hematite and rutile which are certainly hypogene. Chalcopyrite replaces magnetite in 102612; in 102609 chalcopyrite, rutile and magnetite are intergrown. Pyrite is frequently seen in wallrock adjacent to veins, and in 103010 and 102998, it is replaced by chalcopyrite. Bornite and molybdenite are uncommon; they occur in the wallrock (actually clasts) of the Intrusive Breccia 103023.

Of relationships between opaque minerals and silicates, the association, already noted, of rutile and chlorite is the most prominent. Disseminated chalcopyrite replaces igneous minerals (e.g. plagioclase in 102609) but not alteration products (biotite in 102609).

Summary. Careful observation of alteration assemblages of the immediate selvages of quartz-Cu,Fe sulphide veins indicates that the fractures have carried either distinct fluids at different stages, or a single fluid of changing chemistry. The general association of potassic alteration with quartz-Cu,Fe sulphide veins (Fountain, 1972) still stands, despite the few apparent exceptions. The occurrence of other alteration types also follows Fountain's scheme. The common occurrence of K-feldspar, with or without sericite, in the inner selvages (whereas

Fig. 3-12 Map of occurrences of sericite and albite in alteration assemblages of quartz-Cu,Fe sulphide veins. Geological contacts and outer 0.3% Cu contour as in fig. 2-3.

Fig. 3-13 Map of occurrences of anhydrite veins, chabazite-bearing veins, pyrite-clay veins and sphalerite-pyrite veins. Two symbols separated by a slash indicate a vein fitting two categories. Geological contacts and outer 0.3% Cu contour as in fig. 2-3.



sericite without K-feldspar occurs only once) is an important observation which will be cited in discussions of the alteration chemistry (Chapter 10). The appearance of albite appears to be associated with the boundary of the ore-zone to the southwest.

(iii) ANHYDRITE VEINS

White and purple anhydrites occur as veins at depth in the north-western part of the deposit (fig. 3-13). Samples were obtained only from diamond drill-core. They contain also quartz, chalcopyrite, bornite, and secondary gypsum. They cannot be related to other vein-types except by inference: solid inclusions of anhydrite occur in the quartz and sulphides of quartz-Cu,Fe sulphide veins. Anhydrite, quartz and sulphides were all deposited by the same fluid, but the anhydrite has been removed by groundwater except where sheathed by an insoluble mineral or where it sealed the rock sufficiently to exclude water. Gustafson & Hunt (1975) reported the latter phenomenon in the El Salvador deposit, Chile. The northwestern part of the Panguna deposit is such a sealed area, and the anhydrite so preserved occurs both as a wallrock alteration product (replacing plagioclase and biotite in 102675) and as veins containing also small quartz crystals. The solution of anhydrite containing small quartz crystals may give rise to the sugary quartz habit described for certain quartz-Cu,Fe sulphide veins.

(iv) QUARTZ-PYRITE VEINS

In the field, a set of quartz-pyrite veins was distinguished from quartz-Cu,Fe sulphide veins by the apparent absence of ore minerals other than pyrite and (commonly) by the milkiness of the quartz. Subsequent studies of fluid inclusions and mineragraphy have led to the

reclassification of a few specimens as quartz-Cu,Fe sulphide veins. The distinction of a class of quartz-pyrite veins is nonetheless justified; in 103015 and 103028 quartz and pyrite were deposited on to previous fracture-fillings of quartz-Cu,Fe sulphide. In these cases, the quartz-pyrite was distinctive in containing neither chalcopyrite nor two types of fluid inclusion characteristic of the quartz-Cu,Fe sulphide filling. In other cases, however, minor amounts of chalcopyrite and molybdenite occur and the distinction is justified by fluid inclusions alone (see Chapter 6). In 103017 the pyrite crystals have many complex facets with polygonal striae, and are veined by chalcopyrite, sphalerite and marcasite. The class of quartz-pyrite veins probably comprises at least three different generations of veins: those from outside the deposit (103043, 103044, 103045), those which seem to form a halo to the Leucocratic Quartz Diorite (see fig. 6-4) and others such as 103015 and 103028 from within the deposit. No distribution map is given, since many of the veins sampled have not been studied in sufficient detail to confirm their identity. In 103015 and 103028, the wallrock alteration is considered to belong to the quartz-Cu,Fe sulphide mineralisation phase. The quartz-pyrite generation of quartz in 103015 is associated with chlorite. The selvages of two veins from far outside the deposit were examined. In 103044, the selvage is rich in chlorite, and chlorite and epidote occur intergrown with vein quartz throughout the vein. The chlorite replaces highly altered rock probably consisting largely of quartz and feldspar. In 103045 there appears to have been a sericitic selvage, although little is preserved with the thin section.

In the orebody, quartz-pyrite veins are younger than some quartz-Cu,Fe sulphide veins around (but not in) the Leucocratic Quartz Diorite, where clear inter-vein relationships were seen. Where quartz-pyrite occurs as a second fracture filling it is also younger than the first fracture filling of quartz-Cu,Fe sulphide.

(v) THICK, MASSIVE PYRITE VEIN

A single example (103474), over 30 cm thick, was found near a contact of the largest Leucocratic Quartz Diorite stock (fig. 3-14). It consisted of massive pyrite with occasional vugs and a very small amount of included chalcopyrite. No contiguous wallrock was obtained. No other veins were observed to intersect this vein.

(vi) PYRITE ± BLEACHED SELVAGE

Thin pyrite veins occur along two arcs (fig. 3-14), one peripheral to the southern margin of the orebody, the other encircling the Leucocratic Quartz Diorite. The two examples to the north of the deposit may lie on an extension of the former arc, or may belong to yet another group. Most of the veins contain only pyrite, but a vein of chalcopyrite with a bleached selvage may also belong to this class. In 103470 small quartz crystals project into the pyrite from the margin, and the bleached selvage of altered wallrock consists of quartz and sericite.

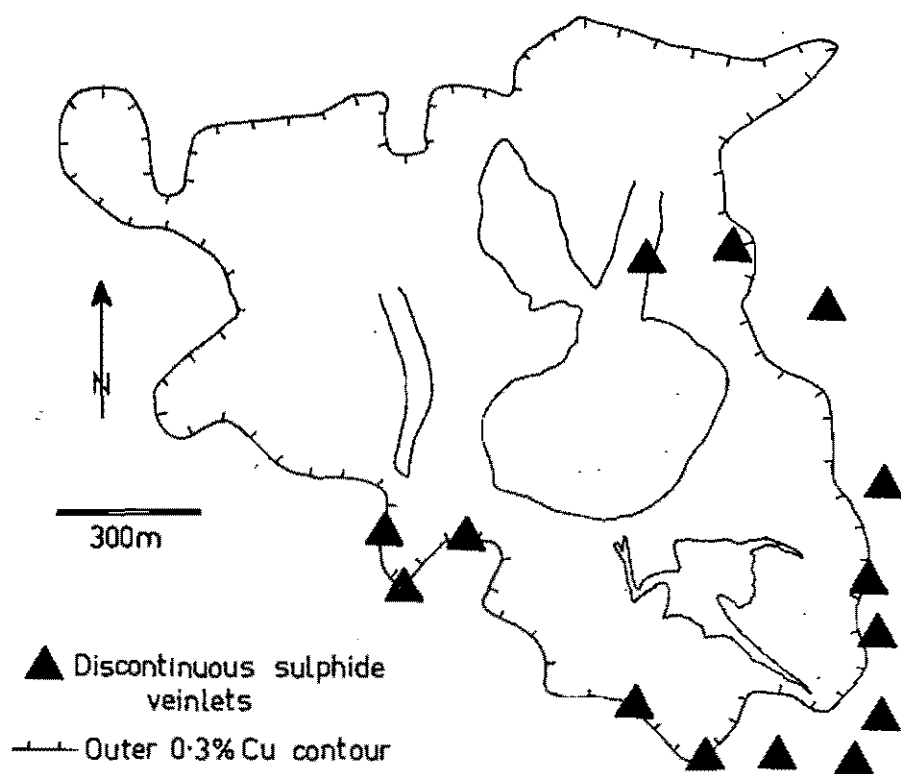
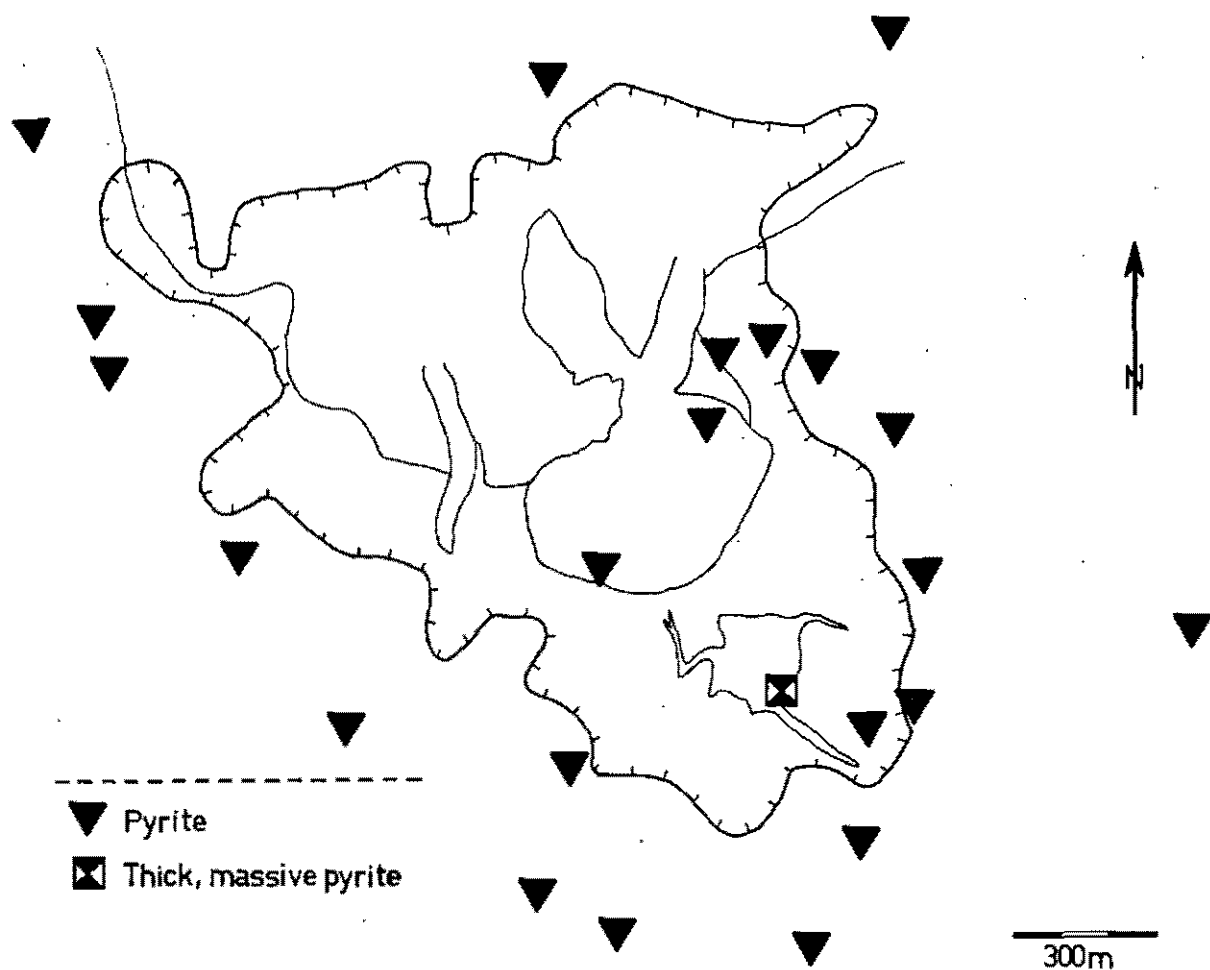
Around the Leucocratic Quartz Diorite, with which one set of these veins appears to be contemporaneous, thin pyrite veins cut quartz-pyrite and quartz-Cu,Fe sulphide veins.

(vii) DISCONTINUOUS SULPHIDE VEINLETS

Fractures containing discontinuous fillings of any or all of pyrite, chalcopyrite and molybdenite, some with minor quartz (103466) occur in what may be a ring around the Leucocratic Quartz Diorite (fig. 3-15). The wallrock alteration effects of two specimens are clearly later than biotite alteration (103466, 103467) and amphibole-

Fig. 3-14 Map of occurrences of thin pyrite veins and the thick, massive pyrite vein. Geological contacts and outer 0.3% Cu contour as in fig. 2-3.

Fig. 3-15 Map of the occurrences of discontinuous sulphide veinlets. Geological contacts and outer 0.3% Cu contour as in fig. 2-3.



plagioclase-magnetite alteration (103466). In 103467, where the same fracture seems to have controlled biotitisation, biotite is largely replaced by chlorite along a thin chlorite-plagioclase selvage. In 103466 chlorite replaces plagioclase, and epidote and chlorite replace biotite in the selvage of the veinlet. The intervein relationships between type (vii) and others give conflicting information, but the relationship with the Leucocratic Quartz Diorite suggests contemporaneity with that intrusion.

(viii) CHABAZITE-BEARING VEINS

Rare veins bearing chabazite were noted south of the deposit (fig. 3-13). Molybdenite is intergrown with the chabazite of 103040, which also contains quartz and pyrite. Wallrock alteration was not examined.

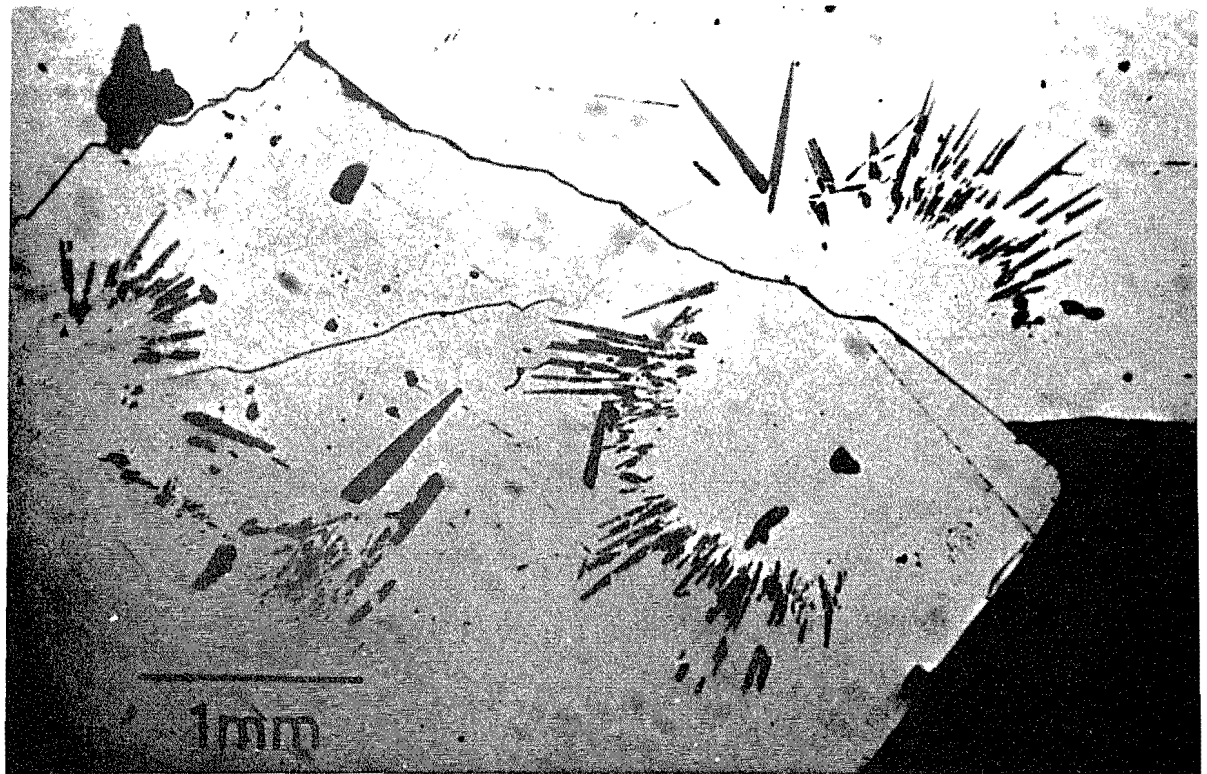
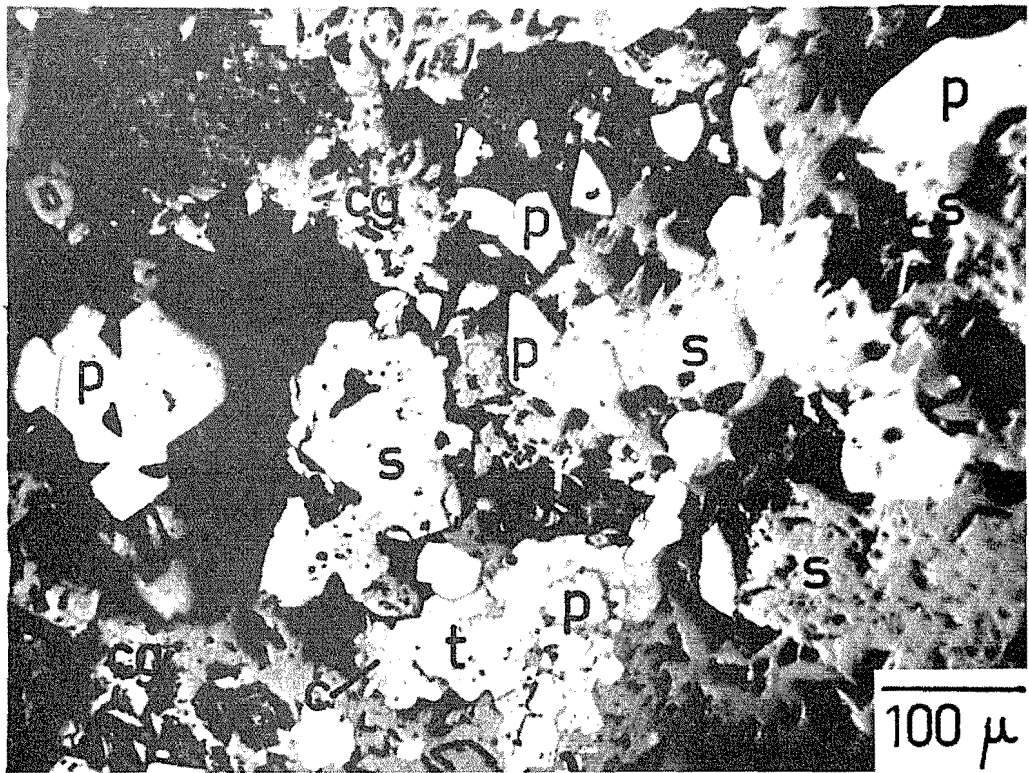
(ix) SPHALERITE-PYRITE VEINS

Sphalerite and pyrite are the main components of an uncommon, but widely-distributed vein type (fig. 3-13). Chalcopyrite, galena and tennantite may also be present (fig. 3-16). The pyrite characteristically includes radiating arrays of specular hematite blades (fig. 3-17). Quartz, calcite and siderite gangues were observed.

The paragenetic sequence is made up of several stages. Carbonate in 103480 is replaced by the sulphides. Hematite and pyrite seem to have been concurrent throughout, and sphalerite and galena were also deposited together. Chalcopyrite replaces sphalerite in 103042. Sphalerite and chalcopyrite replace pyrite, except in 103480 where some grains show several cycles of pyrite and sphalerite. Tennantite in 103480 replaces pyrite and may be in equilibrium with sphalerite.

Fig. 3-16 Photomicrograph of specimen 103480. Pyrite (p) is replaced by sphalerite (s), chalcopyrite (c) and tennantite (t). cg - carbonate gangue. Black areas are surface imperfections. Plane-polarised, reflected light.

Fig. 3-17 Photomicrograph of pyrite containing radiating blades of hematite, specimen 103475. Black areas are surface imperfections. Plane-polarised, reflected light.



Brecciation took place after the deposition of all sulphides, and in 103048 was succeeded by the deposition of barren quartz. The veins in several cases occur in minor fault zones in which there is clay, and movement along the fault after sulphide deposition may have led to the brecciation.

Because of the association with argillaceous fault zones, contiguous wallrock is hard to obtain. The sphalerite-carbonate vein in 103473, is marginal to a quartz-Cu,Fe sulphide vein with biotite inclusions, and the chlorite which cuts the quartz vein may be an alteration product associated with sphalerite deposition.

(x) PYRITE-CLAY VEINS

Pyrite and clay occur in many minor faults, widely distributed in the Panguna area but particularly concentrated (according to the sampling pattern used here) along the southern margin of the deposit between the Biuro Granodiorite and the Leucocratic Quartz Diorite (fig. 3-13). Some contain quartz. 103042, identified as a pyrite-clay vein in the field, was later found to contain chalcopyrite, galena and sphalerite in addition to pyrite, and the pyrite was found to include a little specular hematite. Thus it bears some resemblance to type (ix) veins. In 103477, however, only pyrite was observed. It is suggested, because of the certain degree of similarity, that the formation of pyrite-clay and sphalerite-pyrite veins may be closely related.

(xi) GYPSUM VEINLETS

Veinlets of gypsum are found only with anhydrite (e.g. 102675, 102676). They are thought to be the product of supergene hydration of anhydrite.

(xii) BARREN QUARTZ VEINS

Barren quartz veins were recognised as an early (pre-amphibole vein) generation of veins by Fountain (1972). Of the barren quartz veins sampled for this study, not all were early. Those suitable for fluid inclusion study proved with one exception to be indistinguishable from quartz-Cu,Fe sulphide veins in their inclusion assemblages. They are therefore classified thus, leaving only the quartz healing the brecciated sphalerite-pyrite of 103048 in category (xii).

(xiii) CALCITE

Vein calcite, as well as occurring in vein types (ii) and (ix), has been noted as a second fracture filling in 103010 and 103468. In both, fine dogtooth crystals have been deposited on to earlier quartz bearing chalcopryrite in 103010 and (?) chalcocite in 103468. Several sources for the calcite can be suggested: hypogene, associated with clay-calcite or propylitic alteration, or supergene, replacing anhydrite and gypsum. There are gypsum and calcite zones (Baumer & Fraser, 1975), the top of the calcite zone being generally above that of the gypsum zone. Since the boundary surfaces of the zones follow the topography to a degree, it is likely that the zones are of supergene origin.

(xiv) VIVIANITE VEINLETS

Blue vivianite, coarsely crystalline or earthy, occurs in a heavily fractured zone of the Biotite Granodiorite (103469). It apparently replaces pyrite and may be a supergene phenomenon since it occurs near the topographic surface. Hydrothermal apatite is probably the source of the phosphate. Baldwin *et al.* (1978) have noted vivianite veinlets in a Collapse Breccia bearing apatite northeast of the Biotite Granodiorite.

SUMMARY OF OBSERVATIONS ON VEIN ORDER

For group Vb, the vein distribution maps suggest that the emplacement of the Leucocratic Quartz Diorite and the formation of type (vii) and certain type (vi) veins were associated. Evidence suggesting that certain type (iv) veins were also associated with this event is presented in Chapter 6. Inter-vein relationships suggest that within this group of associated phenomena, the order was (iv) first, then (vi), both post-dating some type (ii) veins not necessarily related to the Leucocratic Quartz Diorite. Within the Leucocratic Quartz Diorite itself, two generations of type (ii) veins - first (iia), then (iib) - took place. In other places, type (iv) veins succeed type (ii).

In group Vc, brecciation, and probably the introduction of clay, post-date the deposition of sphalerite and pyrite. The common association of sphalerite-pyrite with brecciation and clay suggests that all are closely related phenomena.

Vivianite (xiv) and certain calcite (xiii) veins may belong to group Vd supergene veins.

CHAPTER FOUR: FLUID AND SOLID INCLUSION STUDIES

GENERAL

The measurement of the temperatures of phase transitions in fluid inclusions demands accurate instrumentation (see below) and sufficient knowledge of the chemical systems in the inclusions for the interpretation of temperature data (Roedder, 1967; Yermakov, 1965). As is customary, freezing data are compared with the system NaCl-H₂O (Potter, 1978), in full realisation that small amounts of polyvalent ion in solution may bring about large errors. Salinity determinations on inclusions with daughter salts are made, where possible, by reference to the system NaCl-KCl-H₂O (Ravich & Borovaya, 1949), but other properties of salt-rich systems must at present be referred to the system NaCl-H₂O (e.g. Sourirajan & Kennedy, 1962; Keevil, 1942; Urusova, 1975).

The notation used in the following chapters is explained in the Introduction Chapter.

EQUIPMENT

Most of the heating and freezing measurements were made on Chaixmeca apparatus, on one set at the Centre de Recherches Pétrographiques et Géochimiques (Nancy, France) and on another at the University of Tasmania. The characteristics of the Chaixmeca stage have been discussed by Poty *et al.* (1976). Below 0°C, a temperature measurement is accurate to $\pm 0.2^\circ\text{C}$ and at 500°C, to $\pm 3^\circ\text{C}$. Readings were made up to 580°C. The stages were calibrated relative to the melting points of the following substances:

n-hexane		-95°C
n-octane		-56.8°C
CO ₂ (in fluid inclusions supplied by the Chaixmeca Co.)		-56.6°C
CCl ₄		-23.0°C
Merck Schmelzkoerper	9670	70°C
"	9735	135°C
"	9800	200°C
"	9847	247°C
NaNO ₃		306.8°C
K ₂ Cr ₂ O ₇		398°C

One of the calibration curves used in Nancy is presented (fig. 4-1).

A small number of readings were made on a heating stage built at the University of Tasmania and are accurate to $\pm 5^\circ\text{C}$ at 500°C . They are distinguished in the table of data (Appendix 2). This stage was calibrated in the same way as the Chaixmeca stages. Some readings greater than 580°C were made at Nancy on a modified Leitz 1350°C heating stage. These measurements (also distinguished in the Appendix) were necessarily approximate, since the Leitz stage was calibrated only at $398 \pm 3^\circ\text{C}$ (fusion of $\text{K}_2\text{Cr}_2\text{O}_7$) and at $1063 \pm 15^\circ\text{C}$ (fusion of Au).

A Chaixmeca crushing stage was used for semiquantitative determinations of CO_2 according to the method of Roedder (1970).

TREATMENT OF DATA

The pilot study (those readings made on the stage built at the University of Tasmania) indicated certain difficulties which were to influence the entire study. For a set of measurements on apparently similar inclusions in a single specimen, or even within a single crystal, a given parameter often exhibits a broad range of values. The possible reasons for this are several, e.g.

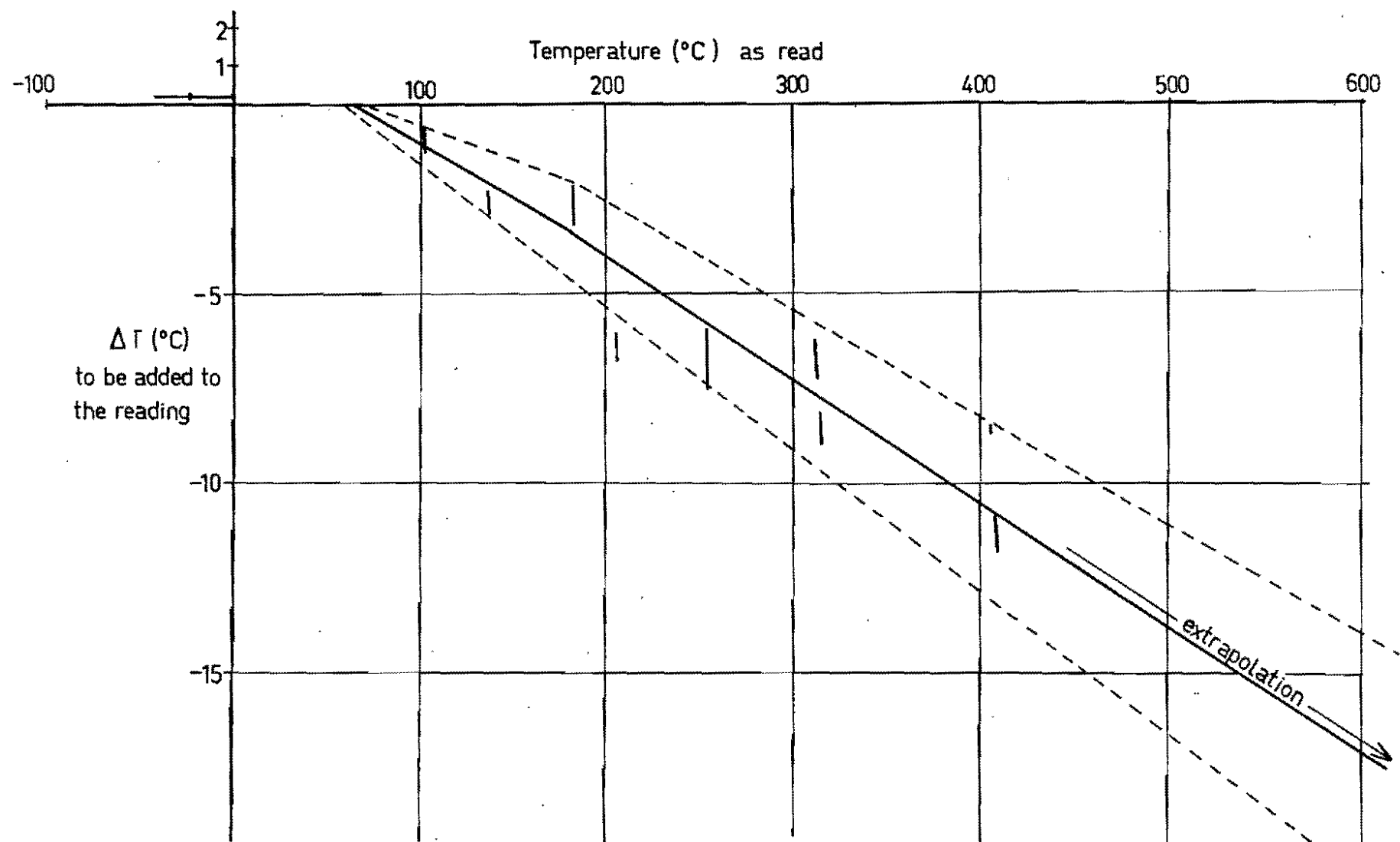


Fig. 4-1 Calibration curve of the Chaixmeca microthermometry apparatus at the University of Tasmania, Nov. 1975.

- (a) the presence of more than one generation of inclusions
- (b) the trapping of solid or gaseous phases along with liquid
- (c) necking down
- (d) leakage, especially under experimental conditions
- (e) metastability of an included phase under experimental conditions.

Point (a) is relevant in this case because primary inclusions are hard to identify. Point (b) must be considered because several solid phases and two fluid phases were present during the deposition of much of the quartz at Panguna. The necking down of fluid inclusion cavities, i.e. the annealing of the host mineral, will occur relatively rapidly at the high temperatures indicated for porphyry copper mineralisation, possibly leaving little evidence of the process. By a similar process involving the transfer of host material across the inclusion cavities, primary inclusions might move out of alignment with growth zones, or secondary inclusions might shift away from fracture planes, making the habits of inclusions difficult to specify. A test of the importance of necking down *per se* is discussed in Chapter 5. Leakage was not a serious problem at temperatures below 400°C in the situation discussed by Roedder & Skinner (1968), and though most measurements at Panguna were at temperatures over 400°C, they were for fluids of low vapour pressure relative to those examined by Roedder & Skinner (see Chapter 7). Leakage, when observed in Panguna samples, was total; no case of the loss of a small quantity of fluid only was observed. Such partial leakage is probably more likely under higher confining pressure, e.g. during temperature changes soon after the deposition of the veins, many of which have passed through the transformation from β -quartz to α -quartz.

A set of fluid inclusion data representing one episode of trapping ought to give a sharp peak on a frequency distribution graph, provided

none of the inclusions has undergone any of the effects (b) to (d) listed above. These effects would be expected to perturb measurements by variable, although not random, amounts. The expected type of perturbation of the sharp peak for each effect acting alone is shown diagrammatically in fig. 4-2 (it has been assumed that most inclusions in the sample have not been perturbed at all, i.e. that the original mode is preserved). In this study, one or more modes are defined in most histograms where there are sufficient data; the modes are assumed to be measures of original fluid properties unless there is evidence to the contrary. In the case of T_h measurements on salt-rich inclusions there is such evidence in the form of a metastability phenomenon (see Chapter 5). A metastability phenomenon could displace a frequency distribution along the temperature axis in such a way as to be undetectable. Metastability must be watched for, and any data so affected must be treated with due caution.

It was found desirable to avoid inclusions of very irregular form, because these yielded dispersed data, presumably spurious because of necking down or other perturbations. Data were gathered from inclusions in several parts of a specimen where possible. The number of readings necessary for an apparently-representative set of data could only be judged by trial and error. Thirty or more inclusions, spread over different parts of a specimen, were studied if possible, to check on polymodality. As few as ten measurements were in some cases sufficient to define the properties of a single fluid.

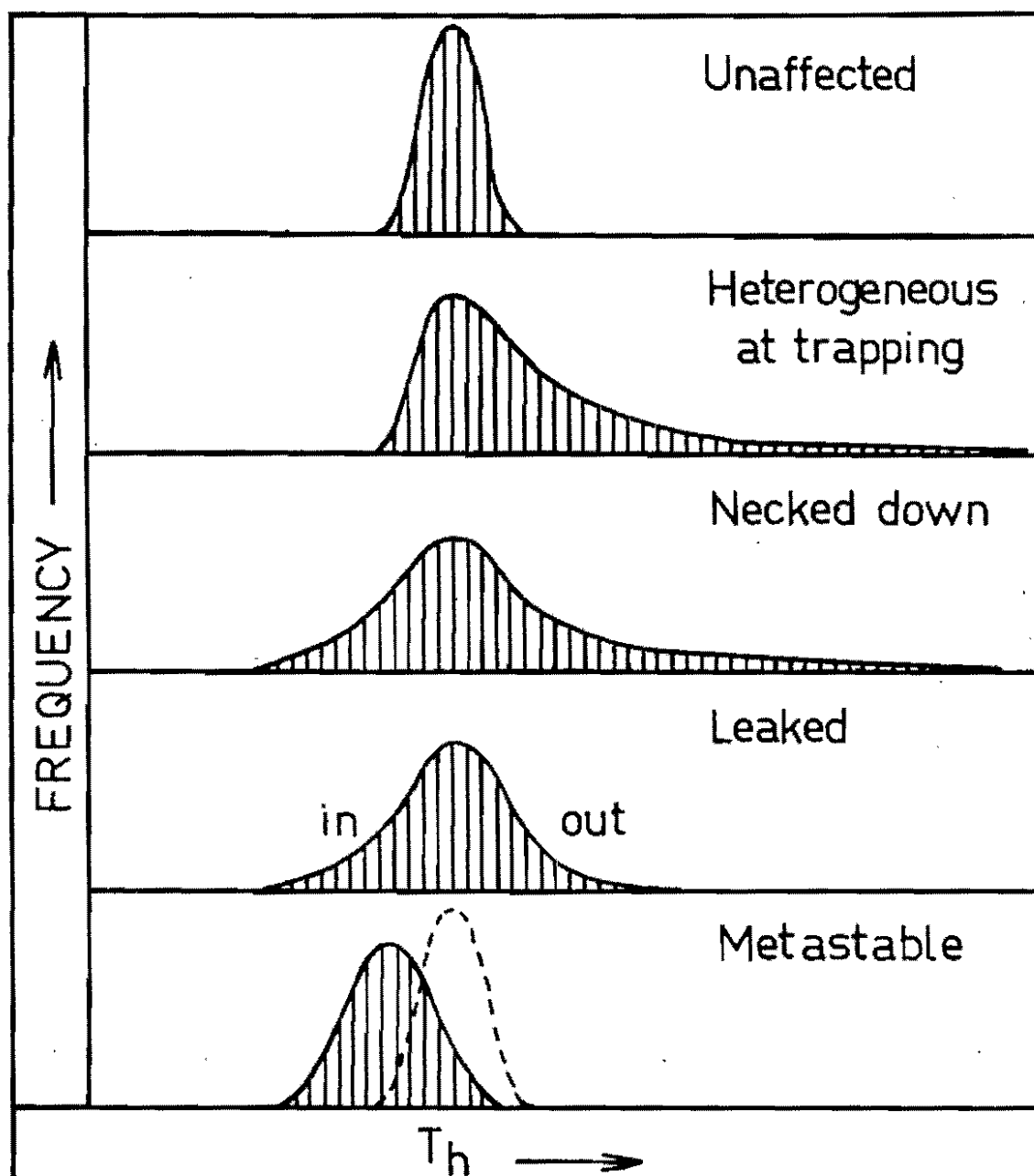


Fig. 4-2 Effects of the perturbation of fluid inclusions on measurements. Solid inclusions in quartz (specimen 102619).

CLASSIFICATION AND DESCRIPTION OF INCLUSIONS

Solid inclusions. A variety of solid inclusions was found in hydrothermal and igneous quartz. It is informative to consider these along with the fluid inclusions.

In quartz from type (ii) veins, the following types of solid inclusions occur:

(i) Colourless crystals of an anisotropic material of high relief and moderate birefringence. The outlines are commonly rectangular and sometimes elongate (fig. 4-4, L, M, N). Electron microprobe analysis of several of these which had been polished to the surface of specimens revealed Ca and S, so that the optical and chemical properties of these are consistent with those of anhydrite.

(ii) Colourless crystals of an isotropic mineral with a refractive index almost indistinguishable from that of quartz (fig. 4-3). They are rounded in outline, although one attached to a type II inclusion had a form suggesting an imperfect cube. Although quite common in some specimens, these are very difficult to see. Under crossed nicols they appear as faint grey patches in quartz of light yellow interference colour. In plane polarised light they are invisible at all but the smallest diaphragm aperture.

Repeated electron microprobe analyses of a polished section of 102619 failed to find any substance other than quartz or tin oxide in areas where these inclusions were thought to intersect the surface. Since the properties of the inclusions resemble those of halite, the grinding was done with kerosene as a lubricant, and dry tin oxide was used for the final polish. The section was ground and polished between each attempt at microprobe analysis. This process tends to leave tin oxide in surface cavities, and this may have masked the inclusions.

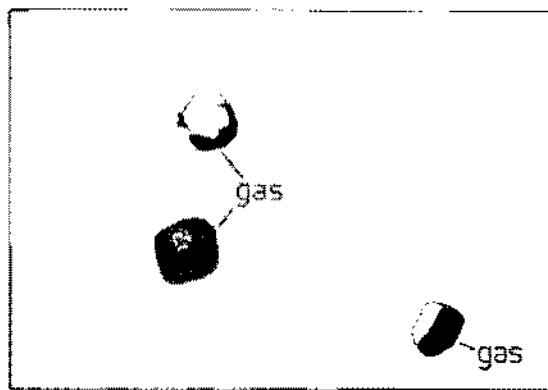
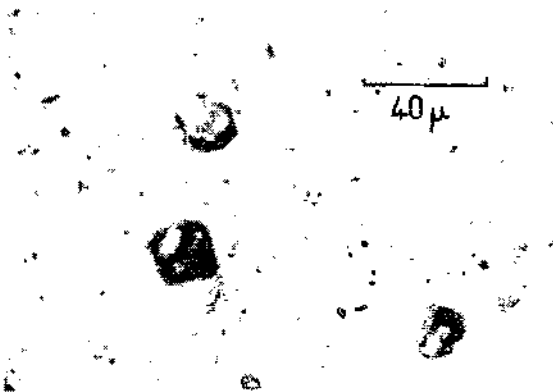
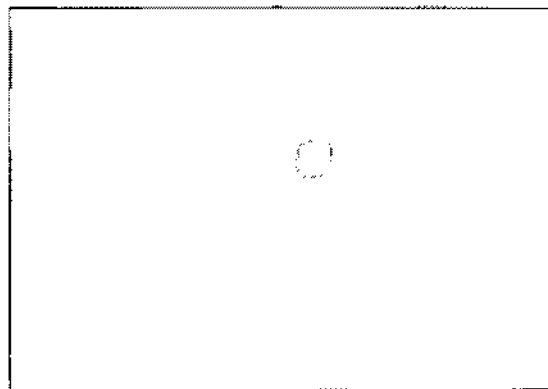
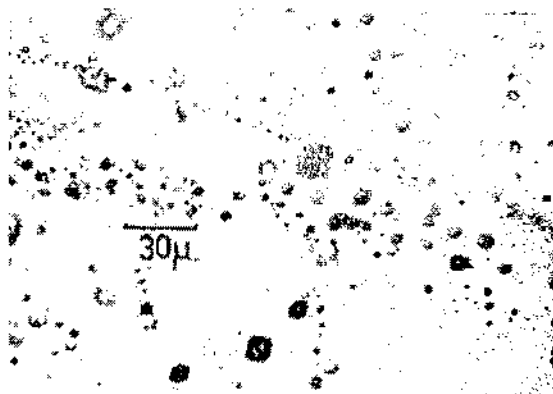


Fig. 4-3 Solid inclusions in quartz.
(specimen 102619).

Grinding with kerosene as lubricant does preserve halite - this was observed in fluid inclusion cavities opened by polishing.

A thin section of the same specimen was exposed to Cr K_α X-rays (50kV, 40 mA) for ten minutes. Halite irradiated with X-rays develops an orange-brown colour (Przibram & Caffyn, 1956), and an irradiation of that duration was sufficient to colour halite daughter crystals in type III inclusions in the section. The colour persisted long enough for examination under the microscope. The solid inclusions in question developed no colour, and are therefore not halite.

(iii) Platy, pleochroic inclusions (the colours ranging between red-brown, mauve and light blue on rotation) of high relief and moderate to high anomalous birefringence. They are found along the margins of many veins and mark growth zones in 103012. One polished to the surface of 103012 gave a semiquantitative electron microprobe analysis consistent with titaniferous biotite.

(iv) Red platelets of high relief and high, anomalous birefringence, occurring very sparsely as solid inclusions in a few specimens (e.g. 102636). They are thought to be hematite, and are much more commonly seen in type III inclusions (see below).

(v) Opaque inclusions are common. Some are large enough to be identified as chalcopryite in polished sections. Most are of irregular shape, but occasionally the triangular section of a chalcopryite disphenoid is recognised.

(vi) Very thin, colourless needles in a few specimens may be rutile or apatite.

Composite solid inclusions have been found, e.g. anhydrite-hematite-opaques in 102636 (fig. 4-4 L), anhydrite-chalcopryite in 103028 and biotite-hematite in 103012. Gas occurs attached to sporadic solid inclusions of anhydrite, biotite, the unidentified mineral

and opaques, and more rarely there is what may be a film of liquid about a solid inclusion. The composite inclusions serve to demonstrate the coexistence of the solid and fluid phases concerned.

The red solid inclusions are also found in a type (i) vein, 103049, and with inclusions of chlorite in a type (iv) vein, 103015.

Quartz phenocrysts from the Biotite Granodiorite contain solid inclusions resembling anhydrite, a Cu,Fe sulphide (fig. 4-5 E; confirmed by electron microprobe), hematite and a colourless material of low relief (see fig. 6-1). The last are common and are easily picked under crossed nicols by their bluish-grey interference colour, which may be due to the rotation of light at the inclusion walls. Semiquantitative electron microprobe analysis showed these to contain Na, K, Ca, Al and Si, and thus they were probably inclusions of magmatic glass. Some contain, or consist entirely of, alkali feldspar. Some may contain internal bubbles, cf. Etminan (1977) who found a bubble apparently containing halite in a glass inclusion at Sar Cheshmeh. Gas and rarely salt-rich liquid adhere to such inclusions in Biotite Granodiorite phenocrysts at Panguna (figs. 4-5 D, E; 6-1). This is evidence for the coexistence of halite-rich fluid and a vapour with silicate liquid in the Biotite Granodiorite.

Fluid inclusions. The fluid inclusions from hydrothermal minerals and from quartz phenocrysts from the Panguna deposit have been classified as follows:

Type I: Inclusions of low to moderate salinity with small bubbles.

Type II: Gas-rich inclusions.

Type III: Inclusions bearing cubes of halite.

Nash (1976) reported these types, and also CO₂-rich inclusions (Type IV), as typical of porphyry coppers. At Panguna, CO₂-rich inclusions were seen only in a small crystal of anhydrite included in vein quartz from 102998, and these are not discussed further.

Fig. 4-4 Photomicrographs of fluid inclusions.

Symbols: g = gas, h = halite, s = sylvite, b = birefringent salt, c = chalcopryrite, o = opaque phase, hm = hematite.

- A: type III, specimen 103019.
- B: type III, specimen 102594.
- C: type III, specimen 103022. The presence of the chalcopryrite crystal on the surface of the growing quartz probably caused the trapping of liquid.
- D: type II, specimen 103031, with a large liquid rim and daughter minerals.
- E: type II, specimen 102594.
- F: type III, specimen 103022. Such inclusions have an equivalent NaCl + KCl salinity of 75%. The chalcopryrite crystal is oriented with an edge towards the observer.
- G: type III, specimen 103031. The opaque crystal is cubic. Gas may have been trapped with the liquid in this case.
- H: type III, specimen 103022, showing the hexagonal form of hematite.
- I: type III, specimen 103004. A flake of hematite, thought to be a trapped solid, protrudes through the inclusion wall. The birefringent salt consists of radiating acicular crystals.
- J: type I, specimen 103017. These secondary inclusions homogenise at the critical point.
- K: type I, specimen 103035.
- L, M, N: Anhydrite solid inclusions, specimen 102636. Note the association with hematite (L), type II inclusions (L, M) and type III (N).
- O-U: type III, specimen 103019. A heating experiment on neighbouring inclusions of different salinities and homogenisation orders. In the large inclusion: $T_s\text{KCl} = 97^\circ\text{C}$, $T_s\text{NaCl} = 409^\circ\text{C}$, $T_h = 464^\circ\text{C}$, decrepitation at 550°C with opaque and birefringent salt remaining. In the small inclusion: $T_h = 380^\circ\text{C}$, $T_s\text{NaCl} = 449^\circ\text{C}$, leaving a birefringent salt and an opaque scarcely resolved in the photograph. Gas may have been trapped in the large inclusion.

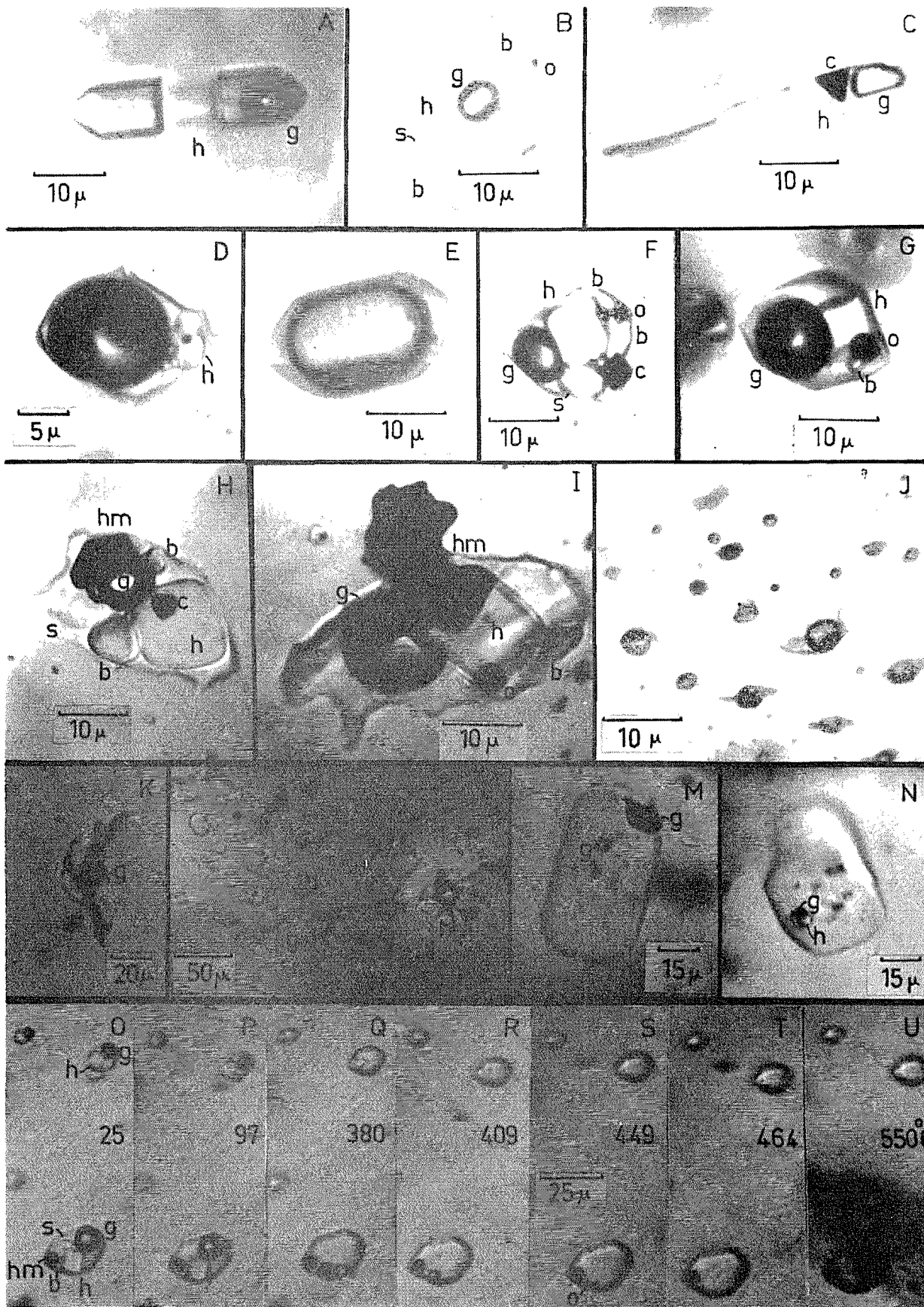
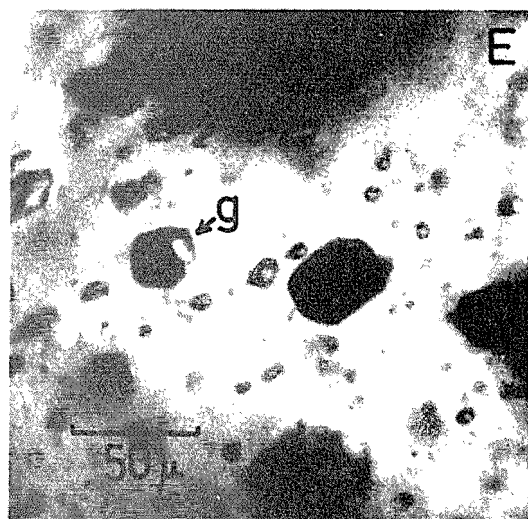
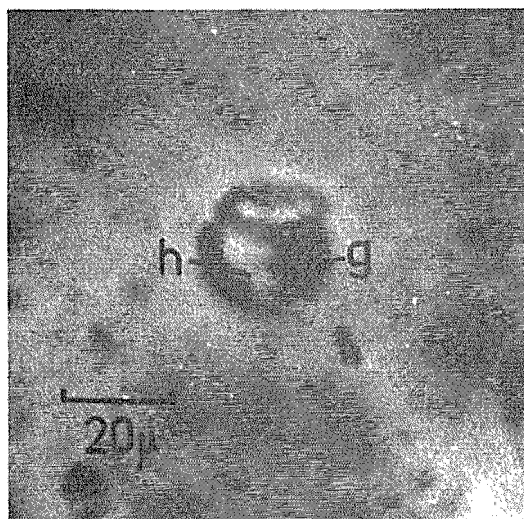
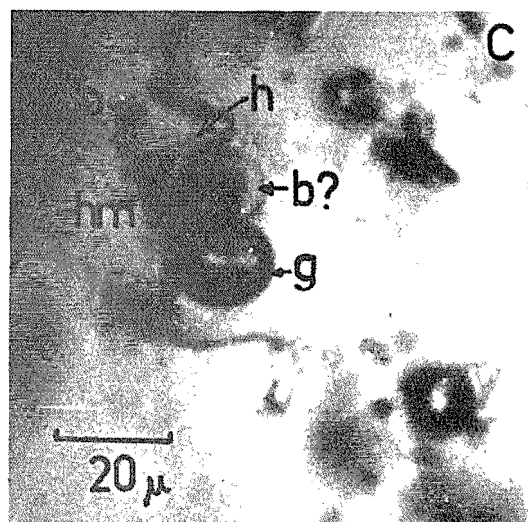
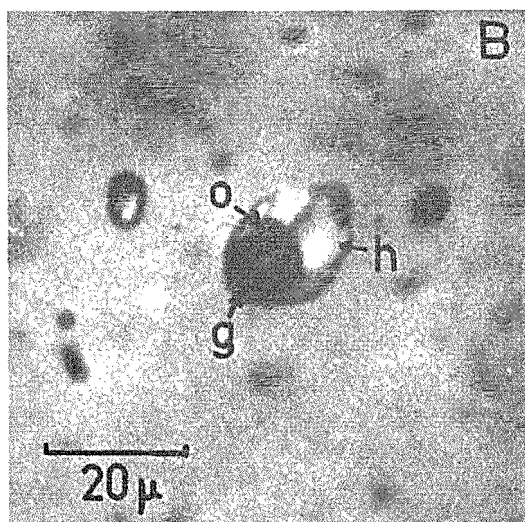
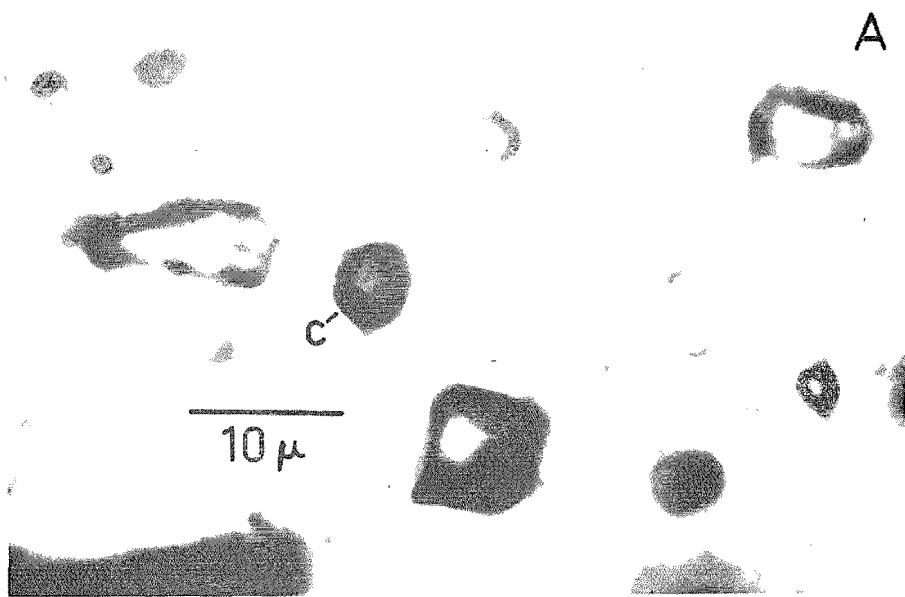


Fig. 4-5 Photomicrographs of fluid inclusions. Abbreviations as in fig. 4-4.

- A. Type II inclusions, specimen 103029. One inclusion contains a crystal of chalcopyrite.
- B. Type III inclusion in a quartz phenocryst, 103001.
- C. Type III inclusion in a quartz phenocryst, 103001.
- D. Primary type III inclusion in a quartz phenocryst, 103001. The inclusion is indistinct because it is underneath a solid inclusion.
- E. Primary type II inclusion adhering to a solid (?Cu,Fe sulphide) inclusion in a quartz phenocryst, 103001.



Type I inclusions are found in all igneous and hydrothermal quartz at Panguna. Most are smaller than 40 μ in diameter and occupy irregular cavities, equidimensional or branched in form. Most are secondary inclusions, but primary type I inclusions have been identified in the growth zones of the last quartz deposited in 102997, 103015 and 103028. They consist of an aqueous liquid and a bubble occupying 5 - 20% (occasionally more) of the cavity volume. Daughter minerals or imprisoned minerals are uncommon; in 103017 an opaque phase was observed in certain groups of type I inclusions and in 103047 a colourless salt of high relief and high birefringence was found in the inclusions in one healed fracture. The salt was insoluble during heating runs. Hematite and other colourless salts occur sporadically, but are not common.

Type II inclusions. These occur in all igneous quartz and in most hydrothermal quartz. The occasional relationship of type II inclusions with growth zones and with solid inclusions (figs. 4-4 L, M; 4-5 E) indicates that at least some of them are primary, but secondary or pseudosecondary habits are more usually encountered. A perfect negative crystal form is predominant in a few veins (e.g. 102676), otherwise the cavities tend to be equidimensional to slightly elongate, and rounded, rarely cusped. Few are larger than 40 μ long.

They have liquid rims, ranging from very small (visible only in cusped cavities) to relatively large and easily visible. Some of the larger rims contain daughter salts, e.g. halite, hematite, opaques, and in 103029, many type II inclusions contain a perfectly-formed crystal of chalcopryrite (fig. 4-5 A). As other authors have suggested (e.g. Roedder, 1971) the larger liquid rims may result from the trapping of a little liquid with the predominant vapour. Indeed, it would be rare in a boiling system to trap a bubble adhering to a surface growing from the

liquid without including a little of the liquid as well. This is probably the situation at Panguna. The occurrence of gas-rich inclusions with various proportions of liquid does not constitute proof of boiling, however, because the necking down of type III inclusions might also produce such type II inclusions. Whether boiling did take place is discussed below.

Type III inclusions. Halite-bearing inclusions are always found in company with type II inclusions. Very few are definitely primary; many are of secondary or pseudosecondary habit. They occupy cavities ranging from perfect negative crystals to complex branching forms. Few are larger than 40 μ in diameter.

Besides a bubble occupying about 10% of the cavity and a salt-saturated liquid, these inclusions contain a rich assortment of daughter minerals (fig. 4-4). Up to nine solid phases have been observed in a single inclusion. Halite and sylvite have been identified according to the usual criteria (Roedder, 1971) and there are possibly five other colourless salts of which at least four are birefringent (see Chapter 5). One of these is thought to be anhydrite because it has a high refractive index and exhibits rectangular and diamond-shaped sections (fig. 4-4 B, H). Another has an acicular habit (fig. 4-4 I). The other colourless salts show various irregular forms. Nearly all dissolve completely by 580°C; those which do not may have been trapped as solids. Red flakes in type III inclusions are thought to be hematite. They darken, at temperatures over 300 - 400°C, as do fine grains of hematite heated in the atmosphere, and become red again on cooling. The flakes occasionally show a perfect, regular hexagonal form. An extremely small platelet, seen only when adhering to and distorting the bubble during the latter stages of heating runs, may be molybdenite. Two other opaque minerals are found in many inclusions. Cubic solids may be pyrite or bornite, and

disphenoidal-tetrahedral solids are probably chalcopyrite (fig. 4-4 C, F, G, H). No opaque grain was ever seen to move in response to passing a magnet near a specimen. It is common to find two opaque grains in a single inclusion. The opaques and the hematite do not dissolve during heating runs.

Opened fluid inclusion cavities were located on freshly-broken surfaces of vein quartz containing type III inclusions. The surfaces were cleaned ultrasonically before being coated with carbon for examination under the scanning electron microscope. In many of the cavities it was possible to discern daughter minerals. These were analysed semi-quantitatively on the electron microprobe analyser, and the following salts were identified (see figs. 4-6, 4-7).

(a) chlorides: pure NaCl, pure KCl and crystals containing various proportions of Na, K and Ca with minor Fe, Mn and Zn.

(b) a Cu,Fe sulphide, probably chalcopyrite.

(c) a mineral containing Ca, P and minor Fe, Mn, Cl (and K?), probably apatite. These crystals are large relative to the cavities they lie in, and may have been trapped as solids. This is evidence that hydrothermal apatite may have been deposited at Panguna. A concentration of such apatite may have been the source of phosphate in the vivianite veinlets (Chapter 3, xiv). In one of the chloride crystals there was a trace of S, probably as sulphate.

Decrepitation products on the polished surface of a piece of quartz which had been heated rapidly in air to 700°C were also analysed by electron microprobe. The spectra in fig. 4-8 are for four sample locations across the decrepitation product shown in the accompanying electron micrograph. Si was detected to varying degrees, depending on the thickness of the decrepitation product layer over the quartz. The peaks shown as Ca are due in part to potassium K β radiation. Taking

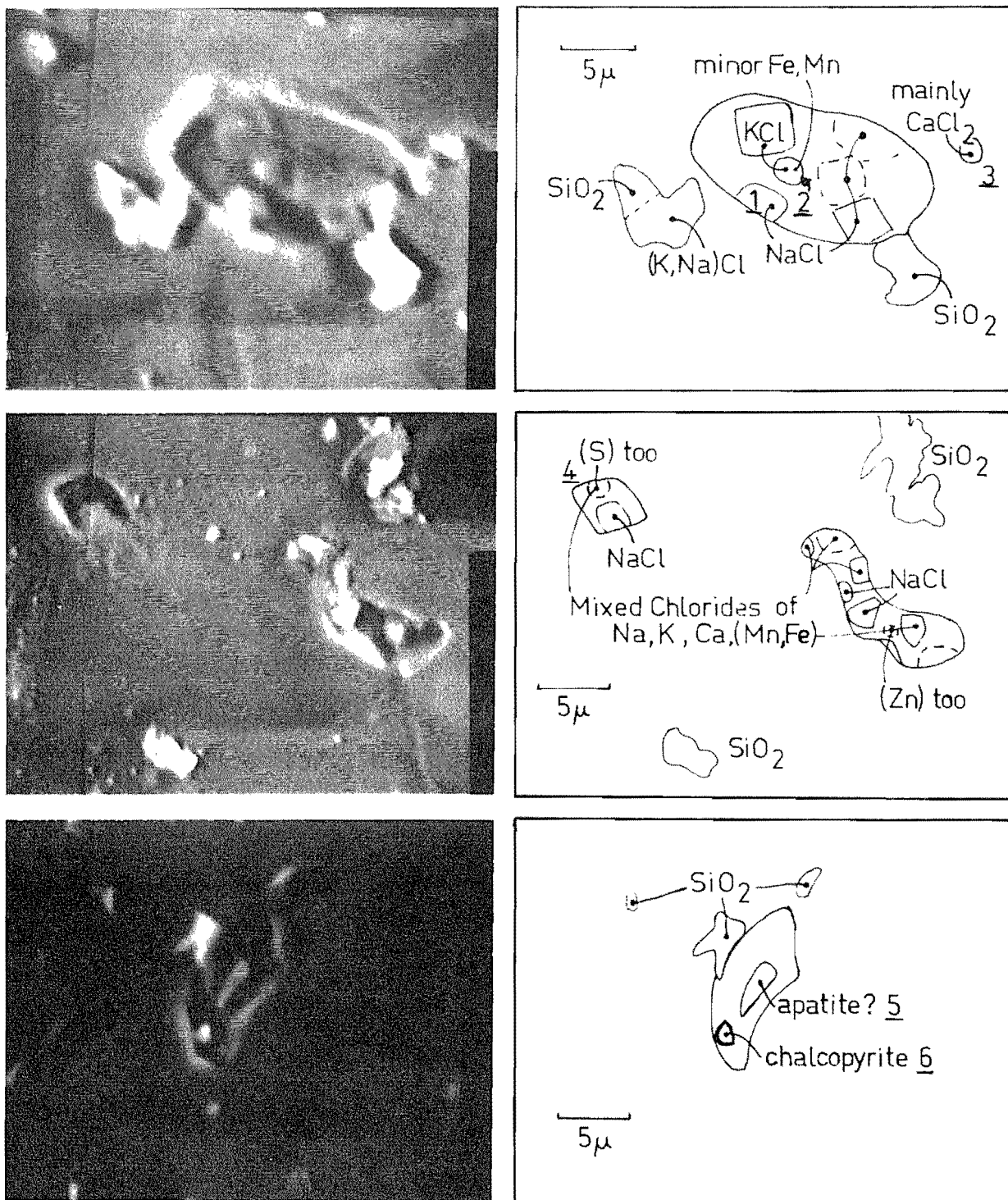
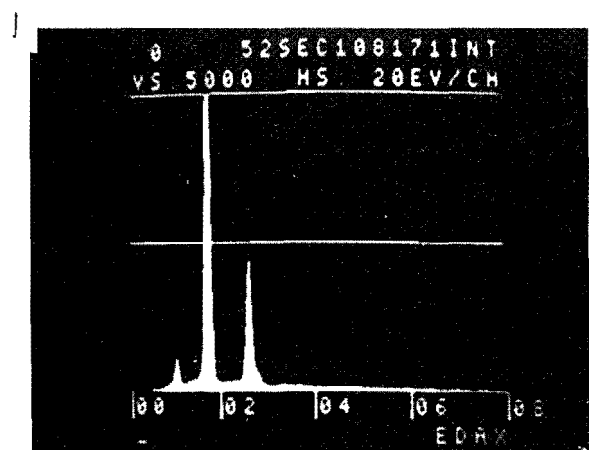


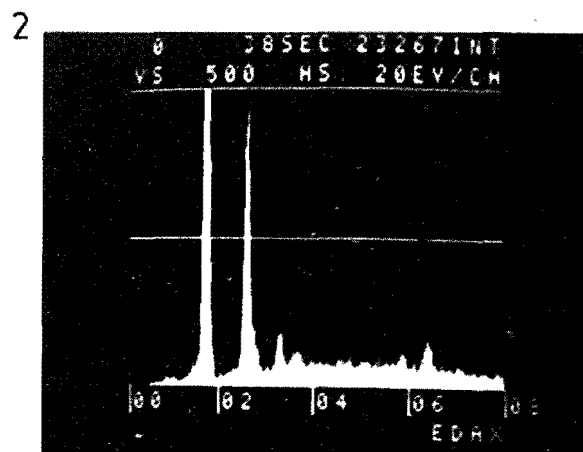
Fig. 4-6 Back-scattered electron images of opened fluid inclusions, and diagrams showing the compositions of daughter minerals or trapped minerals (according to semiquantitative electron microprobe analysis). Numbers refer to numbered analyses in fig. 4-7.

Fig. 4-7 Spectra gathered in semiquantitative energy-dispersive electron microprobe analyses of the numbered crystals in fig. 4-6. Si gives a large peak in each case because the electron beam penetrates quartz.

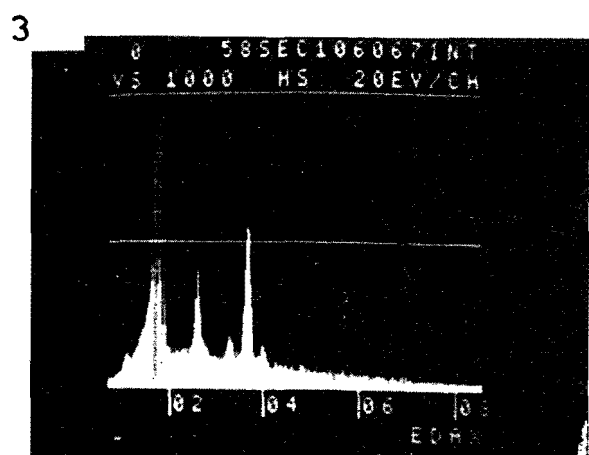
1. NaCl
2. a mixed chloride of K, Mn, Fe.
3. a mixed chloride of K, Ca, Na.
4. a mixed chloride of K, Ca, Mn, Fe, Na with a little S.
5. a mineral containing Ca, P, Cl (minor K, Mn, Fe).
6. a Cu,Fe sulphide.



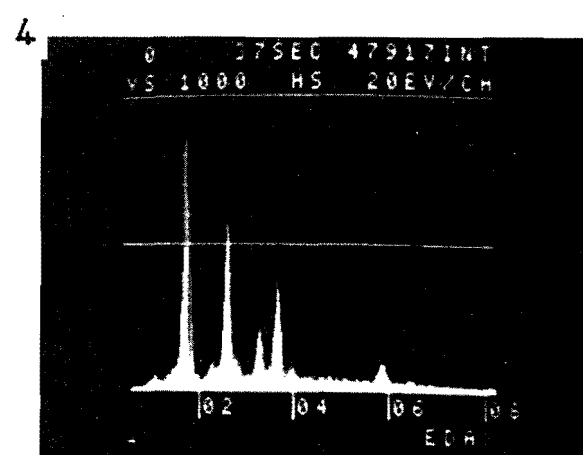
NaSi Cl



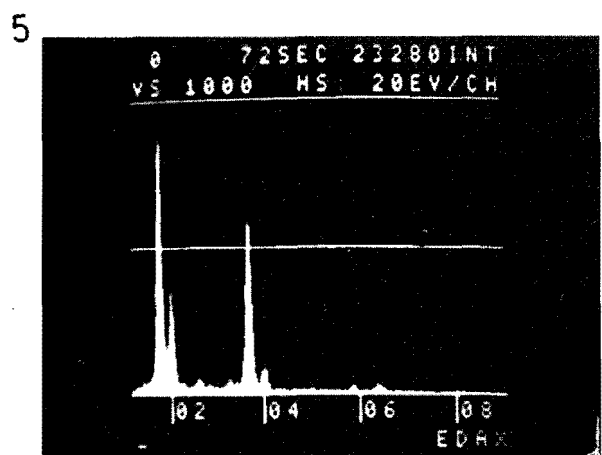
Si Cl K Mn Fe



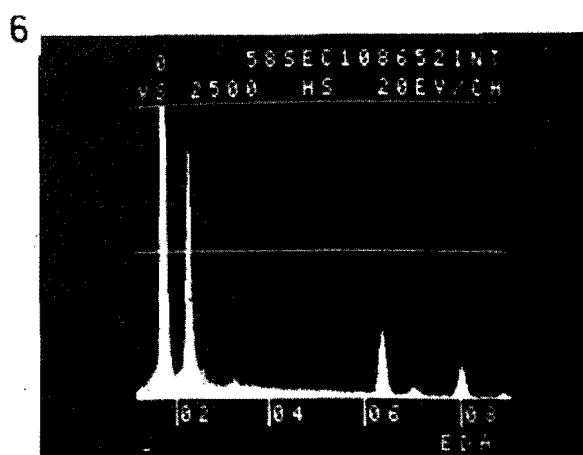
NaSiCl K Ca



NaSiClKCa Mn Fe



Si P Cl K Ca Mn Fe



Si S Fe Cu

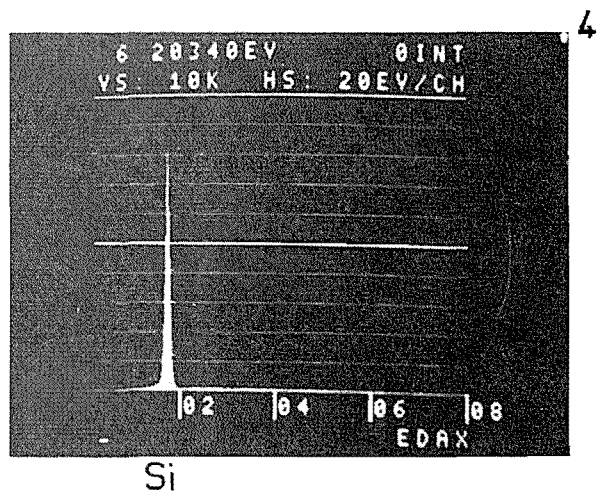
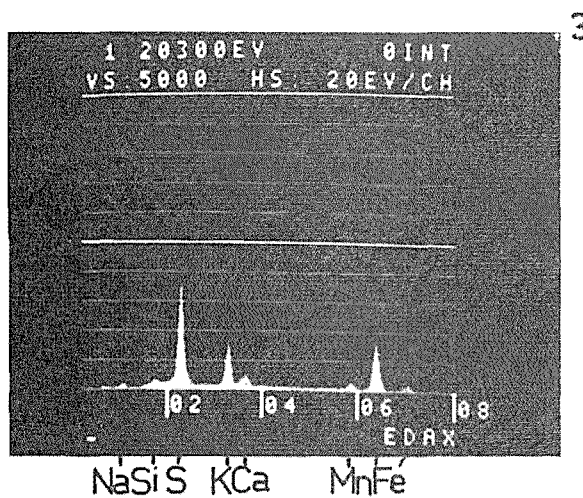
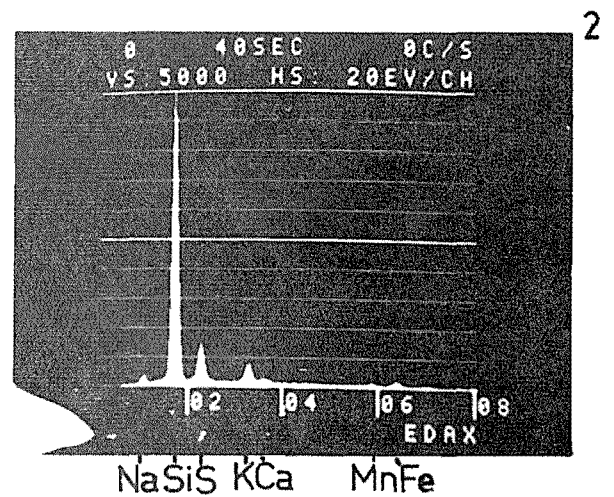
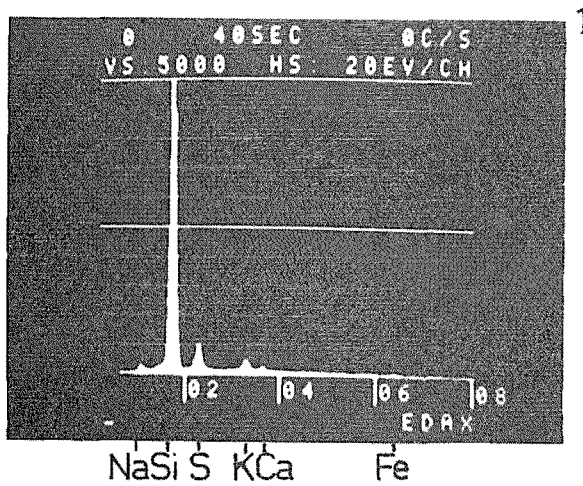
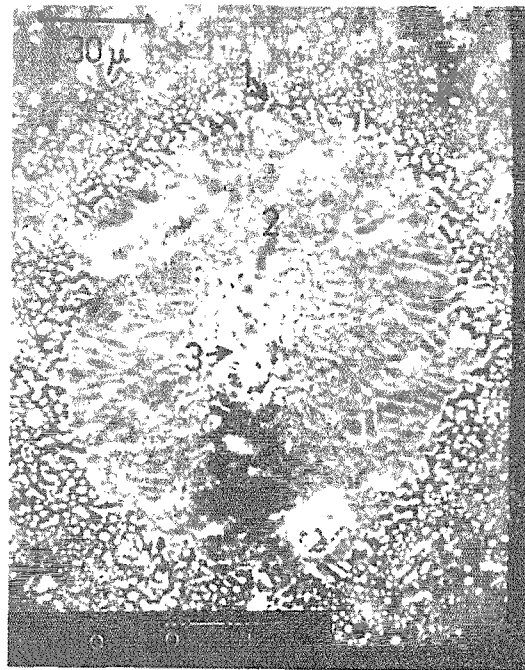


Fig. 4-8 Back-scattered electron image of decrepitation products of type III inclusion, with spectra gathered in semiquantitative energy dispersive electron microprobe analyses of the numbered areas.

Table 4-1

X-RAY COUNTS ON DECREPITATION PRODUCTS, SPEC. 103031

Element	1	2	3	4	5
Na	4950	6791	1551	7676	3032
Mg	1553				
Si	16921	6363	26266	74067	12304
S	28845	28301	28159	28525	28715
Cl				15368	
K	11990	7578	12822	13074	12654
Ca	4482	3627	6127	6773	4572
Mn	1801	1282	3462	4057	2721
Fe	4346	2933	6113	10487	6251
Ni	2239			7413	1124
Cu	1976	941	2176	9698	1090
Zn	1513	876	2116	6893	

N.B. Counts on S standardised to ~28500.

Counts on Ca are partly due to K k_{β} radiation.

account of the low count-rate of Na relative to heavier elements, it can be seen that K, Na, S, Fe and minor Mn and Ca are the chief constituents of the decrepitation products. Cl is notably absent. Mn and Fe are more abundant in the coarser central products. Table 4-1 gives X-ray counts for the elements found in other decrepitation products in the same specimen. The counts on S are standardised to about 28500 in each case. Although only semiquantitative because they were made on unpolished surfaces, the analyses are useful for comparison. Analyses 1, 2, 3 and 5 are typical of most such decrepitation products. The presence of a considerable amount of chlorine in one crystal is indicated by analysis 4; in the same place, Fe, Ni, Cu, Zn, Mn and (to a lesser extent) K and Na are all enriched relative to S. The decrepitation products are thus very different from the daughter salts of inclusions opened cold. Metzger *et al.* (1977) cited "phase transformations and other undesirable changes" during decrepitation of the inclusions as disadvantages of analysing decrepitation products. In this instance, the process of decrepitation evidently brings about reaction and fractionation of the constituents of the inclusions. Alkalis, Cl, and some of the base metals may be transported as volatiles such as NaCuCl_2 , Na_2CuCl_3 , NaFeCl_3 and NaFeCl_4 , which have escaped from the area around the ruptured inclusions in all cases examined but one. This observation provides a clue to the possible processes of metal transport at high temperatures. The volatile species could be important in the vapour phase, and also, possibly, in the salt-rich liquid. This point will be considered further in Chapter 10.

The crushing of quartz under anhydrous glycerine indicated that there is a negligible amount of CO_2 in type III (and type II) inclusions.

Hematite. It has been noted that hematite occurs both as solid inclusions and in type III inclusions, in both igneous and hydrothermal quartz. Rarely, it protrudes through the walls of a type III inclusion cavity (fig. 4-4 I). It seems unnecessary to invoke self-oxidation by hydrogen diffusion through the quartz lattice, as suggested by Roedder & Skinner (1968), to explain the presence of insoluble hematite in type III inclusions. A flake of hematite on the surface of a growing quartz crystal would be a likely site for the trapping of fluid (as would grains of anhydrite and sulphides, which may also be insoluble on heating). The relatively small number of solid hematite inclusions, and the size variation (relative to cavity volume) and sporadic occurrence of hematite crystals in type III inclusions are consistent with the trapping of salt-rich liquid about flakes of hematite already present on the quartz surface. Hematite is also prominent in obviously secondary or pseudosecondary type III inclusions, where it again occurs sporadically. The reason for this is discussed in Chapter 5.

Boiling. The invariable association of type III with type II inclusions raises the question of whether the salt-rich liquid trapped in type III inclusions was boiling. This association is common in porphyry copper deposits (Nash, 1976) and suggests, but does not establish, that the boiling of salt-rich liquid was characteristic of porphyry copper environments. To prove the intimate coexistence of two fluids, it would be necessary to find a growth zone or a healed fracture bearing both types of fluid inclusion, and unaffected by any subsequent necking down, introduction of other fluids, etc. No unequivocal examples of these were found. Appealing to less direct evidence, it has been noted that gas was contemporaneous with most solid inclusion species, viz. anhydrite, hematite and opaque solids. The same species all occur in type III inclusions. Thus the solid inclusions and types II and III fluid

inclusions appear to be contemporaneous. The best example is 102636, where an association of anhydrite, hematite and opaque solid inclusions have gas adhering to them (fig. 4-4 L). Also in 102636, solid inclusions of anhydrite themselves contain type II and type III fluid inclusions (but not both in the same solid inclusion), which are apparently primary or pseudosecondary. Anhydrite and chalcopryrite solid inclusions with gas adhering to them were also noted in 102619, 102676, 103009, 103010 and 103028. In 102619 there is gas adhering to the isotropic, colourless solid inclusions mentioned above. There is thus indirect, but plausible, evidence that boiling was taking place, and that types II and III inclusions were closely related.

CHAPTER FIVE: FLUID INCLUSIONS IN QUARTZ-Cu,Fe SULPHIDE VEINS

Every specimen of quartz-Cu,Fe sulphide vein or breccia matrix contained fluid inclusions of types I, II and III. Type II inclusions are usually more common than type III inclusions, which in turn are usually more common than type I inclusions. The significance of these observations on relative abundance is questionable because they reflect a variety of controlling factors, e.g. the probable tendency of the host crystal to trap more of one fluid than the other in a two fluid phase system, and the amount of fracturing of the host during the various hydrothermal stages. Primary type II inclusions occur, e.g. in 103006, and the salt-rich liquid is also thought to be a primary fluid (see Chapter 4). Type I inclusions are invariably secondary inclusions in quartz which also contains inclusions of types II and III.

TYPE I INCLUSIONS

Data were obtained from the heating and freezing of type I inclusions. Freezing measurements were not possible in every inclusion because some were too small and others were optically unsuitable in other ways for the melting of ice to be observed. Some could not be induced to freeze at all, even on being cooled to -80°C , and others retained metastable ice at temperatures over 0°C . In general, the melting of ice was the only phase change seen in type I inclusions being warmed from low temperatures; no CO_2 hydrate was seen. Only in 103031 was more complex behaviour observed, and this, too, may be related to metastability (see below).

T_h data were obtained for 497 inclusions and T_f data for 223 inclusions (fig. 5-1). Paired T_h and T_f data are plotted in two ways because of the diversity of data within single specimens. Firstly, (T_h, T_f) pairs for individual inclusions have been plotted as small, black points; secondly, mean data for three or more accordant, neighbouring inclusions are represented as larger, open circles. The data were grouped and averaged in this way in order to eliminate inclusions perturbed by leakage, necking down, etc. since trapping. Comparison of the two methods shows that for higher salinities in particular ($T_f > -6^\circ\text{C}$) the field of individual data points is much broader than the field of averaged data points. This probably does not mean that the inclusions have been perturbed, however, because it is difficult to account for any increase in the salinity of type I inclusions (which precipitate no halite) by leakage or by necking down. So most of the points plotted in fig. 5-1 probably represent true fluid compositions, with the exception of those with $T_f < -28^\circ\text{C}$. These all occur in 103031. The T_f readings obtained from these may not correspond to the melting of ice in the inclusions, in a few of which another phase change seemed to occur at higher temperatures (up to $+10^\circ\text{C}$). Several precipitated a salt resembling halite on attaining room temperature and the halite crystals dissolved at $95 - 140^\circ\text{C}$. Therefore the low-temperature fusions reflect the non-equilibrium properties of relatively concentrated, supersaturated brines and are probably not to be interpreted in terms of the equilibrium system $\text{NaCl-H}_2\text{O}$. Most type I inclusions contain liquid of low salinity, 0 - 5% eq. NaCl (although it must be remembered that the study excluded a number of inclusions which could not be frozen, possibly because of their composition). These low-salinity liquids mostly homogenise in the temperature range $150 - 360^\circ\text{C}$. More saline liquids, 5 - 23% eq. NaCl, homogenise between 240°C and 380°C .

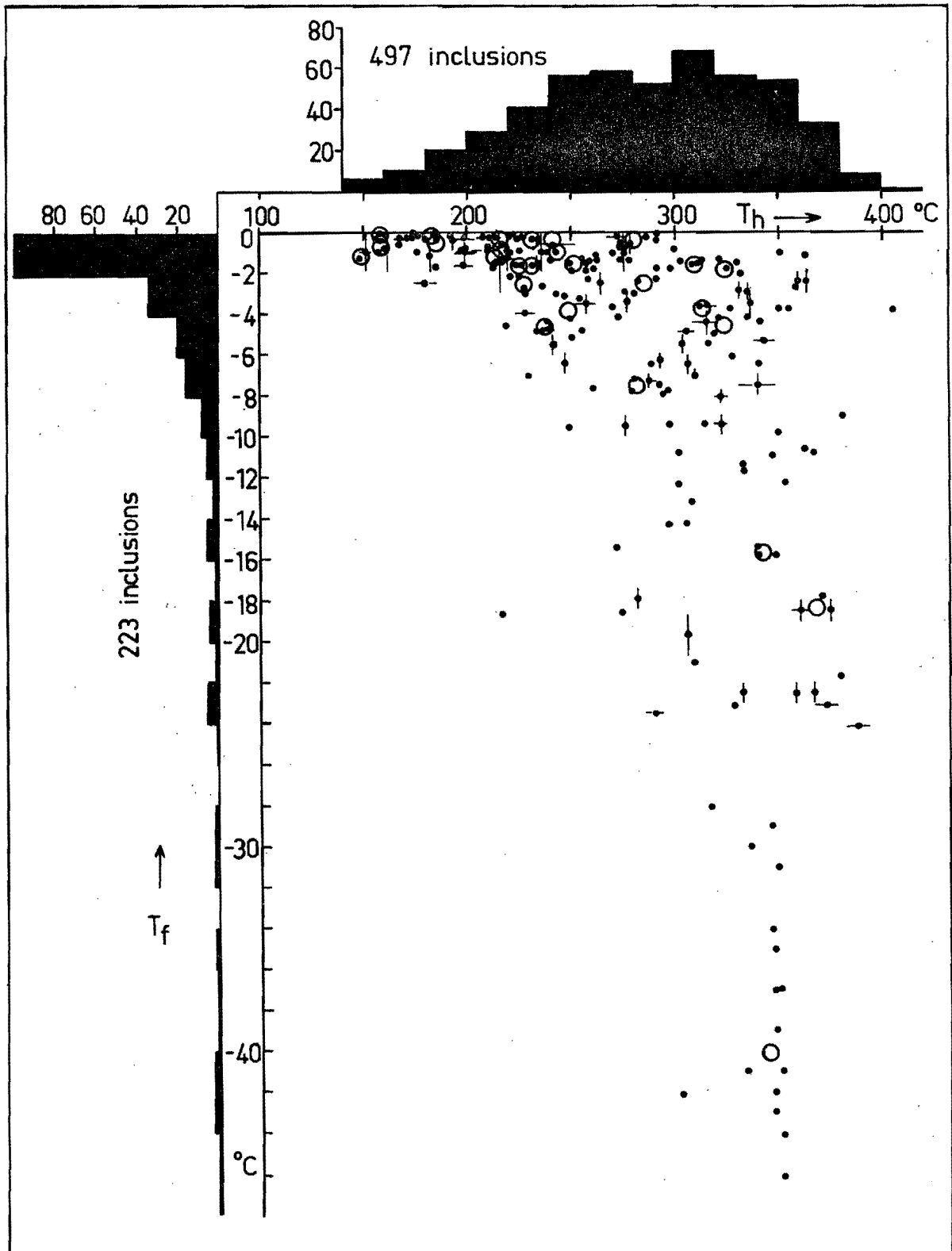
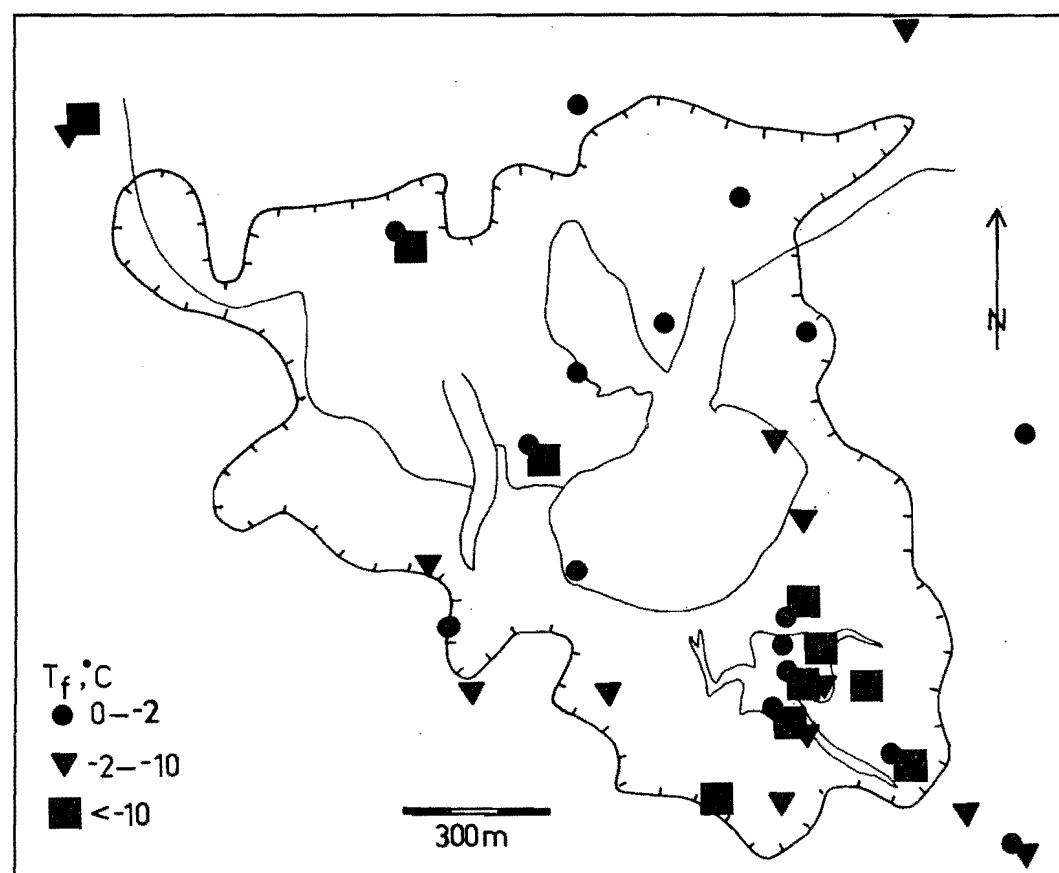
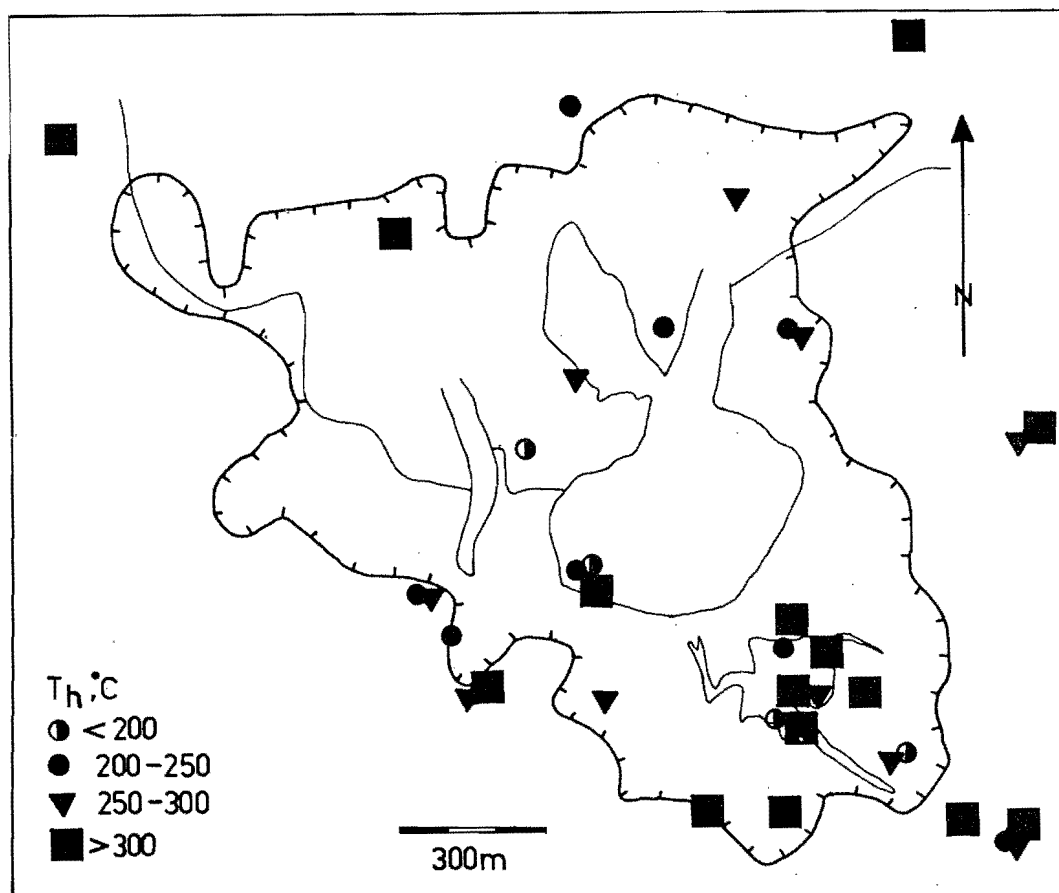


Fig. 5-1 T_h and T_f data for type I inclusions from quartz-Cu,Fe sulphide veins. The histograms include all data available. T_h is plotted against T_f for those inclusions for which both parameters were measured; the black dots indicate data for individual inclusions (bars indicating uncertainty) and the open circles indicate data averaged from three or more neighbouring inclusions in close agreement.

Fig. 5-2 Map of the distribution of T_h for type I inclusions from quartz-Cu,Fe sulphide veins. Symbols are shown only where a result is satisfactorily defined (see text). Overlapping symbols indicate several results in a single specimen. Geological contacts and the outer 0.3% Cu contour as in fig. 2-3.

Fig. 5-3 Map of the distribution of T_f for type I inclusions from quartz-Cu,Fe sulphide veins. Symbols are shown only where a result is satisfactorily defined (see text). Overlapping symbols indicate several results in a single specimen. Geological contacts and the outer 0.3% Cu contour are as in fig. 2-3.



The ice in all of them melts at $T_f \geq -24^{\circ}\text{C}$, which is essentially consistent with the phase properties of the system $\text{NaCl-KCl-H}_2\text{O}$ (eutectic at -22.9°C , Cornec & Krombach, 1932).

Distributions of T_h and T_f for type I inclusions in quartz-Cu,Fe sulphide veins are plotted relative to the geology in figs. 5-2 and 5-3, respectively. These diagrams suffer from limitations, e.g. the variations in the number of data on which each plotted temperature is based, the sampling pattern and the exclusion of some inclusions in the case of T_f , as pointed out above. Not all specimens were studied for type I inclusions. In some specimens a T_h or T_f mode was defined by a number of inclusions in agreement, but not necessarily from the same area of the specimen. In others, two or more inclusions, closely associated, gave closely similar T_h and T_f readings. The maps include examples of both. The distributions are apparently unzoned, both for temperature and for salinity. Several samples preserve evidence of more than one generation of fluid. The grouping of higher salinities and higher temperatures around the Leucocratic Quartz Diorite is in part an artefact of the close sample spacing in this interesting area. Nonetheless, the characteristic wide ranges of salinity and temperature around the Leucocratic Quartz Diorite show that that part of the deposit has undergone a complex history of invasion by these fluids.

The fluid inclusions peculiar to certain healed fractures in 103047 are distinct from other type I inclusions in quartz-Cu,Fe sulphide veins in having a T_h range of $390 \pm 10^{\circ}\text{C}$ and in each containing a small daughter salt. Two of the inclusions gave T_f readings of -11.2 and -12.0°C . The salt has not been identified. It is colourless, occurs as equant grains of high relief and is very highly birefringent, too much so to be anhydrite. It may be a carbonate.

Pressure corrections. At a pressure of 300 bars (see Chapter 7), the pressure corrections (from Potter, 1977) for fluids of the salinities encountered in type I inclusions at Panguna are listed in Table 5-1. All fall within the range $25 \pm 10^{\circ}\text{C}$. These corrections are added to the T_h readings to give the formation temperatures which therefore span a range of 170 - 400°C .

TYPE II INCLUSIONS

Type II inclusions, some with large liquid rims and others with small rims, were heated and frozen. The formation of ice or hydrates could be observed only in inclusions with large rims, and these usually either fail to homogenise by 600°C , or decrepitate before homogenising. They were probably mixtures of liquid and vapour at trapping, and so give spurious measures of temperature and composition. There is so little liquid visible in inclusions with small liquid rims that only those in cusped cavities can be used in heating runs. The precision of T_h measurements on such inclusions is poor, often $\pm 10^{\circ}\text{C}$.

The vapour in type II inclusions is thought to have been in equilibrium with salt-rich liquid at temperatures over 400°C (see Chapter 4). An inclusion which consisted of vapour only when it was trapped must homogenise at $T_h \leq T_c$, and T_c is a function of the salinity of the inclusion. Since vapour salinities are very much lower than liquid salinities in the relevant parts of the NaCl-H₂O system (Sourirajan & Kennedy, 1962), it is to be expected that T_h readings on type II inclusions will in general be less than the temperature of trapping of the vapour, the upper limits being 390 - 425°C , corresponding to 2 - 5 wt. % salt in the vapour. An inclusion formed of a gas-liquid mixture will homogenise at a higher temperature limited by the critical

Table 5-1

PRESSURE CORRECTIONS FOR T_h OF TYPE I INCLUSIONS,
FOR A FORMATION PRESSURE OF 300 BARS (Potter, 1977).

Salinity % NaCl	$T_h, ^\circ\text{C}$					
	150	200	250	300	350	400
1	30	24	15	15	-	-
5	~32	25	21	19	~20	-
10			25	20	~20	~20
15			30	22	18	~15
20			35	25	20	~18
25			27	20	17	15

The corrections listed are added to T_h ($^\circ\text{C}$).

temperature of the whole mixture. Of the cusped type II inclusions selected for their small liquid rims, 34 homogenised by 440°C (fig. 5-4). Many others retained two fluids to much higher temperatures. Most of the data are from two specimens only (103026, 103029); these are veins which seem to have formed near 400°C on the basis of data from type III inclusions (see fig. 5-7). In veins formed near 600°C , (e.g. 103012), very few inclusions with small liquid rims homogenised at temperatures less than 420°C . The histogram has a well-defined mode at $390 \pm 10^{\circ}\text{C}$, suggesting a minimum T_c estimate of 400°C , i.e. a minimum salinity estimate of 2.6% (Sourirajan & Kennedy, 1962), for the vapour in the set of veins formed near 400°C . The relevance of these observations to pressure determination is considered in Chapter 7.

DENSITY AND COMPOSITION OF TYPE III INCLUSIONS BY VOLUME MEASUREMENT

The volumes of some type III inclusions and their component phases were determined from micrometer measurements made under the microscope. These measurements were only possible on regular geometric forms, viz. negative crystals. Volume determinations can be made only on cavities with the c-axis oriented perpendicular to the line of sight, and even these are subject to large errors because it is impossible to tell whether the prismatic part of the cavity is oriented with a face or an edge closest to the observer, i.e. it is not possible to distinguish whether $2b$ or $2b'$ (fig. 5-5) or a section between these extremes is being measured. At the extremes, and for a measurement b , the volume of the prismatic part of the cavity is

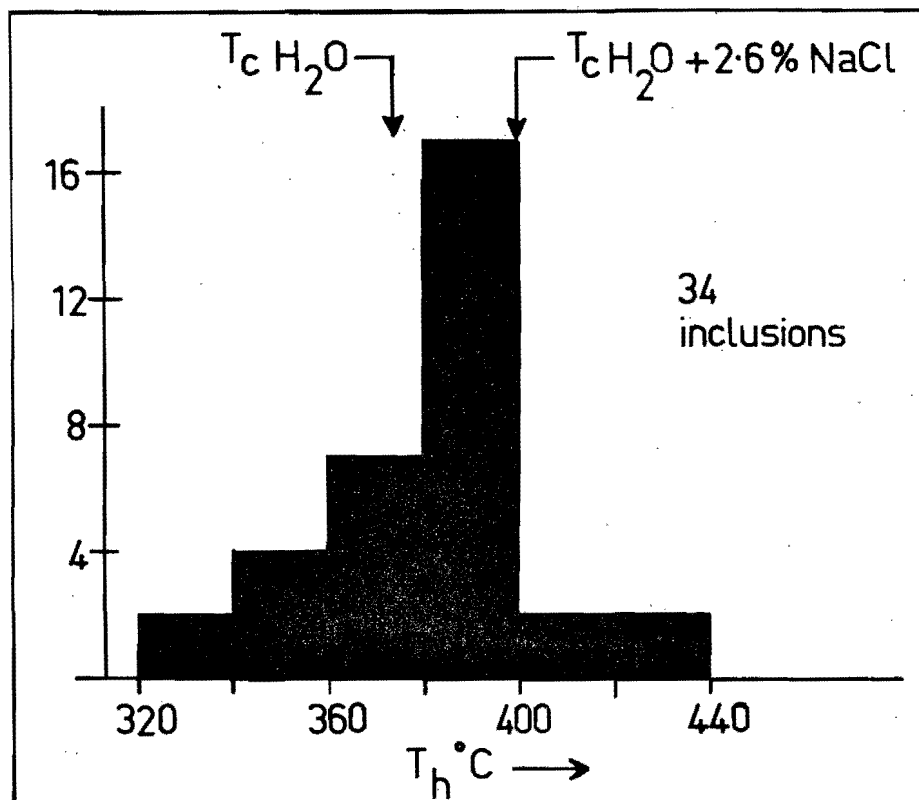


Fig. 5-4 T_h histogram for type II inclusions from quartz-Cu,Fe sulphide veins.

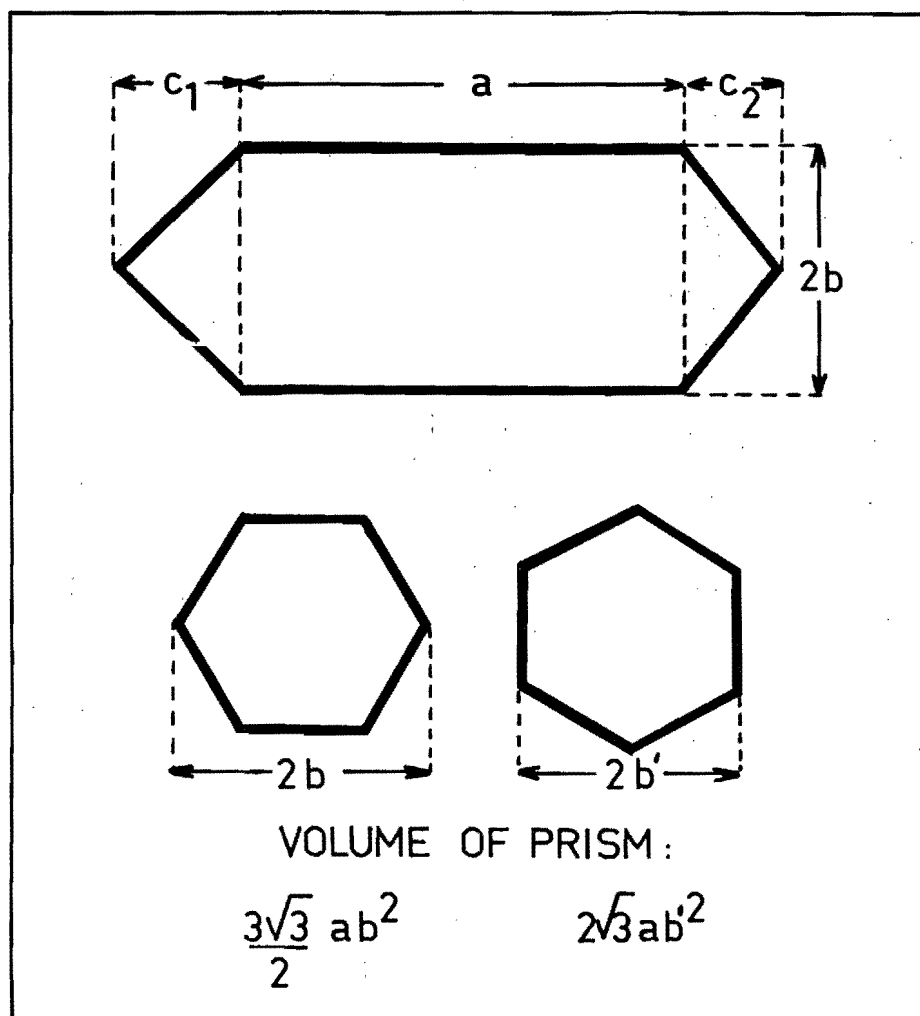


Fig. 5-5 Diagrams explaining the calculation of the volume of a negative quartz crystal (see text).

$$\frac{3 \sqrt{3} ab^2}{2} \quad \text{with face closest,} = 2.60 ab^2$$

$$2 \sqrt{3} ab^2 \quad \text{with edge closest,} = 3.46 ab^2$$

and the volume of a cylinder of height a and radius b lies between these:

$$\pi ab^2 = 3.14 ab^2$$

Here, the calculations are made by assuming that b as measured is the radius of a cylinder, and the error engendered is thus about $\pm 15\%$.

A similar argument applies to the pyramidal caps, which are approximated by cones of volume

$$\frac{c_1 + c_2}{3} \pi b^2$$

The other forms are simpler: NaCl is a cube, $\rho = 2.2 \text{ g/cm}^3$, KCl is a cube, $\rho = 2.0 \text{ g/cm}^3$; other salt - assumed to be a sulphate, a cuboid, $\rho = 2.7 \text{ g/cm}^3$; chalcopyrite - assumed to be a regular tetrahedron of edge d and volume $d^3/6\sqrt{2}$, $\rho = 4.2 \text{ g/cm}^3$; bubble - a sphere, $\rho = 0 \text{ g/cm}^3$. The density of water saturated with KCl and NaCl at 25°C is 1.23 g/cm^3 (Cornec & Krombach, 1932). The calculation of each of these volumes engenders further error.

Of twenty-two density measurements (Table 5-2), sixteen lie in the range $1.2 - 1.5 \text{ g/cm}^3$, and the rest broaden the range to $0.9 - 1.7 \text{ g/cm}^3$. Where there are several results for a single specimen, the range for that specimen is the same as for all of the data, so that much of the variation may be due to error. Urusova (1975) reported a density of 1.1 g/cm^3 for a NaCl-H₂O mixture of 50% NaCl at 450°C and 500 kg cm^{-2} .

Table 5-2

DENSITY DETERMINATIONS ON TYPE III INCLUSIONS

Specimen	Densities, g/cm ³
102594	1.4, 0.9
102676	1.1
103012	1.7, 1.5, 1.5, 1.2, 1.3, 1.2
103019	1.4
103022	1.2, 1.3, 1.5, 1.3, 1.3
103031	1.4, 1.5, 1.0, 1.1, 1.3, 1.2
103035	1.2

Table 5-3

VOLUMETRIC SALINITY MEASUREMENTS FOR TYPE III INCLUSIONS

Specimen	% H ₂ O	% KCl	% NaCl	% Total salts	% Salt content from micro- thermometry*
103031	42	10	48	58	
103031	45	10	45	55	63
103031	39	25	36	61	

103012	21	15	64	79	
103012	39	11	50	61	68

103022	38	8	54	62	
103022	47	14	39	53	75
103022	48	11	41	52	

* Mean result for inclusions in which T_sKCl and T_sNaCl were measured (6 for 103031, 4 for 103012, 9 for 103022).

Some volumetrically-determined compositions calculated for inclusions in 103012, 103031 and 103022 are listed in Table 5-3. Only the volumes of KCl, NaCl and the bubble have been measured; the volume and weight contributions of other salts, if any, have been ignored in the calculations. Although the results for each specimen are variable, they compare approximately with salinities determined by microthermometry (the last column of the table) in 103012 and 103031. The microthermometric results (see below) are also based on the assumption that the inclusions contain only H₂O, NaCl and KCl.

In certain inclusions it was possible to measure the volumes of the chalcopryrite crystals and thence calculate the copper content of the salt-rich liquid. In 103022 a plane of secondary type III inclusions was examined. The distribution of hematite and chalcopryrite crystals in the inclusions is not uniform, despite the apparent uniformity of the halite cubes relative to cavity size (borne out by the small T_{gNaCl} range of this specimen, see fig. 5-7). The halite must therefore have crystallised after the fluid in the fracture had split up into the present array of inclusions. If a solid phase were to precipitate in the fracture prior to the split-up, it would act as the nucleus for a secondary inclusion. If two solid phases were to precipitate independently, it would be rare for a single secondary inclusion to nucleate on both solid species. A section of fracture consisting of 24 inclusions was closely examined, and it was found that: (i) 15 inclusions each contained a large chalcopryrite crystal, but no hematite; (ii) 7 inclusions contained hematite, but either no visible chalcopryrite (small opaque phases can be hard to see against cavity walls), or a very small chalcopryrite crystal relative to the size of the cavity; (iii) 2 inclusions contained a small chalcopryrite crystal but no hematite. All of these combinations can be explained if the fluid in the fracture deposited chalcopryrite and

hematite first, *then* split into discrete inclusions, *then* precipitated halite. No hematite was deposited after the splitting up of the fluid, but a little chalcopryrite was deposited. This gave rise to the small chalcopryrite crystals seen in some of the 7 inclusions localised around hematite and in the 2 inclusions which contained neither a large chalcopryrite nor a hematite crystal. The Cu content of the inclusions with large chalcopryrites is a maximum estimate of the Cu content of the original fluid. The Cu content of inclusions with hematites and small chalcopryrites is a minimum estimate of the Cu solubility, as well as an estimate of the Cu solubility at the temperature of the split-up. Two large chalcopryrites gave 3200 and 3000 (mean 3100) ppm Cu, and two small gave 510 and 290 (mean 400) ppm. Distributing the Cu in the large chalcopryrites over all 24 inclusions (which are of comparable size) gives an estimate of the original Cu concentration, 1900 ppm, provided no fluid was lost from the fracture during the split-up into discrete inclusions. The amount of Fe corresponding to chalcopryrite is then 1670 ppm, and the amount of S as sulphide, 1910 ppm. More Fe is probably present as dissolved species at room temperature, along with a little as hematite. S will also be present as sulphate, both dissolved and as daughter salt crystals at room temperature.

COMPOSITION OF TYPE III INCLUSIONS BY MICROTHERMOMETRY

The solution temperatures of NaCl and KCl in type III inclusions give estimates of the composition of the salt-rich liquids in terms of the system NaCl-KCl-H₂O, from the data of Ravich & Borovaya (1949).

The degree to which type III inclusions reproduce the properties of their parent fluids has been investigated by taking readings on isolated planes of secondary inclusions. Such sets of readings ought to

represent fluids originally homogeneous with respect to salinity; any subsequent change can be attributed to leakage or necking down. It is difficult to assess visually the importance of necking down, for inclusions in the process of necking down are not often seen. This is because quartz anneals relatively fast at the high temperatures to which these veins have been subjected. T_{SNaCl} histograms for three planes of inclusions from different specimens are presented in fig. 5-6. In each case, 80% of the readings lie within a 15°C interval. The T_{SNaCl} distributions of individual veins have much broader ranges (fig. 5-7). This suggests that the fluid composition at a point changed with time.

Measurements of T_{SNaCl} indicate the relative salinities of the inclusions, although T_{SKCl} values are also required to estimate the actual salinities. Despite the broad spreads of the T_{SNaCl} distributions in fig. 5-7, many specimens are quite distinguishable according to their T_{SNaCl} ranges and modes. The spatial distribution of T_{SNaCl} modes has the following characteristics (figs. 5-8, 5-9):

- (i) a ridge of high salinities (T_{S} mode $\geq 500^{\circ}\text{C}$) running northeast through the centre of the deposit,
- (ii) a marginal zone of relatively low salinities (T_{SNaCl} mode $\leq 420^{\circ}\text{C}$) flanking the 0.3% Cu contour and apparently bounding higher salinities to the southwest of the deposit. No such zone was located to the north and east, and near the Leucocratic Quartz Diorite, where the history may have been more complex, high and low salinities overlap. The salinity distribution is therefore asymmetric with respect to the copper mineralisation.

Minor features include some low T_{SNaCl} modes ($\leq 420^{\circ}\text{C}$) east of the centre of the orebody (but neither bounding higher salinities nor, as a group, flanking the 0.3% Cu contour), and small highs consisting of T_{SNaCl} modes of 490°C near two of the Leucocratic Quartz Diorite stocks.

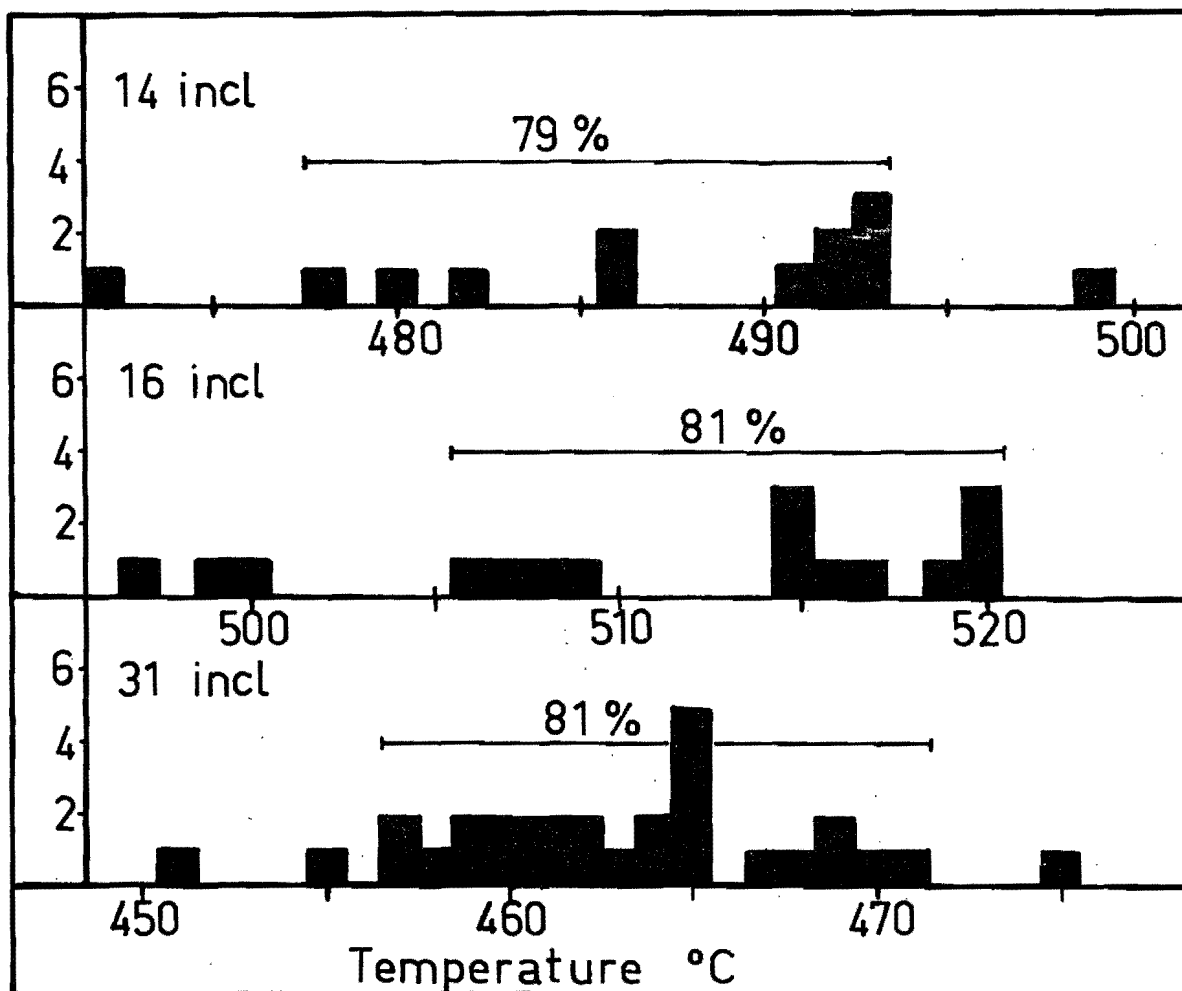
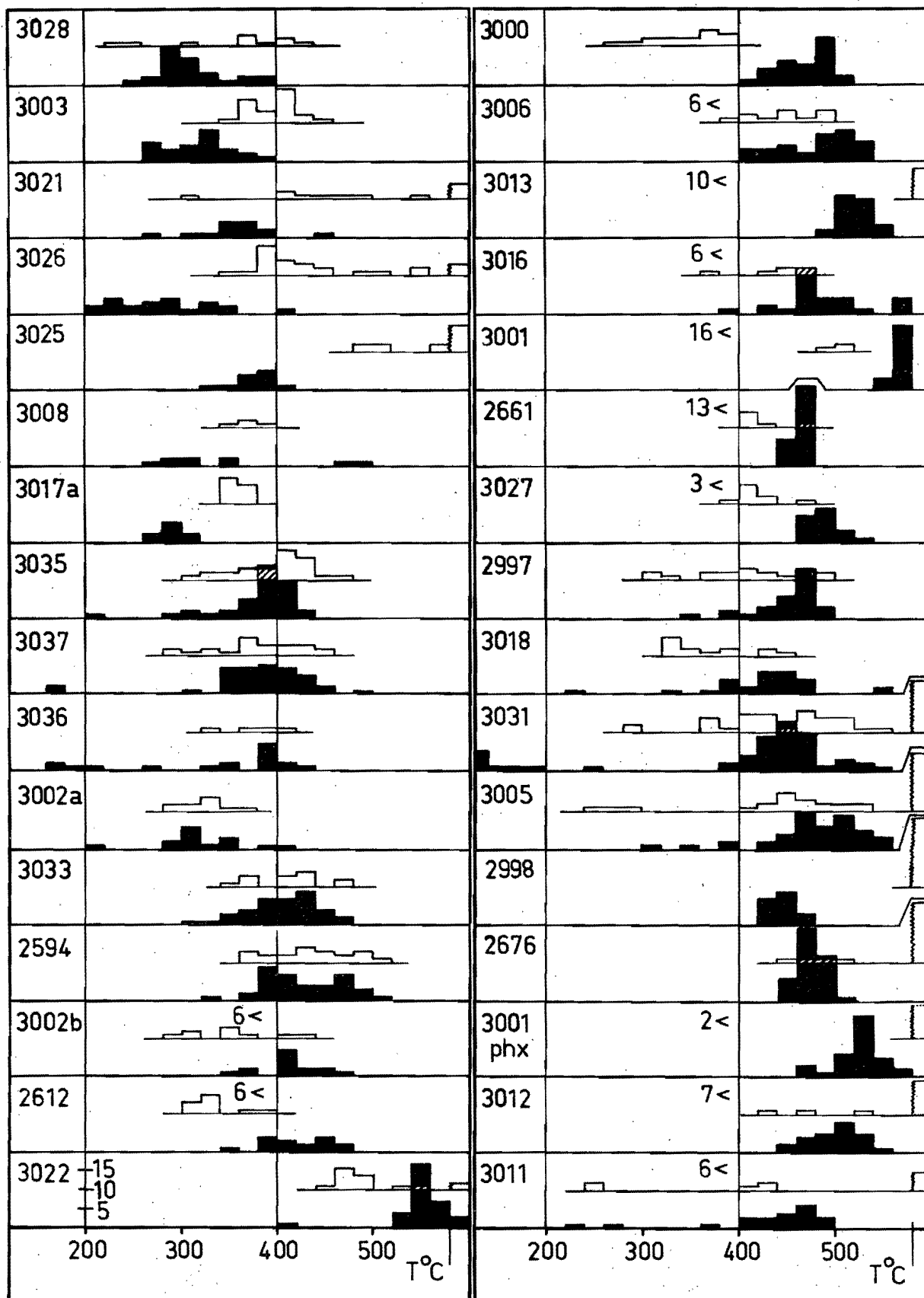


Fig. 5-6. T_{gNaCl} histograms for three discrete planes of secondary or pseudosecondary type III inclusions. The number of measurements, some of which do not fall inside the range shown, is indicated at the left. The intervals into which the central $80 \pm 1\%$ of readings fall are indicated.

Fig. 5-7 Data for type III inclusions in quartz-Cu,Fe sulphide veins and phenocrysts (phx). The black histograms give T_SNaCl and the white T_h . Hatching indicates the overlap of columns. Spatially separate groups of inclusions from a single sample are differentiated by letters e.g. 3002a, 3002b. The symbol "13<" indicates that 13 T_h measurements were not precisely recorded but were recorded as being less than T_SNaCl in their respective inclusions. The temperature scale breaks at 580°C; columns beyond this correspond to higher temperature results which could not be measured with the Chaixmeca apparatus. See fig. 5-15 for T_h measurements >580°C made with a Leitz 1350° stage on specimens 2998, 2676 and 3031. Specimen numbers are prefixed by 10 in the University of Tasmania catalogue.



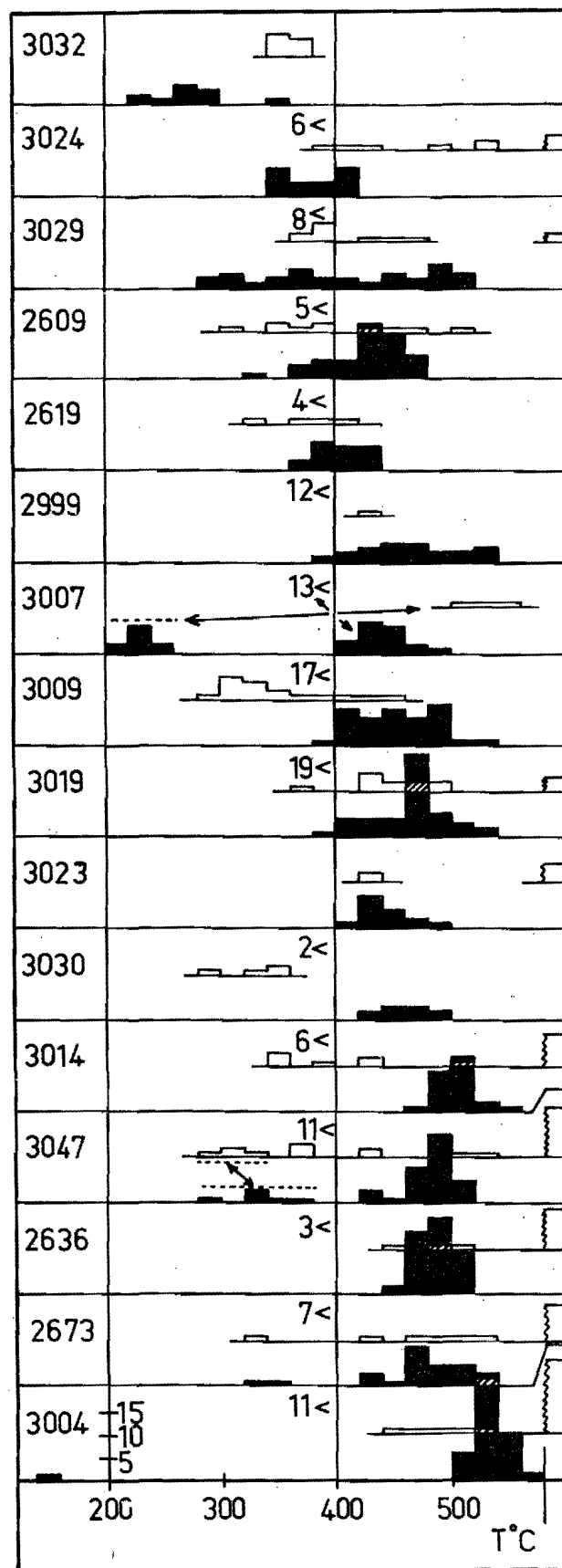
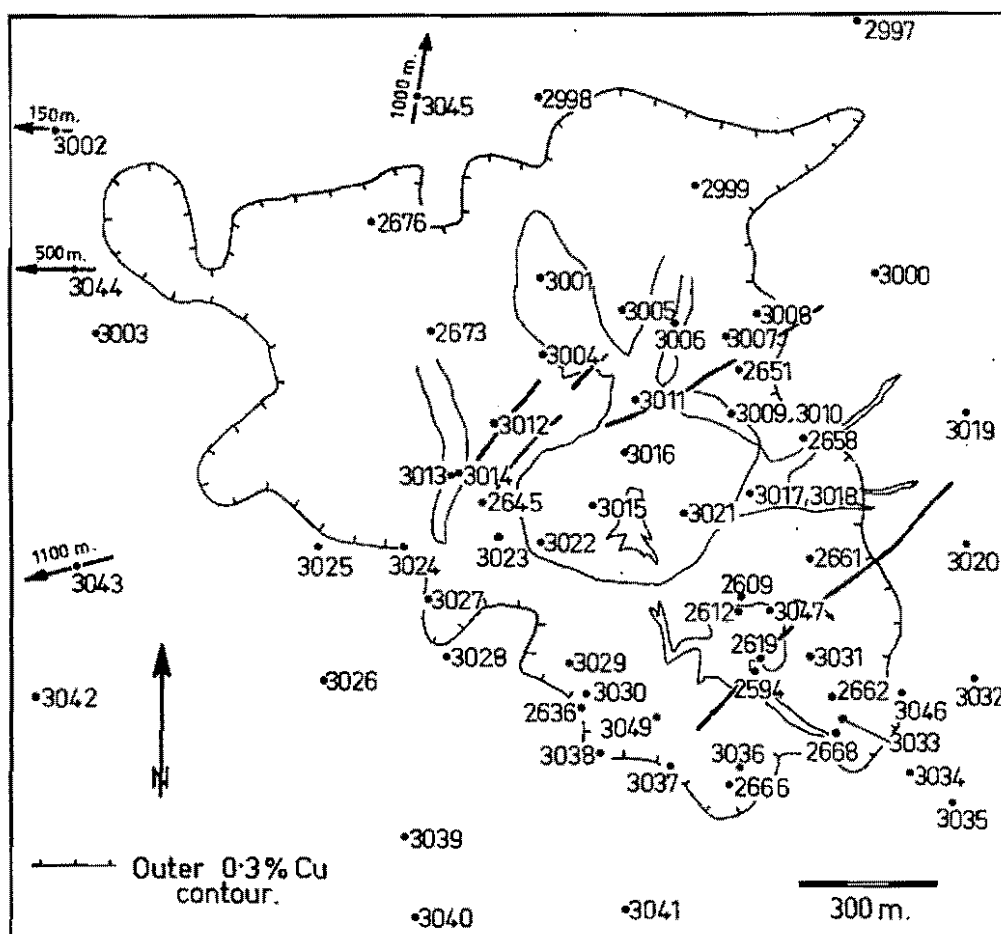
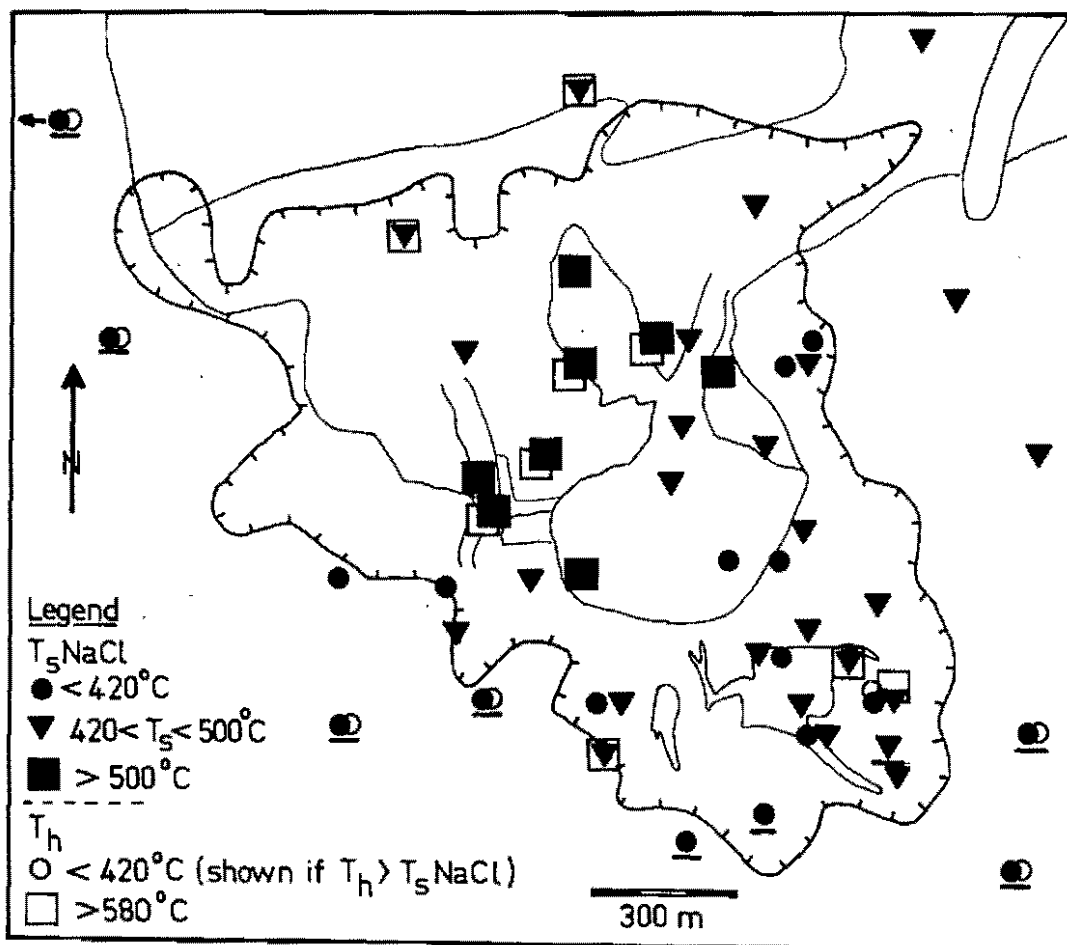


Fig. 5-7 cont.

Fig. 5-8 Data from type III inclusions: modal values of T_h (white symbols) and T_{SNaCl} (black symbols) are plotted relative to geological contacts and the outer 0.3% Cu contour (see fig. 2-3). Symbols are shown only for specimens which yielded sufficient data to define a mode (see appendix for numbers of data). T_h modes are shown only for specimens where $T_h \geq T_{SNaCl}$. Underlined symbols indicate specimens that define the zone of cooling along the southwestern margin of the deposit.

Fig. 5-9 Sample localities of specimens used in the fluid inclusion study, relative to geological contacts (see fig. 2-3). The location of no.3048 is not shown, being imprecisely known. It is from the quadrilateral between points 3004, 3011, 3022 and 3013. Sample numbers are prefixed by 10 in the University of Tasmania catalogue.



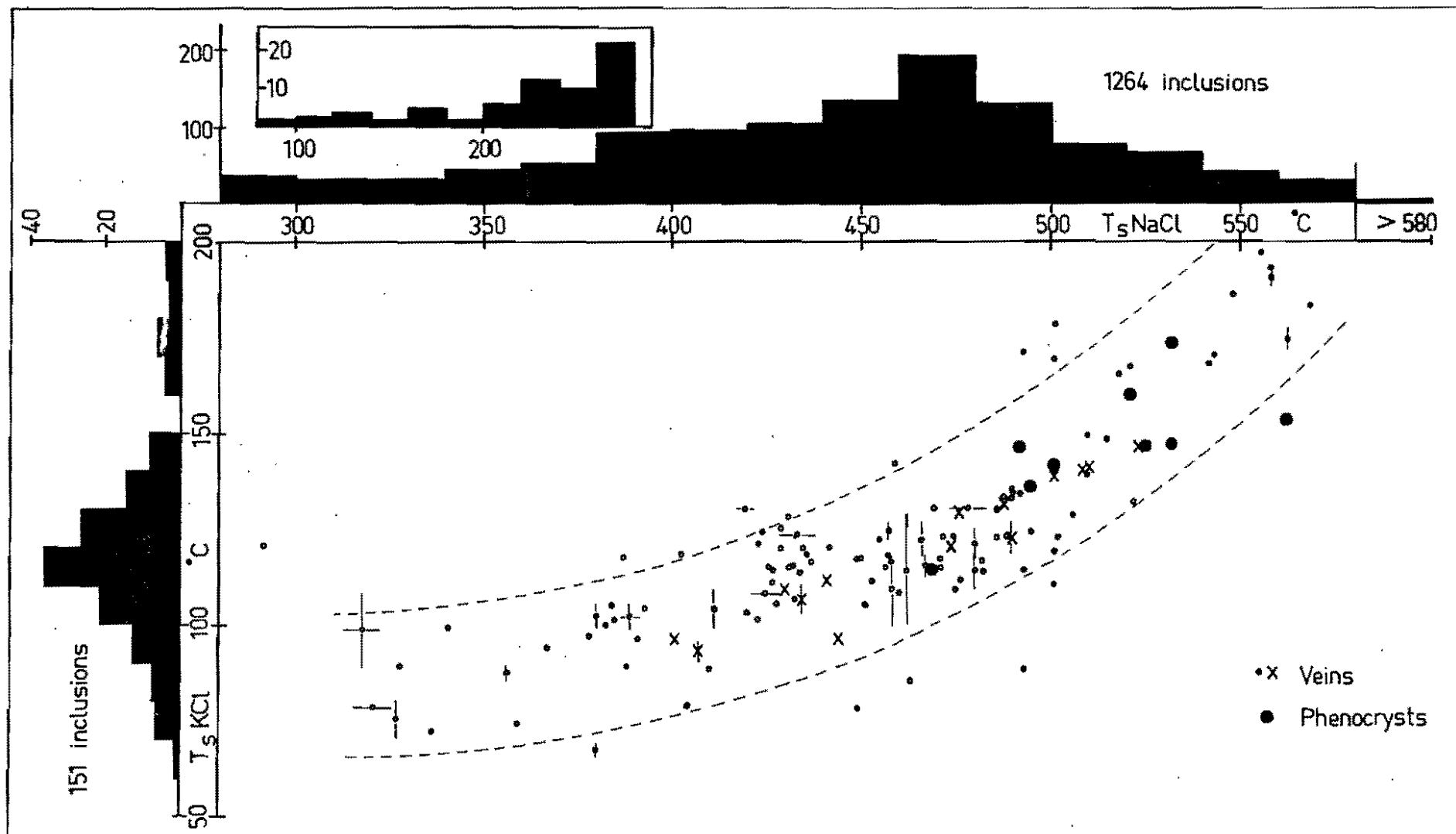
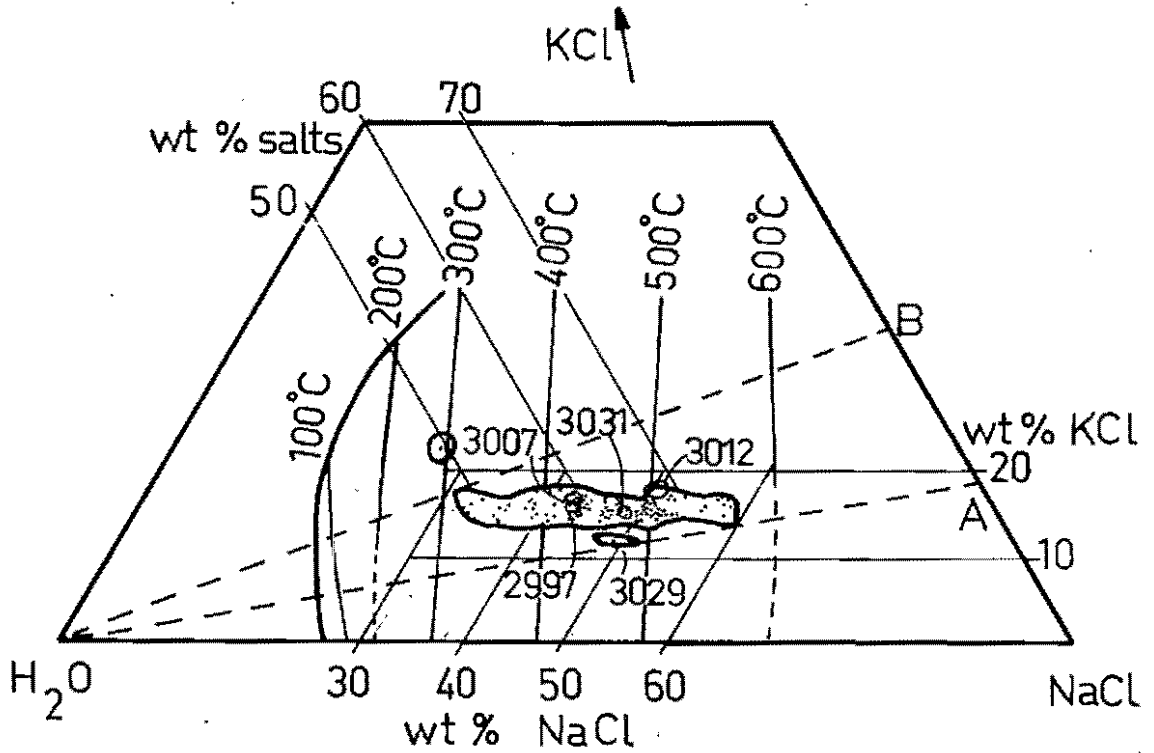
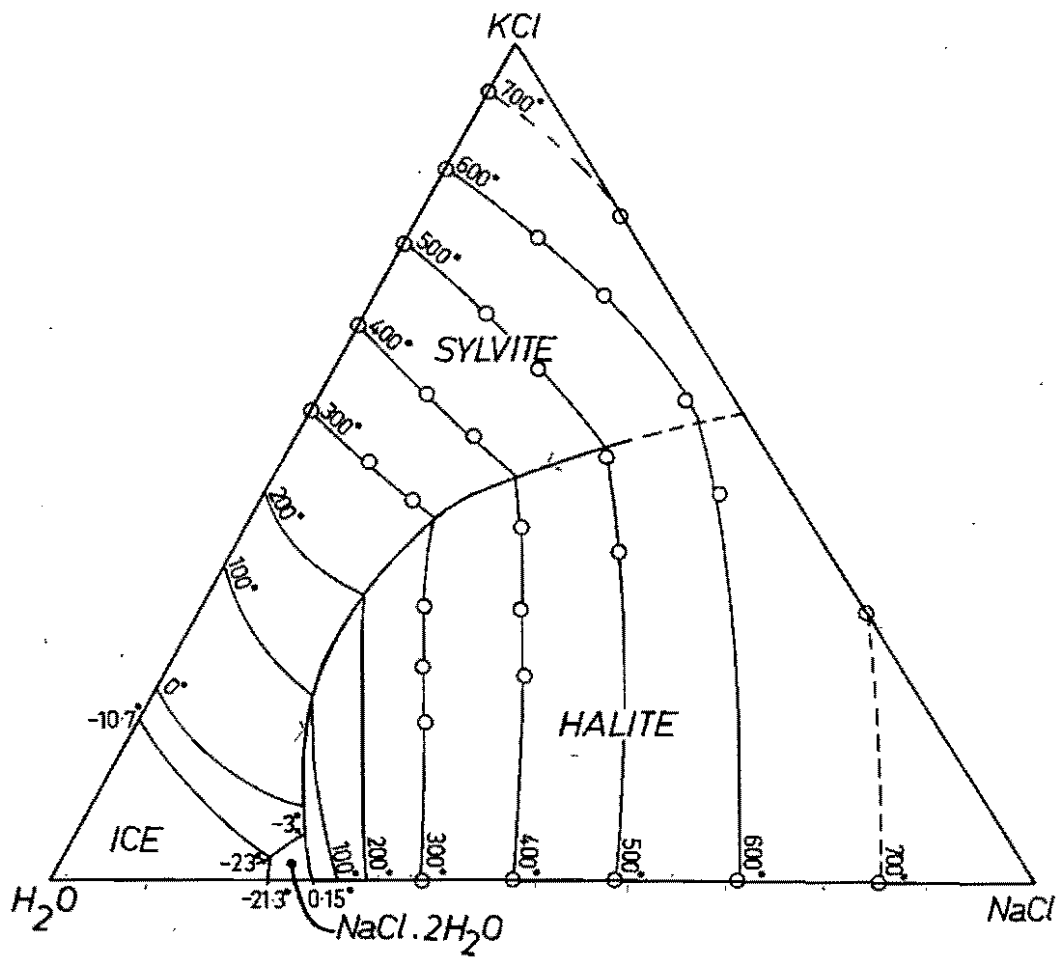


Fig. 5-10 $T_s\text{NaCl}$ and $T_s\text{KCl}$ data for type III inclusions from quartz-Cu,Fe sulphide veins and quartz phenocrysts. All data available are given in the histograms. $T_s\text{NaCl}$ is plotted against $T_s\text{KCl}$ for those inclusions in which both parameters were measured. Vein and phenocryst data are distinguished as shown. The crosses represent data from a single vein, 103006. Bars indicate the uncertainty of the readings.

Fig. 5-11 The ternary diagram NaCl-KCl-H₂O, after Ravich & Borovaya (1949). The isotherms of the liquidus surface are shown in °C, and the regions of the liquidus are labelled according to the equilibrium solid phase in each. Circles indicate Ravich & Borovaya's data points; data for isotherms at $T < 200^{\circ}\text{C}$ were taken by the authors from other sources.

Fig. 5-12 A portion of the ternary diagram NaCl-KCl-H₂O, after Ravich and Borovaya (1949), showing the cotectic NaCl-KCl and isotherms (100 - 600°C) of the part of liquidus at which NaCl is saturated. The field of microthermometric data for inclusions in which both T_{gKCl} and T_{gNaCl} could be measured is superimposed on it; the smaller fields of five numbered specimens are also shown. The ratio K/Na (atomic) has the value 0.17 along line A and 0.46 along line B. Specimen numbers are prefixed by 10 in the University of Tasmania catalogue.



Paired $T_g\text{NaCl}$ and $T_g\text{KCl}$ readings have been obtained for 125 inclusions covering a $T_g\text{NaCl}$ range of $294 - 570^\circ\text{C}$. These are plotted in fig. 5-10 alongside the histograms of all $T_g\text{KCl}$ readings (151) and all $T_g\text{NaCl}$ readings (1264). The points plot, with some lateral spread, along a single curve. The contributions of single specimens are mostly concentrated in small intervals of the curve, but for 103006 (points plotted as crosses) the points follow the curve over a $T_g\text{NaCl}$ range of 130°C . The NaCl-KCl- H_2O ternary diagram (fig. 5-11) of Ravich & Borovaya (1949) permits this curve to be interpreted as a compositional variation. In fig. 5-12, the data from Panguna are reproduced on a portion of Ravich & Borovaya's diagram. The salinities of inclusions in which both $T_g\text{KCl}$ and $T_g\text{NaCl}$ could be measured vary between 46 and 76 wt. % NaCl + KCl. In 90% of inclusions with $T_g\text{NaCl} > 300^\circ\text{C}$ the disappearance of KCl on heating could not be seen well enough for $T_g\text{KCl}$ readings to be made, but there is no reason to suppose that these deviate from the trend established by the other 10%. Those with $T_g\text{NaCl} < 300^\circ\text{C}$ are represented by one point only on the $T_g\text{KCl}$ vs. $T_g\text{NaCl}$ plot, and this point does deviate from the trend. It is from 103047 and its possible significance will be considered later (Chapter 9). The rest of the points indicate a KCl content constant at $16 \pm 2\%$ throughout a range of NaCl content from 60% (high $T_g\text{NaCl}$) to 30% (low $T_g\text{NaCl}$). As $T_g\text{NaCl}$ decreases, the ratio KCl/NaCl decreases from 0.59 to 0.22 by weight, or 0.46 to 0.17 by molar proportions. The areas marked with specimen numbers in fig. 5-12 encompass data from those specimens for which K/Na ratios from leaching experiments are also available. The two sets of ratios are compared in Table 5-3. Each ratio determined by microthermometry differs by a maximum of 0.06 from the corresponding leachate ratio in a range (determined by microthermometry) of 0.29, with excellent agreement for 103012 and 103031.

Eighty-five paired measurements ($T_S\text{NaCl}$, T_S salt A) were made on inclusions with one or more colourless salts in addition to halite and sylvite. The majority of these salts proved to be soluble within the temperature range of the Chaixmeca stage. The data are plotted in fig. 5-13 as points of the ($T_S\text{NaCl}$, T_S salt A) plane, with the lines $T_{S\text{salt A}} = T_{S\text{NaCl}}$ (line A) and $T_{S\text{salt A}} = T_{S\text{KCl}}$ (line B) for comparison, and the T_S salt A data are also presented as a histogram. Four temperature modes are clearly distinguished in the histogram and labelled First (bottom) to Fourth (top). Multiple (up to three) $T_{S\text{salt A}}$ measurements were made in each of several inclusions. Invoking the principle that each salt in an inclusion will form just one crystal if it nucleates, it is possible to distinguish two salts corresponding to the first mode, i.e. in certain inclusions (two in this case), two salts were seen to disappear in the temperature interval corresponding to the first mode. The second, third and fourth modes apparently correspond to one salt each on the basis of multiple $T_{S\text{salt A}}$ measurements in another inclusion. Similarly, it is possible to show that the salt corresponding to the second mode differs from that of the third and from that of the fourth, and that one of the salts corresponding to the first mode, the salt of the third and the salt of the fourth are all different. Both salts in the first mode are different from the salt of the third mode. These observations are summarised in the following deductions to demonstrate the minimum number of different salts consistent with the observations. The possible salts are named 1A, 1B (first mode), 2 (second), 3 (third) and 4 (fourth). Equality symbolises sameness, and inequality difference.

Observations: (a) $1A \neq 1B$

(b) either $1A$ or $1B \neq 3$; either $1A$ or $1B \neq 4$; $3 \neq 4$.

(c) $1A \neq 3$; $1B \neq 3$

(d) $2 \neq 3$; $2 \neq 4$.

Deduction: either $1A$ or $1B \neq 2$.

CASE 1: If $1A \neq 4$, then $1B$ could be $= 4$; and if $1B \neq 2$ then $1A$ could be $= 2$. Therefore the minimum number is three salts.

Likewise if $1B \neq 4$ and $1A \neq 2$.

CASE 2: If $1A \neq 4$ then $1B$ could be $= 4$, and if $1A \neq 2$ then $1B$ could be $= 2$. But $1B = 2$ and $1B = 4$ is consistent with the observations $2 \neq 4$. So either $1B \neq 4$ or $1B \neq 2$, but not necessarily both. Therefore the minimum number is four salts.

Likewise if $1B \neq 4$ and $1B \neq 2$.

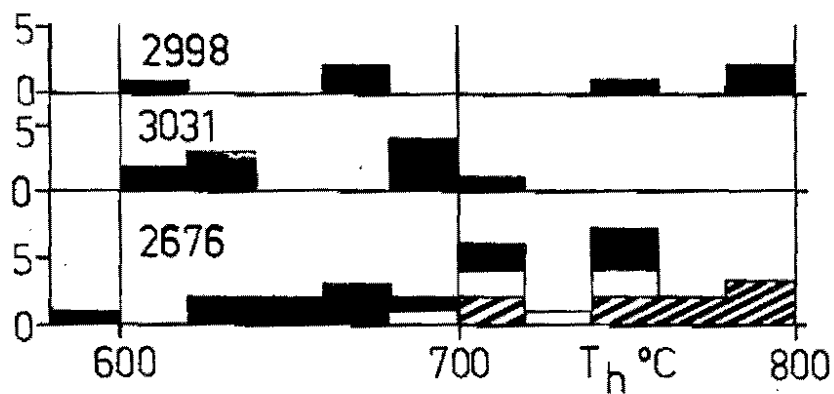
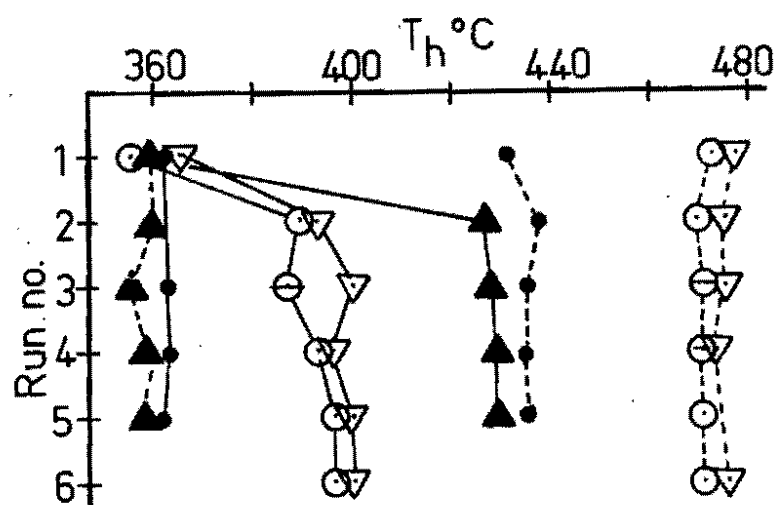
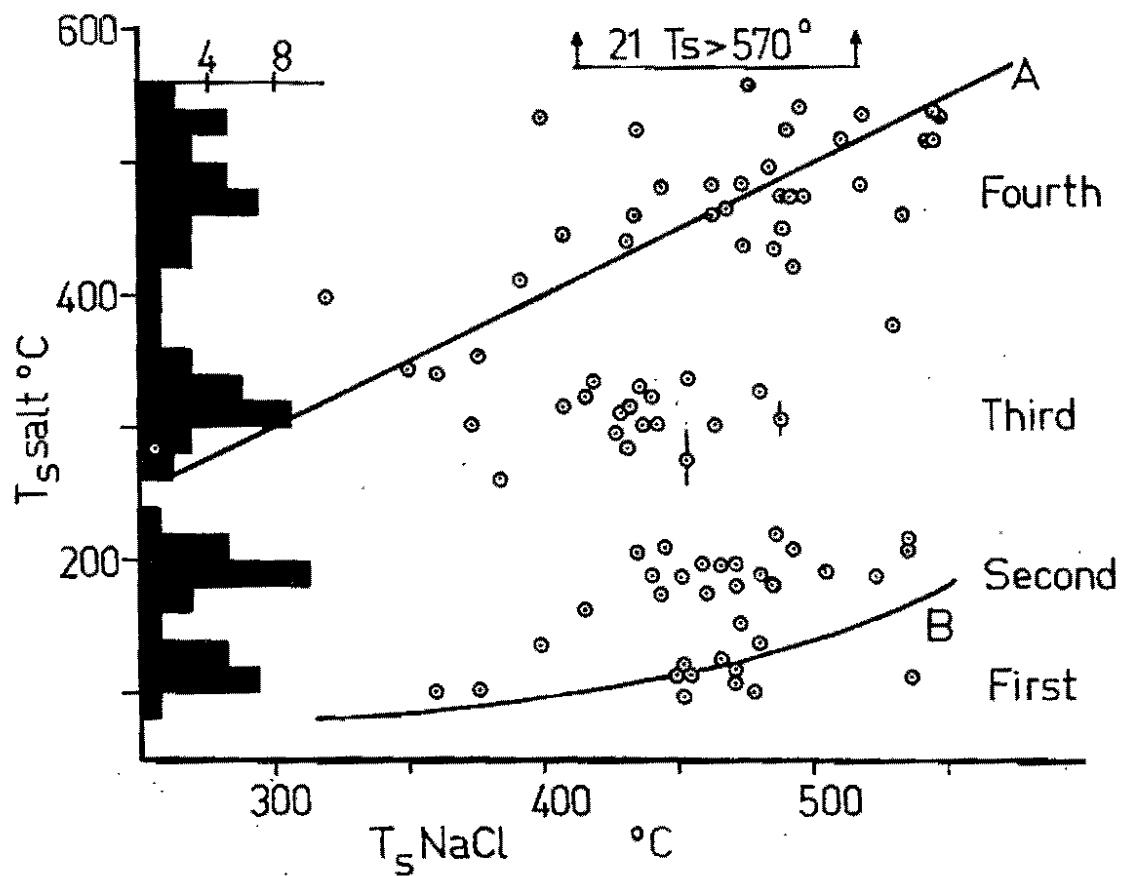
So there are at least three different salts, and there may be four or five.

None of the salts corresponding to the three lower modes appears to vary in solubility as a function of $T_S\text{NaCl}$. The points composing the fourth mode plot near or above the $T_S\text{NaCl}$ line. Because anhydrite is known to have been at or near saturation during mineralisation, this salt is tentatively identified as anhydrite. The optical properties of such daughter minerals - high birefringence, high relief, and the prismatic and diamond-shaped profiles (figs. 4-4 B, G, H) - are consistent with the properties of anhydrite. The links between optical properties and the other modes have been only tenuously established. The acicular salt (fig. 4-4 I) belongs in the first mode; the salts corresponding to the other modes are all birefringent and of higher refractive index than KCl.

Fig. 5-13 $T_{\text{Ssalt A}}$ vs T_{SNaCl} for type III inclusions. The points and the histogram are for salts A other than NaCl and KCl. Line A is $T_{\text{Ssalt A}} = T_{\text{SNaCl}}$; line B is $T_{\text{Ssalt A}} = T_{\text{SKCl}}$. The symbol "21 $T_{\text{S}} > 570^{\circ}\text{C}$ " indicates 21 salts A which did not dissolve by 570°C , and the T_{SNaCl} range in which these occurred.

Fig. 5-14 A metastability effect in type III inclusions. T_{h} and T_{SNaCl} are plotted as functions of the numbers of successive heating runs on four different inclusions. Solid lines are for T_{h} ; broken lines are for T_{SNaCl} . Each inclusion has a different symbol. A bar in a symbol indicates the uncertainty of a reading.

Fig. 5-15 T_{h} data greater than 580°C for specimens 2998, 3031 and 2676. The white and hatched areas in the lower histogram indicate distinct groups of neighbouring inclusions. The measurements were made on a Leitz 1350^o heating stage. The data are for inclusions with T_{SNaCl} data as given in fig.5-7 (T_{h} shown "> 580°C "). Specimen numbers are prefixed by 10 in the University of Tasmania catalogue.



TEMPERATURES FROM TYPE III INCLUSIONS

The behaviour of the inclusions. The broad spread of T_h readings for groups of inclusions giving a relatively narrow range of T_{SNaCl} suggests that the trapping of gas with salt-rich liquid may have been frequent in type III inclusions at Panguna. Necking down appears to be less important, as indicated by T_{SNaCl} measurements (fig. 5-6). Other difficulties which compromise the usefulness of T_h data from type III inclusions are described below.

A metastability effect has been noted. Up to seven successive heating experiments were performed on several inclusions which were allowed to cool to room temperature between each run and were heated at the same rate ($2 - 3^{\circ}\text{C}/\text{min}$) each time. For four such inclusions, T_{SNaCl} and T_h are plotted as a function of experiment number in fig. 5-14. T_h increased sharply at first in three cases, becoming constant after the third or fourth run, while T_{SNaCl} remained relatively constant in all cases. Most type III inclusions showed this effect, with the size of the initial increase variable. No leakage has been observed in conjunction with the increase in T_h , so that the increase is thought not to be due to minute fractures around the inclusions (suggested by Larson *et al.*, 1973). Another phenomenon which may be relevant is permanent viscous strain in the host crystal. Variation of the heating rate and the repetition of experiments over a long time (say, several months) after the initial series of runs might be useful in any further work on this aspect of fluid inclusion behaviour.

Another difficulty concerns the order-of-homogenisation phenomena. In an inclusion of a liquid trapped when it was in equilibrium with vapour, the bubble should disappear at a temperature no less than T_{SNaCl} . Such is the case at Panguna, generally, for veins with T_{SNaCl} modes $\leq 400^{\circ}\text{C}$

or with T_h readings greater than 580°C . For the rest of the veins, the bubble disappears before the halite during heating runs. The histograms in fig. 5-7 are laid out to illustrate the transition between NaCl-first and bubble-first homogenisation at $T_{\text{SNaCl}} \approx 400^{\circ}\text{C}$, and the change in behaviour where $T_h > 580^{\circ}\text{C}$. For veins with T_{SNaCl} near 400°C the difference between T_h and T_{SNaCl} is small, and there is a mixture of homogenisation orders. In veins with higher T_{SNaCl} the difference tends to be greater, and it is often consistent in a group of cognate inclusions (e.g. in 102662, where 25 secondary inclusions in one healed fracture gave $T_{\text{SNaCl}} = 426 \pm 10^{\circ}\text{C}$ and $T_h = 320 \pm 15^{\circ}\text{C}$ during one heating run). The problem of homogenisation order exists regardless of the metastability effect, which is of insufficient magnitude to reverse the order of homogenisation. The homogenisation-order phenomenon has been described previously, in particular by Touray (1970) who ascribed it to pressure effects - i.e. the difference $T_{\text{SNaCl}} - T_h$ is a minimum estimate of the pressure correction required for T_h . The occurrence of both homogenisation orders, systematically changing with salinity, and the acceptance of the boiling hypothesis, both rule this explanation out for Panguna.

Chivas & Wilkins (1977) have reported both metastability and homogenisation-order effects in specimens from the porphyry copper prospect at Koloula on Guadalcanal, southern Solomon Islands. They observed that prolonged heating caused T_h and T_{SNaCl} to converge (upwards and downwards respectively) to a common temperature, and suggested that an observed slow solution of quartz, changing the cavity volume and the solution composition, was responsible. Solution of the cavity walls would be sufficient only if the volume change accompanying the transition from quartz to dissolved silicate species resulted in a net increase in unfilled cavity volume. This would be plausible, in view of the structural "holes" present in salt melts (Bloom, 1967). However, the solution of

cavity walls has not been observed at Panguna, no change in $T_g\text{NaCl}$ has been seen to accompany an increase in T_h , and the order of homogenisation appears to be a function of formation temperature. Therefore the phenomena which have been observed at Panguna seem to require a more elaborate explanation than those at Koloula.

Solution of silica. The effect of dissolving SiO_2 on $T_g\text{NaCl}$ in a salt-rich liquid can be examined by means of the following rough calculation. Let us suppose that the solution of SiO_2 takes place according to the reaction



so that NaCl is removed, and HCl added, to the salt-rich liquid.

The maximum effect on the salt content is at $m = 1$, when the solution of 60 g SiO_2 takes up 117 g NaCl and 18 g H_2O . In 1 kg of salt-rich liquid (50% NaCl, 50% H_2O):

$$\text{after dissolving } n \text{ g } \text{SiO}_2, \text{ amount of salt remaining} = 500 - \frac{117n}{60} \text{ g}$$

$$\text{amount of water remaining} = 500 - \frac{18n}{60} \text{ g}$$

$$\text{new salinity, } S = \frac{500 - 117n/60}{1000 - n(117 + 18)/60} \times 100 \quad \% \text{ NaCl.}$$

n	S	n	S
1	49.9	10	49.1
2	49.8	15	48.7
5	49.6	20	48.3

From Keevil (1942), a decrease of 1% salinity at 50% NaCl corresponds with a decrease of about 11°C in $T_g\text{NaCl}$ - i.e. about 1% of SiO_2 in solution in the calculation above. The effect is smaller for a fixed amount of dissolved silica if $m > 1$, and the actual effect on $T_g\text{NaCl}$ may

be reduced because Na silicate species are substituted for NaCl in the liquid. If T_{SNaCl} is reproducible to say $\pm 2^{\circ}\text{C}$, it will be possible to dissolve more than 0.2% SiO_2 in the salt-rich liquid without significant change in T_{SNaCl} . Chivas & Wilkins did not report the size of the change of T_{SNaCl} in their serial heating runs.

Supersaturation. It is thought that the salt-rich liquids with $T_{\text{h}} < T_{\text{SNaCl}}$ were supersaturated at the time of trapping. The behaviour of type III inclusions on the heating stage is consistent with the possibility of supersaturation. In one case, it was found to be possible to cool a liquid with $T_{\text{SNaCl}} = 430^{\circ}\text{C}$ to 300°C and to hold it there for 24 hours without the crystallisation of halite. Halite in this case crystallised at $200 - 220^{\circ}\text{C}$, the temperature apparently depending little on the cooling rate (which could be varied easily by a factor of 10). Long-term supersaturation thus appears possible in salt-rich liquid, and is even more likely to occur where motion of the liquid inhibits the nucleation of solids. The likelihood of supersaturation will be discussed again in Chapter 9.

Interpretation of T_{h} data. Subject to the effects of metastability and original heterogeneity, T_{h} measurements on type III inclusions are the best estimates of formation temperature where $T_{\text{h}} \geq T_{\text{SNaCl}}$. This involves two sets of inclusions: those with $T_{\text{SNaCl}} \leq 400^{\circ}\text{C}$, and those with $T_{\text{h}} > 580^{\circ}\text{C}$. For those liquids thought to be supersaturated, T_{h} should also be a true estimate of the formation temperatures, subject to the same qualifications, and T_{SNaCl} a maximum estimate. For reasons which will emerge more fully in Chapter 9, the T_{h} modes of certain specimens as measured here seem to be too low. The low temperatures may be due to the metastability effect.

Frequency distribution histograms of T_h are presented in fig. 5-7. Few of these are based on enough data to give convincing modes, and the data commonly define very broad ranges. In 103026, 103022 and 103009 the histograms are skewed with tails to the high temperature side, as has been predicted for boiling systems (Chapter 3).

Upper temperature limit. A minimum trapping temperature of 580°C is indicated for associated groups of fluid inclusions in vein quartz in 102636, 102676, 102998, 103005, 103011, 103012, 103031 and 103047. For 102676, 102998 and 103031 attempts were made to measure the high T_h values on a Leitz 1350° heating stage. The histograms are given in fig. 5-15. From the data for 102998, it can be concluded only that the formation temperature was greater than 600°C ; for 103031, $600 - 720^{\circ}\text{C}$ is indicated. In the histogram for 102676, the white and hatched areas denote readings made on two discrete sets of inclusions, one of which formed at a temperature over 680°C and the other over 700°C . In all three specimens, some unmeasured T_h values would have been greater than 800°C (i.e. the bubbles persisted to 800°C at which temperature the heating runs were stopped). These are unlikely to be meaningful as formation temperatures if the veins were formed in solid andesite or diorite, because partial melting of the wallrock should begin at such temperatures (Wyllie, 1977). Rather, they are due to the incorporation of gas with salt-rich liquid, or necking down, or both. The distribution of inclusions with $T_h > 580^{\circ}\text{C}$ is shown in fig. 5-8.

Lower temperature limit. It has been noted (Chapter 3) that the history of certain parts of the deposit is complex, probably more complex than in other parts. A simple relationship between geology and fluid properties is therefore likely to be significant even if it does not apparently apply to the time-integrated data everywhere in the orebody,

and anomalies are probably attributable to the superposition of other generations of fluid. This reasoning is used in the following discussion.

The lower temperature limit of quartz-Cu,Fe sulphide veining is set by the group of veins with $T_g\text{NaCl}$ modes $\leq 400^\circ\text{C}$. Specimens 103003, 103017, 103026, 103035 and possibly 103037 have satisfactorily-defined T_h modes of 410° , 390° , 360° , 420° and 370°C respectively. On the basis of fewer data, 102666, 102668, 103002, 103028, 103032, 103033, 103034, 103036 and 103038 have T_h values in a similar range and these, together with 103003, 103026, 103035 and 103037 define a cooling zone bounding the deposit along its southern and southwestern margins and corresponding approximately with the outer 0.3% Cu contour there. Specimens 103008, 103017 and 103021 may represent the eastern edge of a different phase of mineralisation, different because their locus does not bound all quartz-Cu,Fe sulphide mineralisation in the eastern part of the deposit. Since the metastability effect has not been dealt with in this study, these temperatures are only approximate. Nonetheless, comparison with $T_g\text{NaCl}$ readings of other veins shows them likely to be the lowest formation temperatures in the deposit. On the evidence available, $350 - 430^\circ\text{C}$ is accepted as an estimate of the temperature at the edge of the deposit.

Temperature estimates independent of the fluid inclusion data.

From the study of sulphur isotope fractionation in coexisting anhydrite and chalcopryrite (see Chapter 11), 102676 gave $588 \pm 40^\circ\text{C}$ and 102675 (which is from a nearby vein in the same diamond drill hole) gave $797 \pm 70^\circ$, estimates which compare favourably with fluid inclusion temperatures of $600 - 700^\circ\text{C}$ or greater in quartz from 102676. Ayres *et al.* (in press) have presented additional sulphur isotope temperatures of 350 and 520°C for anhydrite-chalcopryrite pairs (these

are reinterpreted in Chapter 11). Together, the sulphur isotope temperatures span the whole fluid inclusion temperature range for the quartz-Cu,Fe sulphide mineralisation.

Another independent temperature estimate, derived from the compositions of hydrothermal biotites (the method of Beane, 1974) was presented by Ford (1976) who analysed biotite separates for Fe^{2+} and Fe^{3+} by wet chemical techniques. The temperature range was 370 - 540°C, again comparing reasonably with the fluid inclusion data. Beane, however, devised his method for biotites coexisting with magnetite and sanidine. It seems likely, however, that hematite (rather than magnetite) coexists with biotite at Panguna. There is textural evidence for this in 103012, in which a small red flake, similar to others thought to be hematite, makes up a composite solid inclusion with a flake of biotite. This is despite the experimental results of Eugster & Wones (1962) who showed hematite, sanidine and annite to be an unstable assemblage above about 400°C, at pressures below 1 kb. Panguna biotites are not, of course, pure annite. If the compositions (from Ford, 1976) are expressed in terms of the three end-members annite, phlogopite and proton-deficient oxyannite, the activity of annite is 3.5×10^{-3} (Beane, 1974). But there is also a large contribution from a titaniferous end-member (Ford's microprobe analyses indicate up to 4.2% TiO_2). Somewhere between these difficulties may lie the reason for the coexistence of biotite and hematite at Panguna. This undoubtedly affects Beane's method, but the size of the effect is not known.

LEACHING STUDIES OF VEIN QUARTZ

Samples from six quartz-Cu,Fe sulphide veins and one quartz-pyrite vein were carefully selected so as to be as free as possible of impurities. The chief impurities, once the selvage has been carefully removed, are anhydrite and Cu,Fe sulphides. There are also the isotropic, colourless inclusions described (Chapter 4) in certain specimens; these, depending on their composition, could seriously limit the value of the data obtained by this method. Alkali feldspar crystals detached from the selvage were observed in a few samples (e.g. 103001). Denis (1974) established that these are a major source of error in the determination of K/Na ratios. In addition, biotite, hematite and rutile may be present in very minute quantities.

The crushing, leaching and leachate analyses were carried out in the laboratories of the Centre de Recherches Pétrographiques et Géochimiques in Nancy, France. The method is basically that described by Poty *et al.* (1974) but the techniques were modified by M. Denis and B. Charoy in order to deal with the possible presence of small amounts of alkali feldspar. The process was as follows:

- (i) Careful examination and selection of pure quartz by hand.
- (ii) Samples of about 20 g were placed in cold concentrated HF for two hours. This treatment removes alkali feldspar more readily than it removes quartz from a mixture of the two minerals. The samples were then:
- (iii) Boiled for two hours in HNO_3 ,
- (iv) boiled for two hours in deionised distilled water,
- (v) placed in circulating deionised distilled water in contact with an ion-exchange resin for four days,
- (vi) placed in stainless steel tubes (cleaned by a similar process to steps iii-v) and crushed inside the tubes under a heavy-duty press.

(vii) leached with 60 ml deionised water. Millipore filtration was used to collect the leachate. Before each crushing and leaching a control blank solution was prepared by leaching the uncrushed quartz in the stainless steel tube. The blank was also filtered.

The leachates and control blanks were analysed for Na, K, Ca, Mg and Fe by atomic absorption spectrophotometry and for Cl and SO_4 by colorimetry. No carbonate determinations were made because the leachates were exposed to the atmosphere during preparation.

Denis (1974) tested the method by varying the grain size of the samples at the cleaning stage, by varying the volume of the leachate, by omitting the HF stage, by performing second leachings on certain samples of crushed quartz and by performing duplicate runs on different pieces of quartz from the same sample. The method outlined above embodies his findings; in particular it is worth noting that no difference in K/Na ratio was observed between first and second leachates on a given crushed sample. Denis (pers. comm.) recommended that at least five samples be done for each specimen in order to ensure that the results are valid. There was, however, sufficient quartz for only two runs on each of the vein specimens from Panguna except for 103046 where there was only enough for one.

Sample 103046 contained pyrite, even after the selection of material. During the cleaning in boiling HNO_3 , this became oxidised to S which had to be removed by further oxidation to SO_4 . Hence the SO_4 analysis for this specimen is regarded as unreliable. The analytical data and their ratios are set out in Table 5-4., alongside comparable micro-thermometric data. There is no way of separating out the contributions of the ubiquitous type I and II inclusions, but because of the abundance and high salinity of the type III inclusions theirs is thought to be the dominant ion contribution to the leachate. This is one of the assumptions

Table 5-4

ANALYSES OF FLUIDS LEACHED FROM CRUSHED QUARTZ

Tas. Uni. Number	CRPG No.	Analyses of leachates							Ratios (in ionic proportions)						K/Na		Ion Sums*	
		Na ppm	K ppm	Ca ppm	Mg ppm	Fe ppm	SO ₄ ppm	Cl ppm	Ca/Na	Fe/Na	Ca/SO ₄	Cl/SO ₄	Na/Cl	Leachate	T _S Data	Σ ⁺ averaged	Σ ⁻ averaged	
103031	675	11.22	5.43	0.87	0.20	3.26	3.30	32.75	0.05	0.12	0.63	26.80	0.53	0.28	0.26	0.87	0.98	
	676	14.93	7.16	1.12	0.15	4.67	4.00	44.38	0.05	0.13	0.58	29.96	0.52	0.28				
103012	677	9.45	4.41	0.14	0.30	2.23	3.00	24.00	0.01	0.10	0.11	21.60	0.61	0.27	0.28	0.66	0.74	
	678	5.59	2.72	0.23	0.16	1.13	2.80	14.90	0.03	0.08	0.20	14.37	0.58	0.28				
103007	679	3.23	1.45	0.17	0.10	N.D.	1.98	10.44	0.03	-	0.21	14.24	0.48	0.26	0.31	0.38	0.62	
	680	2.88	1.22	0.34	0.03		0.86	9.34	0.08		0.95	29.32	0.47	0.25				
103029	688	4.48	1.07	0.66	0.07	1.16	1.96	11.00	0.10	0.11	0.81	15.15	0.63	0.14	0.20	0.30	0.34	
	689	4.63	1.07	0.30	0.14	0.99	1.95	11.44	0.04	0.09	0.37	15.84	0.62	0.14				
103028	690	0.51	0.22	0.65	0.00	0.11	0.97	2.35	0.83	0.09	1.61	6.54	0.33	0.25		0.125	0.153	
	691	0.95	0.39	0.04	0.01	<0.10	1.90	2.00	0.03	<0.04	0.05	2.84	0.73	0.24				
102997	692	17.6	10.4	0.96	0.11	7.77	3.50	51.75	0.04	0.18	0.66	39.92	0.52	0.35	0.29	2.88	2.98	
	693	16.75	10.1	0.83	0.13	6.33	4.50	48.35	0.03	0.15	0.44	29.01	0.53	0.35				
103046	694	0.85	0.25	0.30	0.00	0.15	‡	4.70	0.24	0.07	-	-	0.28	0.17		0.068	0.132	
	BLANKS	0.00	0.00	0.00	0.00													
		-0.03	-0.01	-0.04	-0.01													

* Units: $\frac{\text{ppm}}{\text{atomic weight}}$ x valency

Weight of quartz sample: 20g approx.
 Volume of leachate : 60 ml
 Analytical precision : Better than ± 0.1 ppm
 for all elements
 CRPG No. refers to the catalogue of leachate
 analyses kept at the Centre de Recherches
 Pétrographiques et Géochimiques, Nancy, France.

‡ SO₄ not determined: oxidation
 of pyrite during cleaning led
 to contamination.

Σ⁺, - sums of positive, negative
 charge, assuming all Fe to be
 Fe³⁺

tested in the comparison between the microthermometric and leach-analysis K/Na ratios.

The K/Na ratios are consistent for each pair of analyses. Low K/Na ratios (< 0.20) occur in 103029 and 103046 in which type II inclusions are very much more abundant than other types. For the rest of the samples, in which the analytical data should reflect mainly type III inclusions, the K/Na ratios range between 0.24 and 0.35.

The Na/Cl ratio is consistent for each pair except for 103028, so that in general, Na and Cl are suitable standards with which to compare the other ions. Less consistency within pairs is shown by the other ionic ratios, particularly those involving SO_4 . The presence of microscopic solid anhydrite inclusions in the quartz might be expected to affect the analyses of Ca and SO_4 . The Ca/ SO_4 ratio ought to tend to unity in this case, but is actually usually much less. This indicates contributions from sulphate species other than anhydrite - either the oxidation products of sulphides, or other daughter-salt sulphates.

Na, K and Fe are the predominant cations in the leachate and Cl is the predominant anion. If the positive and negative charge sums (measured arbitrarily as analysis in ppm \times valency/formula weight) are compared, a consistent deficiency in cations is revealed. The positive charge sum includes all Fe as Fe^{3+} , and the negative charge sum may be low because CO_3 has not been considered. Either factor, if a source of error, would bring about a larger deficiency than that reported here. Presumably, other cations must be involved, probably mainly H. The electron microprobe analyses of daughter minerals show perceptible Mn also, but in relatively minor amounts. If it is assumed that the total deficiency is accounted for by H, then the $\log \text{K/H}$ and $\log \text{Na/H}$ (ionic proportions) of the leachates are less than 0.5. According to data for 1 kb (Montoya & Hemley, 1975) such ratios are quite inconsistent with the

silicate alteration assemblages seen in the vein selvages. Albite occurs at about 400°C, and sanidine and sericite, or sanidine only, at temperatures up to and beyond 600°C. It seems likely, therefore, that the leach-ratio deficiencies do not give a valid measure of the acidity of the fluid in the type III inclusions. If the acidity of the leachate were due to contributions from the vapour phase, into which HCl would be fractionated preferentially, this would imply disequilibrium between one fluid, most likely the vapour, and the silicates. If liquid and vapour were both in equilibrium with the silicate assemblages, both should have the same alkali:H ratios.

It seems inconceivable that any other ion, even Mn, should make up most of the deficiency in cations. If the missing ions are H, then the silicate mineralogy implies a large excess of this species in the inclusions. Clearly, the properties of the original salt-rich liquid are not consistent with those of the leachate. A change may have occurred in the ionic composition since crushing; this would necessarily take place by ion exchange. The size of the cation deficiency therefore casts a great deal of doubt on the value of these analyses. The only conclusions in which any confidence is justified are:

- (i) the presence of soluble Fe as a main constituent of the fluids, along with Na, K and Cl.
- (ii) there are two cases of close agreement between K/Na ratios obtained by leaching and by microthermometry.

SUMMARY

The temperatures of the salt-rich liquids have been specified approximately, and only at the extremes. Despite the difficulties, it can be seen in fig. 5-8 that the T_h and T_{NaCl} distributions are similar

in being asymmetric with respect to the copper mineralisation and in having the same central ridge. They are dissimilar in that the high temperatures along the northern margin of the orebody and in the area around the Leucocratic Quartz Diorite are not matched by salinities as high as those along the central ridge. The spatial distribution of phase behaviour (homogenisation order) in type III inclusions can also be seen from fig. 5-8 to resemble T_s and T_h distributions. The patterns of T_h and T_{sNaCl} data are not simple; one way of explaining this is to postulate several mineralising events, as suggested also by field observations of the veins. This, the mechanisms of the chemical variation of the salt-rich liquid and the relationship of the fluid inclusion data to the known properties of simple salt-water systems will all be discussed in subsequent chapters.

CHAPTER SIX: FLUID INCLUSION STUDIES IN HOSTS OTHER THAN QUARTZ-
Cu,Fe SULPHIDE VEINS

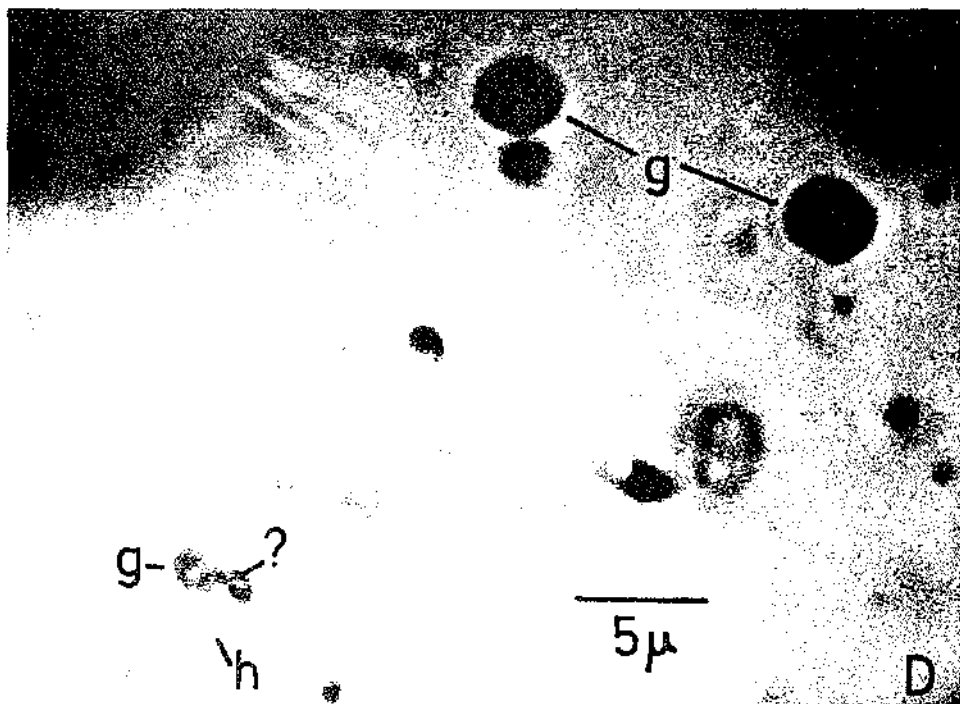
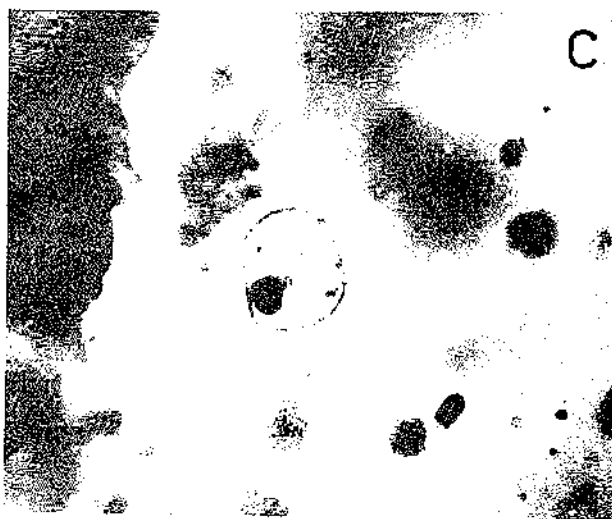
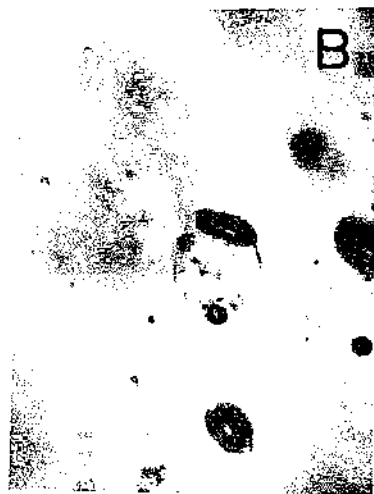
QUARTZ PHENOCRYSTS

Samples with quartz phenocrysts were taken from the Biotite Granodiorite, from an Intrusive Breccia, from a Feldspar-Quartz Porphyry dyke cutting the Biotite Granodiorite and from the Biuro Granodiorite. All phenocrysts contain fluid inclusions of types I, II and III and the suite of solid inclusions described in Chapter 3. Type II inclusions are more abundant than type III, and type I inclusions are variable in abundance, usually less common still. Primary type II inclusions are found adhering to solid inclusions of glass and Cu,Fe sulphide (fig. 4-5, 6-1). Definite primary type III inclusions are rare, and are again associated with solid inclusions (fig. 4-5). Many phenocrysts exhibit one prominent growth zone (commonly near the rim) marked by plentiful glass and primary type II inclusions. A few type III inclusions may also be associated with these zones.

It seems from the fluid inclusion assemblages that three fluids - silicate liquid, salt-rich liquid and vapour - coexisted in the Biotite Granodiorite magma at the level of the ore-zone. In the other intrusions, only vapour and silicate liquid are proven to have coexisted, although salt-rich liquid is present as inclusions of indeterminate habit. Fluid and solid inclusions are much less abundant in quartz phenocrysts from the Biuro Granodiorite than from phenocrysts in the Biotite Granodiorite and its associated intrusive phases. The presence in the phenocrysts of solid inclusions of Cu,Fe sulphide, (?) anhydrite and hematite, all characteristic hydrothermal solid inclusions at Panguna, suggests that some of the quartz in the phenocrysts may have been deposited from the

Fig. 6-1 Photomicrographs of inclusions.

- A. A silicate solid inclusion, originally probably glass, from a quartz phenocryst in 103001. The dark objects are gas-rich inclusions.
- B. The same inclusion after heating to 950°C. The rim has melted, and the gas-rich inclusions have coalesced and become rounded.
- C. Another silicate solid inclusion from the same phenocryst in 103001, after heating to 950°C.
- D. Type II and III inclusions in quartz from an amphibole-bearing vein, 103049. g = gas, h = halite.



salt-rich liquid. In the same way, the glass inclusions suggest the deposition of igneous quartz. This indicates the presence of several fluids at equilibrium, all saturated with respect to silica.

The prominent growth-zones marked by glass and type II inclusions may represent a sudden change in physical conditions - perhaps a pressure release - causing the evolution of vapour.

Temperatures were measured for type III inclusions from 103001, 103011 and 103015 (Biotite Granodiorite), 103006 (Intrusive Breccia) and 103021 (Quartz-Feldspar Porphyry). In each case the phenocrysts were taken from near quartz veins, so that salt-rich liquid from the veins could have been preserved as secondary inclusions in the phenocrysts. The T_{SNaCl} values in vein and phenocryst are essentially indistinguishable in 103006 and 103011, but one of the inclusions in the phenocryst in 103001 is apparently primary. For 103001, 103015 and 103021 the T_{SNaCl} values are distinct in vein and phenocryst; in 103001 the distinction is reinforced by the presence of a primary inclusion in the phenocryst and a difference in T_{h} values (cf. figs. 5-6 and 6-2).

The T_{SNaCl} range of salt-rich liquids from the phenocrysts is broad, 400 - 560°C to include most T_{SNaCl} data (fig. 6-2). Paired (T_{SNaCl} , T_{SKCl}) readings were obtained for seven inclusions, three of them in 103006. These are plotted with (T_{SKCl} , T_{SNaCl}) data from quartz-Cu,Fe sulphide veins in fig. 5-10 and all data conform to the same trend. Likewise, $T_{\text{Ssalt A}}$ data from the phenocrysts conform to the patterns established for the veins (fig. 5-13). Two cases where $T_{\text{Ssalt A}}$ exceeded 580°C were noted.

T_{h} readings also covered a broad range. They were generally less than T_{SNaCl} in 103006, 103011 and 103021. In 103001 and 103015 all T_{h} values were beyond the range of the Chaixmeca apparatus (>580°C). However, four type III inclusions in a phenocryst from 103001 were

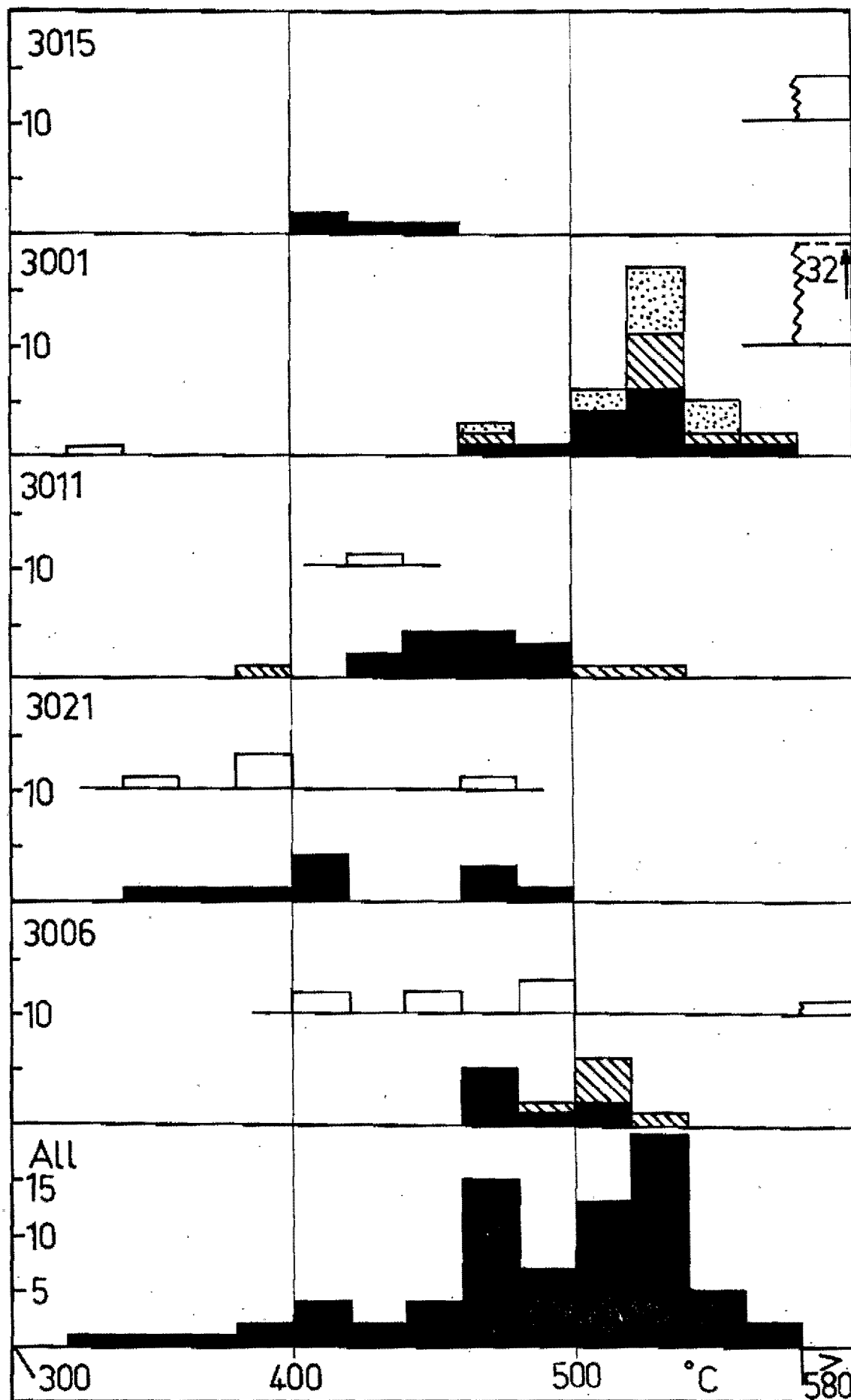


Fig. 6-2 Data from type III inclusions in quartz phenocrysts. Specimen numbers, shown at top left of each part, are prefixed by 10 in the University of Tasmania catalogue. Th data are shown as white columns, TsNaCl as black or patterned columns. The patterns distinguish data from different phenocrysts.

Table 6-1

ANALYSES OF A SOLID INCLUSION IN A QUARTZ PHENOCRYST FROM 103001

	Core (poorly polished)		Half way to rim	
Na ₂ O	2.32	0.41	11.34	1.93
Al ₂ O ₃	19.03	2.02	20.05	2.07
SiO ₂	66.68	6.01	67.58	5.93
K ₂ O	10.85	1.25	0.47	0.05
CaO	1.12	0.11	0.56	0.05
Total (pre-normalisation)	91.30	9.80	98.10	10.03
	Half way to rim		Rim	
Na ₂ O	7.14	1.23	11.23	1.91
Al ₂ O ₃	19.39	2.04	20.41	2.11
SiO ₂	67.02	5.97	66.81	5.87
K ₂ O	5.89	0.67	0.43	0.05
CaO	0.56	0.05	1.11	0.10
Totals	101.10	9.96	100.60	10.05

Left hand columns: weight percentages.

Right hand columns: molecular proportions (per 16 oxygens).

examined on the heating stage of the C.S.I.R.O. Minerals Research Laboratories by Dr. P.J. Eadington, who obtained T_h readings of 944, 945, 1023 and 1023°C. At such temperatures, the solid inclusions thought to be devitrified glass were observed to melt around the edges, and bubbles in or on the surface of one of them disappeared. Other bubbles on the surface became rounded. The inclusion in fig. 6-1 was heated briefly to 950°C, so must have begun to melt at a lower temperature. The surface bubbles are thought to have been magmatic vapour attached to the impurity on the surface of the growing quartz phenocryst. Near the bubbles, therefore, the included silicate material would be melting in the presence of water and quartz.

The phase diagram of muscovite granite - H₂O (Wyllie, 1977, fig. 6) is appropriate for the compositions of the Panguna intrusive rocks. At 800 - 1000 bars, the likely pressure of crystallisation of the plutons (the lithostatic pressure corresponding to a hydrostatic pressure of 300 bars), quartz crystallises at temperatures below 800°C. Thus the type III fluid inclusions are indicating unreasonably high temperatures. It is not known whether quartz can contain fluid tightly at these high temperatures. As for the silicate solid inclusions, they too may be indicating unreasonable temperatures in that very little melting has taken place by 950°C. They may not, in fact, represent the melt composition at all. One of them, exposed on the surface of the polished section, was analysed in detail on the electron microprobe and found to contain sodic alkali feldspar with a potassic core (Table 6-1). There was no excess silica (this may have diffused into the host) and no concentration of Ca, Fe or Mg at the polished section. Diffusion appears to have separated Na from K within the inclusion.

The measurements do not help greatly in establishing the temperature of formation of the quartz phenocryst. The only indisputable observation

is that type III inclusions in this phenocryst as a group have much higher minimum T_h values than the groups of type III inclusions examined in vein quartz.

In the light of the discussion in Chapter 5, it seems unlikely that fluid inclusions with $T_h < T_{\text{SNaCl}}$ could have been trapped under magmatic conditions. Thus only the salt-rich liquids in 103001 and 103015 remain as candidates for salt-rich liquid in equilibrium with magma.

The similar chemical variation patterns of the salt-rich liquids from the quartz phenocrysts and the quartz-Cu,Fe sulphide veins, and the occurrence of primary inclusions as described above, strongly suggest that some, at least, of the liquids share a common origin, namely within the magmas of the intrusive suite at Panguna. In addition, the occurrence in phenocrysts of Cu,Fe sulphides both as solid inclusions and as trapped or daughter-mineral phases in type III inclusions indicates the association of magmatic salt-rich liquid and copper.

AMPHIBOLE-MAGNETITE-QUARTZ VEINS

A single specimen, 103049, was studied for fluid inclusions. The amphibole contains abundant type II inclusions and rare reddish solid inclusions (hematite ?). The quartz also contains these, and less abundant type I and type III inclusions. No definite primary or secondary inclusions were identified. The data are presented in fig. 6-3.

Type I inclusions homogenised at $330 \pm 10^\circ\text{C}$. The salinity was 0 - 3% eq. NaCl, corresponding to a T_f range of 0 to -1.8°C . For a formation pressure of 300 bars the pressure correction is $15 - 20^\circ\text{C}$ (Potter, 1978) so that the trapping temperature of these fluids was $348 \pm 13^\circ\text{C}$.

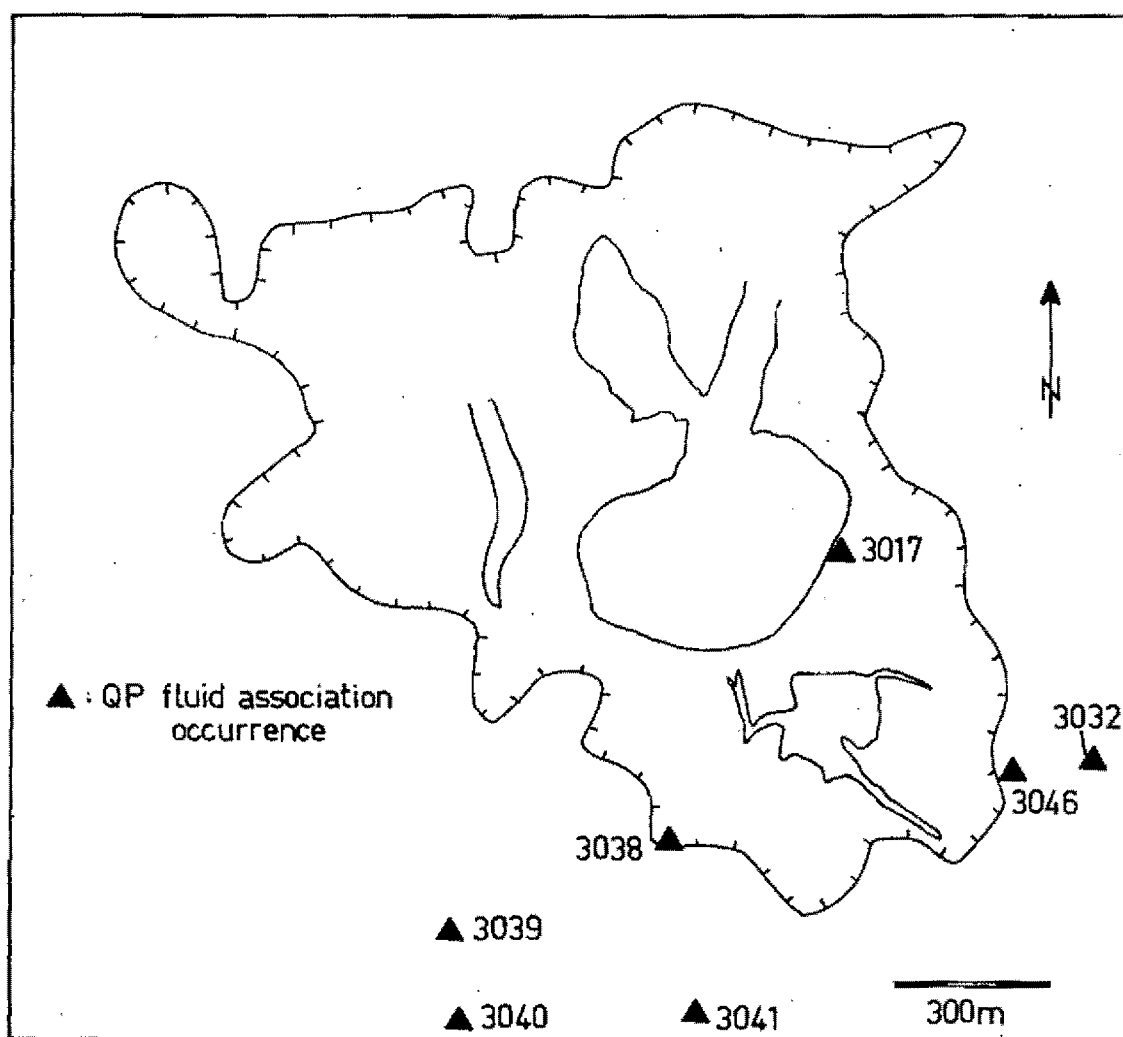
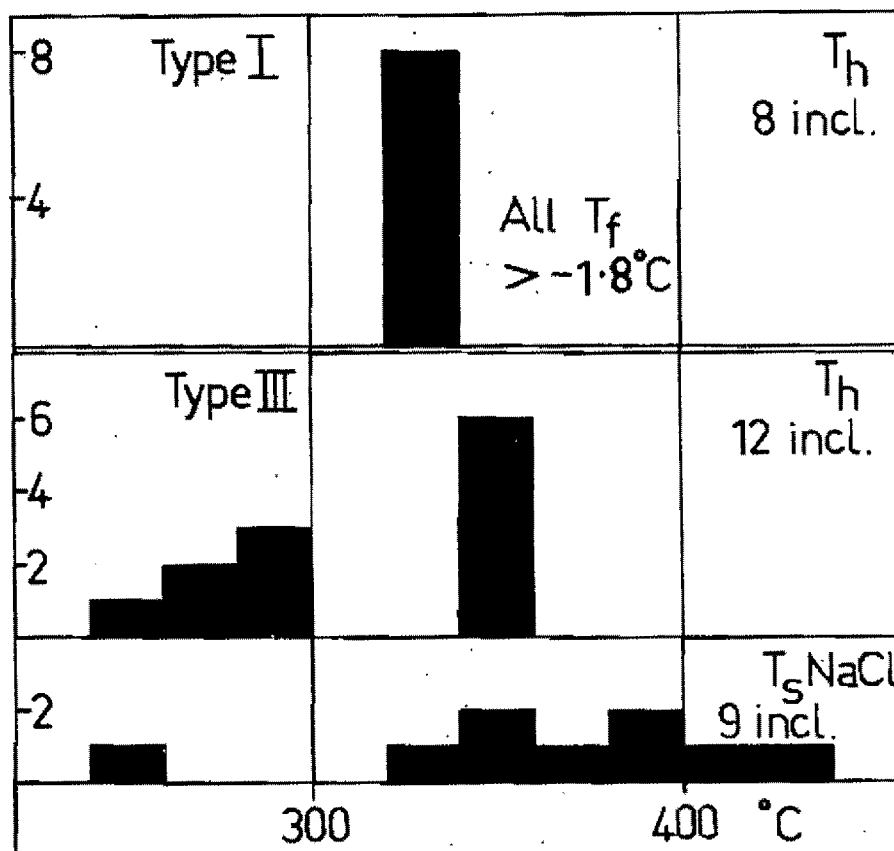
Type III inclusions have nucleated only one daughter mineral, which appears to be halite. The salt-rich liquid may have been boiling, because one gas-rich inclusion of composition intermediate between types II and III was observed. The data from type III inclusions are heterogeneous, and of little help in specifying the properties of a single fluid. The T_{SNaCl} range is 320 - 440°C, and this gives maximum formation temperature estimates for the inclusions since $T_{\text{h}} < T_{\text{SNaCl}}$ in all but one inclusion, i.e. the liquids were probably supersaturated. This behaviour differs from that of type III inclusions in quartz-Cu,Fe sulphide veins in which T_{h} is generally greater than T_{SNaCl} in inclusions with $T_{\text{SNaCl}} < 400^\circ\text{C}$. This vein may have formed from a boiling salt-rich liquid. Alternatively, the deposition of the vein minerals may have been a high temperature pneumatolytic event, (accounting for the abundance of type II inclusions in the amphibole) the salt-rich liquid in the quartz having been incorporated during later copper mineralisation. The salt-rich liquid does not, however, resemble salt-rich liquids from quartz-Cu,Fe sulphide veins, either in the daughter salts observed, or in homogenisation order. Ford & Green (1977) suggested a temperature of 600 - 650°C, based on the $\delta^{18}\text{O}$ of the quartz, for another of these veins.

QUARTZ-PYRITE VEINS

All quartz-pyrite veins contain type I inclusions, and some contain types II and III. In specimens 103015 and 103028 it was possible to distinguish two generations of quartz filling the one fracture. The younger generation in each case was associated with pyrite and contained only type I inclusions, and the older contained fluid and solid inclusions typical of quartz-Cu,Fe sulphide veins. Other quartz-pyrite veins were distinguished from quartz-Cu,Fe sulphide veins by the presence

Fig. 6-3 Fluid inclusion data from type I and III inclusions
in quartz from in the amphibole-bearing vein 103049.

Fig. 6-4 The distribution of QP association fluids (see text
for explanation). Geological contacts and the outer
0.3% Cu contour are as in fig. 2-3.



of a special association of types I and II inclusions exhibiting various homogenisation phenomena at temperatures largely over 360°C . These phenomena include the following, which are characteristic of fluids homogenising at or near the critical point (see Yermakov, 1965, p.364 ff.).

For type I inclusions:

1. $T_h > 360^{\circ}\text{C}$, bubble diminishes rapidly just before homogenisation to liquid.
2. Homogenisation at the critical point.
3. Liquid boils just before homogenisation to gas.

and for type II inclusions:

4. Homogenisation to gas, largely at $360 - 420^{\circ}\text{C}$; liquid diminishes rapidly just before homogenisation.

In addition, there are type I inclusions with homogenisation temperatures up to 520°C . These homogenise by a gradual decrease in the volume of the bubble.

The veins which contain such inclusions (fluids termed the QP association from here on) were found only in specimens 103017, 103032, 103038, 103039, 103040, 103041 and 103046 (fig. 6-4). These have been interpreted as forming an arc encircling the Leucocratic Quartz Diorite (Eastoe, 1978), but an alternative interpretation should also be considered. This considers 103039, 103040 and possibly 103041 to belong to another group, possibly an earlier halo. In Chapter 9, reasons for favouring this alternative interpretation are discussed. Type I inclusions of lower homogenisation temperatures and type III inclusions are usually also present in veins bearing QP association inclusions. In 103017, type III inclusions bearing hematite are found in those parts of the quartz unaffected by the dense swarms of healed fractures with QP association inclusions. Solid inclusions of hematite have been observed

in the quartz, much of which was therefore probably deposited by salt-rich liquid. Type III inclusions in the rest of the quartz could have been destroyed during the intense fracturing. The QP association fluids may be associated with a later generation of lustrous pyrite crystals and quartz with very small, primary type II (?) inclusions along the growth zones. The later minerals were deposited on to a pre-existing vein, probably a quartz-Cu,Fe sulphide vein.

Salinity. Relatively few type I inclusions were large enough for freezing experiments. The points plotted in fig. 6-5 are individual (T_h, T_f) pairs distinguished according to specimen and to vein type (as suggested in Chapter 2, the "quartz-pyrite" classification may comprise three vein types: veins from outside the deposit, those bearing QP association fluids and others from within the deposit but bearing no QP association fluids).

Quartz-pyrite veins from outside the deposit contain mainly waters with T_f ranges of 0 to -2°C and $< -16^{\circ}\text{C}$, i.e. 0 - 3% and $> 20\%$ eq. NaCl respectively (fig. 6-5, square symbols). Certain inclusions have T_f values below -21.1°C ; these may contain salts other than NaCl. Specimen 103015 (within the deposit, but without QP fluids) gave T_f readings grouped around -4°C ($\sim 7\%$ eq. NaCl). QP association inclusions which homogenised to liquid gave T_f readings in the range -5°C to -20°C and lower (8 to $>22\%$ eq. NaCl). For inclusions which homogenised at the critical point, there are conflicting indications of salinity. A T_c -range of $370 - 420^{\circ}\text{C}$ implies salinities of 0 - 4% eq. NaCl, but T_f readings on two such inclusions (in 103017 and 103040) were -15°C and $-22 \pm 3^{\circ}\text{C}$, implying very much higher salinities in terms of the system NaCl-H₂O. While small amounts of divalent ion in solution may radically affect the freezing properties of such solutions, the critical point data of Marshall & Jones (1974) suggest that divalent ions will have only a small

effect on critical phenomena. Salinity estimates based on T_c are therefore regarded as more reliable than those based on T_f . Inclusions homogenising to gas at $T_h < 400^\circ\text{C}$ must contain less than 3% eq. NaCl (Sourirajan & Kennedy, 1962).

Temperatures. T_h histograms are presented in fig. 6-6. The quartz-pyrite veins from outside the deposit all contain inclusions which homogenised at $T_h < 320^\circ\text{C}$. Only 103045 contains a significant number of inclusions homogenising at higher temperatures. 103015 from the pit contains primary inclusions homogenising at $300 - 330^\circ\text{C}$. For these, for the T_h readings for veins from outside the deposit and probably for the lower-temperature inclusions from 103017 and 103032 (for which there are no salinity estimates), the pressure corrections are given in Table 5-1.

The temperatures of formation of the QP association are best discussed in the light of the arguments presented in Chapter 9. The temperatures of critical and near-critical phenomena are at worst minimum estimates of the formation temperatures of the fluid inclusions concerned, but they may well be true estimates. The liquids of higher salinity and higher T_h (as in 103017) formed at higher temperatures. The histogram for 103017 indicates many T_h readings in the range $400 - 460^\circ\text{C}$, and a "tail" of higher values stretching off beyond 500°C . This "tail" suggests that the liquids may have been boiling, and thus that the more common T_h readings below 460°C may be true formation temperatures. The decrepitation temperatures of QP association inclusions in 103017 are $560 - 570^\circ\text{C}$.

Relationship with type I inclusions from quartz-Cu,Fe sulphide veins.

The broken line in fig. 6-5 encompasses the field of T_h , T_f data for quartz-Cu,Fe sulphide veins (from fig. 5-1). Except for four inclusions from 103043 with $T_f < -24^\circ\text{C}$, all (T_h , T_f) points for veins outside the

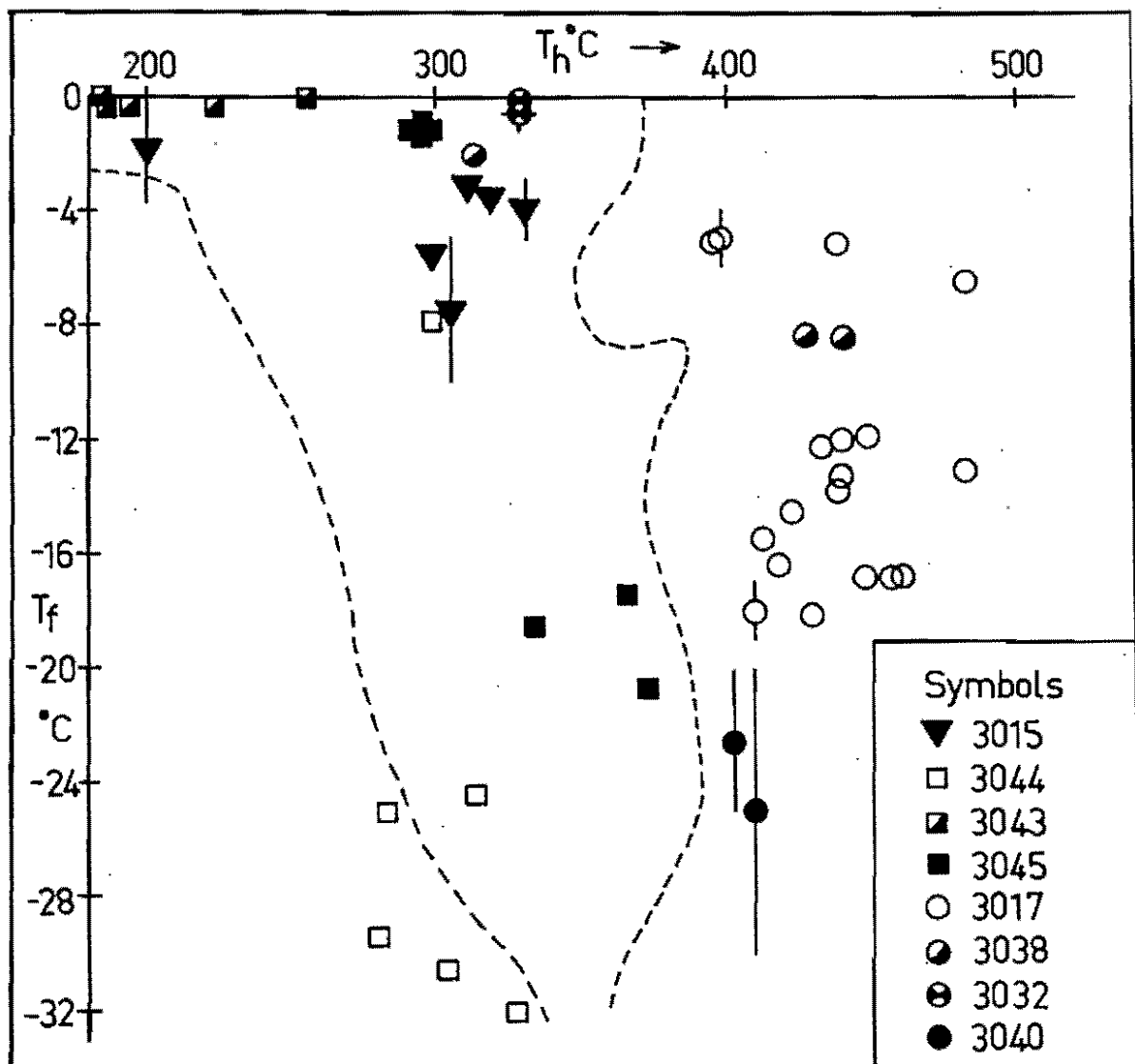


Fig. 6-5 T_h data vs. T_f data for type I inclusions from quartz-pyrite veins. Each symbol corresponds to a single specimen; the specimen numbers in the legend are prefixed by 10 in the University of Tasmania catalogue. Bars give the uncertainty of data. The dashed line encompasses the field of data from type I inclusions in quartz-Cu,Fe sulphide veins.

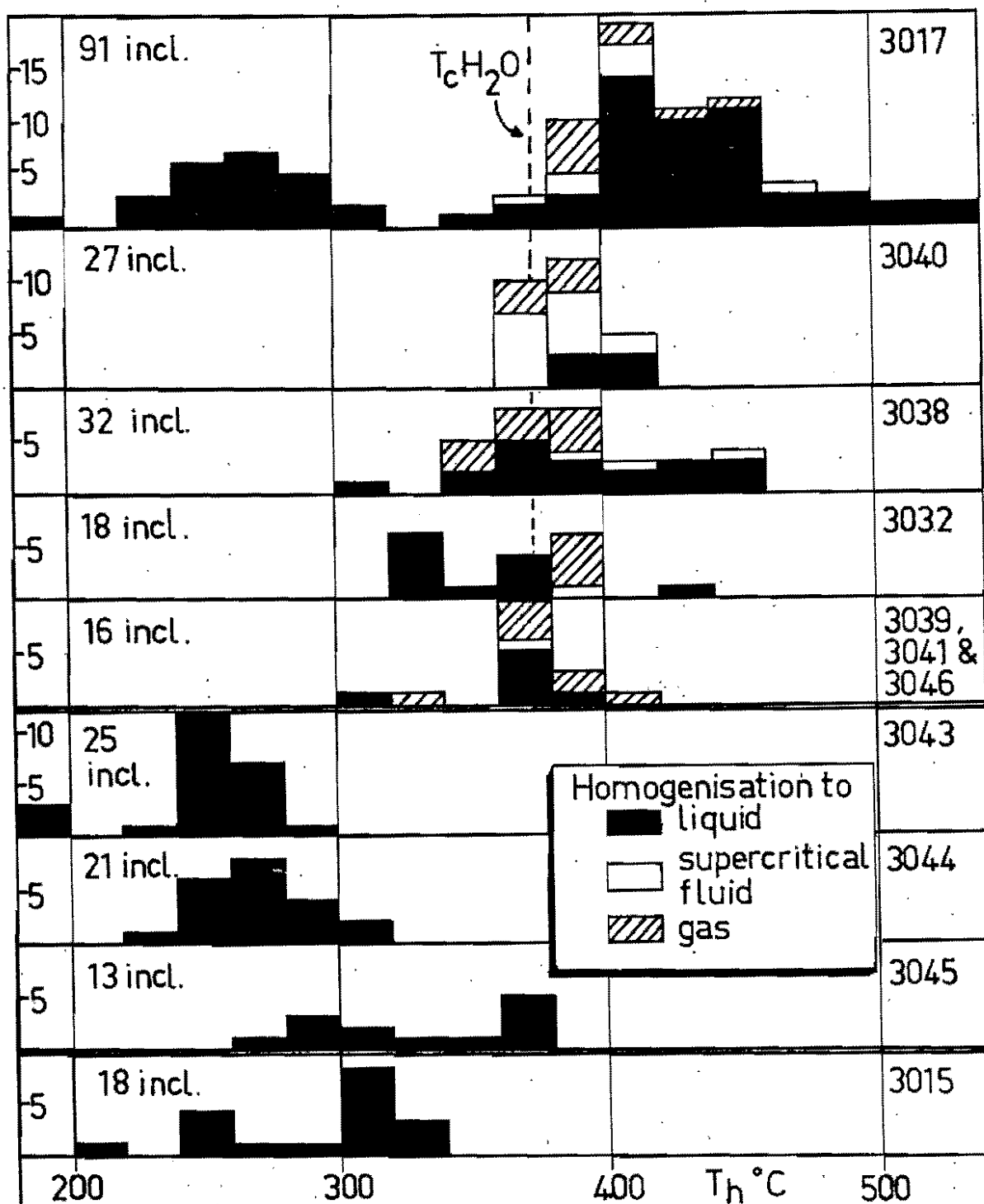


Fig. 6-6 Histograms of T_h data for type I inclusions (and a few type II) from quartz-pyrite veins. The top five histograms are for specimens bearing QP association fluid inclusions (see text). The critical temperature of water is indicated. 3043-3045 are specimens from outside the ore-zone, and 3015 from within the ore-zone. Specimen numbers are prefixed by 10 in the University of Tasmania catalogue.

deposit and for 103015 within the deposit also lie in this field. The QP fluid association plots outside the field, on the high temperature side, but differs from the fluids in other type I inclusions only in temperature. Therefore the QP association could be the result of heating of fluids like those preserved in type I inclusions in quartz-Cu,Fe sulphide veins. The higher salinities (and T_h measurements) in QP association fluids may have resulted from the boiling of less-saline waters.

PYRITE ± BLEACHED SELVAGE

Although this vein-type appears to be free of gangue minerals at hand specimen scale, a thin section of 103470 revealed small quartz crystals projecting into the seam of pyrite from the margin. A little of the quartz is enclosed by the pyrite. The quartz contains fluid inclusions, the larger and more visible of which are mostly type II inclusions. There are also much less abundant type I inclusions and some intermediate between types I and II. No type III inclusions were observed. Some very small primary inclusions associated with a growth zone of the quartz were difficult to classify, but the larger ones seem to be type II inclusions. The deposition of the quartz (and pyrite) was probably associated with a vapour phase, and possibly also with a boiling liquid of low to moderate salinity. No heating or freezing measurements were made.

SPHALERITE-PYRITE VEINS

A specimen of quartz associated with pyrite and small quantities of sphalerite, chalcopyrite and galena, 103042, contained type I inclusions suitable for study. The inclusions were of indeterminate habit, but no other type of inclusion was found in the specimen. The T_h mode was 310°C and salinities range between 0 and 2% eq. NaCl (fig. 6-7). A pressure correction of about 15°C (Potter, 1978) is implied for a pressure of 300 bars. The formation temperature of 330°C is to be compared with sulphur isotope temperatures of $270 - 310^{\circ}\text{C}$ for other pyrite-sphalerite veins (see Chapter 11). The T_h, T_f plot for 103042 indicates fluids indistinguishable from those most frequently represented in the type I inclusions in quartz-Cu,Fe sulphide veins (fig. 5-1).

QUARTZ HEALING BRECCIATED SPHALERITE

Type I inclusions from 103048 were indeterminate in habit, and gave T_h readings in the range $200 - 320^{\circ}\text{C}$. T_f readings were mainly between 0 and -2°C , giving a pressure correction of about 15°C . These fluids, too, compare closely with the fluids in type I inclusions in quartz-Cu,Fe sulphide veins.

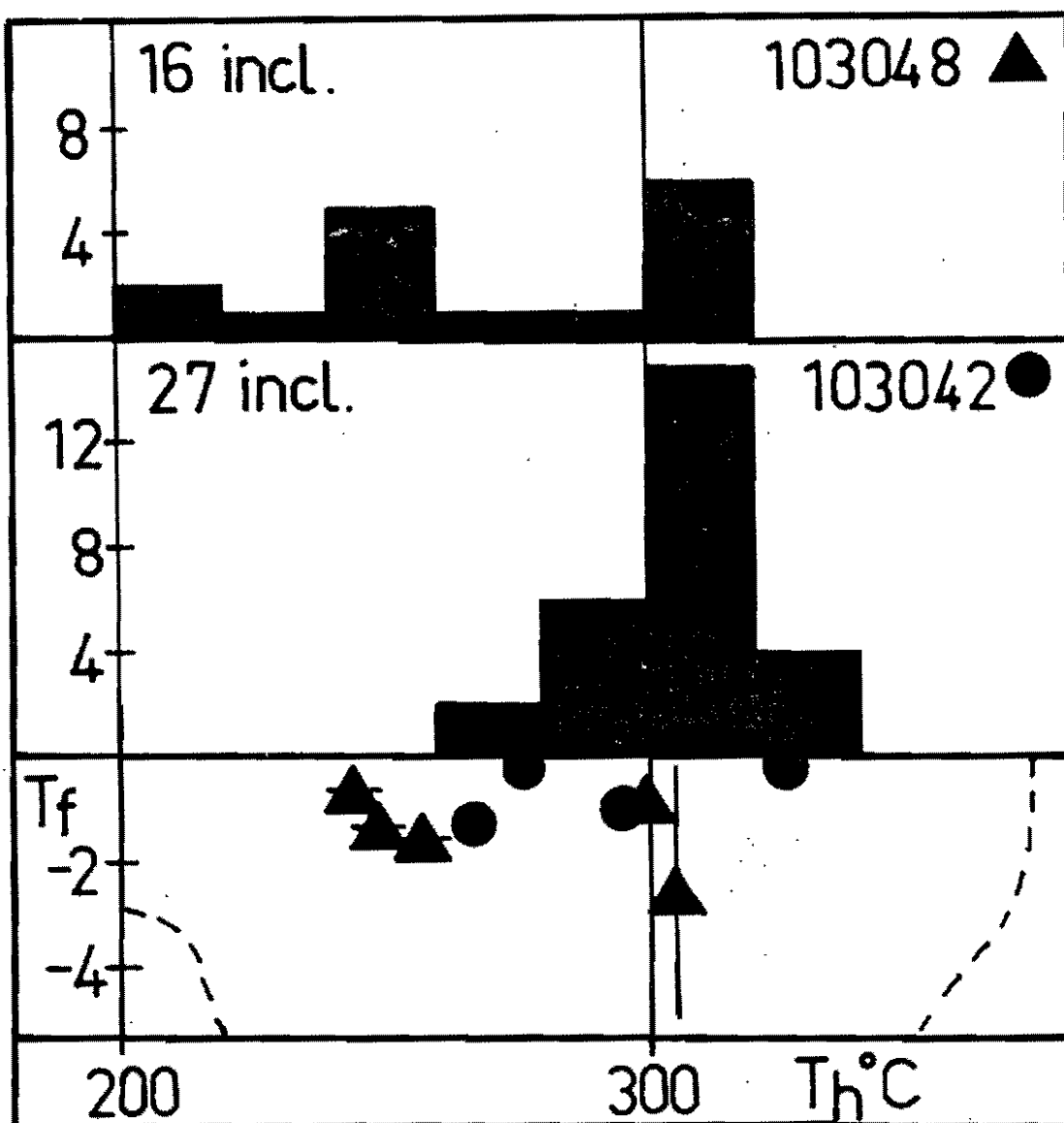


Fig. 6-7 T_h histogram and T_h vs. T_f for 103048 (quartz healing brecciated sphalerite) and 103042 (a quartz-pyrite-clay vein with minor sphalerite, chalcopyrite and galena).

CHAPTER SEVEN: PRESSURE ESTIMATES

Three methods of estimating the pressure during mineralisation are available from the fluid inclusion data. The first applies to the QP fluid association (see Chapter 6); the second and third apply to the salt-rich liquids and their vapours.

QP ASSOCIATION

A fluid inclusion which homogenises at T_C must have been trapped at $P \geq P_C$ and $T \geq T_C$. In 103017 the mode of T_C is 410°C , and in 103040 the mode is 400°C (see fig. 6-6). These correspond respectively to P_C values of 280 and 270 bars in the system $\text{NaCl-H}_2\text{O}$ (Sourirajan & Kennedy, 1962). These are minimum pressure estimates, on the assumption that there are no other substances present in sufficient quantity to change the critical properties of the fluids (experiments with a crushing stage revealed little, if any, CO_2 in these specimens). Similar pressure estimates apply to the other specimens in which there were homogenisations at the critical point.

TYPE II INCLUSIONS

The data obtained from type II inclusions have been discussed in Chapter 5 (see fig. 5-4). When type II inclusions homogenise, the temperature and pressure in the inclusions must be less than T_C and P_C of the vapour they contain. In 103026, which appears to have formed near 400°C on the basis of type III inclusion data, the type II inclusions with small liquid rims homogenise at temperatures less than 400°C . The 400°C formation temperature must apply to the type II inclusions if the salt-rich

liquid was in equilibrium with the vapour. Assuming the system NaCl-H₂O to be an adequate representation of the vapour, the P_c at 400°C is 290 bars. A similar estimate may apply for 103029, where the formation temperature of the vapour is less certain. These are maximum possible pressures of formation. In veins formed at higher temperatures, much higher maximum pressure estimates may apply. Consistent with this, the homogenisation temperatures of type II inclusions in 103012 and 103022 were observed to be higher, generally >420°C (but not measured precisely) in inclusions with small liquid rims.

TYPE III INCLUSIONS

If the salt-rich liquids in type III inclusions are adequately represented by the system NaCl-KCl-H₂O, the data of Ravich & Borovaya (1949) can be used to estimate the vapour pressures of the boiling liquids. A few such liquids at Panguna saturated or close to saturation in NaCl contained about 3 parts NaCl to 1 of KCl by weight; such a liquid has a vapour pressure greater than 200 bars between 450 and 600°C (fig. 7-1). An upper limit of 300 bars has been interpolated in a part of Ravich & Borovaya's diagram where the data are sparse. At higher temperatures the pressure diminishes, approaching 50 bars at 700°C. The most concentrated liquids at Panguna have about 4 parts NaCl to 1 of KCl by weight; this permits pressures a little higher than in the 3:1 case (by 10 - 20 bars at saturation). The most dilute liquids contain about 2 parts NaCl to 1 of KCl, and these would have a vapour pressure between 200 and 250 bars (values again interpolated).

The salt-rich liquids could deviate from the conditions of the experiments of Ravich & Borovaya because of the presence of other salts (probably lowering the vapour pressure) or volatiles other than water

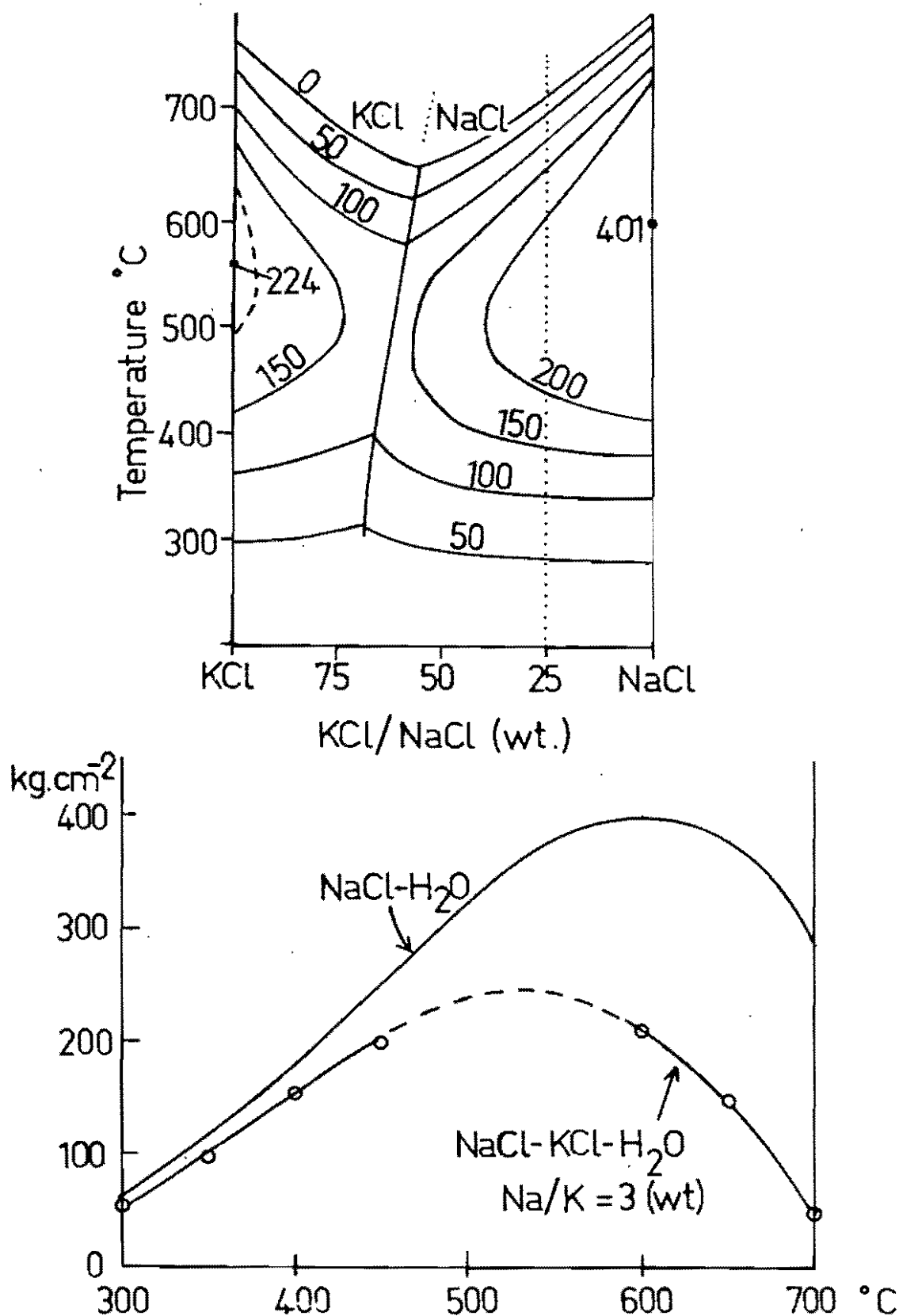


Fig. 7-1 Vapour pressures in the system NaCl-KCl-H₂O. The upper figure gives vapour pressure isobars in kg/cm^2 for saturated liquids with KCl/NaCl ratios as indicated on the abscissa, and at temperatures from 300 to 700°C. The lower diagram gives vapour pressure curves for two liquids of fixed KCl/NaCl ratio. After Ravich & Borovaya (1949). One bar $\approx 1 \text{ kg cm}^{-2}$.

(raising it), if the liquids were unsaturated with respect to NaCl (raising the vapour pressure) and also if they were supersaturated (lowering it). Unsaturation is most likely in the case of the most dilute and certain more concentrated liquids (see Chapter 5). Saturation or supersaturation appears to be the case for the rest. Therefore the best pressure estimate by this method is 200 - 300 bars for the liquids which appear to be saturated in NaCl.

SUMMARY

QP association fluids, the specimens in which most of the type II inclusion data were collected and the lower-temperature saturated salt-rich liquids are all associated with the edge of copper mineralisation (see Chapters 5 and 6). Therefore all of the considerations above are consistent with a pressure of 270 - 290 bars near the edge of the deposit. Within the deposit, the pressure may have been lower where those salt-rich liquids thought to have been supersaturated were present, or higher where there were higher-temperature saturated or unsaturated salt-rich liquids. These matters will be examined again in Chapter 9.

CHAPTER EIGHT: THE HISTORY OF THE DEPOSIT

The vein classification (Table 3-1) does not include any sub-division of quartz-Cu,Fe sulphide veins beyond distinguishing veins with a central sulphide seam from those with disseminated sulphide only near the Leucocratic Quartz Diorite. However, there are other indications that more than one phase of quartz-Cu,Fe sulphide veining took place. Such veins intersect each intrusive body in the deposit, yet the relationships between the intrusives and copper mineralisation (and silicate alteration) differ widely (Fountain, 1972). The Leucocratic Quartz Diorite and the southern part of the Kaverong Quartz Diorite are strongly mineralised and are largely altered to potassic assemblages. The Biotite Granodiorite is weakly mineralised (except in the marginal Intrusive Breccias) and is altered largely to phyllic and argillic assemblages. The Biuro Granodiorite is very weakly mineralised and relatively unaltered. The two pyrite haloes delineated in this study give a further indication of multiple veining phases.

Adding the fluid inclusion data to the intersection relationships between veins and intrusives (the only useful field criteria for classifying quartz-Cu,Fe sulphide veins) allows an improved interpretation. Areas of high salinity or high temperature (or both) are considered as possible centres of mineralisation and suggest a centre in and near the Leucocratic Quartz Diorite (Phase B) and another along the west edge of the Biotite Granodiorite (Phase C). Data from veins thought to be associated with these centres have been excluded from the map. The residual fluid inclusion data (fig. 8-1) have been termed Phase A. In the following discussion of their relationships, the three phases are best treated in the order C, B, A.

PHASE C

The centre along the west edge of the Biotite Granodiorite is defined by specimens 103001, 103004, 103005, 103006, 103012, 103013, 103014 and 103022. It is younger than the Biuro Granodiorite because 103013 and 103014 cut that intrusion. It is, hence, younger than other mineralisation in the vicinity, since the Biuro Granodiorite intersects all other mineralisation and alteration patterns around it (Fountain, 1972). The specimens listed belong to the core area of a phase of mineralisation (phase C) which probably also includes all other quartz-Cu,Fe sulphide veins cutting the Biotite Granodiorite and its minor phases. The edge of phase C has not been located, except perhaps to the east where low salinities occur within the orebody (specimens 103007, 103008, 103017 and 103021). So the minimum extent of phase C includes the Biotite Granodiorite and the Biuro Granodiorite, and part of the area between them (fig. 8-1).

PHASE B

The centre in and near the Leucocratic Quartz Diorite is marked by a concentration of quartz veins (fig. 3-1) and high copper grades (Baldwin *et al.*, 1978), as well as by high T_h data from specimens 103031 and 103047. It is encircled by a halo of pyrite veins and possibly by another halo of quartz-pyrite veins bearing the QP-fluid association (specimens 103017, 103020, 103032, 103040, 103046; see fig. 8-1). This phase (B) may itself have comprised two stages because there are two generations of quartz-Cu,Fe sulphide veins. High salinities and temperatures at the southern margin of the orebody (102636, 103029, 103030) belong to a separate centre about 100 m from the nearest Leucocratic Quartz Diorite contact. This centre, too, may belong to phase B.

RELATIONSHIP OF B AND C

Since they affected different parts of the orebody, it cannot be shown that phases B and C took place simultaneously or otherwise, but the mode of occurrence of the pebble dykes suggests that phases B and C waned concurrently. The pebble dykes mapped by mine geologists are parallel, and occur only in two discrete groups (fig. 2-3). One group cuts the centre of phase B mineralisation and the other cuts the centre of phase C. It is suggested that all of the pebble dykes formed in a single episode of violent boiling, as low salinity waters inundated the waning mineralisation centres along newly-created, deeply-penetrating, NE-NNE fractures. Phase B, if it comprised two stages, may have been active both before and during phase C activity.

PHASE A

If mineralisation belonging to phases B and C is excluded (i.e. veins enclosed by the haloes about the Leucocratic Quartz Diorite, and those which cut the Biotite Granodiorite or the Biuro Granodiorite or the area between them), the asymmetric element of the salinity and temperature distributions remains (fig. 8-1). This is called phase A. Since only a minimum extent could be established for phase C it is possible that phase C data remain in fig. 8-1. However, the sparseness of phase C veining, even at the implied centre of this phase, and the simplicity of the proposed phase A pattern, suggest that few if any are left. There is a broad field of veins with $T_g\text{NaCl}$ from 450°C to 490°C , bounded to the south and southwest by a zone of lower salinities, i.e. a zone of dilution by groundwater. There is also a fall in temperature from more than 700°C in the north to $350 - 430^{\circ}\text{C}$ along the same zone to the south and southwest. Phase A has a pyritic halo (fig. 4, Baumer &

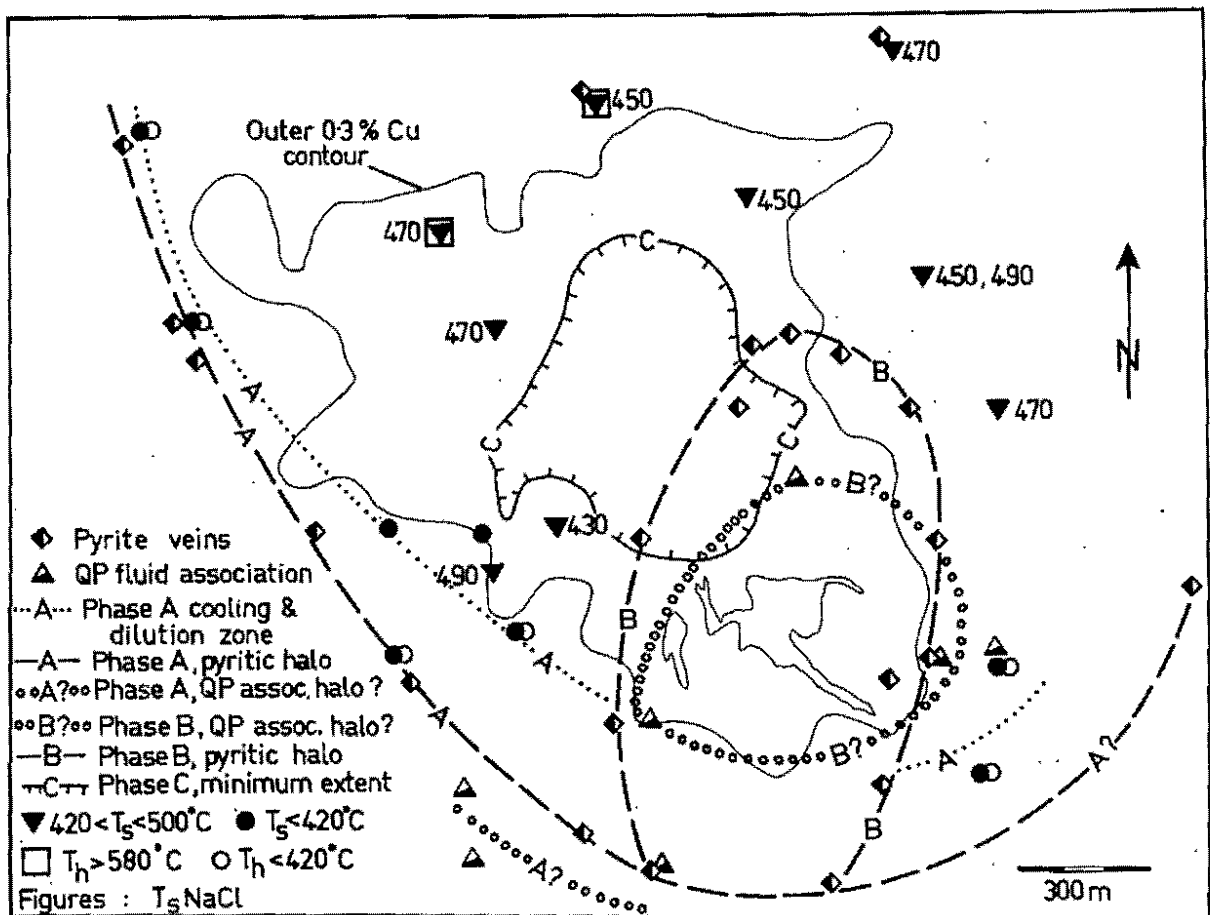


Fig. 8-1 Map of phase A fluid distribution. The fluid inclusion data enclosed by the phase B haloes and the minimum extent of phase C have been excluded. The contact of the Leucocratic Quartz Diorite and the outer 0.3% Cu contour are as in fig. 2-3.

Fraser, 1975) slightly beyond and parallel to the zone along which dilution occurred. This is shown separately in fig. 8-1. There could also be a QP association halo similar to the one suggested for phase B. Three quartz-pyrite specimens (103039, 103040, 103041) with QP association fluid inclusions occur beyond the ore-zone and may be part of a halo running parallel to the zone in which salt-rich liquid was cooled and diluted. Other parts of the proposed halo were not accessible for sampling. Previously (Eastoe, 1978), all of the specimens with QP association fluids were ascribed to a single halo encircling the Leucocratic Quartz Diorite.

The asymmetric temperature and salinity distributions of phase A (with respect to the 0.3% Cu contour) are consistent with the formation of phase A while the southern part of the Kaverong Quartz Diorite was hot. According to data from specimens 102676 and 102998, the temperatures were sub-magmatic (700°C or greater).

Two hypotheses relating phase A to the intrusive sequence arise. The first is that phase A was related to the emplacement of the Kaverong Quartz Diorite and predated the Biotite Granodiorite. This hypothesis is favoured by the association of the biotitisation of the southern margin of the Kaverong Quartz Diorite (to give the Biotite Diorite) with copper mineralisation. Such biotitisation continues beyond the economic deposit and is not spatially related to the Biotite Granodiorite which appears to be unaffected by it. The phase A zone of cooling and dilution, and the pyrite halo, are parallel to the margin of the Biotite Diorite (in particular, in tracing the form of the southeastward projection, most of which has been displaced by the Biotite Granodiorite). The second hypothesis relates phase A to the intrusion of the Biotite Granodiorite while the Kaverong Quartz Diorite was still hot.

The central position of the Biotite Granodiorite with respect to copper mineralisation and the presence in its melt of boiling, salt-rich liquid (demonstrated by primary type II and III fluid inclusions in quartz phenocrysts) favour the second hypothesis. Yet there do not appear to be any fluid inclusion data centred on the Biotite Granodiorite. For this reason, and because of the Biotite Diorite-copper association, the first hypothesis is preferred here.

The evolution of salt-rich liquid from the Biotite Granodiorite must have had some effect, as yet not accounted for, on the surrounding rocks. The only mineralisation obviously associated with the Biotite Granodiorite seems to be the sanidine-biotite-quartz-chalcopyrite matrix in parts of the Intrusive Breccias. The mineralisation is sharply bounded at the breccia-country rock contacts, suggesting that fluid transport was mainly upwards through the steeply-dipping breccia bodies rather than outwards at this stage (fig. 8-2). Ford (1976) suggested that the Biotite Granodiorite stock reached a level higher than the roof zones of the Kaverong Quartz Diorite and the Leucocratic Quartz Diorite. If this is so, mineralisation associated with the Biotite Granodiorite may have taken place above the exposed orebody, or may not have occurred at all because of unsuitable physical conditions at higher levels.

CONDITIONS DURING PHASE B

The symmetry of the pyrite halo around the Leucocratic Quartz Diorite implies that the temperature distribution had changed between phases A and B. By analogy with phase A, where the pyrite halo was probably associated with the dilution and cooling of salt-rich liquid, the presence of a closed pyritic halo indicates that cooling and dilution of the salt-rich liquid took place around the whole cell of phase B mineralisation, and that groundwater had already inundated the ore-zone.

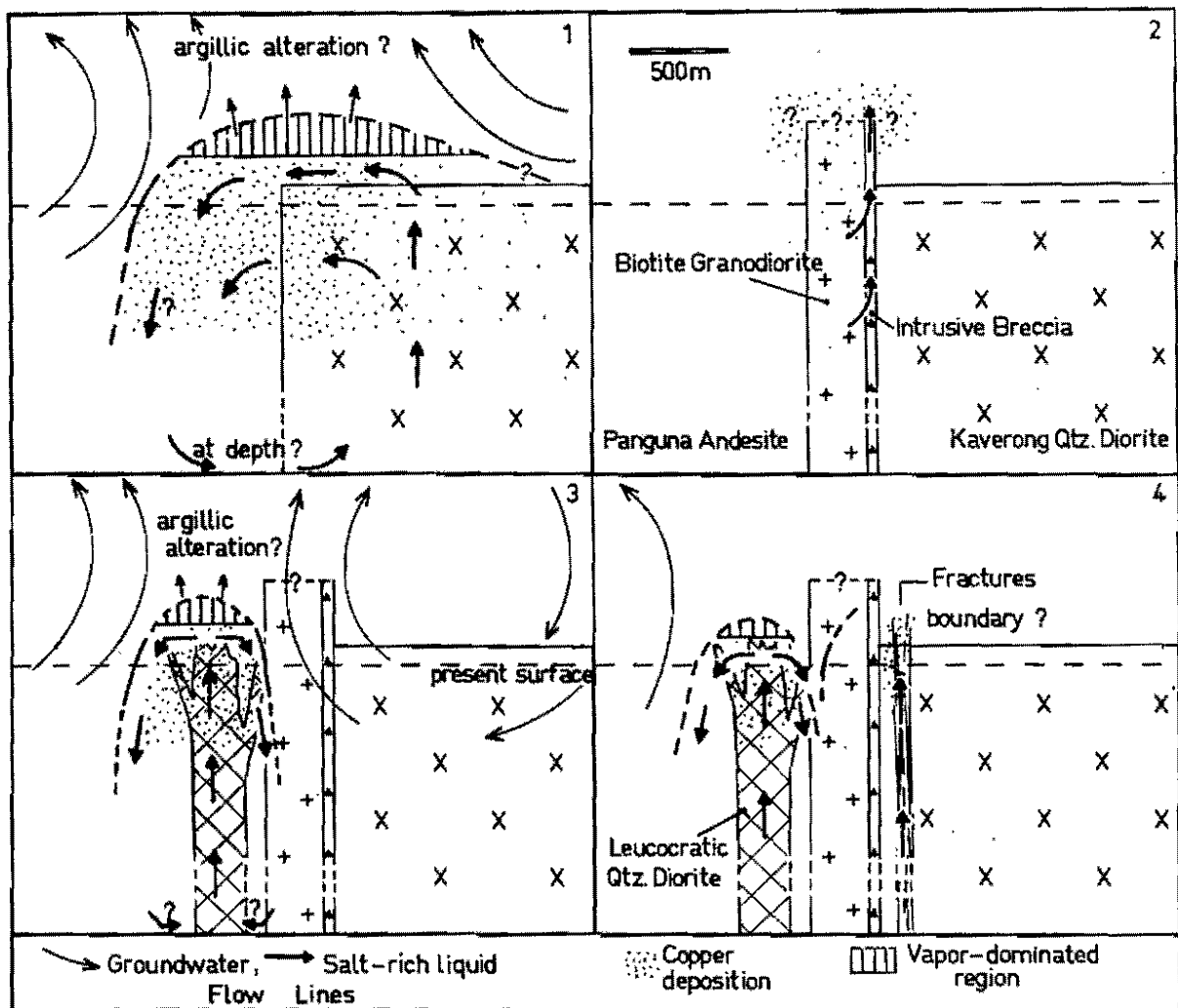


Fig. 8-2 Four proposed stages in the evolution of the Panguna deposit. The sketches are of a vertical section through the centre of the Leucocratic Quartz Diorite and oriented NNW.

1. Phase A.
2. Intrusion of the Biotite Granodiorite.
3. Phase B.
4. Phase C (phase B probably continuing).

The horizontal scale is approximate and the vertical scale is not specified. The forms of the intrusions are simplified, and the Intrusive Breccia at the contact of the Biotite Granodiorite has been projected onto the section. The present surface is approximated by a horizontal broken line.

Phase B therefore occurred well after the waning of phase A and the cooling of the entire system, including the Biotite Granodiorite (because this is cut by the phase B pyrite halo). Page & McDougall (1972) detected a difference of 0.5 - 1.5 m.y. between the K-Ar ages of fresh Kaverong Quartz Diorite and the younger hydrothermal alteration of the smaller porphyry stocks, and this is sufficient time for the proposed change in thermal regime.

EVENTS PRIOR TO PHASE A

It has already been noted (Chapter 3) that a phase of amphibole-magnetite-quartz veining preceded all quartz-Cu,Fe sulphide veining. The alteration accompanying the amphibole-magnetite-quartz veining is pervasive in the Panguna Andesite out to the propylitic alteration zone. West of the deposit, however, three quartz-Cu,Fe sulphide veins (103003, 103025, 103026) have outer selvages containing plentiful biotite. A little amphibole, possibly igneous, remains and is rimmed by biotite in 103026, but other ferromagnesian minerals have been entirely replaced. Plagioclase phenocrysts are rimmed and veined with biotite, and much of the groundmass consists of fine-grained biotite; the texture is one of replacement. In 103003 and 103025 the textures are hornfelsic. In 103003, plentiful randomly-oriented plates of biotite occur between plagioclase phenocrysts. 103025 is a fine-grained hornfels consisting largely of biotite and quartz. It is possible that at least two of these specimens preserve a contact-metamorphic biotite hornfels which predates the amphibole-magnetite-quartz event and survives only beyond the edge of amphibole alteration. This biotite does not appear to be associated with the quartz-Cu,Fe sulphide veins. The inner selvages of 103003, 103025 and 103026 consist of albite \pm chlorite \pm sericite. Only in veins closer

to the orebody is secondary biotite visibly associated with quartz-Cu,Fe sulphide veins. Biotite hornfels is characteristic of the British Columbian porphyry copper deposits, where it is occasionally confused with potassic alteration (Sutherland Brown, 1976b). The outer boundary of the hornfels commonly coincides roughly with the pyritic zone in the British Columbian deposits; this seems likely at Panguna, too, on the evidence of the three specimens. If there was an early biotite hornfels at Panguna, then it has been very effectively masked by the subsequent amphibole alteration. None of the specimens with alteration amphibole (103049, 103466, 103467) gives any indication that amphibole has replaced pre-existing biotite.

SUMMARY

Mineralisation appears to have taken place at intervals throughout the intrusive cycle. There was a hiatus between an early group of phenomena (the Kaverong Quartz Diorite, phase A and possibly the Biotite Granodiorite) and a later group (the Leucocratic Quartz Diorite, the Biuro Granodiorite, phases B and C, and the pebble dykes). During the hiatus, groundwater invaded the ore-zone. The sequence of events suggested by the arguments in this section is shown in Table 8-1.

The interpretation here differs in one major respect from that of Baldwin *et al.* (1978) who suggest that the Biotite Granodiorite, while not itself the progenitor of significant copper mineralisation, remobilised and assimilated phase A copper and upgraded the ore in the zone adjacent to its contact. They do not recognise a phase of mineralisation corresponding to the phase C of this study. The upgrading along the Biotite Granodiorite contact may be a broader manifestation of the contact-controlled escape of volatiles (in parts more spectacularly

evidenced as mineralised breccias). Otherwise, the fluids responsible for the upgrading have not been identified in this study. The veins which cut the Biotite and Biuro Granodiorites must be ascribed to another event, however minor in economic importance. Both this study and that of Baldwin *et al.* (1978) agree that the relatively low-grade Biotite and Biuro Granodiorites are not a low-grade core in the sense of Lowell & Guilbert (1970); rather they intersect pre-existing mineralisation.

Table 8-1

THE SEQUENCE OF EVENTS AT PANGUNA

IGNEOUS EVENTS		HYDROTHERMAL/PNEUMATOLYTIC EVENTS	AGE
Nautango Andesite			1.6 m.y.
<hr/>			
		Pebble Dykes Pyrite-clay veining Sphalerite-pyrite veining Quartz-pyrite veining Groundwater inundation	
Biuro Granodiorite] order?	PHASE C - quartz-Cu, Fe sulphide-anhydrite veining +	
Leucocratic Quartz Diorite		PHASE B (2 stages) - quartz-Cu, Fe sulphide- anhydrite veining + quartz- pyrite veining + pyrite veining.	3.4±0.3 m.y.
<hr/>			
		Groundwater inundation	
<hr/>			
Quartz-feldspar porphyries Intrusive Breccias Biotite Granodiorite		Intrusive Breccia matrix	
<hr/>			
		PHASE A - quartz-Cu, Fe sulphide-anhydrite veining + pyrite veining Amphibole-magnetite-quartz veining and alteration.	
Kaverong Quartz Diorite (and contact metamorphism)			4.5±0.5 m.y.
<hr/>			
Kieta Volcanics			?Oligocene - lower Miocene

K-Ar dates from Page & McDougall (1972).

CHAPTER NINE: FLUID SYSTEMS AND PORPHYRY COPPER FORMATION

THE WATER IN TYPE I INCLUSIONS

Low-salinity waters, unsaturated in NaCl at room temperature, have been present throughout the evolution of the orebody at Panguna, either immediately outside the ore-zone or pervading the whole area. The evidence for this is as follows:

- (i) The dilution of salt-rich liquid near the edge of copper mineralisation;
- (ii) The presence of secondary type I inclusions in all quartz-Cu,Fe sulphide veins and quartz phenocrysts. These cover the entire temperature range between copper mineralisation and about 150°C.
- (iii) The presence, both inside and outside the ore-zone, of veins (mainly quartz-pyrite) containing only type I inclusions.

The waters in type I inclusions cannot readily be identified as meteoric or otherwise. Ford & Green (1977) suggested that the isotopic data for phyllic and argillic alteration products of the Biotite Granodiorite would be consistent with equilibrium with magmatic water at 500°C, or with meteoric water, ^{18}O -shifted in the propylitic zone, at 300°C (see Chapter 1). Combining this with textural evidence, they recognised the possibility of two generations of sericite-bearing alteration assemblages. This study has confirmed the availability of fluids at both temperatures in the Biotite Granodiorite. In specimen 103015, phyllic alteration is associated with water of low salinity. The younger generation of quartz in this vein (from the chlorite-sericite zone of the Biotite Granodiorite) encloses pyrite, chlorite and type I fluid inclusions, some of which are primary. The pressure-corrected

temperature is $320 - 350^{\circ}\text{C}$ and the salinity is near 5% eq. NaCl. If isotopic and fluid inclusion data are considered together, this observation demonstrates that some of the phyllic alteration was due to low salinity meteoric water. Other sericite occurrences in the Biotite Granodiorite are clearly associated with quartz-Cu,Fe sulphide veins, and by implication, with magmatic waters.

It seems reasonable to suppose that all other low-salinity water in the deposit was also meteoric. Such water was present in the ore-zone only between and after pulses of salt-rich liquid, apparently flooding the ore-zone from outside. The variable salinities of type I inclusions from within the ore-zone (salinities are commonly far above the 0 - 3% eq. NaCl commonest in type I inclusions and probably representing uncontaminated groundwater) must have been due to the mixing of salt-rich liquid with the encroaching groundwater. The waning of the salt-rich liquid system and the inward movement of groundwater appears to have been of short duration compared with the period of copper mineralisation. The phase A salt-rich liquid boundary, for example, is relatively sharp, not smeared out. But because the fluids were distributed in fractures, pockets of salt-rich liquid could easily have remained to be mixed later with groundwater. This is consistent with the diminishing range of salinity in type I inclusions with decreasing T_h (fig. 5-1); as time progressed, and groundwater cooled the deposit, so less salt remained.

The pressure at the edge of the ore-zone was 270 - 290 bars (Chapter 7), the pressure of groundwater surrounding it. Cathles (1977) showed that the heating of water around an intrusion has little effect on the pressure distribution. Assuming that groundwater filled fractures all the way to the surface (there is no way of proving this), the depth of cover was about 3 km at the time of copper mineralisation.

The convection of groundwater, driven by heat from the cooling intrusion, is the model which best fits the phenomena described in this section. There is no evidence, however, that copper mineralisation is connected with this type of fluid system. The other mechanisms discussed in Chapter 1 will now be considered in the light of the data from Panguna.

THE ORTHOMAGMATIC MODEL AND THE VAPOUR-PLUME MODEL

At least some of the boiling salt-rich liquid in the deposit was of magmatic origin. This assertion is supported by the occurrence of primary type II and III inclusions in quartz phenocrysts of the Biotite Granodiorite, and by the continuity of properties between salt-rich liquids in veins and those in the phenocrysts. In particular, all K/Na ratios of salt-rich liquids lie on a single trend, and the temperatures of certain veins approach magmatic temperatures. That the salt-rich liquids were boiling wherever they occurred, and that they were associated with copper deposition, are interpretations which have been discussed in earlier chapters. Either the orthomagmatic model (the derivation of salt-rich liquid direct from silicate liquid by exsolution) or the vapour-plume model (Henley & McNabb, 1978, i.e. the derivation of salt-rich liquid indirectly by condensation from magmatic vapour) might be consistent with these observations.

Quantities of salt-rich liquid. Both mechanisms are capable of supplying a large amount of salt-rich liquid. This can be shown by the following rough calculations:

Consider 1 kg of magma exsolving volatiles. The experiments of Ryabchikov (1975), as well as the fluid inclusions in quartz phenocrysts show that under the conditions of crystallisation of high-level

calc-alkaline intrusions, two non-silicate fluids, vapour and salt-rich liquid, coexist with silicate liquid and crystals. Ryabchikov estimates that the magma will exsolve 1 - 2% by weight of water and that this water will contain a mole fraction of chlorine equal to 0.02 ± 0.01 . Taking the mean in each case, the bulk composition of the non-silicate fluids will be 15 g H₂O + 1.0 g NaCl (assuming all chlorine is in the form of NaCl). The compositions of coexisting liquids and gases under various conditions in the system NaCl-H₂O are taken from Sourirajan & Kennedy (1962) and these can be used to work out the distribution of NaCl between vapour and liquid (both generated direct by exsolution). The results of three calculations are set out in Table 9-1.

Table 9-1

T, °C	P, bars	NaCl:H ₂ O (weight)*		Distribution of NaCl (% of total NaCl)	
		in liquid	in gas	in liquid	in gas
700	500	75:25	2:98	71	29
700	1000	60:40	4:96	40	60
700	1100	50:50	7:93	56	44

* from Sourirajan & Kennedy (1962).

The calculations are rough, not least because the liquid compositions are taken from a part of Sourirajan & Kennedy's diagram where there are very large interpolations. Also, 800°C would be a better magmatic temperature estimate, but data are not available above 700°C. At 800°C, the vapours should contain more of the NaCl, so that the calculations above serve to demonstrate that a significant amount of the NaCl exsolved by the magma will be carried away as vapour.

Condensation over the first hundred degrees of cooling of the vapour will remove about 99% of the salt from the vapour at 500 bars (see fig. 19 of Sourirajan & Kennedy, 1962, reproduced here as fig. 9-1); on cooling from magmatic temperatures to 600°C (the temperature of minimum NaCl solubility in the vapour at 400 - 600 bars) virtually all of the salt is removed. At 800 bars, the solubility minimum is at 650°C, and cooling will still remove most of the salts from the vapour. This is the lithostatic pressure corresponding to a hydrostatic pressure of 300 bars; if formed at 800 bars or higher, the vapour will undergo a rapid temperature and pressure decrease on moving towards groundwater and will condense out most of its salt as salt-rich liquid. Comparable amounts of salt-rich liquid can thus be formed by the two mechanisms.

K/Na ratios. The condensate as a whole will clearly preserve the K/Na ratio of the vapour, and since the temperature fall to 600°C will probably occur over a short distance above the intrusion, the condensate is unlikely to be separated into fractions differing in K/Na. This should provide a test for distinguishing the two types of salt-rich liquid, because preliminary calculations by Lagache & Weisbrod (1977) indicate that KCl and NaCl fractionate between liquid and vapour to different extents. The vapour has a lower K/Na than the liquid for fluids in equilibrium with two alkali feldspars. For instance, at 640°C and 900 bars, the molar K/Na ratios are 0.28 for the liquid and 0.18 for the vapour. Although not buffered in the same way by feldspars, the orthomagmatic fluids at Panguna should undergo similar fractionation because fluid properties, not those of the solid phases, control the difference between liquid and vapour. If orthomagmatic and condensate salt-rich liquids are separated, then two different trends of K/Na ratios ought to be present, probably in different places. At Panguna, only one K/Na trend has been detected; this trend applies to three separate phases of

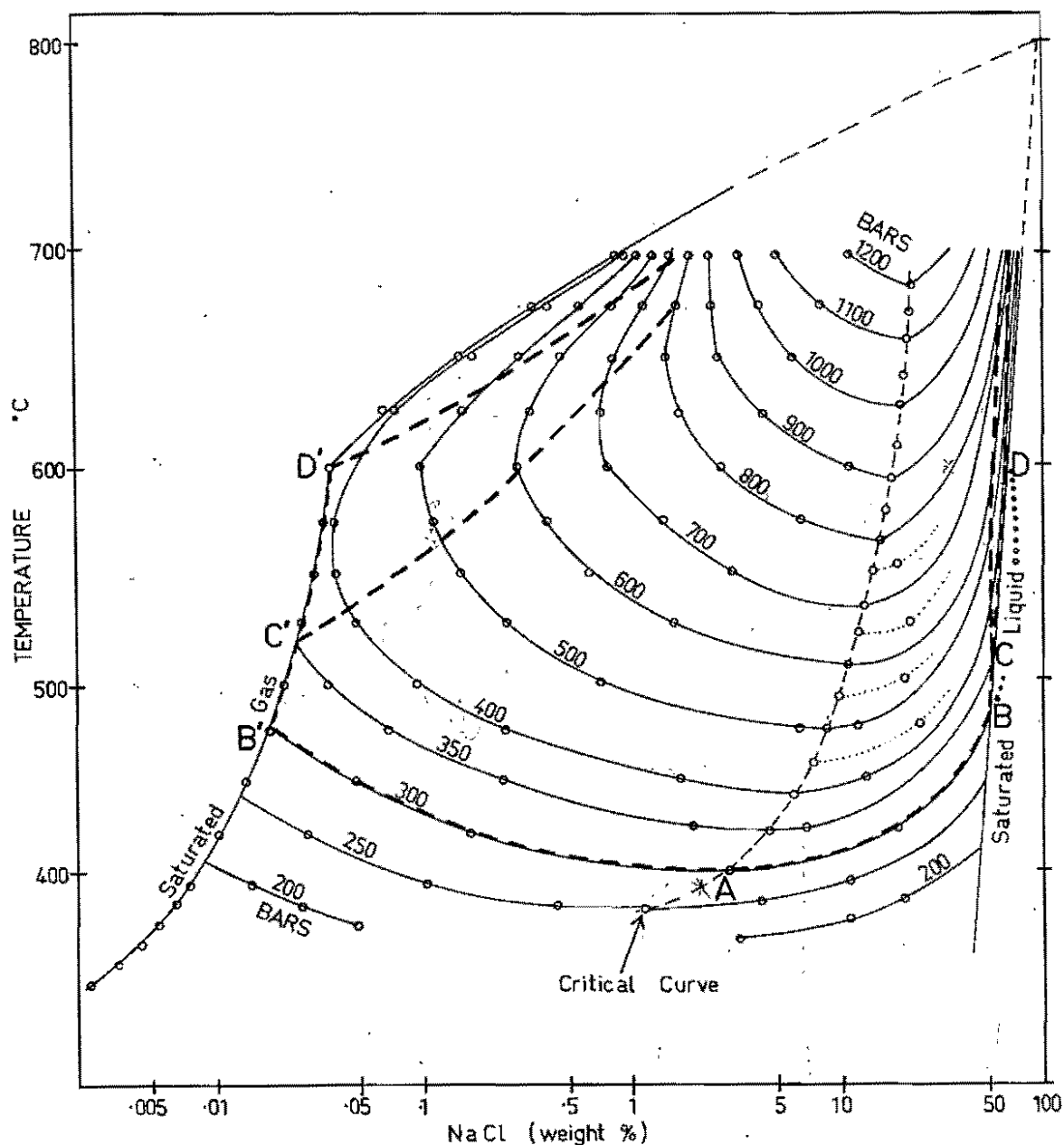


Fig. 9-1 Isobars of the two-phase region in the system NaCl-H₂O, from Sourirajan & Kennedy (1962). Each isobar gives the compositions of coexisting vapour and liquid at various temperatures. Possible paths of fluid-evolution at Panguna are shown, and are discussed in the text. The part of the path representing supersaturated salt-rich liquid is shown in dots between B and D.

evolution of salt-rich liquid (see fig. 5-10) and also includes orthomagmatic salt-rich liquid from the Biotite Granodiorite. It may be concluded that only one sort of salt-rich liquid was present at near-magmatic temperatures, and that the source was orthomagmatic. The single exception to the trend, 103029, might be explained as condensate salt-rich liquid, since the K/Na ratio is low relative to other salt-rich liquids.

It seems much more likely, however, that the temperature gradient above the part of the intrusion exsolving volatiles, or the subsolidus part where boiling takes place, is very steep. Most of the condensation which must occur over the first hundred degrees of cooling will take place where the condensate cannot really remain separate from the orthomagmatic salt-rich liquid. Because of its density, the salt-rich condensate will descend, eventually mixing with and becoming indistinguishable from the orthomagmatic salt-rich liquid. In this case, the vapour plume model becomes a giant reflux condenser.

Whether salt-rich condensate was being separated, or refluxed and mixed with orthomagmatic salt-rich liquid, cannot be determined from the fluid inclusion evidence from Panguna. The single trend of K/Na data does, nonetheless, rule out any significant deposition of quartz-Cu,Fe sulphide veins from a separate condensate.

FLUID EVOLUTION ACROSS THE TWO-PHASE REGION

Predictions. No matter what the mechanism of generation of the two fluid phases associated with the ore-zone, be it boiling or condensation, the fluid evolution across the two-phase region can be considered in a way similar to the treatment given by Henley & McNabb (1978). Those authors examined the changes across an isobaric section at 500 bars, at which pressure it is possible to vary the compositions of two unsaturated

NaCl-H₂O fluids in equilibrium from the critical point up to magmatic temperatures. The 500 bar isobar in fig. 9-1 is the locus of the fluid compositions. The two-phase region characteristic of porphyry copper deposits would thus be bounded by a surface defined by the critical temperatures and pressures of the fluid system, and the fluids within the two-phase zone would converge towards a common composition as the boundary surface was approached.

It has already been noted (Chapter 6) that fluids with homogenisation properties indicating that they are near the critical point at 400°C are characteristic of a set of quartz-pyrite veins and (Chapter 8) that these veins may be parts of outer haloes to phase A and phase B mineralisation. The pressure at the edge, in this case, is about 300 bars according to inclusions which homogenise at the critical point. It will now be supposed that these fluids were, in fact, on the boundary surfaces of the respective two-phase regions. Using phase data for the NaCl-H₂O system (Sourirajan & Kennedy, 1962), here shown as fig. 9-1, the evolution of composition of the two fluids across a horizontal section of the two-phase region will be examined for the case with a boundary pressure of 300 bars.

The critical boundary is represented by point A on the 300 bar isobar. In the two-phase region adjacent to the boundary, the fluid evolution in a horizontal section will be isobaric, the compositions diverging from A towards B and B'. These fluids are unsaturated in NaCl.

At B and B', the liquid and vapour become saturated in NaCl. This happens at a temperature near 475°C. If the temperature is raised still further (on moving still further into the two-phase region), the isobaric evolution of coexisting vapour and liquid is no longer possible under equilibrium conditions. Several paths are possible, differing in the temperature at which the fluids depart from the saturation curves.

Any path which follows the saturation curves to temperatures over 600°C is not possible because of the maximum in the vapour pressure of saturated $\text{NaCl-H}_2\text{O}$ at 600°C (Keevil, 1942). A boiling, saturated liquid moving away from a hot source would have to increase its vapour pressure as its temperature fell towards 600°C . This, in fact, would not occur; while the salt-rich liquid would still move outwards, in liquids above 600°C , the pressure would increase to the value of the maximum vapour pressure and the liquids would cease to boil. They would therefore be unable to cool. Toulmin & Clark (1967) have shown that expansion and mixing with groundwater are the only significant means of cooling fluid in a large, established hydrothermal system. Mixing with groundwater cannot be feasible at the centre of the system (see below for a discussion of where such mixing occurs); this leaves only expansion, which for a sub-critical, incompressible liquid implies boiling.

Permissible paths may leave the saturation curves if the fluids become unsaturated at temperatures below 600°C - such paths leave the curves at C, C' and D, D' in fig. 9-1. These paths permit two fluids to coexist at pressures and temperatures which decrease monotonically together. They have been drawn to approach lithostatic pressure, 800 bars, as magmatic temperatures are approached. Since only unsaturated fluids can coexist at the magmatic pressure of 800 bars or greater (see fig. 9-1) this will be the ultimate direction of the departure from saturation.

At submagmatic temperatures, however, supersaturation may permit more complex phenomena. Since the vapour pressures of supersaturated $\text{NaCl-H}_2\text{O}$ liquids are not known, it is difficult to predict anything other than general limits to the behaviour of the fluids. The vapour pressures of supersaturated liquids will certainly be less than those of saturated liquids. Pressures may, as we shall see below, fall below the boundary

pressure, 300 bars. Ostensibly, the possibility of supersaturation makes it possible to circumvent the pressure barrier imposed on saturated liquids, so that a liquid boiled to saturation and then supersaturation at a temperature over 600°C could continue boiling and cooling to lower temperatures. In practice, however, the link (i.e. boiling) between cooling and increase in concentration, combined with any regularities in the vapour pressures of the supersaturated liquids, might severely limit the range of possible paths. A possible indication of the operation of such a constraint will be discussed below.

Comparison of predictions and observation. In Chapters 5 and 6, various homogenisation phenomena of type III inclusions were described. It was found that there were certain regularities: in particular that the threshold of saturation was crossed twice; that $T_h > T_{\text{SNaCl}}$ for the highest and lowest temperature salt-rich liquids (i.e. these were unsaturated); and that $T_{\text{SNaCl}} < T_h$ for an intermediate range of fluids. Fig. 9-2 is a selection of histograms taken from earlier figures and typifying these varieties of behaviour. The distribution of the various behaviour types is shown on a map of the deposit in fig. 9-3.

The low-temperature group of unsaturated fluids comprises fluids with T_h up to 460°C and salinity up to 20% eq. NaCl, and also the most dilute of the salt-rich liquids. For the latter, T_h is usually near 400°C . The group of salt-rich liquids with $T_h \approx T_{\text{SNaCl}}$ in the range $400 - 430^{\circ}\text{C}$ also probably belong to the unsaturated group because of the metastability phenomenon (Chapter 5) which raises T_h during series of heating runs.

The liquids for which $T_{\text{SNaCl}} > T_h$ cover the whole upper salinity range from 430 to 580°C . These have been interpreted as supersaturated liquids (Chapter 5), some supersaturated by several tens of degrees. They occur in the temperature range in which saturation is suggested by

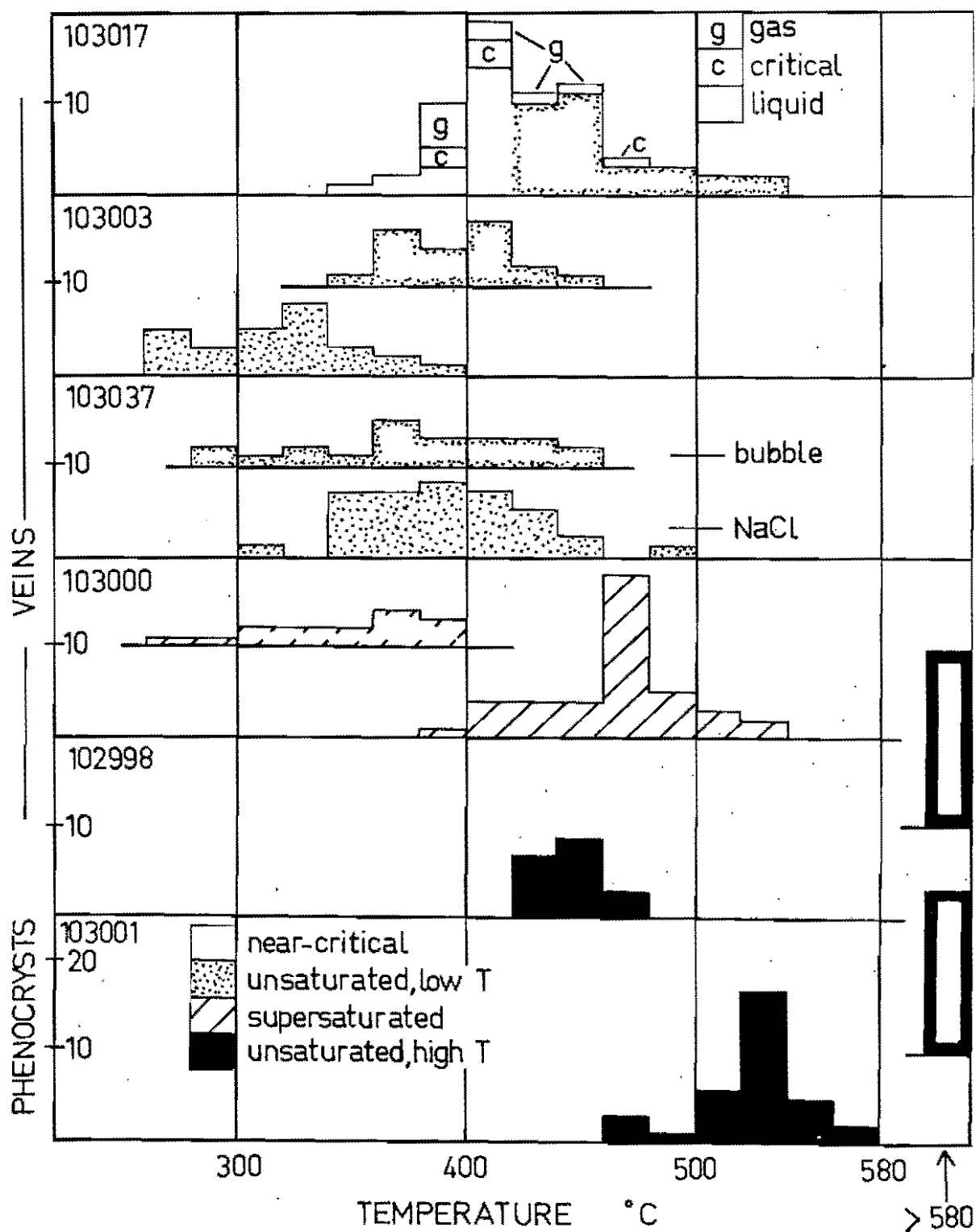


Fig. 9-2 A selection of histograms of fluid inclusion data (from figs. 5-7, 6-2 and 6-6), chosen to illustrate the various types of phase behaviour in salt-water liquids.

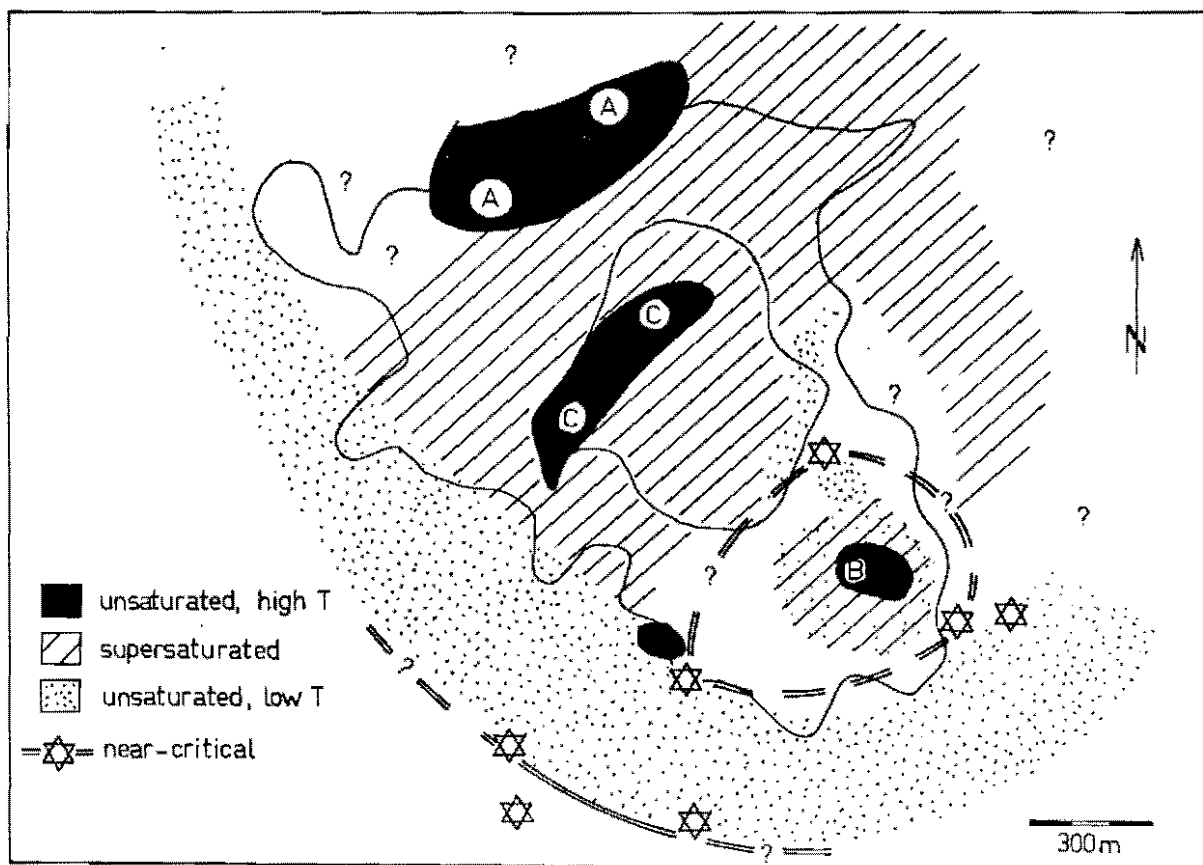


Fig. 9-3 Distribution of the various types of phase-behaviour in salt-water liquids. Letters refer to phases A, B and C of Chapter 8. The outer 0.3% Cu contour is shown as in fig. 2-3, and the minimum extent of phase C as in fig. 8-2.

phase data for NaCl-H₂O. The only alternative explanation of this behaviour would require a different pressure-temperature path for the salt-rich liquids, so that the ones with $T_{\text{SNaCl}} > T_{\text{h}}$ are trapped, then become saturated in halite, then boil (rather than being trapped after becoming saturated and then supersaturated without precipitating NaCl, while boiling). This does not seem consistent with the presence, without exception, of vapour inclusions in veins where type III inclusions behave in this way. The supersaturation hypothesis is thus preferred here.

The precise lower temperature limit of supersaturation is masked by the metastability effect, but is probably a little higher than 430°C where the crossover of homogenisation order occurs. The threshold appears to be the same for all phases of mineralisation. The precise upper limit is also difficult to fix because no specimen pinpointing a high-temperature crossover of T_{h} and T_{SNaCl} has been found. The crossover is implied by the presence of unsaturated liquids at temperatures over 580°C. These unsaturated liquids occur in phases A, B and C and are notably abundant in phenocrysts from the Biotite Granodiorite.

In a supersaturated liquid, T_{SNaCl} must be an upper limit on the temperature of formation. In phases A and B, where the highest T_{SNaCl} mode is 500°C, there is therefore a temperature gap of at least 80°C unrepresented by fluid inclusions. The salinities and K/Na ratios are, nonetheless, continuous between supersaturated and unsaturated liquids. In phase C, salinities range up to 580°C. The most concentrated liquids (in 103022, 103001) are highly supersaturated, while unsaturated liquids from the same phase have $T_{\text{SNaCl}} = 500 - 520^\circ\text{C}$. This suggests that the higher salinities are the result of concentration by boiling of the liquids of lower salinity. Since saturation must therefore have occurred at a temperature nearer to 500 - 520°C, there is again a temperature gap

unrepresented by fluid inclusions. The lowest of the few T_h measurements done on high-temperature unsaturated liquids is about 600°C in 103031; this may fix the upper end of the temperature gap, at least for that specimen. Within the temperature gap lies the high-temperature crossover point of T_h and T_{SNaCl} . The high-temperature unsaturated liquids have T_{SNaCl} in the range $500 \pm 30^{\circ}\text{C}$, and the supersaturated liquids diverge from this range. This suggests that the saturation point or points occur in the range $500 \pm 30^{\circ}\text{C}$; there is no ostensible reason to suppose that a single crossover temperature applied to all phases of salt-rich liquid.

Despite the uncertainties in the temperature determinations, the observed phase properties of the boiling salt-rich liquids at Panguna closely match what was predicted from the $\text{NaCl-H}_2\text{O}$ phase diagram. The sequence of homogenisation behaviour fits well, given the added complication of metastable supersaturation, and the ranges predicted for the upper and lower saturation points are quite reasonable. It must be remembered that the comparison of the experimental work of Sourirajan & Kennedy (1962) with the observations at Panguna rested on the assumption that the critical fluids of the QP association composed external haloes to the two-fluid-phase regions in which the deposit formed. This led to the pressure estimate at the edge. The match so obtained between experiment and nature strongly suggests that the assumption is valid.

The hydrothermal system at Sar Cheshmeh. The only previous set of results with which this model can be compared are those of Etminan (1977) from Sar Cheshmeh (see Chapter 1). Etminan found boiling liquids of lower salinity (unsaturated at room temperature) around the zone of salt-rich liquid corresponding to the main phase of mineralisation. He did not, however, report the presence of a critical-point boundary, and he did not give a map of the salinity distribution within the zone of salt-rich liquid. Both homogenisation orders are reported: $T_h > T_{\text{SNaCl}}$ is

characteristic of fluids found in the intrusive breccia and a later phase of dykes. Overall, Etminan's report is not sufficiently detailed to show whether the same sort of fluid evolution occurred at Panguna and Sar Cheshmeh, but the data on main-phase fluids suggest that a detailed study could obtain such information.

CONDITIONS IMPOSED BY THE REAL SYSTEM

The presence of KCl. An assumption, tacit until now, has been that the NaCl-H₂O system is an adequate physical approximation of the porphyry copper fluid system. The real salt-rich liquid contains about 15% KCl. The close correspondence of real and predicted fluid behaviour described in the previous section suggests that this assumption, too, is valid, in any case from the point of view of temperatures. Vapour pressures are much reduced relative to the NaCl-H₂O system when KCl is added (Ravich & Borovaya, 1949). According to those data (fig. 7-1 of this thesis) the vapour pressures of boiling NaCl-KCl-H₂O liquids saturated in NaCl could not exceed 300, perhaps 250 bars. Within the zone of supersaturation, then, there was probably a zone of pressure lower than hydrostatic pressure outside the deposit (270 - 280 bars, the critical point estimates), unless other volatiles exerted sufficient partial pressures, possibly 10% of the total pressure, over the salt-rich liquids. It is known that there was very little CO₂ in the fluids; other possibilities will be considered in Chapter 10.

The temperature at the maximum vapour pressure of saturated salt-rich liquids varies between 600°C (NaCl-H₂O) and about 500°C (the mixture with KCl:NaCl of about 3:2 by weight). Other mixtures have intermediate values (Ravich & Borovaya, 1949). The position of the maximum vapour pressure is difficult to judge accurately, even where Ravich & Borovaya have drawn

curves (see fig. 7-1); it is necessary to extrapolate for Panguna liquids so that at best the temperature can only be estimated at $550 \pm 50^{\circ}\text{C}$. It has been explained above that this would be a maximum limit for T_{gNaCl} if saturated liquids only were involved. At Panguna, supersaturated liquids were present, some of them concentrated by boiling, yet T_{gNaCl} does not exceed 580°C . The correspondence between the observed maximum value of T_{gNaCl} and the temperature of the maximum vapour pressure may be fortuitous, or it may indicate that they are related for supersaturated liquids just as they would be for saturated liquids.

The role of groundwater. In theory, it would be possible to modify the compositions of two coexisting fluids along the paths in fig. 9-1 while maintaining a constant bulk composition. In natural situations, the great density contrast between the two fluids will bring about their separation in an open, fractured medium. Volatiles, mainly water, will be removed, driving the denser fluid towards saturation and supersaturation in NaCl as has been described. The observed return to unsaturation at lower temperatures cannot, therefore, be brought about without a diluent from outside the ore-zone, in this case groundwater.

The change from salt-rich liquid (giving inclusions saturated in NaCl at room temperature) to groundwater (giving unsaturated inclusions) occurs in the range AB of fig. 9-1. Here, there is a large change in liquid salinity for a relatively small change in temperature. The change should therefore be confined to a narrow zone. Any smoothing of the transition will take place by the outward diffusion of salts or the inward diffusion of water. This should not broaden the boundary zone significantly; Turner *et al.* (1970) have shown experimentally that two convecting liquids with a large density contrast will remain physically separate across a sharp interface essentially unaffected by diffusion even when horizontal. So most of the lateral salinity change due to mixing

with groundwater will occur in a relatively narrow zone, such as has been observed in phase A at Panguna. By implication, most of the motion in the liquids must be vertical.

THE RELATIONSHIP OF FLUID DISTRIBUTION WITH METAL AND ALTERATION ZONING

The association of potassium silicate alteration with salt-rich liquid, and of groundwater with propylitic alteration, is well-established at Panguna. Few other absolutely consistent relationships are apparent, comparing fig. 2-4 and fig. 9-3, but this is doubtless due to the complexity of superposition in much of the deposit. Southwest of the deposit, there appears to have been no superposition of salt-rich liquids after phase A. There, the critical-point boundary thought to belong to phase A corresponds with a segment of the phase A pyritic halo (see fig. 2-4). It also corresponds with the appearance of chabazite in veins (fig. 3-13). Fountain (1972) shows wallrock biotite alteration continuing out to this halo. The boundary of supersaturated salt-rich liquid (essentially the same as the boundary of all salt-rich liquid) corresponds with the southwestern part of the outer 0.3% Cu contour, and a decline in the density of quartz veining (fig. 3-1). Between these two boundaries, this study has shown that propylitic alteration appears, either pervasively (103035) or as a thin inner selvage (103025, 103026). The same relationship between fluids and copper grades has not been observed to the north and east of the area affected by phase A. This is because the margin of the orebody was not to the north, but the reason is not evident in the case of the eastern side. Probably, the fluid boundary was not located because the area concerned could not be sampled. Three of the four sphalerite occurrences with chalcopyrite (fig. 3-7) are in the low-temperature, unsaturated zone of fig. 9-3. This suggests that groundwater may have been the source of the zinc. Consistent with that

suggestion, Ford (1976) reported a halo of Pb-Zn trace enrichment in the propylitic zone southwest of the deposit. There may also be a vague enrichment of trace Cu in the same halo. Low salinity waters at temperatures near 300°C deposited veins bearing sphalerite, tennantite and galena within the ore zone and outside it. Again, in 103017, pyrite probably associated with QP association fluids occurs with minor marcasite, chalcopyrite, sphalerite and very minor tennantite. Given the low salinities of some of the salt-rich liquids in 102594, a groundwater origin could be possible for the unusual metals - As, Pb, Zn, Sn, Co and Ni - found with the bornite in that specimen.

Thus there are indications that groundwater could have contributed to the accumulation of metals (including Cu) in the Panguna deposit. The influence of groundwater, however, was confined to the zones of dilution of salt-rich liquid - relatively narrow in phase A. This, and the presence of Cu,Fe sulphide with salt-rich liquid in quartz phenocrysts, indicates that most of the copper, in phase A at least, was of magmatic origin. For the later phases, new and remobilised copper cannot be distinguished. In phase B, for instance, groundwater may have deposited, or re-deposited, Cu, Fe and Mo as the discontinuous sulphide veinlets which seem to compose a halo to the Leucocratic Quartz Diorite, largely beyond the halo of thin pyrite veins (fig. 3-15). The centres of phases B and C certainly correspond with the highest grades in the deposit (as shown by Baumer & Fraser, 1975); this implies that the intensification of mineralisation in later phases, either by the introduction of new material or by the reworking of old, was significant in raising copper grades.

TEMPERATURES AND PRESSURES IN THE TWO-PHASE REGION

Temperatures. There was a single source of heat - the magma that supplied the salt-rich liquid - during each phase of copper mineralisation. Therefore fluid temperatures should decline away from the hot centre, probably in steps governed by the distribution of the various zones of fluid. No outward increases in temperature would be expected. The temperature at the critical-point boundary was about 400°C . This calls into question the T_h data for certain veins thought to have formed from supersaturated salt-rich liquid, namely those with $T_h < T_{\text{SNaCl}}$ and $T_h < 400^{\circ}\text{C}$. It appears that T_h gives too low an estimate of the formation temperature in these cases, possibly because of the metastability effect discussed in Chapter 5. The temperatures of these supersaturated liquids are bracketed by 400°C and by T_{SNaCl} which is generally 500°C or less.

Pressures. At the critical-point boundary, the pressure was 270 - 290 bars, assumed to be the hydrostatic pressure of groundwater surrounding the two-phase region. At magmatic temperatures inside the two-phase region, and possibly at a point below the level of the ore-zone, fluids were under lithostatic pressure (>800 bars). Between the two pressure regimes, the pressure need not have decreased monotonically. It has already been suggested that the vapour pressures of superstaured salt-rich liquids were less than the pressure at the critical-point boundary. Fig. 9-4 shows the pressure variation across a horizontal section of the deposit as a function of temperature, and relative to the vapour pressure curve of a saturated salt-rich liquid approximating the Panguna liquids in composition (the curve is from Ravich & Borovaya, 1949). The letters A, B and C correspond with the lettering of fig. 9-1. Point C has been put at 500°C ; as explained above, this is thought to have

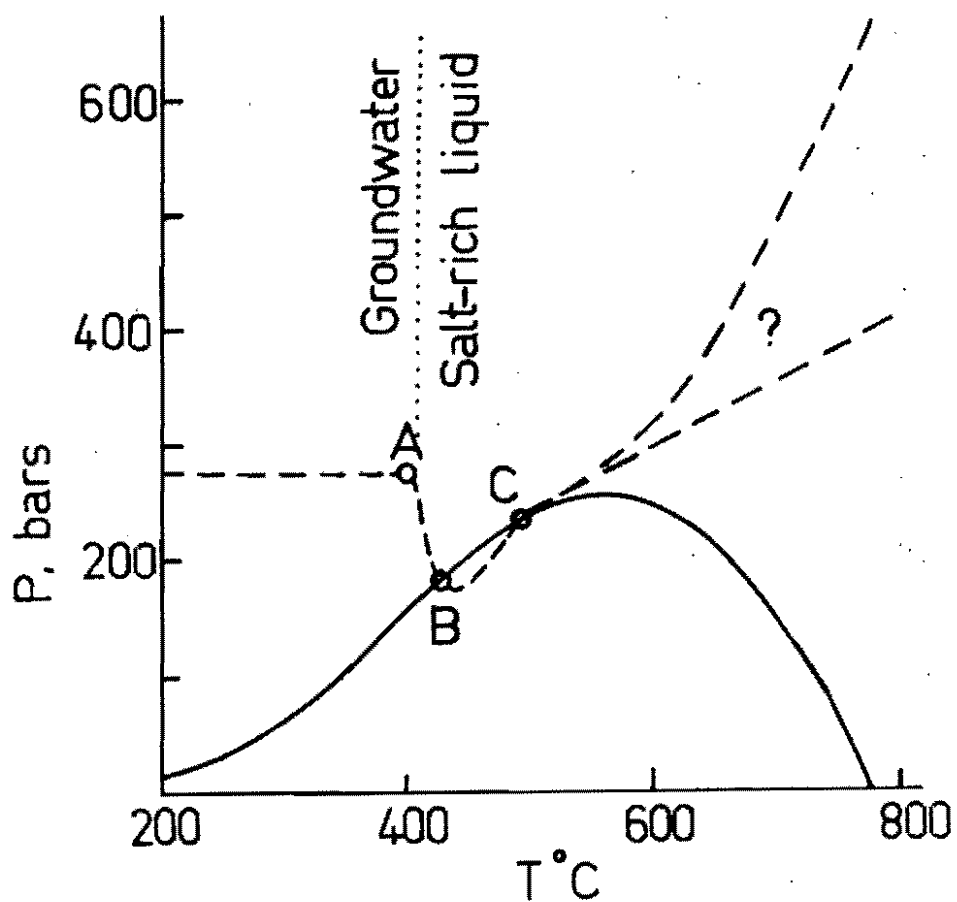


Fig. 9-4 Variation of vapour pressures (dashed line) in the two-phase region as a function of temperature, and relative to the vapour pressure curve (solid line) of a saturated salt-rich liquid (after Ravich & Borovaya, 1949). The lettering corresponds with that used in fig. 9-1.

been the higher temperature of saturation in NaCl. At temperatures over 500°C, pressure and temperature probably increased together, but exactly how is not known. Because of the relationship between temperature and distance from the heat-source (previous paragraph) the abscissa corresponds in a non-proportional way with the distance from the hot centre.

The pressure regime described so far would occur in the two-phase region once it had reached a steady state. None of the evidence from fluid inclusions relates to the conditions during the establishment of such a system, in particular to the phenomena leading to the formation of the fracture-systems that control copper mineralisation. Higher fluid pressures (over 800 bars at the level being considered) would be required. The emplacement of the stocks was probably accompanied by the explosive release of volatiles, a phenomenon quite distinct from, but perhaps the precursor of, those fluid phenomena accompanying copper mineralisation.

K/Na RATIOS IN THE SALT-RICH LIQUIDS

Any adequate model for the fluid interaction at Panguna must be able to account for the linear increase in K/Na ratios with decreasing salinity (see fig. 5-12). From the discussions above, it emerges that the K/Na phenomenon and salinity are not related to temperature monotonically, even though low salinities and high K/Na generally correspond with lower temperatures. Therefore a satisfactory explanation must deal primarily with the salinity dependence of K/Na, and the constancy of the KCl concentration over the whole range of salinity. Five processes may be relevant.

(i) K/Na fractionation during boiling. Lagache & Weisbrod (1977) have predicted that K/Na (gas) will be less than K/Na (liquid) in systems buffered by two alkali feldspars, e.g. at 400 bars and 500°C,

K/Na (gas) = 0.69 K/Na (liquid). Even without the feldspar constraint, boiling should enrich the residual liquid in K relative to Na, and should also increase the KCl content and the total salinity if it occurs to a significant extent. Thus it cannot explain the low K/Na ratios of the supersaturated liquids with $T_{\text{gNaCl}} > 550^{\circ}\text{C}$. Supersaturated liquids at lower T_{gNaCl} should also have K/Na increased by boiling, yet their K/Na ratios do not differ from the ratios of unsaturated liquids of similar salinity.

(ii) The precipitation of halite. Solid inclusions which might be halite have been seen in vein quartz (Chapter 4), but these did not give a positive reaction to a test for NaCl. In any case, the precipitation of halite could not explain the change in K/Na over the whole range, specifically for all unsaturated liquids. Nor could it account for the low K/Na ratios in liquids supersaturated to $T_{\text{gNaCl}} > 550^{\circ}\text{C}$ by boiling.

(iii) K/Na fractionation due to differential diffusion. Turner *et al.* (1970) have shown that at low temperatures, K ions have a slightly higher flux per unit concentration gradient than Na ions at an interface separating two fluids of different density. At higher temperatures, the difference in flux per unit gradient would be expected to diminish. Therefore differential diffusion will reduce the K/Na ratio of salt-rich liquid near the boundary, but perhaps imperceptibly at high temperatures. This mechanism cannot affect liquids away from the boundary with groundwater.

(iv) Mixing of two liquids. The dilution of salt-rich liquid, particularly along the boundary with groundwater, appears to generate much of the observed variation in salinity. The linear trend of salt-rich liquid compositions in fig. 5-12 strongly suggests that they can all be derived by mixing two end-member liquids. One end-member is the

salt-rich liquid derived from the magma. The evolution of several phases of salt-rich liquid from closely-related magmas might reasonably be expected to yield just one such isochemical end-member. The other must be derived from around the ore-zone, and must have about 15% KCl and up to 30% NaCl (the most dilute salt-rich liquids on the linear trend have a total salinity of 45%). It must be generated by a mechanism than can be repeated for each phase of mineralisation.

Groundwater at the critical point boundary has 2 - 3% eq. NaCl; similar or more saline waters are found in veins outside the mine area. The groundwater is boiled between the critical point boundary and the boundary where salt-rich liquid becomes predominant, according to the fluid evolution model proposed so far. Some of the QP association fluids have salinities near 20% eq. NaCl. It seems likely, then, that groundwater was being concentrated by boiling in a zone enveloping the ore-zone, eventually yielding salt-rich liquid. Since the groundwater was in equilibrium with propylitic alteration assemblages (in which Na is fixed in albite, but little or no K is fixed) for some distance around the deposit in each phase of mineralisation, it could have been relatively rich in potassium. The lack of a suitable buffering reaction argues against chemical control; besides, the groundwater immediately adjacent to phase B and C salt-rich liquids must have been altering phase A potassic assemblages to some extent, a chemical environment quite different from that experienced by phase A groundwaters. A reproducible control might have to be physical rather than chemical. Turner *et al.* (1970) state that density difference is capable of keeping two liquids separate across a sharp boundary, so that similarity in density is a requirement for effective mixing. It may be that the inferred groundwater-derived end-member composition has a density at which mixing with the magmatic salt-rich liquid becomes rapid enough to dominate composition

change due to boiling, alteration and other effects. Condensate salt-rich liquid could not have been the diluent because as explained earlier in the chapter, it would initially have a lower K/Na than the orthomagmatic salt-rich liquid.

One lower temperature, lower salinity inclusion relatively rich in KCl was found in 103047. It has a K/Na ratio of 0.64 (atomic). It belongs to a group of secondary inclusions which appear to have necked down, and which now give heterogeneous data ($T_{\text{SNaCl}} = 294 - 363^{\circ}\text{C}$, 6 readings; $T_{\text{h}} = 298 - 331^{\circ}\text{C}$, 4 readings). Thus the high K/Na ratio may be spurious. The fluid also contains too much KCl to be a sample of the diluent.

The mixing mechanism cannot account for the concordance of K/Na values from the highly supersaturated liquids with the general trend. A close examination of the graph of T_{SNaCl} vs. T_{SKCl} (fig. 5-10) reveals that there may indeed be a slightly different trend for $T_{\text{SNaCl}} > 500 - 520^{\circ}\text{C}$. The difference is not perceptible in the triangular diagram (fig. 5-12) for the small salinity range involved.

(v) Rock-fluid interaction. Various studies, e.g. Orville (1963), Ryabchikov (1975) and Lagache & Weisbrod (1977) have examined the relationship between the K/Na ratio of salt-water fluids in equilibrium with alkali feldspars or with calc-alkaline assemblages and temperature, pressure and salinity. All have shown a temperature dependence; K/Na decreases with falling temperature. In addition, Lagache & Weisbrod have shown that there is a pressure dependence based on the unmixing of gas and liquid at lower pressures, but that there is neither a salinity nor a pressure dependence for the liquid phase K/Na. This already suggests that the K/Na variation at Panguna is not primarily a chemical phenomenon. There is no strict temperature dependence of K/Na; rather, liquids with similar salinities, but different temperatures have similar K/Na ratios.

The KCl content, if buffered by some chemical reaction, should not remain constant (as it in fact does) over the whole temperature range.

The decrease in K/Na with decreasing temperature in feldspar-buffered systems is the opposite of what happens in general (if not absolutely strictly) at Panguna. There is no reason why the K/Na ratios at Panguna should be subject to that constraint, for the liquid was apparently not in equilibrium with two feldspars at any stage. In the magma, there are plagioclase phenocrysts, but no alkali feldspar phenocrysts. In the ore-zone, plagioclase is destroyed and alkali feldspar is formed beside quartz-Cu,Fe sulphide veins. Optical investigation of the selvage feldspars of veins near the groundwater to salt-rich liquid boundary revealed plentiful albite. Microprobe investigation revealed a potassic feldspar as well, but the relationship of the two feldspars is not clear. Certainly, the K/Na ratios for these veins are quite inconsistent with the published data for feldspar-buffered systems near 400°C.

An exchange of alkalis between wallrock and liquid must nonetheless have occurred. The effect must have been subordinate to, and opposite to, that of mixing on the alkali composition of the liquid. The veins in which liquids are thought to have been supersaturated to $T_{\text{gNaCl}} \geq 550^{\circ}\text{C}$ by boiling and in isolation from mixing effects have well-developed inner selvages of sanidine. The formation of this sanidine would deplete the liquid in K and enrich it in Na, decreasing the K/Na ratio as observed.

Summary, implications and comparison with other deposits. Given a magmatic supply of salt-rich liquid with $T_{\text{gNaCl}} = 500 \pm 30^{\circ}\text{C}$ and characteristic K/Na, no single mechanism is able to explain the K/Na variation of liquids evolving to both higher and lower salinities. In the direction of lower salinity, mixing with another salt-rich liquid seems best able to account for observations, if a reproducible salt-rich liquid can be generated around the ore-zone. Where mixing does not occur, i.e.

in the direction of higher salinity, alkali exchange with the wallrock would explain the trend. The boiling of groundwater has been suggested as a source for the non-magmatic salt-rich liquid, and this is quite possible according to the physical model explained earlier.

It is interesting to examine K/Na data from other deposits. Those few gleaned from recent publications (Roedder, 1971; Moore & Nash, 1974; Etminan, 1978) and a personal communication (Wilkins, 1978, for the Ok Tedi deposit) have been plotted as $T_S\text{KCl}$ vs. $T_S\text{NaCl}$ with the Panguna trend for comparison in fig. 9-5. As a group, Sar Cheshmeh, Frieda and Ok Tedi overlap the Panguna trend for $300^\circ\text{C} < T_S\text{NaCl} < 500^\circ\text{C}$; individual deposits, however, cover only parts of that range. For these, a mixing process like that at Panguna is plausible. The only real departure from the Panguna trend seems to be in the case of Bingham, and even this is not a large departure. On the other hand, Cloke *et al.* (in press) reported that salt-rich liquids from the Granisle and Bell porphyry copper deposits, British Columbia and from a Pb-Zn skarn at Naica, Mexico, plot along lines indicating evolution of composition by precipitation of halite. The physics of such systems must be quite different from what has been inferred at Panguna. There may thus be two - or more - distinct physical types of hydrothermal system responsible for porphyry copper formation, these reflecting differences in the physical situations, e.g. availability of groundwater.

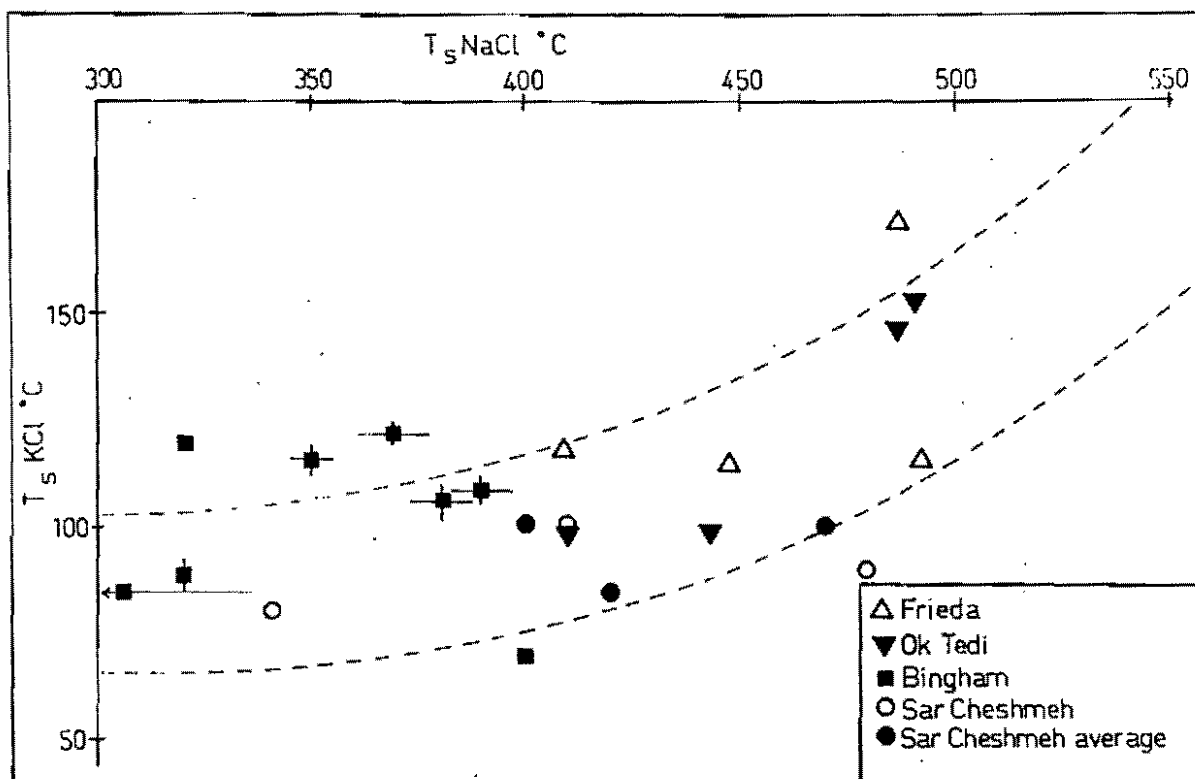


Fig. 9-5 $T_s \text{ KCl}$ vs. $T_s \text{ NaCl}$ for other porphyry copper deposits. The dashed lines give the trend of Panguna data (see fig. 5-10). Data sources: Frieda (this study, see appendix); Ok Tedi (Wilkins, pers. comm.; the $T_s \text{ NaCl}$ data are based on single heating runs); Bingham (Moore & Nash, 1974); Sar Cheshmeh (Etminan, 1977).

ADDING THE VERTICAL DIMENSION

The differences in density of the salt-rich liquids, the vapours and the groundwaters imply that fluid evolution in the vertical dimension will be as important to an understanding of porphyry copper formation as the changes that occur across a horizontal section. The vertical extent of sampling at Panguna was insufficient to give any indication of what happens above and below the essentially-horizontal section of the mine as it was in 1974. The horizontal section of the fluid system is the only available constraint for the following discussion of changes above and below.

Vertical and horizontal flow. The likelihood of mainly vertical fluid motion has been discussed above. The vapour, with a density of 0.3 g/cm^3 or less, would rise vertically on both sides of the boundary between salt-rich liquid and groundwater. Salt-rich liquid ($1.2 - 1.5 \text{ g/cm}^3$) would sink relative to groundwater ($0.8 - 0.9 \text{ g/cm}^3$, Potter & Brown, 1977), while groundwater adjacent to the ore-zone would be buoyant relative to both salt-rich liquid and surrounding, cooler groundwater. All groundwater adjacent to the two-phase region of the porphyry copper system was probably moving towards (from below), and upwards beside, the two-phase region in a convecting flow regime extending through a volume of rock much greater (both vertically and horizontally) than that of the eventual ore-deposit (see fig. 9-6). The mixing of groundwater and salt-rich liquid was a second-order effect superimposed on the vertical movements.

The sinking of the salt-rich liquid might be expected to carry copper mineralisation to some depth around the source intrusion. James (1971) has described deep mineralisation at Bingham as ragged skirts draped around the central pluton at depth and joining as a hood through the top of the pluton (not over it). This means that the top of the

pluton was already solid, and that the magmatic fluids were being derived at depth. At Panguna, phase A mineralisation about the Kaverong Quartz Diorite seems to have had a hot, relatively barren "centre" in the unbiotitised part of the intrusion. The biotitised part (the Biotite Diorite) was certainly solid, but at temperatures over 700°C during mineralisation. So phase A mineralisation could be a portion of an asymmetric shell to the Kaverong Quartz Diorite, or may be part of a hood passing into the intrusion. The asymmetry of the fluid distribution makes the distinction difficult. In the case of phase B, the mineralisation is a hood passing through the top of the Leucocratic Quartz Diorite, which seems too small to have provided fluid without tapping magma at depth. Part of the veining occurred before the stock had solidified and part after; veins of an early set become increasingly indistinguishable from wallrock with distance from the contact towards the centre of the stock, while a later set cuts across the whole stock. Phase C mineralisation took place in solid rocks, and bears no obvious relationship to an intrusion. In phases B and C and possibly A there has been a transfer of salt-rich liquid vertically upwards through solid rock. Despite the density of salt-rich liquid, this will occur for the following reasons:

- (i) the buoyancy of salt-rich liquid, vapour or a single-phase aqueous fluid (whichever is appropriate to the pressure regime at depth) relative to silicate liquid (density $> 2 \text{ g/cm}^3$) will favour the accumulation of all non-silicate fluids at the highest still-liquid part of the magma. Also, it may only be in the highest parts of the magma chamber that the temperature and pressure conditions are suitable for the exsolution of non-silicate fluids.
- (ii) Once a stock has penetrated and fractured the country rock permeated elsewhere at the same level by groundwater, and has itself partly

solidified and become fractured, it will become a conduit for non-silicate fluids from below. Even the dense salt-rich liquid will be pumped up the stock by the difference between hydrostatic pressure at the top and lithostatic pressure (plus any tectonic overpressure) in the magma where the exsolved fluids are accumulating. Each hundred bars of pressure difference could support a column of about 770 m of liquid of density 1.3 g/cm^3 . At Panguna the difference was greater than 500 bars.

At some level in the stock, and not in general at the top (James, 1971), the salt-rich liquid ceases to rise and moves horizontally into the country rock before turning down. The reasons for this are not completely clear, but it could be connected with a sudden change of pressure regime. A column of salt-rich liquid could not be supported because of its density in rock permeated elsewhere by groundwater. Therefore the salt-rich liquid would spread horizontally at the change in regime from lithostatic to hydrostatic. The change appears to occur near the top of the intrusion. At this level, the cooling of magmatic vapour would also be important, and large quantities of salt-rich condensate would be generated. This liquid would either descend and then spread horizontally at its confluence with orthomagmatic salt-rich liquid, or be entrained in convecting groundwater.

The top of the system. James (1971) suggested that copper mineralisation also occurred in a stockwork immediately above the zone of lateral spreading of salt-rich liquid. Higher in the system, according to Sillitoe (1973), pyrite or marcasite, gypsum and sulphur would be deposited, and fumaroles might be the surface expression of the system. Observations on the ore-zone at Panguna suggest that the convection of groundwater heated by the intrusion and the rising of vapour into a plume over the ore-zone and the intrusion are the fluid phenomena which dominate the top of the system. The interaction of groundwater and vapour would

depend on the size of the system and on fluid velocities. For example, rapidly-rising vapour might entrain groundwater and as a result be cooled and condensed before rising very far above the ore-zone. The mixed fluid would be very reactive as a result of inheriting HCl, SO₂ or other volatiles from the vapour. The presence of fumaroles at the surface would not require the persistence of vapour from the deposit to the surface. In some of Cathles' (1977) calculated models, groundwater boils in a discrete two-phase region within 1 km of the surface.

There would be no salt rich condensate in the plume at temperatures lower than the solubility minimum of NaCl in the vapour (450 - 475°C at 250 - 300 bars; Sourirajan & Kennedy, 1962). It is possible, however, that salt-rich liquid could be generated higher in the system by the boiling of groundwater (as at the level of the ore-zone).

The type of critical-point boundary proposed at Panguna has a lower limiting pressure of 221 bars (P_CH₂O). In fact, the limit might be higher because groundwater is seldom free of dissolved salts. In a hydrostatic pressure regime, a pressure of 221 bars corresponds with a depth of about 2.4 km. The critical-point boundary could thus persist at most 600 m above the section examined. It need not have closed over the ore-zone because the upward transport of vapour may dominate other fluid phenomena in the centre of the system at these levels.

The system below the exposed ore-zone. The sinking of salt-rich liquid from the ore-zone has already been discussed. Salt-rich liquids were boiling in all parts of the exposed ore-zone, and in order for boiling to continue at depth in a salt-rich liquid of constant salinity, the local geothermal gradient would have to exceed about 25°C/100 bars (rough estimate from Sourirajan & Kennedy, 1962, fig. 19). Increases in salinity due to boiling would necessitate larger gradients. In an area subject to magmatic activity, abnormally large geothermal gradients are

to be expected, and thus it is likely that boiling could continue below the ore-zone. It also seems probable that the sinking salt-rich liquid would eventually be recycled in a convecting cell.

Other fluid phenomena at depth would depend on whether groundwater persists below the exposed ore-zone. In the initial discussion of the horizontal spreading of the salt-rich liquid, it was suggested that such spreading might occur at the boundary between hydrostatic and lithostatic pressure regimes, i.e. at the lower limit of groundwater. If, however, groundwater did continue below the section studied, the interaction with salt-rich liquid would take on a different character. The critical-point boundary would move to higher temperatures and salinities with increasing depth and pressure - e.g. at 400 bars it would be at 440°C and 6% eq. NaCl and at 500 bars, 475°C and 9% eq. NaCl. Groundwater would be subject to convection over a vertical distance of several km, and any regular increase in groundwater salinity with depth is therefore unlikely. Rather, the higher salinities at the critical-point boundary would be due to mixing with salt-rich liquid, i.e. the critical-point boundary, or the onset of boiling, would occur within the zone of mixing. It appears, then, that no groundwater salt would be involved in the interaction of groundwater and salt-rich liquid, and this would lead to a different K/Na variation in the salt-rich liquids.

Summary. The fluid phenomena which have been deduced for the Panguna deposit could occur only within a narrow range of pressures and corresponding depths, although the entire hydrothermal system extended over a larger vertical range. This qualitative examination suggests that the change of pressure regime from lithostatic to hydrostatic was important in determining the level at which mineralisation took place.

COMPARISON OF PANGUNA WITH PREVIOUSLY-SUGGESTED FLUID MODELS

In Chapter 1, current ideas on the fluid-intrusion interactions responsible for porphyry copper formation were reviewed. These can now be evaluated against the proposed hydrothermal system at Panguna.

An orthomagmatic model, by which salt-rich liquid and vapour are exsolved by a cooling, crystallising magma, is certainly consistent with part of the observation at Panguna. An additional source of salt-rich liquid is required and the physics of the system suggest that it is groundwater concentrated by boiling. The boiling of groundwater under other circumstances has also been suggested (Chapter 8) as an explanation of the pebble dykes. So despite their relative disfavour to date, boiling groundwater models seem to account for important features of the Panguna deposit. The mechanism of condensing a salt-rich liquid from magmatic vapour should also operate, but it does not contribute to the mineralisation in the way that Henley & McNabb (1978) have proposed. Lastly, the simple convection of groundwater cools the deposit once the source of magmatic salt-rich liquid wanes. None of the mechanisms, then, can be ruled out as irrelevant to the formation and evolution of the Panguna deposit.

Fig. 9-6 is a summary of the ideas discussed so far in the form of a hypothetical vertical section through a porphyry copper system.

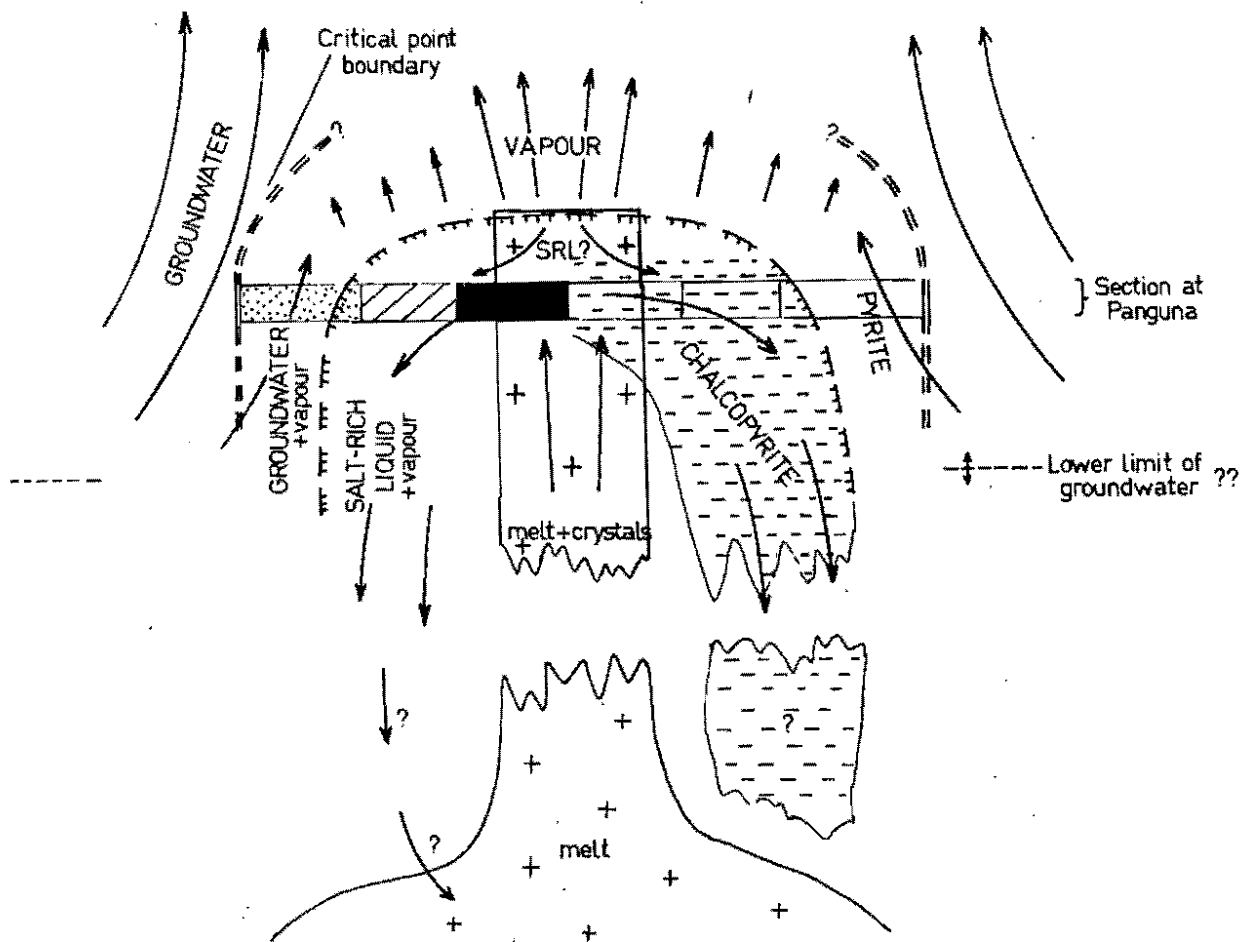


Fig. 9-6 Diagrammatic vertical section of a porphyry copper deposit associated with a stock (+ pattern) showing fluid circulation, phase-behaviour of salt-water liquids (patterns as in fig. 9-4) and estimated pressure and temperature gradients (top). Copper mineralisation is shown as - pattern.

CHAPTER TEN: CHEMICAL CONSIDERATIONS

The variety of mineralisation styles at Panguna presents a multitude of chemical problems. Here, it is intended to examine only phenomena associated with the primary deposition of copper at temperatures over 400°C.

The fluid system consists of salt-rich liquid and vapour at equilibrium, both phases being at equilibrium at a given point with certain crystalline phases. Whereas the liquid cools and evolves in equilibrium with the solids, the vapour is continually removed from the system and can only be considered to be at equilibrium with the solids at its point of origin. The system tends to lose volatiles throughout mineralisation. Neither fluid can be dealt with in terms of aqueous electrolyte chemistry. Because alkali chlorides and water are present in comparable quantities in the liquid, the alkali chlorides cannot be solvated as in more dilute solutions. The alkali chlorides tend to be associated in the temperature range being considered (Montoya & Hemley, 1975). They are, in effect, solvents; solute-solvent interactions are just as likely to involve them as to involve water. Solvation of ions does not occur in the vapour either, associated species being the rule.

Since the temperatures involved range from 400°C up to magmatic temperatures, the discussion is inevitably speculative. Thermodynamic data are not available for some substances at these temperatures and are suspect for others, while fugacity and activity coefficients are in many instances unknown. The following conventions and assumptions are adopted:-

1. The standard states of solids and liquids are the pure substances in their most stable form at T and 1 atm pressure, and for gases, the ideal gas at T and 1 atm. This is the convention adopted in the tables of

Robie & Waldbaum (1968) and JANAF (1971). The former have been used here as a source of data for solid phases and the common gases, and the latter for the gaseous metallic oxides and halides unless otherwise stated.

2. Pressures are therefore expressed in atmospheres and temperatures in Kelvin. This is despite the choice of units earlier in this work. It is easier to relate bars and degrees Celsius to the literature on the physical properties of the systems, and atmospheres and Kelvin to the thermodynamic data. Since two significant figure accuracy is probably more than sufficient in the following calculations, the bar and the atmosphere will be considered as equal, and earlier results in bars will be transposed direct into atmospheres.

3. No pressure correction is applied to the equilibrium constant k . In equilibria involving condensed phases, the pressure dependence of the equilibrium constant is expressed

$$\Delta \log k_{P_2-P_1} = -2.303 \frac{\Delta V_s}{RT} (P_2 - P_1)$$

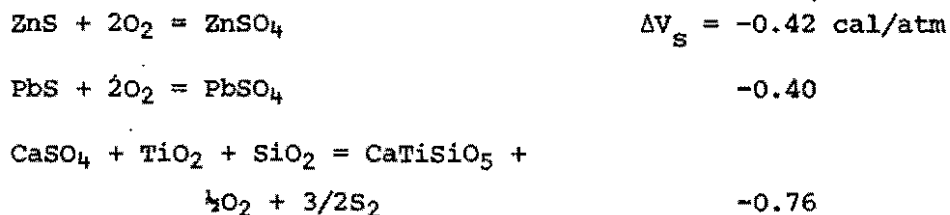
where ΔV_s is the change in molar volume of all condensed species in the particular equilibrium. In this case, P_1 is the standard state pressure, 1 atm. In order that the correction be negligible, say $|\Delta \log k| \leq 0.1$,

$$|\Delta V_s| \leq 1.5 \text{ cal/atm at } P_2 = 300 \text{ atm, } T = 700 \text{ K}$$

$$|\Delta V_s| \leq 0.9 \text{ cal/atm at } P_2 = 800 \text{ atm, } T = 1100 \text{ K.}$$

ΔV_s data are not available for all substances of interest, especially chalcopyrite and bornite but in the following relevant reactions, ΔV_s can be evaluated:-





It will be assumed that the pressure correction is negligible for all other reactions.

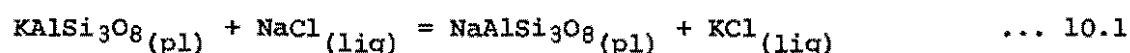
The notation used in this section is tabulated in the Introduction Chapter.

THE BUFFERING OF K/Na IN SALT-RICH LIQUIDS

In Chapter 9, it was suggested that the K/Na ratios of the salt-rich liquids were the product of the mixing of two salt-rich liquids, one derived from the magma and the other from groundwater by boiling. The consistency of the trend over three phases of mineralisation suggests that the alkali ratios in both end members were externally controlled.

The intrusive suite at Panguna is low in potassium. Ford (1976) gave average K_2O contents of 1.72% for the Kaverong Quartz Diorite, and 1.42% for the Biuro Granodiorite, compared with 3.07% for average granodiorite (Taylor, 1969). The Panguna intrusives crystallised phenocrysts of quartz and plagioclase, but not of alkali feldspar. Equilibrium between the salt-rich liquid and the plagioclase, which generally contains less than 0.5% K_2O (Ford, 1976) could result in low K/Na ratios in the liquid. It is possible to do a rough calculation to test this.

Na and K are exchanged between plagioclase and liquid by the following reaction:



Ryabchikov (1975) gives activity coefficients for the orthoclase component in plagioclase, and the activity of the albite component, but they must

be read from small diagrams and so are not available in very precise form.

Values of $k_{10.1}$, the equilibrium constant, are available for temperatures up to 923 K (Hemley, cited in Brimhall, 1977).

$$k_{10.1} = \frac{X_A \gamma_A}{X_O \gamma_O} \cdot \frac{a_{\text{KCl}}}{a_{\text{NaCl}}}$$

(subscripts A for albite component, O for orthoclase). The activities of KCl and NaCl are for the salt-rich liquid; to relate these to mole fractions, it will be assumed that the ratio of activity coefficients is 1. Montoya & Hemley (1975) used such an assumption, but for much less concentrated solutions of salts. Thus

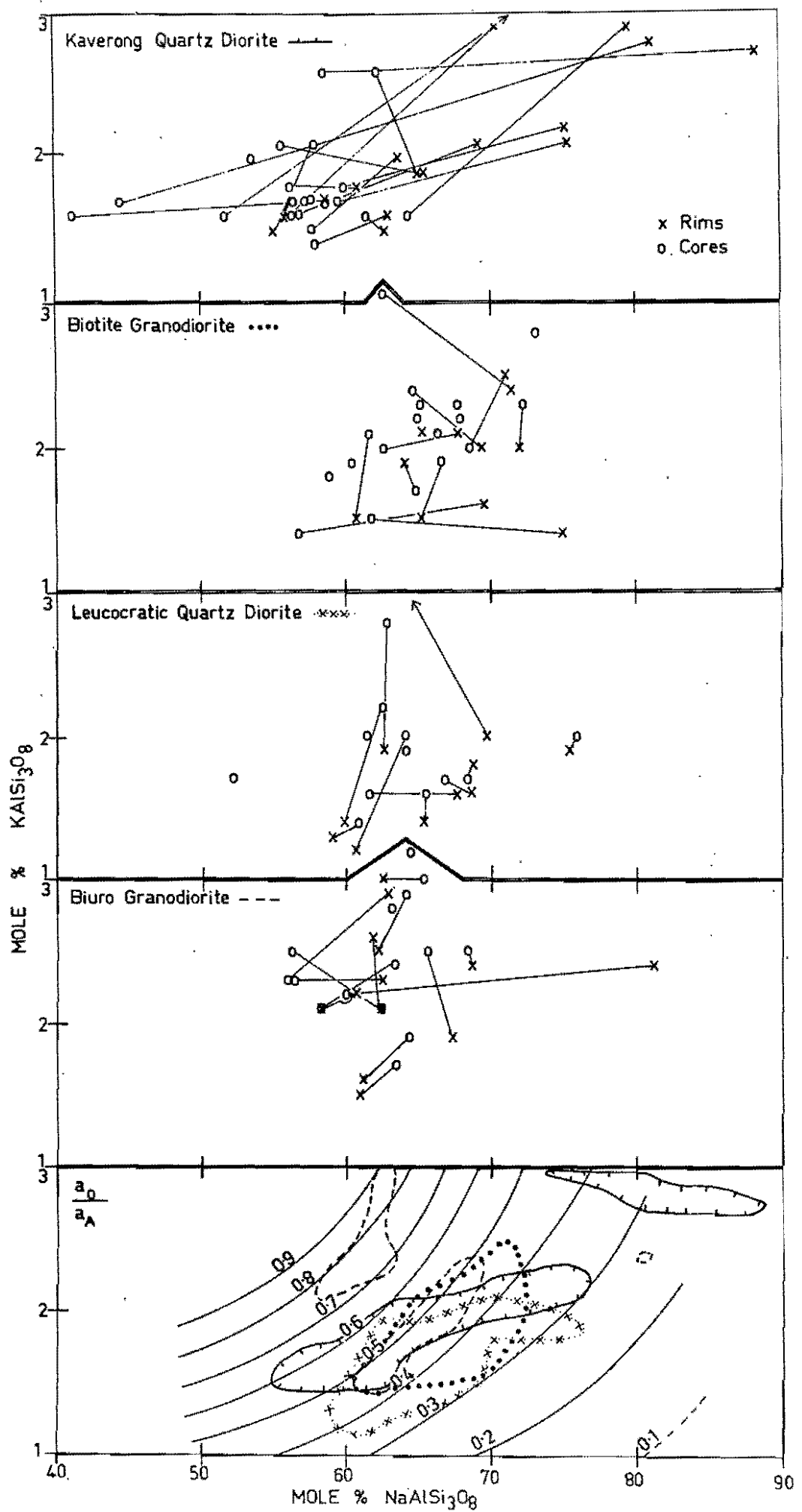
$$\frac{a_{\text{KCl}}}{a_{\text{NaCl}}} = \frac{m_{\text{KCl}}}{m_{\text{NaCl}}} = k_{10.1} \cdot \frac{a_O}{a_A}$$

The constant $k_{10.1}$ increases as a function of temperature over the range 773 - 923 K, and has a value of 0.44 at 923 K. A rough linear extrapolation based on the three data points indicates a value of about 0.6 at 1073 K.

The mole fractions of albite and orthoclase in plagioclase have been taken from Ford (1976) who analysed cores and rims of phenocrysts from the four main intrusions at Panguna. These are plotted, X_O vs. X_A as mole percentages, in fig. 10-1. Where core and rim analyses are available for the same phenocryst they are joined by a straight line. The ratio a_O/a_A has been contoured on the same axes; this was calculated from Ryabchikov's data for 1073 K.

There is commonly a large change in composition between core and rim in a phenocryst. In those few phenocrysts across which Ford did analytical traverses, most of the change takes place in the rim only,

Fig. 10-1 Compositions of plagioclase phenocrysts in the Panguna intrusive rocks. Mole % KAlSi_3O_8 is plotted against mole % $\text{NaAlSi}_3\text{O}_8$ (data from Ford, 1976). Both core and rim compositions are plotted, and are joined where available for single phenocrysts. The lowest diagram is a contour plot of the ratio $a_{\text{or}}/a_{\text{ab}}$ at 1073 K (see text for explanation), with the fields of rim compositions for each of the four intrusions (symbols shown beside names in other diagrams) superimposed.



i.e. this zone represents an event which occurred late in the crystallisation of the phenocrysts. Strong albitisation, by as much as 37 mole %, accompanied by an increase in the K content, is characteristic of the Kaverong Quartz Diorite. In the Leucocratic Quartz Diorite, a reduction in K content and relatively little change in Na is typical. Changes intermediate between these types are found in the other intrusions. Comparing the changes with the a_O/a_A curves, it is seen that all major changes in composition are in the direction of increasing a_O/a_A . Other phenocrysts indicate very little change in the ratio, except for two in the Biuro Granodiorite where there is a definite decrease.

The rim event was probably the exsolution of volatiles from the magmas. Later alteration seems unlikely; in the Kaverong Quartz Diorite, where there is considerable variation in the style of subsequent alteration, the rim compositions bear no relationship to Ford's descriptions of the alteration in each specimen. The fields of rim compositions are superimposed on the a_O/a_A contours in fig. 10-1. The fluid composition is obtained thence with the constant $k_{10.1}$. If $k_{10.1}$ at 1073 K is estimated to be 0.6 - 0.7, a fluid with $m_{KCl}/m_{NaCl} \approx 0.25$ (a likely value for a primary magmatic fluid with $T_{\text{NaCl}} \approx 500^\circ\text{C}$) is possible for $a_O/a_A <$

about 0.4. For those, or lower values of $k_{10.1}$ at 1073 K, equilibrium between liquid with the low K/Na values found at Panguna is possible for many of the phenocrysts in the Kaverong Quartz Diorite, the Biotite Granodiorite and the Leucocratic Quartz Diorite, but only for one from the Biuro Granodiorite. For higher K/Na in the primary salt-rich liquid, the upper limit on a_O/a_A is a little higher. The results seem consistent with the field and petrographic interpretation that the Biuro Granodiorite did not exsolve important quantities of mineralising fluids, whereas the others did.

THE FUGACITIES OF OXYGEN AND SULPHUR DURING COPPER MINERALISATION

The mineral assemblages at Panguna include many species useful for fixing the fugacities of oxygen and sulphur. Most of these, however, occur in low-temperature veins, and diagrams like those of Holland (1965) are useful only at temperatures below 800 K. These parameters are vital to an understanding of the processes taking place in the magma at temperatures much higher than 800 K. Other constraints must be invoked if they are to be evaluated.

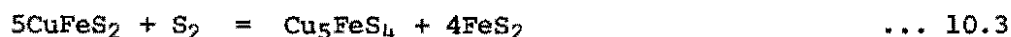
Oxygen fugacity. Coarsely-bladed, primary hematite in quartz-Cu,Fe sulphide veins, and hematite replacing magnetite in vein selvages have been described in Chapter 3, and by Lawrence & Savage (1975). Hematite as a daughter mineral and as solid inclusions is typical of many of these veins, especially the high-temperature ones, but is also completely absent from other veins. Yet others bear magnetite (Lawrence & Savage, 1975) or have selvages containing unaltered magnetite intergrown with chalcopyrite or bornite. Therefore the oxygen fugacity appears to have remained near the hematite-magnetite (HM) buffer



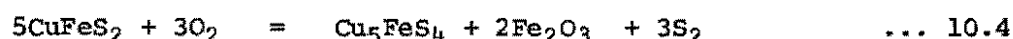
(possibly a little higher on average).

The various estimates of the oxygen fugacity at the HM buffer differ among themselves by at least one log unit, indicating the likely limitations of the thermochemical data being used here. The data used for the HM buffer reaction in figs. 10-2 and 10-3 have been taken from Haas & Robie (1973), and other data are from Robie & Waldbaum (1968). The data are consistent with the coexistence of sphalerite and hematite up to and beyond 850 K, but galena will not coexist with hematite above about 780 K. The occurrence of galena, bornite and hematite in 102594 (formed between 700 and 800 K) brackets the oxygen fugacity for that specimen tightly near the HM value.

Chalcopyrite and hematite usually occur together. At first sight, this might fix an upper limit to the oxygen fugacity at temperatures below 820 K where the tetragonal polymorph of CuFeS_2 becomes unstable (Yund & Kullerud, 1966). The chalcopyrite-bornite-hematite equilibrium

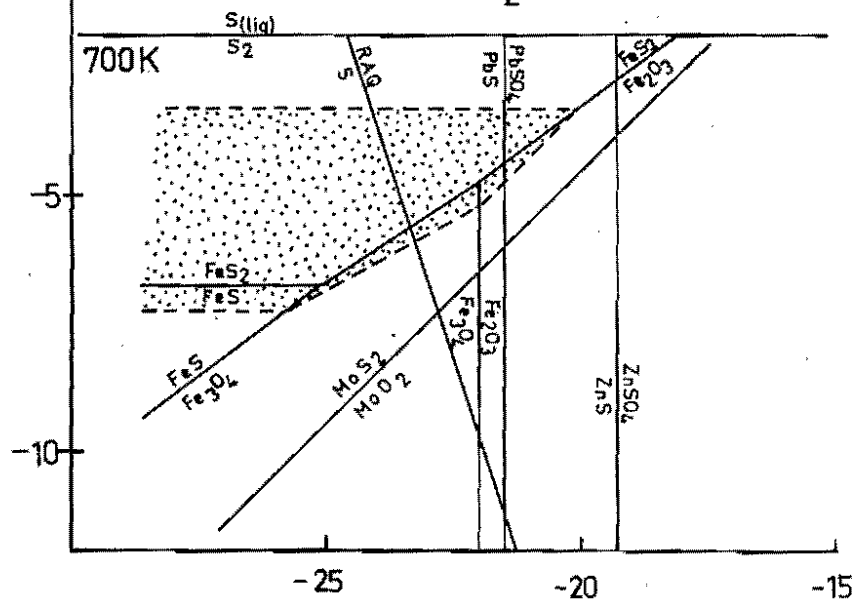
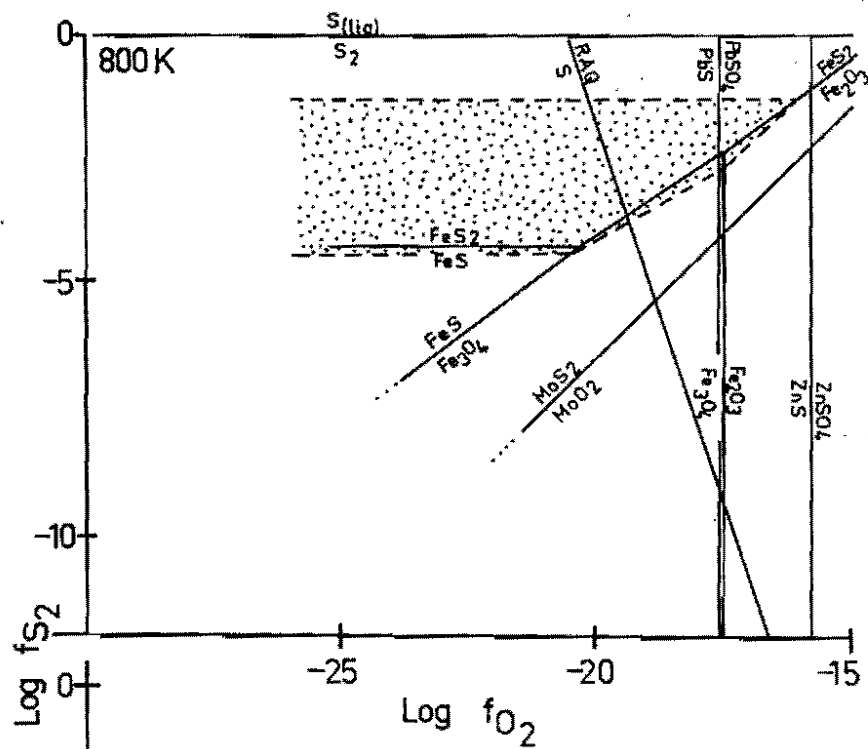
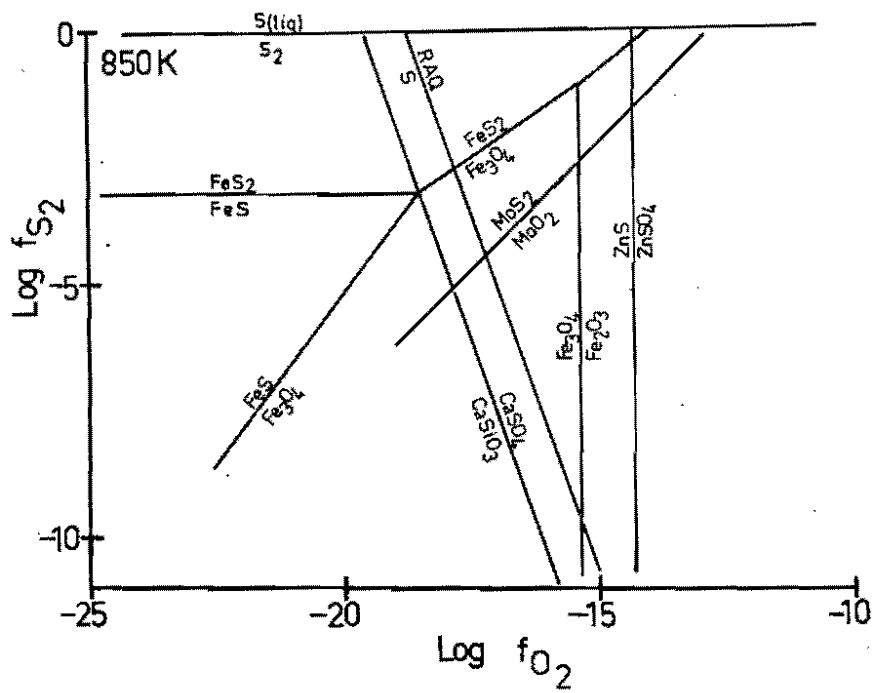


has been plotted using Barton's unpublished data (Barton & Skinner, in press), and the other boundaries of the chalcopyrite fields in fig. 10-2 are based on this, e.g. the boundary representing

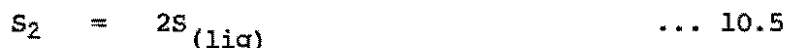


has slope 1 and passes through the point at which hematite, pyrite, chalcopyrite and bornite coexist. The unreliability of the data have already been stressed, however. The apparent convergence of the oxygen fugacities at HM and at the hematite-pyrite-chalcopyrite-bornite point with rising temperature suggests that high CuFeS_2 polymorphs and hematite might not be able to coexist at higher temperatures. No watertight conclusions can be drawn from the thermochemical data, which become even less reliable for the Cu,Fe sulphides above 820 K. Certainly, observation at Panguna suggests the opposite; that hematite and CuFeS_2 do coexist over the whole temperature range. However, it is not certain that the Cu,Fe sulphides now seen in veins formed above 820 K have retained their original compositions. Chalcopyrite, and less frequently bornite, are present yet the broad range of compositions of the cubic Intermediate Solid Solution, the high-temperature equivalent of chalcopyrite (Yund & Kullerud, 1966) implies that other exsolution products such as talnakhite, mooihoekite and haycockite ought to be present. Etch and microprobe investigations (etch methods from Cabri & Hall, 1972) have failed to reveal any of these; Barton (pers. comm, 1977) has commented that the sulphides may have undergone later additions of sulphur during the long hydrothermal history of Panguna.

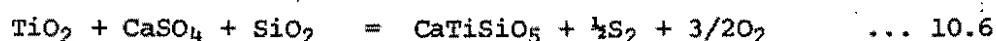
Fig. 10-2 Equilibria relevant to Panguna mineralisation, shown on $\log f_{S_2}$ vs. $\log f_{O_2}$ plots for temperatures of 700, 800 and 850 K. The field of chalcopyrite is stippled. RAQ/S refers to the rutile-anhydrite-quartz-sphene equilibrium (equation 10.6). Standard state pressure of all substances = 1 atm.



Sulphur fugacity. The sulphur condensation reaction



sets an absolute upper limit to the sulphur fugacity because no native sulphur is known in the deposit. The narrow range over which hematite and chalcopryrite coexist below 820 K would bracket the sulphur fugacity closely if it were reliable. It is nonetheless consistent with the broader limits set by the equilibria:



(represented as RAQ/S in figs. 10-2 and 10-3), and



(data for 10.7 from Holland, 1965). Rutile, anhydrite, quartz and molybdenite are characteristically found with chalcopryrite in veins with included hematite. Molybdenite has not been found in veins formed above 850 K, although Holland's data for reaction 10.7 suggest that the co-existence of molybdenite with rutile, quartz, anhydrite and hematite is possible at higher temperatures. Rutile is abundant in the selvages of anhydrite - quartz-Cu,Fe sulphide veins formed above 900 K (e.g. 102998, 102675 and 103012). If the whole assemblage is at equilibrium, then reaction 10.6 sets the only useful lower limit to the sulphur fugacity at high temperatures. The gaseous equilibrium



can be used to set an upper limit at high temperatures in conjunction with the constraint $P_{SO_2} \leq P_{total}$. Let us assume for the moment that $P_{SO_2} \leq 0.1 P_{total}$ (justification will be given in the section below on sulphur gas species), i.e. P_{SO_2} is no greater than the values given in Table 10-1. To find the fugacity of SO_2 , the Lewis & Randall approximation for gas mixtures is used;

viz. "the fugacity of each constituent is equal to its mole fraction multiplied by the fugacity it would exhibit as a pure gas, at the same temperature and the same total pressure."

(Denbigh, 1971)

In this case,

$$f_{\text{SO}_2} = \gamma_{\text{SO}_2} \cdot P_{\text{tot.}} \cdot X_{\text{SO}_2} = 0.1 \gamma_{\text{SO}_2} \cdot P_{\text{tot.}}$$

Using the equilibrium constants in Table 10-1 and fugacity coefficients from Newton (1935), the limiting fugacities of S_2 and SO_2 have been calculated (Table 10-1) and are plotted in fig. 10-3.

The limits at temperatures over 900 K do not appear to overlap any estimated high-temperature continuation (for Intermediate Solid Solution) of the CuFeS_2 fields from lower temperatures unless oxygen fugacities fall well within the magnetite field. The absence of magnetite from many high-temperature vein selvages and replacement textures in others argue strongly against adjusting the oxygen fugacity to fit. The blame might better be placed on the thermochemical data, and the uncertainty as to what happens at high temperatures.

Qualitatively, it is seen that the sulphur fugacity must increase with decreasing temperature to a maximum value near 800 K, and then decrease with continued cooling.

At 800 K, the fugacity of SO_2 for chalcopyrite-hematite-magnetite equilibrium is 11 atm, and the total fluid pressure is about 300 atm. At a log oxygen fugacity 1 unit above HM, the fugacity of SO_2 becomes 316 atm, corresponding to a pressure close to the total fluid pressure. Thus, at 800 K the oxygen fugacity must be very close to the value at the HM buffer as accepted here. This conclusion might be substantially changed by relatively small changes in the thermochemical data.

Table 10-1

FUGACITIES OF S₂ AND SO₂.

A. Maximum f_{S_2} , given $P_{SO_2} = 0.1 P_{tot.}$ ($x_{SO_2} = 0.1$)

T K	P_{SO_2} atm.	γ_{SO_2}	$f_{SO_2} =$ $x_{SO_2} \cdot \gamma_{SO_2} \cdot P_{tot.}$	\log f_{SO_2}	\log $k_{10.8}$	$\log f_{O_2}$ (HM)	$\log \frac{f_{SO_2}}{f_{S_2}^{1/2}}$	\log f_{S_2}
1100	80	1.11	89	2.0	13.4	-8.8	4.6	-5.5
1000	50	1.00	50	1.7	15.1	-11.0	4.1	-4.8
900	40	0.94	38	1.6	17.2	-13.8	3.4	-3.6

$$\log \frac{f_{SO_2}}{f_{S_2}^{1/2}} = \log k_{10.8} + \log f_{O_2}$$

B. Minimum f_{SO_2} , given minimum f_{S_2} (at rutile-anhydrite-quartz-sphene boundary, $f_{O_2} = \text{HM}$).

T K	$\log f_{S_2}$ ($f_{O_2} = \text{HM}$)	$\log \frac{f_{SO_2}}{f_{S_2}^{1/2}}$	$\log f_{SO_2}$	f_{SO_2} atm.
1100	-8.7	4.7	0.35	2.2
1000	-9.4	4.1	-0.60	0.25
900	-9.6	3.4	-1.40	4.0×10^{-2}

C. Range of f_{SO_2} and f_{S_2} (from A and B, above).

T	$\log f_{SO_2}$	$\log f_{S_2}$
1100	1.2 ± 0.8	-7.1 ± 1.7
1000	0.6 ± 1.0	-7.1 ± 2.3
900	0.1 ± 1.5	-6.6 ± 3.0

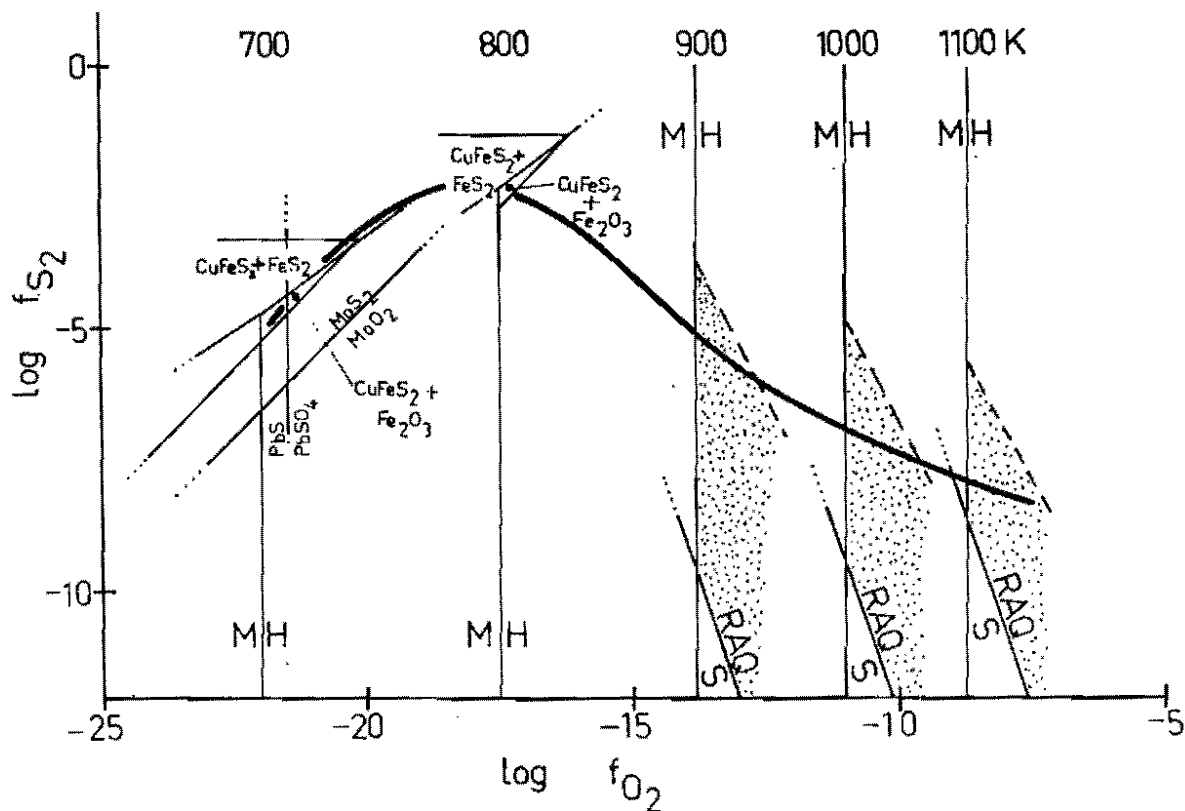
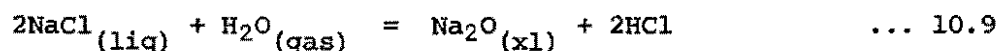


Fig. 10-3 A likely log f_{S_2} - log f_{O_2} path, as a function of temperature. See text for an explanation of assumptions. The stippled areas are the f_{O_2} - f_{S_2} fields at 900, 1000 and 1100 K, limited by the constraints:- hematite-magnetite equilibrium (M/H); rutile-anhydrite-quartz-sphene equilibrium (RAQ/S); $P_{SO_2} = 0.1 P_{tot}$. (dashed line, position calculated from Y_{SO_2} , f_{O_2} and data for equilibrium 10.8). There is no upper limit for f_{O_2} .

THE CHEMISTRY OF THE VAPOUR PHASE

State of water. Increasing pressure favours the polymerisation of H_2O in the vapour phase (Hastie, 1975, p.75 ff.). At pressures of 300 - 800 atm and temperatures near 1000 K the dimer predominates. The fugacity coefficient, as tabulated for example by Anderson (1967), corrects for this source of non-ideality so that the thermochemical data for monomeric water can be used. Mole fractions, however, ought to be calculated taking polymerisation into account. For the calculations which follow, the pressures and fugacities of water listed in Table 10-2 will be used, assuming $P_{H_2O} = P_{tot.}$. This assumption will be re-examined in the section on sulphur species, below.

Fugacity of HCl. Ryabchikov (1975) has suggested the following reaction to evaluate the fugacity of HCl in magmatic fluids



He estimated the activity of NaCl in the salt-rich liquid to be 0.35 ± 0.06 ; at Panguna the approach of salt-rich liquids to saturation near 700 K may mean that the activity approaches 1. Otherwise, Ryabchikov's estimate can be used. The error in this is much less than that involved in the estimation of the activity of Na_2O , which Ryabchikov does by setting limits based on granitoid mineralogy (presence of quartz and feldspars, absence of corundum at one extreme and of wollastonite at the other, fixing $a_{Al_2O_3}$ within limits and thence a_{Na_2O} by a reaction involving the decomposition of albite to its constituent oxides).

At 1000 K, equilibrium with a granitoid assemblage implies a HCl fugacity of 0.4 to 4.0 atm (Table 10-3). At the lower temperatures, the calculations will not correspond exactly with the situation in porphyry coppers; although quartz and one feldspar are present, the activities of the feldspar components will differ from those used by Ryabchikov. The estimates are therefore probably only general indications.

Table 10-2

FUGACITY OF WATER

T, K	P _{tot.} , atm.	$\gamma_{\text{H}_2\text{O}}$	f _{H₂O} , atm.	log f _{H₂O}
700	300	0.77	230	2.4
800	300	0.82	245	2.4
900	300	0.88	264	2.4
1000	500	0.88	440	2.6
1100	800	0.84	670	2.8

Table 10-3

FUGACITY OF HCl

T, K	log k _{10.9}	log f _{H₂O}	log a _{NaCl}	log a _{Na₂O}	log f _{HCl}
700	-27.3	2.4	0.0	-23±1	-1.0±0.5
800	-23.4	2.4	-.69±.16	-21±1	-0.7±0.6
850	-21.8	2.4	-.69±.16	-19.5±1	-0.7±0.6
1000	-17.9	2.6	-.69±.16	-16.8±0.8	0.1±0.5

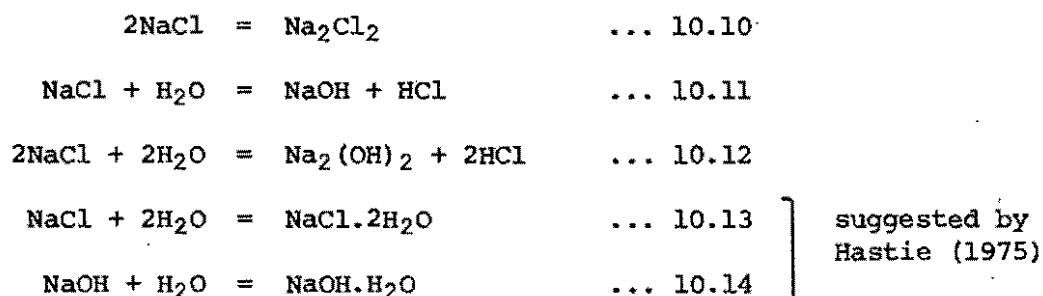
$$\log f_{\text{HCl}} = \frac{1}{2}(\log k + \log f_{\text{H}_2\text{O}} + 2\log a_{\text{NaCl}} - \log a_{\text{Na}_2\text{O}})$$

Table 10-4

DIMERISATION OF NaCl

T, K	log k _{10.10}	P _{tot.} , atm.	P _{NaCl} , atm.	P _{Na₂Cl₂} , atm.
700	8.27	0.36	4.4 x 10 ⁻⁵	0.36
800	6.42	0.05	1.4 x 10 ⁻⁴	0.05
850	5.70	0.05	3.2 x 10 ⁻⁴	0.05
900	4.98	0.09	1.0 x 10 ⁻³	0.09
1000	3.82	1.57	1.6 x 10 ⁻²	1.55

Fugacity of NaCl. For each set of pressure-temperature conditions, the composition of the vapour in the NaCl-H₂O system can be estimated from the fluid evolution paths discussed in the previous chapter, in conjunction with the data of Sourirajan & Kennedy (1962). The species present will depend on equilibrium in the following sets of gaseous reactions:



Thermochemical data are available in JANAF (1971) for all except the hydrate species. Considering initially only reaction 10.10, i.e. a vapour containing only sodium chloride at a total partial pressure P_t , P_t is calculated from the NaCl content of the vapour (wt. % is converted to mole fraction and thence to pressure), with water dimeric. Whether NaCl is mainly dimeric or monomeric does not, as shall be seen, change the final solution because the factor of 2 by which P_t would vary as a result is relatively insignificant in the solution of the two equations

$$P_{\text{NaCl}} + P_{\text{Na}_2\text{Cl}_2} = P_t$$

$$P_{\text{Na}_2\text{Cl}_2} / P_{\text{NaCl}}^2 = k_{10.10} \text{ (assuming } P_i = f_i \text{)}$$

The P_t values in Table 10-4 assume the predominance of dimers, but the same qualitative result, the predominance of dimers, can be obtained assuming mainly the monomer in the mole fraction calculation.

From thermochemical data for reactions 10.11 and 10.12, and the previously-established fugacities of HCl, the following are obtained:

at 1000 K,

$$\log \frac{f_{\text{NaOH}}}{f_{\text{NaCl}}} = -3.5 \pm 0.5; \quad \log \frac{f_{\text{Na}_2(\text{OH})_2}}{f_{\text{NaCl}}^2} = -3.7 \pm 1.0$$

and at 850 K,

$$\log \frac{f_{\text{NaOH}}}{f_{\text{NaCl}}} = -4.2 \pm 0.7; \quad \log \frac{f_{\text{Na}_2(\text{OH})_2}}{f_{\text{NaCl}}^2} = -2.9 \pm 1.4$$

For $\log f_{\text{NaCl}} < 0$, as it is here (considering the predominance of the dimer) NaOH is a minor species, but $\text{Na}_2(\text{OH})_2$ may predominate over NaCl and possibly also over Na_2Cl_2 . Hastie (1975) has explained that the change in slope of the solubility curve of NaCl in water vapour (see fig. 9-1) implies different chemical mechanisms of solution above and below 873 K and that these are consistent with reaction 10.14 above 873 K, and reaction 10.13 below 873 K. In the absence of the required thermochemical data, no firm conclusions can be drawn on the likely fugacity of NaCl. It is evident that NaCl will be a minor species, dominated by Na_2Cl_2 , and possibly by the hydrated species. The values of P_{NaCl} in Table 10-4 will be diminished by the formation of hydrates. The values in Table 10-4 will be used as maximum estimates of P_{NaCl} and f_{NaCl} .

Sulphur species. At temperatures over 673 K, only H_2S , S_2 and SO_2 need be considered among all the possible sulphur-bearing species in hydrothermal fluids (Barnes & Czamanske, 1967; Ohmoto & Rye, in press). S_2 is usually considered only because its fugacity is a useful chemical parameter.

In a system containing only H_2O and sulphur species, the constraints are

$$x_{\text{SO}_2} + x_{\text{H}_2\text{S}} + x_{\text{H}_2\text{O}} = 1$$



It has been shown in a previous section that the fugacity of sulphur cannot be limited without making assumptions about the fugacity of SO_2 . Here, we shall begin by examining the relative fugacities of H_2O and H_2S , assuming only that H_2O is a major constituent (and not, for the moment, that $f_{\text{H}_2\text{O}} = \gamma_{\text{H}_2\text{O}} \cdot P_{\text{tot.}}$) and setting a high limit for P_{SO_2} . The relationship of $f_{\text{H}_2\text{O}}$ and $P_{\text{tot.}}$ will then be re-examined, and, finally, the ratio $f_{\text{SO}_2}/f_{\text{H}_2\text{S}}$ will be calculated.

The ratio $f_{\text{H}_2\text{O}}/f_{\text{H}_2\text{S}}$ depends on f_{S_2} and f_{O_2} in the following way:

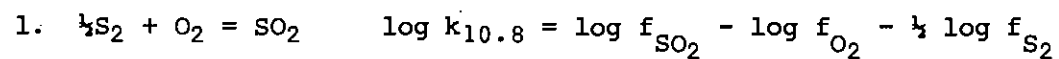
$$\log \frac{f_{\text{H}_2\text{O}}}{f_{\text{H}_2\text{S}}} = \log k_{10.15} + 3/2 \log f_{\text{O}_2} - \log f_{\text{SO}_2}$$

In Table 10-5, this ratio is calculated assuming a mole fraction of 1 for SO_2 in the vapour. For lower mole fractions (an order of magnitude lower would be reasonable), higher $\text{H}_2\text{O}/\text{H}_2\text{S}$ ratios are obtained. Thus only at 700 K might H_2S become important relative to water in the vapour and this is unlikely, because the mole fraction of SO_2 will be very small at 700 K. The fugacity ratio corresponds approximately with the pressure ratio because the ratio of fugacity coefficients is near 1. Except perhaps at 700 K, then, H_2S can be neglected relative to H_2O so that, to a sufficient approximation,

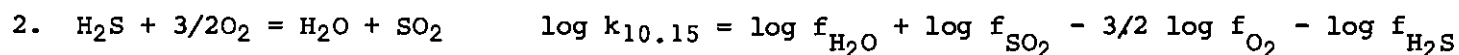
$$x_{\text{SO}_2} + x_{\text{H}_2\text{O}} = 1$$

Equation 10.8 can be used as a constraint only at 700 and 800 K where mineral equilibria provide upper and lower limits. At 900 - 1100 K,

Table 10-5

SULPHUR SPECIES EQUILIBRIA

T	$\log k_{10.8}$	$\log f_{\text{O}_2}$		$\log f_{\text{S}_2}$		$\log f_{\text{SO}_2}$		
		HM	HM+1	HM	HM+1	HM	HM+1	
700	24.0	-22.0	-21.0	-5.0	-4.1	-0.5	0.9	} f_{SO_2} derived from f_{S_2} , chalco- pyrite-hematite assemblage.
800	19.8	-17.5	-16.5	-2.5	-1.7	1.1	2.5	
900	17.2	-13.8	-12.8	-6.6±3.0	-9.1±3.4	0.1±1.5	-0.2±1.8	} f_{S_2} derived from pressure limits on SO_2 and rutile-anhydrite- quartz assemblage.
1000	15.1	-11.0	-10.0	-7.1±2.3	-9.6±2.8	0.6±1.0	0.3±1.4	
1100	13.4	-8.7	-7.7	-7.1±1.7	-9.6±2.1	1.2±0.8	0.9±1.1	



T	$\log k_{10.15}$	$\log f_{\text{O}_2}$		$\log f_{\text{SO}_2}^*$ if $x_{\text{SO}_2}=1$	$\log \frac{f_{\text{H}_2\text{O}}}{f_{\text{H}_2\text{S}}}$		$\gamma_{\text{H}_2\text{S}}^\dagger$	$\log \frac{f_{\text{SO}_2}}{f_{\text{H}_2\text{S}}}$		$\log \frac{f_{\text{SO}_2}}{f_{\text{H}_2\text{S}}}$		$\log f_{\text{H}_2\text{S}}$	
		HM	HM+1		HM	HM+1		$P_{\text{H}_2\text{O}} = P_{\text{tot.}}$, HM	HM+1	HM	HM+1	HM	HM+1
700	34.6	-22.0	-21.0	2.4	-0.8	0.7	1.2	-0.8	0.7	0.3	0.2		
800	29.8	-17.5	-16.5	2.4	1.2	2.7	1.2	1.2	2.7	-0.1	-0.2		
850	27.9	-15.3	-14.3	2.4	2.6	4.1	1.2	2.6	4.1				
900	26.0	-13.8	-12.8	2.5	2.8	4.3	1.2	2.9	4.4	-2.8±1.5	-4.6±1.8		
1000	23.0	-11.0	-10.0	2.7	3.8	5.3	1.2	3.9	5.4	-3.3±1.0	-5.1±1.4		
1100	20.5	-8.7	-7.7	3.0	4.5	6.0	1.4	4.7	6.2	-3.5±0.8	-5.3±1.1		

* coefficients from Newton (1935)

† coefficients from Ryzhenko & Volkov (1971) and Anderson (1967).

mineral equilibria provide only a lower limit to the sulphur fugacity, and an assumption must be made about the partial pressure of SO_2 in order to place an upper limit. If all of the volatiles exsolved by a magma go into a single fluid, the molar ratio $\text{SO}_2:\text{H}_2\text{O}$ can be calculated from Ryabchikov's (1975) estimate, 1 - 2%, of the water lost by the magma, and one he quotes from Vinogradov for the sulphur content of such magmas, 0.04%. These are by weight, so that the molar ratio is 0.02 (H_2O as monomers) or 0.04 (dimers). Thus the limit $P_{\text{SO}_2} < 0.1 P_{\text{tot.}}$ is adopted; if Vinogradov's estimate is low (it is difficult to see how the sulphur content of magmas which characteristically exsolve volatiles could be estimated) the fluid could carry away twice as much sulphur and still fall within the limit.

With this limit, it is possible to calculate the fugacity ratio $\text{SO}_2:\text{H}_2\text{S}$ and thence the fugacity limits of H_2S . The partial pressure of $(\text{H}_2\text{O})_n$ must be greater than $0.9 P_{\text{tot.}}$ and the mole fraction of $\text{H}_2\text{O} \geq 0.9$. By the Lewis & Randall Rule,

$$f_{\text{H}_2\text{O}}(\text{pure}) \geq f_{\text{H}_2\text{O}}(\text{mixture}) \geq 0.9 f_{\text{H}_2\text{O}}(\text{pure at same T \& P})$$

therefore, $0 \geq \log f_{\text{H}_2\text{O}}(\text{mixture}) - \log f_{\text{H}_2\text{O}}(\text{pure}) \geq -0.05$.

This correction may be regarded as negligible, and the fugacity ratio of SO_2 to H_2S calculated using $f_{\text{H}_2\text{O}}(\text{pure})$. The ratios, and the fugacity ranges of H_2S at the various temperatures are listed in Table 10-5, and plotted in fig. 10-4. In the figure, it is clearly shown that SO_2 is the principal sulphur species in the vapour in the porphyry copper environment. This need not be the case in the liquid, as will be seen in Chapter 11.

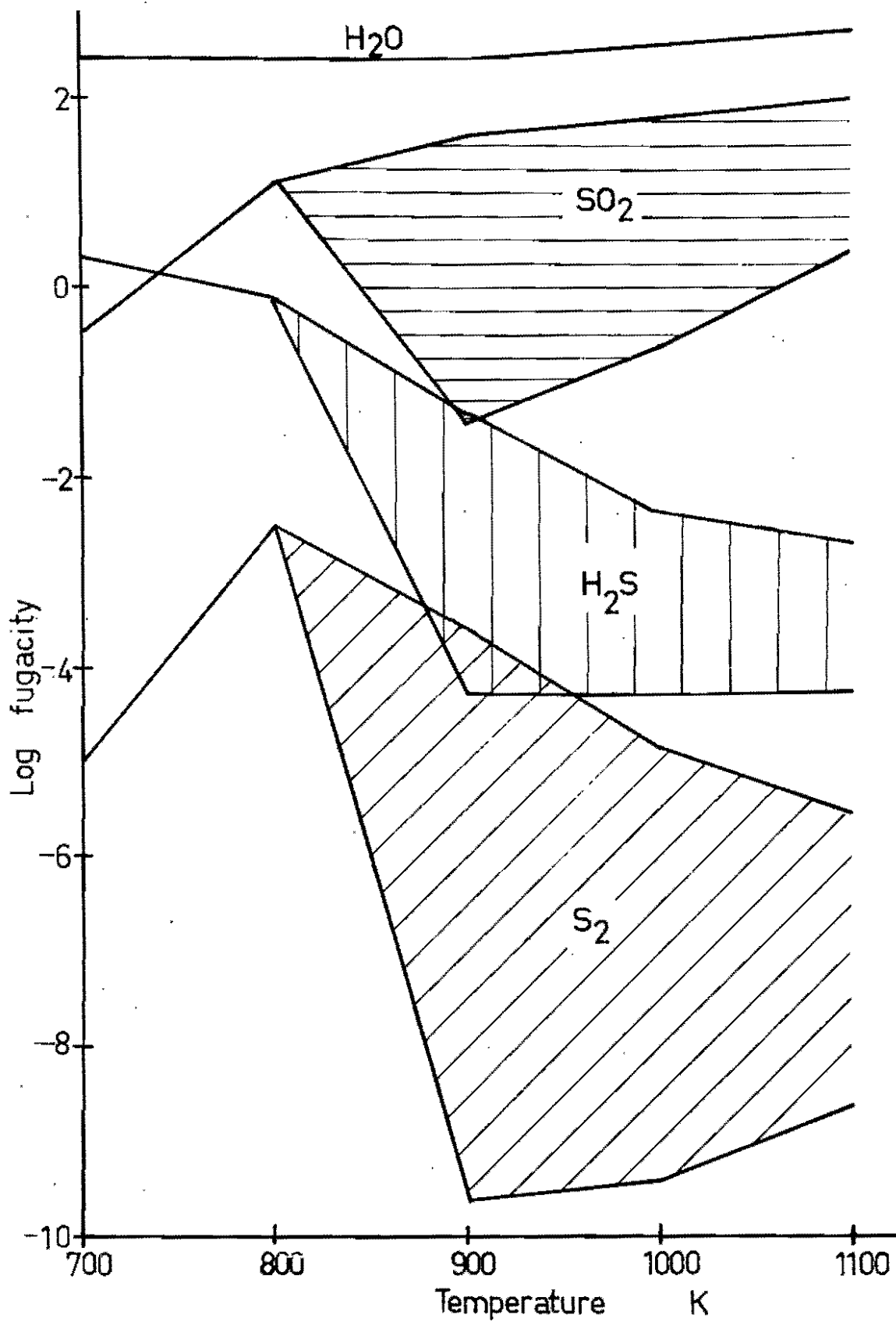


Fig. 10-4 Limits on the fugacities of H₂O, SO₂, H₂S and S₂ over the temperature range 700 - 1100 K at Panguna. Assumptions discussed in text.

BASE METAL TRANSPORT IN THE VAPOUR

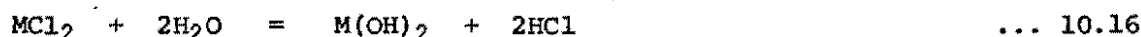
The vapour in porphyry copper systems removes a large amount of water, and may remove significant amounts of other volatiles such as NaCl, SO₂, H₂S, HCl and volatile base-metal species. The Henley & McNabb (1978) vapour plume mechanism, for example, would require significant transport of copper in the vapour. The vapour, as suggested by Krauskopf (1964), may also play a part in the separation of the base metals. The possibility of base-metal transport in vapour when fluid inclusions are decrepitated has been discussed in Chapter 4. The chemical-transport properties of the vapour in porphyry copper deposits will now be examined in the light of current thermochemical data. The approach is to be compared with that of Krauskopf (1964). It differs from Krauskopf's in that newer thermochemical data are available, and in the consideration of complex metal-bearing volatile species.

Enhanced volatility in salt mixtures. Some metal halides, particularly those of trivalent metals, are volatile at high temperatures. The mixing of halide salts gives rise to complex halide species. In a large number of mixed halide systems, the measured vapour pressures are higher than can be explained by the vapour pressures of the individual components. Commonly, then, the formation of complex halides in mixed halide systems enhances the volatility of the simple components. Reviews on this phenomenon include those of Schaefer (1976), Binnewies & Schaefer (1973) and Hastie (1975). Hastie's book includes a set of rules for the estimation of the thermochemical properties of many species, and a discussion of the possible application of the enhanced volatility notion to the problems of ore genesis.

The importance of enhanced halide volatility in chemical transport has been recognised, both in unapplied investigation (Schaefer, 1974) and

in metallurgy (the TORCO, or segregation process for the extraction of copper; Brittan, 1970; and Gross & Stuart, 1971).

Chloride volatility versus hydroxide volatility. Enhanced volatility is also characteristic of non-halide systems, in particular metal oxide - water systems and possibly sulphide systems (Hastie, 1975). Since water is the main constituent of porphyry-copper vapour, the relative importance of chloride and hydroxide volatility must be a first consideration. On p.68 ff. Hastie considers the ratio $P_{M(OH)_2}/P_{MCl_2}$ as a function of the ratio P_{HCl}/P_{H_2O} . From data available for certain cases in JANAF (1971), and from a consideration of the bond-dissociation energies involved, he deduces the following generalised thermochemical data for the reaction



$$\Delta S \approx -4 \pm 2 \text{ cal/deg.mole, } T = 1000 - 2000 \text{ K}$$

$$\Delta H \approx 28 \text{ kcal/mole.}$$

These are based on known thermodynamic data for reactions of type 10.16. Their negligible temperature dependence is characteristic of such vapour phase reactions (for the chloride-chloride reaction case, see below).

Thus $\log k_{10.16} \approx -7$ at 1000 K and -8 at 850 K, and

$$\frac{P_{MCl_2}}{P_{M(OH)_2}} = 10^7 \cdot \left(\frac{P_{HCl}}{P_{H_2O}} \right)^2 = 10^{2.0 \pm 1.0} \text{ at } 1000\text{K, and}$$

$$10^8 \cdot \left(\frac{P_{HCl}}{P_{H_2O}} \right)^2 = 10^{2.0 \pm 1.0} \text{ at } 850 \text{ K.}$$

(using data from previous sections).

Chlorides of divalent metals appear to predominate over hydroxides, but by relatively small factors at the lower limit in each case. An uncertainty of an order of magnitude in $\log k_{10.16}$ would therefore mean that $P_{M(OH)_2} \leq P_{MCl_2}$. No similar considerations are available for the mono-

valent metals, although it has already been seen that $\text{NaOH} \cdot \text{H}_2\text{O}$ may predominate over NaCl at temperatures over 873 K. For the trivalent metals it can be shown similarly that at 1000 K

$$\frac{P_{\text{MCl}}}{P_{\text{M(OH)}_3}} \approx 10^{10} \cdot \left(\frac{P_{\text{HCl}}}{P_{\text{H}_2\text{O}}} \right)^3 = 10^{2.5 \pm 1.5}$$

The conclusions for divalent and trivalent metals are therefore similar. At 1000 K, hydroxides may be present at levels comparable to or less than the concentrations of simple chloride species. This does not rule out the possible predominance of complex chloride species over both. The importance of these will now be considered for Fe, Cu, Zn and Mo.

IRON SPECIES

Ferrous species. Chou & Eugster (1977) showed that FeCl_2 was the dominant iron-bearing species in supercritical chloride solutions at oxygen fugacities up to the hematite-magnetite buffer. The conditions of the experiments do not match those at Panguna; to investigate the effect of Panguna conditions, the following gaseous reaction is considered:



$$\log \frac{f_{\text{FeCl}_3}}{f_{\text{FeCl}_2}} = \frac{1}{2}(\log k_{10.17} - \log f_{\text{H}_2\text{O}} + \frac{1}{2}\log f_{\text{O}_2} + 2 \log f_{\text{HCl}})$$

Using the fugacities established in earlier sections,

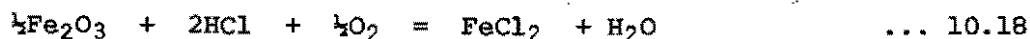
$$\text{At 1000 K, } \log k_{10.17} = 2.3, \text{ and } \log \frac{f_{\text{FeCl}_3}}{f_{\text{FeCl}_2}} = -1.7 \pm 0.5 \text{ at HM}$$

or -1.4 ± 0.5 at HM+1

$$\text{and at 850 K, } \log k_{10.17} = 3.6, \text{ and } \log \frac{f_{\text{FeCl}_3}}{f_{\text{FeCl}_2}} = -2.1 \pm 0.6 \text{ at HM}$$

or -1.8 ± 0.6 at HM+1

Ferrous chloride predominates, then, and will be used as a base for the measurement of the iron content in vapour according to the reaction

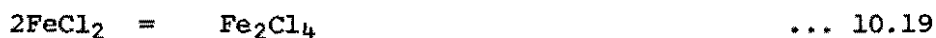


At 1000 K, $\log k_{10.18} = -6.1$ and $\log f_{\text{FeCl}_2} = -14.0 \pm 1.0$ at HM
or -13.5 ± 1.0 at HM+1.

At 850 K, $\log k_{10.18} = -7.2$ and $\log f_{\text{FeCl}_2} = -18.7 \pm 1.2$ at HM
or -18.2 ± 1.2 at HM+1.

Other ferrous species which could be considered are the dimer Fe_2Cl_4 and NaFeCl_3 . The K-analogues of the Na-bearing complexes should behave similarly, and will not be considered here.

Thermochemical data for the reactions



can be estimated with the rules suggested by Hastie (1975, p.135 ff.).

For reactions of the type $A + B = C$,

$$\Delta S = -30 \pm 5 \text{ cal/deg.mole.}$$

Hastie commented that ΔS for such homogeneous gaseous reactions is found to depend chiefly on the change in number of species. As a corollary, ΔS changes little with temperature, and the temperature dependence can be entirely neglected if only whole orders of magnitude are considered.

ΔH is given by a consideration of changes in the number and nature of chemical bonds, and for mixed complexes, by an additional, empirically-based measure of stability enhancement as a function of changes in the coulombic repulsion between metal atoms. For the coulombic effect, the change considered is that taking place on the reaction of two simple dimers to give two molecules of the complex species (see NaFeCl_3 example below).

For the cyclic Fe_2Cl_4 structure $(\text{Cl}-\text{Fe} \begin{smallmatrix} \text{Cl} \\ \diagup \diagdown \end{smallmatrix} \text{Fe}-\text{Cl})$ the contribution of bond dissociation energy is the result of the substitution of four bridging Fe-Cl bonds for two terminal Fe-Cl bonds. Hastie has shown that the energy of a bridging bond in general is about 0.6 of the energy of a terminal bond linking the same types of atoms. In the case of Fe_2Cl_4 there is no coulombic repulsion effect, because both of the metal atoms are the same. The enthalpy change has a negligible temperature dependence (because it is due largely to changes in bond dissociation energies) if only whole orders of magnitude are dealt with.

It is found that $\Delta H = -0.4 \bar{D}_{\text{Fe-Cl}}$, where $\bar{D}_{\text{Fe-Cl}}$ is the average bond dissociation energy of Fe-Cl bonds in FeCl_2 , equal to 97.2 kcal/mole (Vedeneyev *et al.*, 1966). Thus $\Delta H = -38.9$ kcal/mole, and at 1000 K

$$\Delta G = \Delta H - T\Delta S = -9.6 \pm 5.0 \text{ kcal/mole.}$$

$$\log k_{10.19} = 2 \pm 1 = \log \frac{f_{\text{Fe}_2\text{Cl}_4}}{f_{\text{FeCl}_2}} - \log f_{\text{FeCl}_2}$$

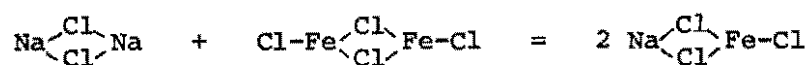
$$\log \frac{f_{\text{Fe}_2\text{Cl}_4}}{f_{\text{FeCl}_2}} \simeq -12 \pm 2 \text{ at HM and at HM+1.}$$

Similarly, at 850 K,

$$\log \frac{f_{\text{Fe}_2\text{Cl}_4}}{f_{\text{FeCl}_2}} \simeq -16 \pm 2 \text{ at HM.}$$

Applying Hastie's rules to reaction 10.20, $\Delta S = -30 \pm 5$ cal/mole.deg and ΔH (bond) = $-0.2 (D_{\text{Na-Cl}} + \bar{D}_{\text{Fe-Cl}}) = -38.9$ kcal/mole (data from Weast, 1975; and Vedeneyev, 1966).

To calculate the coulombic stabilisation, the reaction considered is



Na and Fe are considered to be ions of charge +1 and +2 respectively, so that the change in electrostatic potential energy is

$$\Delta U = 2 \left[\frac{1 \times 2}{r_{\text{Na}} + r_{\text{Fe}}} \right] - \frac{2 \times 2}{2r_{\text{Fe}}} - \frac{1 \times 1}{2r_{\text{Na}}} \simeq -0.9 \text{\AA}^{-1} \text{ (arbitrary units)}$$

(r_i is the ionic radius of ion i , values from Weast, 1975).

From fig. 3-6 of Hastie (1975), this corresponds with a stabilisation of $\Delta H \simeq -15$ kcal/mole.

So the total ΔH of reaction 10.20 is -53.9 kcal/mole.

At 1000 K, $\Delta G = -23.9 \pm 5$, and $\log k_{10.20} = 5 \pm 1$;

$$\begin{aligned} \log \frac{f_{\text{NaFeCl}_3}}{f_{\text{FeCl}_2}} &= 5 \pm 1 + \log f_{\text{NaCl}} \\ &\leq 3 \pm 1 \quad (\text{if } \log f_{\text{NaCl}} \leq \log P_{\text{NaCl}} \text{ as in} \end{aligned}$$

Table 10-4). No better estimate is possible because of the uncertainty about f_{NaCl} ; it can only be concluded that NaFeCl_3 could be the dominant species by a factor of 10^2 to 10^4 .

At 850 K,

$$\log \frac{f_{\text{NaFeCl}_3}}{f_{\text{FeCl}_2}} \leq 4 \pm 1.$$

Ferric species. For the ferric species NaFeCl_4 , there are thermochemical data in the literature. The gaseous reaction considered is:



Galitskiy (1968) gives $\Delta G = -22.7$ kcal/mole at 1000 K, and -27.0 kcal/mole at 850 K.

$$\text{At 1000 K, } \log k_{10.21} = 5.0 = \log \frac{f_{\text{NaFeCl}_4}}{f_{\text{FeCl}_3}} - \log f_{\text{NaCl}}$$

$$\text{and } \log \frac{f_{\text{NaFeCl}_4}}{f_{\text{FeCl}_3}} \leq 3.2$$

$$\text{At 850 K, } \log \frac{f_{\text{NaFeCl}_4}}{f_{\text{FeCl}_3}} \leq 1.5$$

The dimerisation of FeCl_3 takes place by the gaseous reaction



At 1000 K, $\log k_{10.22} = 0.2$, so that

$$\log f_{\text{Fe}_2\text{Cl}_6} = \log k_{10.22} + 2 \log f_{\text{FeCl}_3} \approx -31 \text{ at HM.}$$

Similarly at 850 K, Fe_2Cl_6 is unimportant.

Summarising, for all the ratios obtained above at 1000 K,

$\log f_{\text{H}_2\text{O}} = 2.6$, $\log f_{\text{HCl}} = 0.1 \pm 0.5$, the fugacities of the iron-bearing species in the vapour are:

$\log f$	HM	HM+1
f_{O_2}		
f_{FeCl_2}	-14.0 ± 1.0	-13.5 ± 1.0
f_{FeCl_3}	-15.7 ± 1.5	-14.9 ± 1.5
f_{NaFeCl_3}	$\leq -11 \pm 2$	$\leq -11 \pm 2$
f_{NaFeCl_4}	$\leq -12.5 \pm 1.5$	$\leq -11.7 \pm 1.5$
$f_{\text{Fe}_2\text{Cl}_4}$	-26 ± 3	-26 ± 3
$f_{\text{Fe}_2\text{Cl}_6}$	-31 ± 3	-30 ± 3

Evidently, iron transport in the vapour is of very minor significance, even if the volatility of hydroxide species approaches that of the chlorides.

COPPER SPECIES

There are no data for comparing the volatilities of the hydroxide and chloride species of monovalent copper, but it is possible to compare the various chloride species. Divalent chloride species are assumed not to exist at most of the temperatures of interest because CuCl_2 decomposes at 766 K (Barin & Knacke, 1973). CuCl , its polymers, NaCuCl_2 , NaCu_2Cl_3 , CuFeCl_3 and CuFeCl_4 will be considered.

For chalcopyrite-hematite equilibrium, the CuCl content of the vapour can be calculated for temperatures up to 820 K (the temperature at which the tetragonal polymorph of CuFeS₂ becomes unstable) within the limits of accuracy of the data.



At 800 K, $\log k_{10.23} = -6.1$ (data for chalcopyrite from Barton & Skinner, in press) so that

$$\begin{aligned} \log f_{\text{CuCl}} &= -\log k_{10.23} + 2 \log f_{\text{O}_2} - \log f_{\text{HCl}} - \log f_{\text{S}_2} - \frac{1}{2} \log f_{\text{H}_2\text{O}} \\ &= -28.3 \text{ at HM and } -26.3 \text{ at HM+1.} \end{aligned}$$

For the higher-temperature cubic polymorph, it is estimated that

$G_f = -40 \pm 10$ kcal/mole at 1000 K (an extrapolation of Barton's data for the lower polymorph). In this case, $\log k_{10.23} = -6 \pm 2$ and $\log f_{\text{CuCl}} = -10 \pm 5$ at HM, assuming that the activity of CuFeS₂ in the solid solution is 1.

The polymers of CuCl. Except for the trimer (JANAF, 1971) the data are from Guido *et al.* (1972).



$\log k_{10.24} = 3.2 \pm 0.4$ at 1000 K and 5.5 ± 0.5 at 800 K.

$$\log f \frac{f_{\text{Cu}_2\text{Cl}_2}}{f_{\text{CuCl}}} = \log f_{\text{CuCl}} + \log k_{10.24}$$

-23 at 800 K, HM.

At 1000 K, if $\log f_{\text{CuCl}} < -2.8$, $\log \frac{f_{\text{Cu}_2\text{Cl}_2}}{f_{\text{CuCl}}} < 0$.



$\log k_{10.25} = 20.4$ at 800 K and 13.6 at 1000 K.

$$\log \frac{f_{\text{Cu}_3\text{Cl}_3}}{f_{\text{CuCl}}} = \log k_{10.25} + 2 \log f_{\text{CuCl}} = -36 \text{ at } 800 \text{ K and HM.}$$

$$\text{At } 1000 \text{ K, } \log \frac{f_{\text{Cu}_3\text{Cl}_3}}{f_{\text{CuCl}}} < 0 \text{ if } \log f_{\text{CuCl}} < -6.8$$



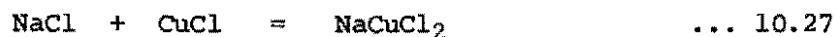
$$\log k_{10.26} = 23.1 \pm 0.6 \text{ at } 800 \text{ K and } 14.6 \pm 0.6 \text{ at } 1000 \text{ K.}$$

$$\log \frac{f_{\text{Cu}_4\text{Cl}_4}}{f_{\text{CuCl}}} = \log k_{10.26} + 3 \log f_{\text{CuCl}} = -61 \text{ at } 800 \text{ K and HM.}$$

$$\text{At } 1000 \text{ K, } \log \frac{f_{\text{Cu}_4\text{Cl}_4}}{f_{\text{CuCl}}} < 0 \text{ if } \log f_{\text{CuCl}} < -4.7$$

None of the polymers is significant beside CuCl at 800 K. The polymers could only be significant at 1000 K if $\log f_{\text{CuCl}}$ exceeded the limits indicated. None seems likely to be significant at Panguna, given the limits calculated roughly from reaction 10.23. Even the trimer can only become significant near the upper limit of f_{CuCl} estimated from equilibrium 10.23, from limits set deliberately very broad. At $\log f_{\text{CuCl}} > -6$, $\log f_{\text{Cu}_3\text{Cl}_3} > -4.4$ and Cu transport in this form becomes important. In systems with higher f_{CuCl} , the trimer may predominate (e.g. the study of Gross & Stuart, 1971) or the tetramer may also be important (J.D. Williams, University of Tasmania, pers. comm., 1978).

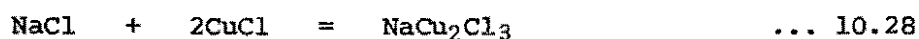
Na-bearing species. Gross & Stuart (1971) found that the formation of the complexes NaCuCl_2 and NaCu_2Cl_3 "contributed a very considerable part" to copper transport at temperatures above 1000 K in the segregation process for copper extraction, but found no evidence of a Na_2CuCl_3 complex. They estimated equilibrium constants based on pressure ratios in torr; these will be used below with the pressures converted to atm. Again, the situation must be re-examined thoroughly for the conditions at Panguna. For the gaseous reaction



$$\begin{aligned} \log k_{10.27} &= \frac{-11900}{T} + 11.6 \pm 0.5 \\ &= -3.3 \pm 0.5 \text{ at } 800 \text{ K (extrapolating) and } -0.3 \pm 0.5 \\ &\text{ at } 1000 \text{ K.} \end{aligned}$$

$$\begin{aligned} \log \frac{P_{\text{NaCuCl}_2}}{P_{\text{CuCl}}} &= \log k_{10.27} + \log P_{\text{NaCl}} \\ &\leq -6.8 \pm 0.5 \text{ at } 800 \text{ K (} \log P_{\text{NaCl}} \leq -3.5 \text{)} \\ \text{or } &\leq -2.1 \pm 0.5 \text{ at } 1000 \text{ K (} \log P_{\text{NaCl}} \leq -1.8 \text{)}. \end{aligned}$$

The NaCu_2Cl_3 species is formed by the gaseous reaction



$$\begin{aligned} \text{for which } \log k_{10.28} &= \frac{-25600}{T} + 25.3 \pm 1.0 \\ &= -6.7 \pm 1.0 \text{ at } 800 \text{ K and } -0.3 \pm 1.0 \text{ at } 1000 \text{ K.} \end{aligned}$$

$$\begin{aligned} \log \frac{P_{\text{NaCu}_2\text{Cl}_3}}{P_{\text{CuCl}}} &= \log k_{10.28} + \log P_{\text{NaCl}} = \log P_{\text{CuCl}} \\ &\leq -38.5 \pm 1.0 \text{ at } 800 \text{ K, HM, } \log P_{\text{NaCl}} \leq -3.5 \\ &\text{and } \leq -2.1 \pm 1.0 + \log P_{\text{CuCl}} \text{ at } 1000 \text{ K; this is much} \end{aligned}$$

less than $\log P_{\text{NaCuCl}_2}/P_{\text{CuCl}}$ at likely values of P_{CuCl} .

At the temperatures cited, neither complex is important compared with CuCl .

NaCuCl_2 may become comparable with CuCl at a temperature greater than 1000 K, possibly at magmatic temperatures.

Fe-bearing species. These can be considered using rules given by Hastie (1975). For



$$\begin{aligned} \Delta S &= -30 \pm 5 \text{ cal/deg.mole} \\ \Delta H (\text{bond}) &= -0.2 (D_{\text{Cu-Cl}} + \bar{D}_{\text{Fe-Cl}}) \quad (\bar{D} \text{ for } \text{FeCl}_2) \\ &= -36.4 \text{ kcal/mole.} \end{aligned}$$

$$\Delta H \text{ (coulombic repulsion)} = -15 \text{ kcal/mole}$$

$$\text{Total } \Delta H = -41 \text{ kcal/mole.}$$

$$\log k_{10.29} = 2 \pm 2 \text{ at } 1000 \text{ K and } 5 \pm 1 \text{ at } 800 \text{ K.}$$

$$\log \frac{f_{\text{CuFeCl}_3}}{f_{\text{CuCl}}} = \log k_{10.29} + \log f_{\text{FeCl}_2}$$

$$= -16 \pm 2 \text{ at HM, } 1000 \text{ K,}$$

$$\text{or much less at HM, } 800 \text{ K.}$$

The species CuFeCl_4 can be treated similarly, but estimating the coulombic repulsion enthalpy term from Hastie's diagram engenders an uncertainty of ± 10 kcal/mole.



$$\Delta S = -30 \pm 5 \text{ cal/deg.mole}$$

$$\Delta H \text{ (bond)} = -0.2 (D_{\text{Cu-Cl}} + \bar{D}_{\text{Fe-Cl}}) = -35.8 \text{ kcal/mole}$$

(\bar{D} for FeCl_3)

$$\Delta H \text{ (coulombic repulsion)} = -20 \pm 10 \text{ kcal/mole.}$$

$$\log k_{10.30} = 6 \pm 4 \text{ at } 1000 \text{ K and } 8 \pm 4 \text{ at } 800 \text{ K.}$$

$$\log \frac{f_{\text{CuFeCl}_4}}{f_{\text{CuCl}}} = \log k_{10.30} + \log f_{\text{FeCl}_3}$$

$$= -10 \pm 6 \text{ at } 1000 \text{ K, HM, and less at } 800 \text{ K.}$$

Neither of the iron-bearing species need therefore be considered.

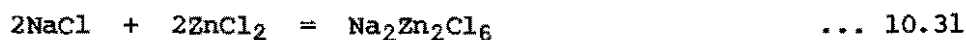
Dewing (1970) found no stable complexes of larger size formed between CuCl and FeCl_3 under the conditions of his experiments (673 - 1073 K, CuCl-FeCl_3 melt present).

Summary. Of the possible copper-bearing species considered, CuCl is the predominant one at 800 K, and probably also at 1000 K. Even at 1000 K, rough calculations suggest that there is only a very small amount of copper in the vapour.

ZINC SPECIES

Some zinc is certainly present in porphyry copper fluids, as indicated by the analysis of fluid inclusion decrepitation products (Chapter 4), but little zinc is deposited in the ore zone. A study of zinc speciation may be useful in explaining this. Chloride species which could transport significant zinc in vapour include ZnCl_2 , Zn_2Cl_4 , NaZnCl_3 , $\text{Na}_2\text{Zn}_2\text{Cl}_6$, the K-analogues of these species, and possibly ZnFeCl_4 . Again, the potassium species will be assumed to behave as the sodium ones.

Na-bearing species. The complexes NaZnCl_3 , and $\text{Na}_2\text{Zn}_2\text{Cl}_6$ were reported by Bloom *et al.* (1970) who gave these thermochemical data:



$$\Delta H = -53.8 \text{ kcal/mole}$$



$$\Delta H = -18.3 \pm 3.4 \text{ kcal/mole.}$$

All species are gaseous, and the temperature range is 577 - 777 K. Since these enthalpies depend largely on bond dissociation energies and bond lengths (Hastie, 1975), they are not significantly temperature-dependent and can be extrapolated. Hastie's rules give

$$\Delta S_{10.31} = -90 \pm 15 \text{ cal/deg.mole}$$

$$S_{10.32} = -30 \pm 5 \text{ cal/deg.mole.}$$

At 1000 K, $\log k_{10.32}$ is -2.6

$$\log \frac{f_{\text{NaZnCl}_3}}{f_{\text{ZnCl}_2}} = \log k_{10.32} + \log f_{\text{NaCl}}$$

$$\leq -4.4 \quad (\text{if } \log f_{\text{NaCl}} \leq -1.8).$$

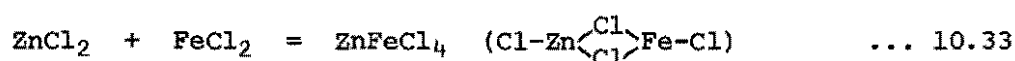
$\log k_{10.31} = -7.9$ at 1000 K, and

$$\log \frac{f_{\text{Na}_2\text{Zn}_2\text{Cl}_6}}{f_{\text{ZnCl}_2}} = \log k_{10.31} + 2 \log f_{\text{NaCl}} + \log f_{\text{ZnCl}_2} \\ \leq -11.5 + \log f_{\text{ZnCl}_2}$$

If $f_{\text{ZnCl}_2} < 500$ ($P_{\text{tot.}} = 500$ atm), $\log \frac{f_{\text{Na}_2\text{Zn}_2\text{Cl}_6}}{f_{\text{ZnCl}_2}} \leq -8.8$.

ZnCl_2 clearly predominates over the NaCl-ZnCl_2 complexes at 1000 K, and a similar result applies at 850 K.

Fe-bearing species. The thermochemical data for the reaction



can be estimated by Hastie's rules.

$$\Delta S = -30 \pm 5 \text{ cal/deg.mole}$$

$$\Delta H (\text{bond}) = -0.2 (\bar{D}_{\text{Zn-Cl}} + \bar{D}_{\text{Fe-Cl}}) = -34 \pm 2 \text{ kcal/mole}$$

($\bar{D}_{\text{A-Cl}}$ for ACl_2 ; data from Vedeneyev *et al.*, 1966).

ΔH (coulombic repulsion) = 0 (because the ionic radii of Fe^{2+} and Zn^{2+} are equal; Weast, 1975). Hence there is no stability enhancement, and the species should be unimportant relative to ZnCl_2 and FeCl_3 . To test this:

$$\text{At 1000 K, } \Delta G_{10.33} = 4 \pm 7 \text{ kcal/mole}$$

$$\text{and } \log k_{10.33} \leq 0.7$$

$$\log \frac{f_{\text{ZnFeCl}_4}}{f_{\text{ZnCl}_2}} = \log k_{10.33} + \log f_{\text{FeCl}_2} \\ \leq -14.7 \pm 1.0 \text{ at HM.}$$

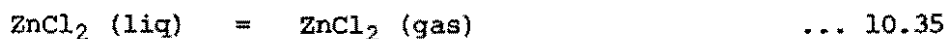
ZnCl_2 . Thus only ZnCl_2 (and possibly its dimer) are important.

The fugacity of ZnCl_2 can be estimated roughly from the reaction



at 850 K, approximately the formation temperature of 103014, in which there is sphalerite. No explicit thermodynamic data for ZnCl_2 gas are

available, but Barin & Knacke (1973) give ΔG_f^O for the liquid (-128.7 kcal/mole), and the equilibrium vapour pressure. It will be assumed that $f_{\text{ZnCl}_2} = P_{\text{ZnCl}_2} = 6.6 \times 10^{-2}$ atm.



For pure liquid, $\log k_{10.35} = \log f_{\text{ZnCl}_2} = -1.2$, and $\Delta G_{10.35} = 4.7$ kcal/mole. Thus $\Delta G_f^O \text{ ZnCl}_2 (\text{gas}) \approx -124$ kcal/mole. So for reaction 10.34, using only data from Barin & Knacke,

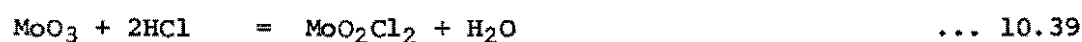
$$\log k_{10.34} = -3.7$$

$$\begin{aligned} \text{and } \log f_{\text{ZnCl}_2} &= \log k_{10.34} - \log f_{\text{H}_2\text{S}} + 2 \log f_{\text{HCl}} \\ &= -3.7 \pm 1.8 \end{aligned}$$

The calculation would not give a meaningful result at 1000 K because ZnS does not appear to be stable at Panguna at that temperature. If the amount of ZnCl_2 in the salt-rich liquid is the same at 850 K and 1000 K, the amount of Zn in the vapour at 1000 K should be much larger than at 850 K. Vapour pressures of pure liquid ZnCl increase about sixteenfold over the same temperature interval (Barin & Knacke, 1973).

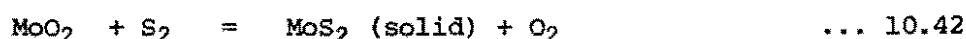
MOLYBDENUM SPECIES

Both the oxides and chlorides of Mo are volatile, and the +4, +5 and +6 valence states may be important. There are thus many reactions to consider. Thermochemical data are available for the following (all species gaseous):



The rules used previously cannot be applied to complex halide species of molybdenum. Table 10-6 is a listing of the equilibrium constants and fugacity ratios for the equations above under Panguna conditions. The +6 oxidation state predominates, largely as OH-bearing species. Glemser & Wendlandt (1963) have suggested that even larger hydroxy-oxide species may be the most significant in the transport of Mo. The species $\text{Mo}_7\text{O}_{18}(\text{OH})_6$ is consistent with the chemical-transport data at pressures up to 330 atm. At higher pressures, they suggested a species involving two H_2O molecules. There are no thermochemical data for these species, but their predominance would be consistent with the stability trend established for the simpler species. Certainly, all available data suggest the predominance of hydroxy-oxide species under Panguna conditions. Krauskopf (1964), concluded that oxides predominated over chlorides under most f_{HCl} conditions at 1 kbar total pressure.

There is no evidence that molybdenite is a stable solid phase at Panguna at magmatic temperatures. If molybdenite was stable at 850 K (e.g. in 103014, where several type III inclusions gave $T_h > 580^\circ\text{C}$), the equilibrium fugacity of MoO_2 would have been as follows.



Mills (1974) gives estimates of ΔG_f° for MoS_2 .

$$\log k_{10.42} = 13.3$$

$$\begin{aligned} \log f_{\text{MoO}_2} &= -\log k_{10.42} + \log f_{\text{O}_2} - \log f_{\text{S}_2} \\ &= -24.1 \pm 1.5 \end{aligned}$$

and from the data in Table 10-6, $\log f_{\text{MoO}_2(\text{OH})_2} = -3.6 \pm 1.5$

Table 10-6

MOLYBDENUM SPECIES

At 1000 K, $\log f_{\text{H}_2\text{O}} = 2.6$, $\log f_{\text{HCl}} = 0.1 \pm 0.5$, $\log f_{\text{O}_2} = -11.0$ (HM)

Reaction	$\log k_{10.1}$	
10.36	11.2	$\log [f_{\text{MoCl}_4}/f_{\text{MoO}_2}] = 6.4 \pm 2.0$
10.37	7.9	$\log [f_{\text{MoO}_3}/f_{\text{MoO}_2}] = 7.6$
10.38	7.5	$\log [f_{\text{MoO}_2(\text{OH})_2}/f_{\text{MoO}_3}] = 10.1$
10.39	10.6	$\log [f_{\text{MoO}_2\text{Cl}_2}/f_{\text{MoO}_3}] = 8.4 \pm 1.0$
10.40	-8.35	$\log [f_{\text{MoCl}_6}/f_{\text{MoO}_3}] = -15.6 \pm 3.0$
10.41	-5.2	$\log [f_{\text{MoCl}_6}/f_{\text{MoCl}_5}] = -9.1 \pm 0.5$

At 850 K, $\log f_{\text{H}_2\text{O}} = 2.4$, $\log f_{\text{HCl}} = -0.7 \pm 0.6$, $\log f_{\text{O}_2} = -15.3$

Reaction	$\log k_{10.1}$	
10.36	15.7	$\log [f_{\text{MoCl}_4}/f_{\text{MoO}_2}] = 8.1 \pm 2.4$
10.37	8.8	$\log [f_{\text{MoO}_3}/f_{\text{MoO}_2}] = 8.5$
10.38	9.6	$\log [f_{\text{MoO}_2(\text{OH})_2}/f_{\text{MoO}_3}] = 12.0$
10.39	13.7	$\log [f_{\text{MoO}_2\text{Cl}_2}/f_{\text{MoO}_3}] = 9.9 \pm 1.2$
10.40	-6.0	$\log [f_{\text{MoCl}_6}/f_{\text{MoO}_3}] = -17.4 \pm 3.6$
10.41	-5.0	$\log [f_{\text{MoCl}_6}/f_{\text{MoCl}_5}] = -10.7 \pm 0.6$

DISCUSSION OF VAPOUR CHEMISTRY

The fugacities of the various important metal species can now be compared.

	<u>850 K</u>	<u>1000 K</u>
$\log f_{\text{CuCl}}$	-28.3	-10 ± 5 ?
$\log f_{\text{NaFeCl}_3}$	-15 ± 2	-11 ± 2
$\log f_{\text{ZnCl}_2}$	-3.7 ± 1.8	? ($> -3.7 \pm 1.8$)
$\log f_{\text{MoO}_2(\text{OH})_2}$	-3.6 ± 1.5	? ($> -3.6 \pm 1.5$)

Under magmatic conditions (T 1000 K) the transport of Fe in the vapour is insignificant. The transport of Cu is also unimportant if $\log f_{\text{CuCl}} < -6.8$, which seems likely on the basis of the deliberate broad limits ($\log f_{\text{CuCl}} = -10 \pm 5$) arising from the rough calculation on equilibrium 10.23. If all of the metals have relative volatilities that are similar under magmatic conditions to those at 850 K, then it may be possible to separate Zn and Mo from Cu and Fe in the process of evolving a boiling salt-rich liquid from silicate melt and crystals. This could account for the general lack of Zn in porphyry coppers, and for the separation of Mo from Cu in certain deposits.

The condensation of salt-rich liquid by the Henley & McNabb (1978) mechanism will fractionate whatever metals are carried in the vapour into the condensate to some extent. No Henry's Law constants are available. Whether or not this leads to the formation of porphyry-molybdenum deposits, Cu and Mo may behave differently enough to be separated under porphyry copper conditions. That Zn should follow Mo, on the indications given here, is a problem, because Zn-enrichment is not characteristic of porphyry molybdenums.

Lastly, the likely copper concentration of the salt-rich condensate can be examined. For 1 ppm of Cu in vapour consisting otherwise of water,

the mole fraction of CuCl is

$$\frac{1/63.5}{1/63.5 + 10^6/36} = 6 \times 10^{-7} \text{ for dimeric H}_2\text{O.}$$

At a total pressure of 800 atm, then, $P_{\text{CuCl}} = 4.8 \times 10^{-4} \text{ atm} \approx f_{\text{CuCl}}$ for a vapour concentration of 1 ppm. At 1000 K, $\log f_{\text{CuCl}}$ has been estimated at -10 ± 5 . Under conditions at which CuCl is dominant ($\log f_{\text{CuCl}} < -6.8$) the concentration of Cu in the vapour is less than 1 ppb; the presence of, say, 5% NaCl in the vapour makes little difference to the calculation. If all of the copper is transferred to a liquid consisting of 50% NaCl and 50% H₂O, then 10% of the mass of the vapour is being condensed and the copper is enriched 10 times to less than 10 ppb. If the vapour contained only 2% NaCl, the enrichment factor would be 25 and the upper limit on copper concentration in the liquid 25 ppb. This falls short of the observed copper concentrations in type III inclusions by many orders of magnitude, and would be a further argument against any significant copper deposition from the condensates of the magmatic vapour. This, as stated earlier, seems likely from the broad overlap of the limits of f_{CuCl} for equilibrium with hematite and chalcopryrite, and for the dominance of CuCl in the vapour. It appears possible, however, to derive a salt-rich liquid rich in copper for $\log f_{\text{CuCl}}$ between -5 and -6. Clearly, better thermochemical data for the Cu,Fe sulphides are required if this problem is to be resolved beyond doubt.

The findings of this study can be compared with those of Krauskopf (1964). Under the conditions $T = 1100 \text{ K}$, $\log f_{\text{H}_2\text{O}} = 3$, $\log f_{\text{O}_2} = -8$, $\log f_{\text{ES}} = 1$, $\log f_{\text{HCl}} = 0$, he found that

$\log f_{\text{Cu}_3\text{Cl}_3}$	-1
$\log f_{\text{FeCl}_2}$	-5
$\log f_{\text{ZnCl}_2}$	-2
$\log f_{\text{MoO}_3}$	-2

and at 900 K, $\log f_{\text{H}_2\text{O}} = 3$, $\log f_{\text{O}_2} = -14$, $\log f_{\Sigma\text{S}} = -1$, $\log f_{\text{HCl}} = -1$

$\log f_{\text{Cu}_3\text{Cl}_3}$	-7
$\log f_{\text{FeCl}_2}$	-8
$\log f_{\text{ZnCl}_2}$	-5
$\log f_{\text{MoO}_3}$	-5

The estimates made in this study for magmatic conditions apply to intermediate conditions. Both studies agree on the high volatility of Zn and Mo. The volatilities of Cu and Fe are considerably higher in Krauskopf's results than in those of this study. In particular, the importance of Cu_3Cl_3 according to Krauskopf contrasts with its insignificance according to this work. Both studies are limited by unreliable thermochemical data for the Cu,Fe sulphides.

THE ACIDITY OF THE SALT-RICH LIQUID

The salt-rich liquid presents its own problems of speciation, but a consideration of this serves little purpose at present. It is sufficient to remark that all potential vapour species, dominant or otherwise, must exist in the liquid, and probably do so in different relative proportions. The consequences of mineral precipitation in veins and of wallrock alteration will be dealt with here.

K-feldspar, or K-feldspar + sericite, commonly forms an inner alteration selvage to quartz-Cu,Fe sulphide veins. A quartz-sericite assemblage without K-feldspar was noted in only one case, 103021. Sericite-albite assemblages without K-feldspar occur along the boundary between salt-rich liquid and groundwater. To a good approximation, the molality of KCl remained constant in the salt-rich liquids so that any increase in molality of HCl would drive the liquid towards the sericite field (Montoya & Hemley, 1975). The alteration assemblages show that this did not happen

in general; the K-feldspar - sericite boundary was not crossed. Montoya & Hemley's diagrams can be used, with estimates of the molalities of NaCl and KCl at Panguna, to show that the range of pH in which albite and sericite coexist at 400°C is close to the buffered pH of the K-feldspar - sericite assemblage. There appears to have been a control on the amount of HCl in the salt-rich liquids. The reactions controlling HCl include:

- (i) precipitation of quartz. Dissolved quartz is presumed to be in the form of an alkali silicate.



- (ii) precipitation of sulphides, e.g. chalcopyrite, pyrite - see below for equations (10.53, 10.54).

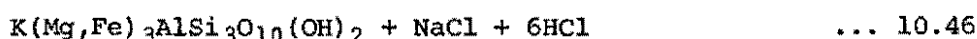
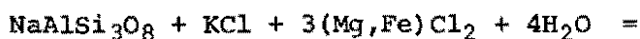
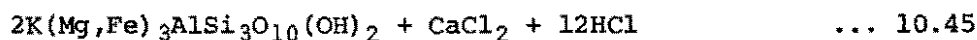
- (iii) precipitation of anhydrite.



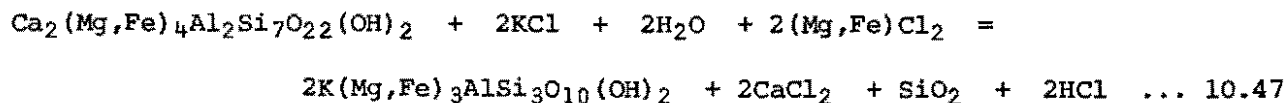
The sources of CaCl_2 and H_2SO_4 are discussed below.

- (iv) wallrock alteration. Biotite is by far the most abundant alteration product associated with quartz-Cu,Fe sulphide veins at Panguna; reactions involving this mineral all either consume or produce HCl. Biotite usually replaces plagioclase and amphibole of either igneous or early hydrothermal origin. Ford (1976) gives analyses of amphiboles and all fall in a range between actinolite and hornblende. Here, reactions are written for both end members, $\text{Ca}_2(\text{Mg,Fe})_5\text{Si}_8\text{O}_{22}(\text{OH})_2$ and $\text{Ca}_2(\text{Mg,Fe})_4\text{Al}_2\text{Si}_7\text{O}_{22}(\text{OH})_2$, and for the anorthite and albite components of plagioclase.

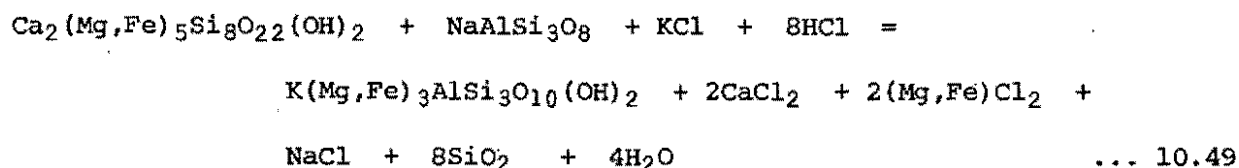
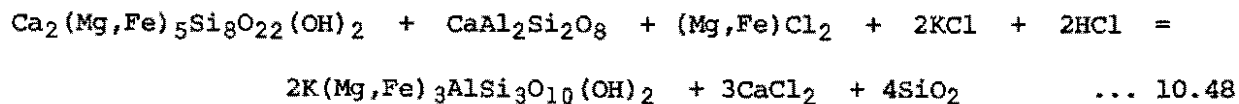
- (a) Plagioclase to biotite.



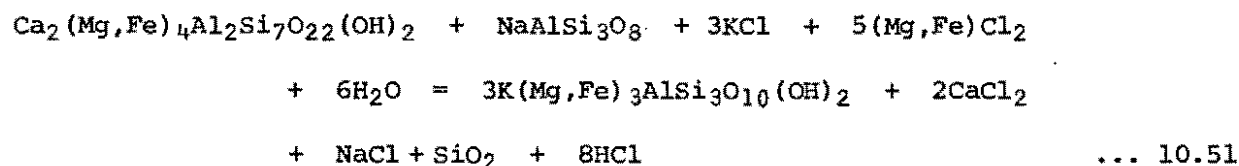
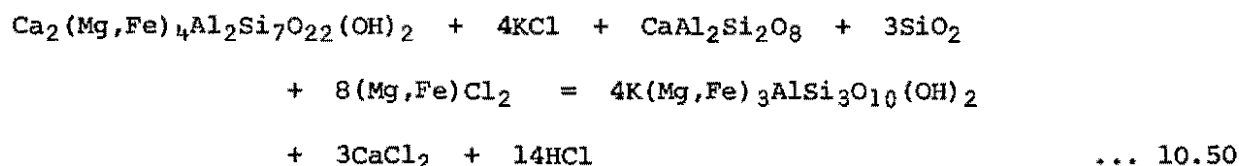
(b) Hornblende to biotite.



(c) Actinolite and plagioclase to biotite.



(d) Hornblende and plagioclase to biotite (combining a and b).



The reactions above are written to conserve aluminium, which shows only small variations between fresh and altered rocks at Panguna (Ford, 1978). The reactions by which sanidine replaces biotite and chlorite replaces biotite both consume HCl, but these are considered unimportant beside the other reactions above. Likewise, the reactions depositing vein material should be insignificant because of the sheer volume of biotitised rock in the orebody, with the possible exception of the deposition of quartz in parts of the orebody where quartz veins make up 5 to 10% of the total volume.

The biotite-amphibole-plagioclase reactions are summarised below as a table, giving the numbers of moles of HCl produced (+) or consumed (-) per mole of reactant on conversion to biotite.

	Albite	Anorthite	No plagioclase
Actinolite	-8	-2	-
Hornblende	+8	+14	+2
No amphibole	+6	+12	-

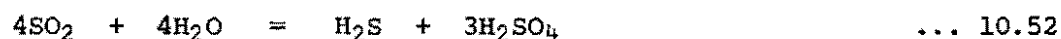
In the intrusions, the alteration of plagioclase predominates, so that there will be a net increase of HCl in the fluid (this may be partly compensated, but not completely, by the consumption of HCl as SiO₂ is supplied from the fluid to alter anorthite). In the Panguna Andesite amphibole of the amphibole-plagioclase-magnetite alteration assemblage is entirely altered, and the plagioclase partly. Since the volume of a mole of amphibole is nearly three times that of a mole of plagioclase, the simultaneous conversion of a mole of each in a rock consisting of approximately equal volumes of each is probably a reasonable approach to reality. If a mole of Ab₅₀An₅₀ reacts with a mole of Hb₅₀Ac₅₀ to give biotite, interpolation of the numbers in the table gives about 3 moles of HCl added to the fluid.

If this extra HCl is not taken up by some other means, sericite will replace K-feldspar. The sporadic chloritisation of biotite, the replacement of biotite by K-feldspar near veins and the deposition of quartz in veins may all be in part a response to local HCl build-up. However, minerals not favoured by increasing HCl content (sulphides and anyydrate) also form in the veins and wallrock. This suggests that some other means of removing HCl is operating. The most obvious one is boiling, for which there is evidence in the form of type II inclusions throughout the deposit. Boiling would thus appear to be an essential element of the porphyry copper mechanism in deposits in which sericite is not an important component of the potassic alteration assemblage. Sericite - K-feldspar assemblages are characteristic of veins cutting the

Biotite Granodiorite (and also occur to some extent in the other porphyries). This is consistent with the predominance of the alteration of plagioclase in the porphyries and the consequent release of large quantities of HCl.

SULPHIDE AND SULPHATE DEPOSITION

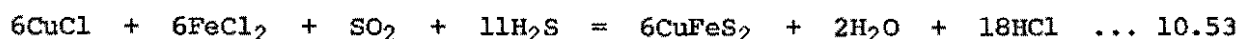
Although the main sulphur-bearing species in the vapour is SO_2 , it will be shown in Chapter 11 that sulphur isotope data are consistent with a predominance of H_2S in the salt-rich liquid. Only 10 - 20% of the sulphur in the liquid is carried as SO_2 . In the vapour, SO_2 will decompose as the temperature falls, probably according to the reaction



(Holland, 1967, p.421). The same could be suggested for the salt-rich liquid, although the chemical evolution is different. The liquid appears to maintain a constant $\text{SO}_2:\text{H}_2\text{S}$ ratio, between 1:9 and 1:4 (see fig. 11-3), while H_2S is withdrawn as Cu,Fe sulphides, so that SO_2 must be withdrawn simultaneously. As sulphate is formed, it will combine with Ca^{2+} from the alteration of plagioclase to give anhydrite. A sufficient explanation of the vein assemblages should account for these features:

- (i) The salt-rich liquids are saturated in Cu,Fe sulphides and anhydrite over the whole temperature range, from magmatic temperatures to 400°C .
- (ii) In the high-temperature veins (e.g. 102675, 102676 and 102998) anhydrite is more abundant than sulphides; sulphides become much more abundant, probably more so than anhydrite, at about 500°C and below (this is difficult to judge because of the solution of anhydrite, but there is nothing to suggest a large-scale removal of anhydrite from wallrock at lower temperatures).

Reaction 10.52 is incapable of accounting for the increase of sulphide relative to sulphate at lower temperatures, although it seems necessary to account for the generation of sulphate at all temperatures, and if it is the only important reaction at high temperatures, could account for the high sulphate to sulphide ratio in the high-temperature veins. Other reactions for the decomposition of SO_2 may become important below 500°C : e.g. for the formation of chalcopyrite



and for pyrite



The reaction forming chalcopyrite removes SO_2 and H_2S in a molar ratio 1:11, and this will tend to deplete the liquid in H_2S (according to the ratios arising from the isotope study). Reaction 10.52 will enrich the liquid in H_2S . A combination of the two processes could account for the constant ratios at lower temperatures.

The reduction of Mo^{6+} species to form molybdenite could also contribute to the oxidation of Fe^{2+} or SO_2 , although the quantities involved would be very small.

METAL ZONING

According to the textures described in Chapter 4, pyrite deposition generally preceded the deposition of chalcopyrite and bornite. The distribution of bornite and digenite relative to chalcopyrite, and of sphalerite relative to the Cu,Fe sulphides are further features that require explanation in a complete chemical model of ore deposition. The formation of a mole of biotite (according to the average reaction considered above in the context of acidity) would consume one mole of $(\text{Mg,Fe})\text{Cl}_2$, while the alteration of plagioclase alone causes a larger

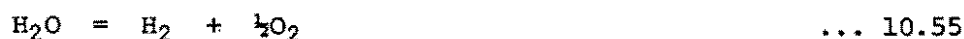
depletion of Fe and Mg in the liquid. Ford (1976) has suggested that the formation of biotite might be a necessary condition for the deposition of Cu,Fe sulphides instead of pyrite and magnetite, through the decrease it brings about in the concentration of Fe species. The liquid may thus evolve in composition, first depositing pyrite, then chalcopyrite, and finally becoming sufficiently enriched in copper over iron to deposit bornite with or without digenite. It is unlikely however, that the situation is as simple as that. The removal of volatiles by boiling may also affect the replacement of pyrite by chalcopyrite and chalcopyrite by bornite. The chemistry of ore deposition at the edges of the deposit may also have been complicated by additions from groundwater (see Chapter 9).

THE OXIDATION STATE OF MAGMATIC FLUIDS

The occurrence of hematite and the expulsion of much SO_2 (see Chapter 11) are consistent with a high oxidation state in the magma and the fluids it was exsolving at the time of copper deposition at Panguna. Magnetite is the usual iron oxide phase in crystallising magmas (e.g. non-mineralised Kaverong Quartz Diorite, where sphene and ilmenite also occur). Oxidation therefore seems to have taken place before copper mineralisation, and Ohmoto & Rye (in press) have suggested the diffusive loss of hydrogen as a possible mechanism. The degree of oxidation of an ordinary pluton (i.e. one without porphyry copper mineralisation) seldom, if ever, attains the degree observed at Panguna. Thus there is little to suggest that diffusion, which ought to be equally effective in all plutons, brings about the oxidation in porphyry coppers. Hematite has been reported in other deposits, e.g. Bingham (Roedder, 1971), Sar Cheshmeh (Etminan, 1977), Frieda (appendix, this study), and there is evidence of

more extreme oxidation at El Salvador (see Chapter 11). The expulsion of two fluids from the magma is evidenced in each of these deposits just as it is at Panguna.

In a magma which has begun exsolving water and other volatiles, the fugacity of hydrogen is governed by the gaseous reaction



$$\log f_{\text{H}_2} = \log k_{10.55} + \log f_{\text{H}_2\text{O}} - \frac{1}{2} \log f_{\text{O}_2}$$

At 1100 K, $\log k_{10.55} = -8.9$. If exsolution starts at $\log f_{\text{O}_2} = \text{HM}-3$ (the estimate of Carmichael *et al.*, 1974, for calc-alkaline magmas with amphibole phenocrysts) and $\log f_{\text{H}_2\text{O}} = 2.8$, then $\log f_{\text{H}_2} = -0.2$. The fugacity coefficient of hydrogen under these conditions is 1.2 (Newton, 1935; critical parameters from Weast, 1975) so that the corresponding partial pressure of hydrogen is 0.5 atm, by the Lewis & Randall Rule. This is a substantial pressure in terms of the ability of a vapour phase to carry hydrogen away from the magma. Continued removal of vapour will therefore lead to the oxidation of the magma and fluids by the loss of hydrogen. At $\log f_{\text{O}_2} = \text{HM}$ the hydrogen fugacity is -1.7, and at $\text{HM}+1$, -2.2. The degree of oxidation will be limited by the decline of the partial pressure of hydrogen.

The expulsion of magmatic volatiles is therefore implicated in the oxidation process, not only at Panguna, but in many porphyry coppers. This mechanism was also suggested to explain progressive oxidation during the crystallisation of the Finnmarka complex, Norway, by Czamanske & Wones (1973). This means that the production of oxidised fluids ought to be preceded by the production of reduced fluids, all as part of a single, continuous process. There is evidence for this (except for the continuity of the process) at Panguna where phase A mineralisation, usually hematite-bearing, was superimposed on to a slightly more extensive and more

pervasive amphibole-plagioclase-magnetite alteration with associated sphene (cf. oxidation state of unaltered Kaverong Quartz Diorite). There is meagre evidence (specimen 103049) that a boiling salt-rich liquid was involved in the formation of the amphibole-bearing assemblage, and that the water in equilibrium with another specimen was of magmatic origin (Ford & Green, 1976). The phase A pyritic halo, described by Fountain (1973) as being most intensely developed at the outer boundary of the amphibole-bearing assemblage, may also have been deposited by the reduced fluids. The pyrrhotite replaced by pyrite in 103029 may also belong to this hydrothermal phase.

Chivas (1976) recognised oxidation resulting from the expulsion of volatiles at the Koloula porphyry copper prospect, Guadalcanal. He attributed part of the copper mineralisation to the first, relatively reduced, fluids which were boiling salt-rich liquids (although the fluid inclusions of these are said to contain hematite by Chivas & Wilkins, 1977).

There is nothing to suggest that the reduced fluids at Panguna deposited copper, although they may have deposited sulphur in the pyritic halo and iron as magnetite and pyrite. Together with the apparently general association of copper deposition and oxidised fluids in porphyry coppers, this suggests that the evolution of copper-rich fluids from the silicate melt is dependent on the state of oxidation of the fluids.

CHAPTER ELEVEN: SULPHUR ISOTOPE STUDY

INTRODUCTION

A small number of samples was examined at the isotope laboratory of the C.S.I.R.O. Minerals Research Laboratories, North Ryde, New South Wales, under the guidance of Messrs. J.W. Smith and M.S. Burns.

Sulphide samples were separated physically if possible, but anhydrite was dissolved away from chalcopyrite in HCl, and samples bearing pyrite, sphalerite and galena were subjected to a chemical separation. A weighed sample was reacted first with cold 1N HCl in a reflux apparatus with a magnetic stirrer. A stream of nitrogen was passed through the reactants to collect any H₂S, and was then passed through a trap containing AgNO₃ solution. Any Ag₂S formed was collected by filtration, dried and weighed. The reactants (minerals + acid) were also filtered, the residue being kept for the next stage and the filtrate for analysis by atomic absorption spectrophotometry. The residue was placed in cold 2N HCl and the whole process was repeated, and the residue from that stage was processed a third time with hot 2N HCl. The final residue, pyrite or chalcopyrite (they cannot be separated by this process) was dried in a nitrogen atmosphere. The three Ag₂S samples and the pyrite (in this case) were burned as described below. Since the process does not separate the minerals quantitatively, the filtrate analyses (Pb, Zn, Cu and Fe) are used to determine the contributions of each mineral to the measured $\delta^{34}\text{S}$ of each Ag₂S sample.

Powdered sulphide samples (10 mg of pyrite, 20 mg of others) were ground with excess Cu₂O and burned at 900°C in a vacuum. Any water vapour in the gaseous products was separated out with an acetone-dry ice

freezing mixture, and any CO_2 was separated from SO_2 with a pentane freezing mixture (Sakai & Yamamoto, 1966).

Anhydrite samples were first converted to BaSO_4 by solution in hot HCl and precipitation with BaCl_2 . Weighed BaSO_4 samples were reduced to BaS with graphite at 1100°C under a stream of nitrogen (basically the method of Rafter, 1957). The BaS was leached out and filtered into AgNO_3 solution, and the resulting Ag_2S was recovered and burned as above.

$\delta^{34}\text{S}$ was measured for each SO_2 sample on a mass spectrometer relative to a laboratory standard. In the case of determinations on Ag_2S from anhydrite, a second standard (seawater sulphate taken as +20.2‰) was also checked. Since this was found to give +19.1‰ relative to the other standard, all $\delta^{34}\text{S}$ readings on sulphate sulphur were corrected according to a linear interpolation between the two standards.

As is customary, the isotopic variation is expressed as $\delta^{34}\text{S}$, defined as

$$\delta^{34}\text{S} = \left[\frac{{}^{34}\text{S}/{}^{32}\text{S} \text{ (sample)}}{{}^{34}\text{S}/{}^{32}\text{S} \text{ (standard)}} - 1 \right] \times 1000 \text{ ‰}$$

The standard is troilite from the Cañon Diablo meteorite. The fractionation of ${}^{34}\text{S}$ between minerals A and B is expressed as

$$\Delta_{\text{A-B}} = \delta^{34}\text{S}_{\text{A}} - \delta^{34}\text{S}_{\text{B}}$$

Recently, Rees (1978) criticised the method of determining $\delta^{34}\text{S}$ on SO_2 samples. He presented inter-laboratory data which showed poor agreement due to the "memory" effect - the retention of SO_2 in mass spectrometer inlet valves between measurements - and to unaccounted-for oxygen isotope interference. The interference is unavoidable when SO_2 is used. On the basis of determination on SF_6 , free of both drawbacks,

Rees *et al.* (1978) have recalibrated seawater sulphate at $\delta^{34}\text{S} = 20.99\%$. The temperatures quoted here may therefore be in slight error because seawater sulphate was taken as $+20.2\%$. Studies of the isotopic variation in a single mineral across a deposit will not be greatly affected, provided all measurements are made in the one laboratory. The determination of temperatures from isotopic fractionation (which, by virtue of the need of a calibration curve, will generally involve data from more than one laboratory) will be subject to unknown error. The uncertainty in sulphate-sulphide temperatures, already large according to the calibration data (Ohmoto & Rye, in press), will be increased because the disagreement between laboratories tends to be larger at higher $\delta^{34}\text{S}$ (Rees, 1978). In this study and in another of sulphur isotopes at Panguna (Ayres *et al.*, in press) and in a study of the calibration (used here) of the galena-sphalerite-pyrite thermometer (Smith *et al.*, 1978) all readings were made in the same laboratory.

THERMOMETRY

Sphalerite-pyrite veins. Sphalerite-pyrite pairs were obtained from six veins, a sphalerite-galena pair from one and sphalerite-galena-pyrite from one. In the last (103473) the expected fractionation order (galena < sphalerite < pyrite) was reversed and the results were rejected. A high result for one of the Ag_2S samples in 103471 was also rejected because the yield of the burn was low, and it led to a low Δ (sphalerite-pyrite) compared with the other sample, which was comparable with other specimens. The $\delta^{34}\text{S}$ and Δ values are set out in Table 11-1.

The mineragraphic study (Chapter 3) confirmed that sphalerite and galena were in equilibrium in 103480. This was the only specimen in which pyrite also appeared to be in equilibrium with sphalerite, but no

$\delta^{34}\text{S}$ could be measured for the pyrite because of the presence of tennantite in the final residue. The galena-sphalerite pair gave a temperature of 300°C . Three of the pyrite-sphalerite pairs in apparent textural disequilibrium gave similar temperatures ($270 - 310^{\circ}\text{C}$). The other two pairs gave much lower temperatures.

The only comparable fluid inclusion data are from 103042 (see Chapter 6) which did not have enough galena or sphalerite for isotopic study. The pressure-corrected trapping temperatures were $330 \pm 5^{\circ}\text{C}$. Taken altogether, the various temperature estimates indicate an average temperature near 300°C for sphalerite-pyrite mineralisation. Osatenko & Jones (1976) report a similar temperature, 266°C , for a sphalerite-pyrite pair from Valley Copper, British Columbia.

Anhydrite-Chalcopyrite. Two samples were obtained from diamond drill core BVP 88 for this study. Ayres *et al.* (in press) made measurements on two other samples. All of the data have been converted to temperatures using calibration equations cited in Ohmoto & Rye (in press), viz.

$$T = \frac{2.85 \times 10^{-3}}{(\Delta \pm 1)^{\frac{1}{2}}} \quad (\text{for } T > 673 \text{ K})$$

Note that the temperatures published by Ayres *et al.* differ substantially from those accepted here (Table 11-2). The temperature range compares favourably with the fluid inclusion temperature range for quartz-Cu,Fe sulphide mineralisation. In the cases of 102675 and 102676, the temperatures match the fluid inclusion data for quartz from 102676 ($T_h = 600$ to $>700^{\circ}\text{C}$).

Table 11-1

 $\delta^{34}\text{S}$, Δ AND TEMPERATURE MEASUREMENTS ON PYRITE-SPHALERITE VEINS

Specimen	$\delta^{34}\text{S}$, ‰			Δ , ‰	$T^{\circ}\text{C}^*$
	galena	sphalerite	pyrite		
103048		+0.2	+2.4	2.2	<150
103481		+1.2	+2.4	1.2	270
103475		+1.6	+3.1	1.5	200
103476		+0.6	+1.7	1.1	310
103471		+1.6	+2.7	1.1	310
103473	-1.5	-1.0		2.5	300

* using data from Smith *et al.* (1978).

Table 11-2

 $\delta^{34}\text{S}$, Δ AND TEMPERATURES FOR ANHYDRITE-CHALCOPYRITE PAIRS

Specimen	$\delta^{34}\text{S}$, ‰		Δ , ‰	$T^{\circ}\text{C}^{\S}$
	anhydrite	chalcopryrite		
102675	+7.6	+0.4	7.2	797 \pm 70
102676	+11.5	+0.5	11.0	588 \pm 40
34640 [†]	+16.0	-0.1	16.1	438 \pm 22
34641 [†]	+11.0	+0.2	10.8	597 \pm 40

[†] from Ayres *et al.* (in press), who gave temperatures of 350 $^{\circ}\text{C}$ and 520 $^{\circ}\text{C}$.

[§] data cited in Ohmoto & Rye (in press).

VARIATION OF $\delta^{34}\text{S}$ IN TIME AND SPACE

Pyrite. Pyrite samples examined in this study had $\delta^{34}\text{S}$ values ranging between +0.5 and +3.1‰ (+2.4, excluding veins with appreciable sphalerite). Ayres *et al.* (in press) found a similar range of 0.0 to +2.3‰. All available measurements for pyrite have been plotted on a map of the deposit (fig. 11-2). Fig. 11-1 shows specimen locations for the sulphur isotope study. There is no systematic distribution of $\delta^{34}\text{S}$ if the data are considered in this way. The data of Ayres *et al.* do not lend themselves to classification in terms of vein-types; most of the pyrite samples had been classified by association with alteration types. Even where a vein type was specified, it is not possible to relate Ayres' classification (after Fountain, 1972) to that used here. Thus only the measurements made in this study can be classified according to vein type.

Apart from the high ^{34}S content of the pyrite from sphalerite-pyrite veins, no real trend is visible, probably because there are not enough samples for most of the vein types.

Chalcopyrite. The range of $\delta^{34}\text{S}$ given by Ayres *et al.* is -1.6 to +1.5‰ within the orebody, and one is -2.5‰ outside the orebody. Given the number of samples involved, the trends suggested by Ayres *et al.* (viz. a difference in mean $\delta^{34}\text{S}$ between samples from near the Leucocratic Quartz Diorite and samples from near the Biuro Granodiorite, and an enrichment in ^{34}S towards the northwest) do not seem to be significant.

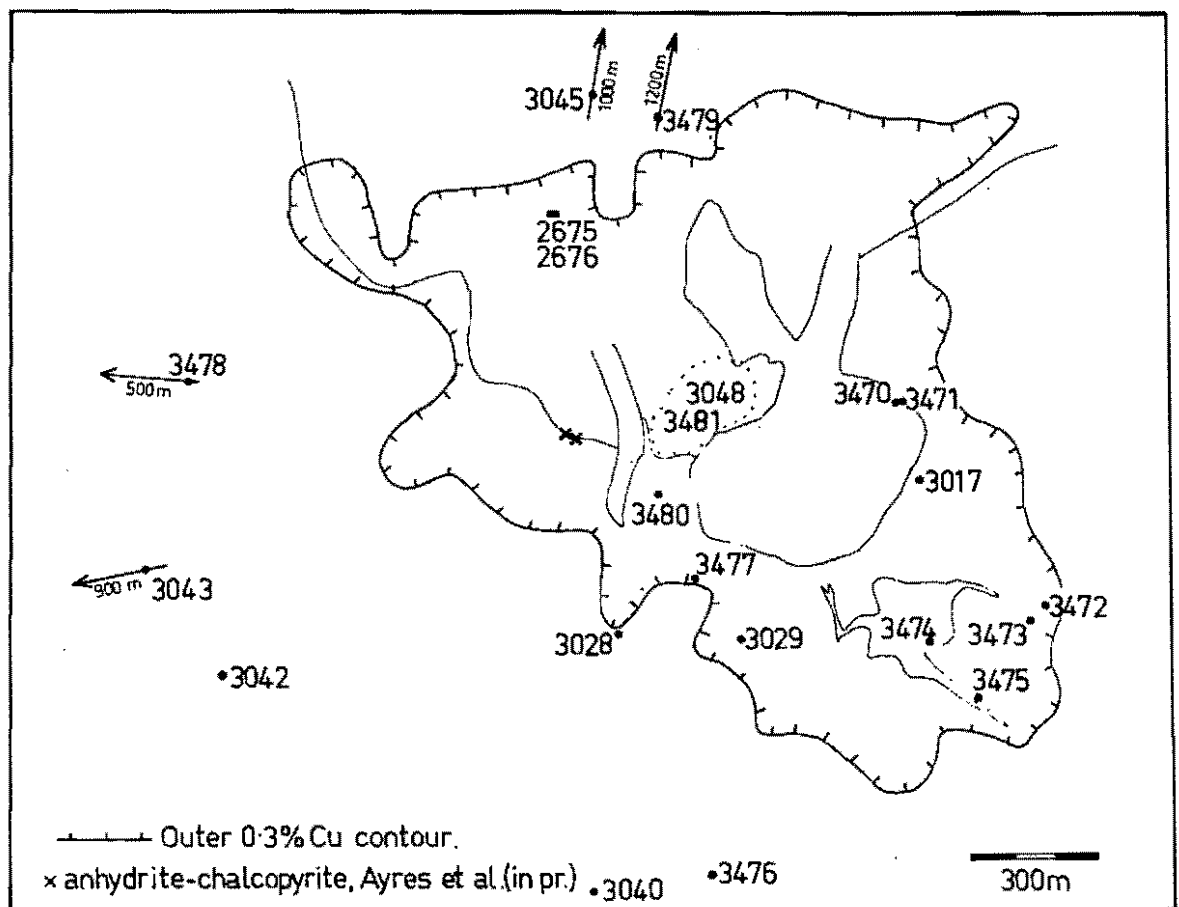


Fig. 11-1 Locality map of specimens used in the sulphur isotope study. Geological contacts and outer 0.3% Cu contour as in fig. 2-3.

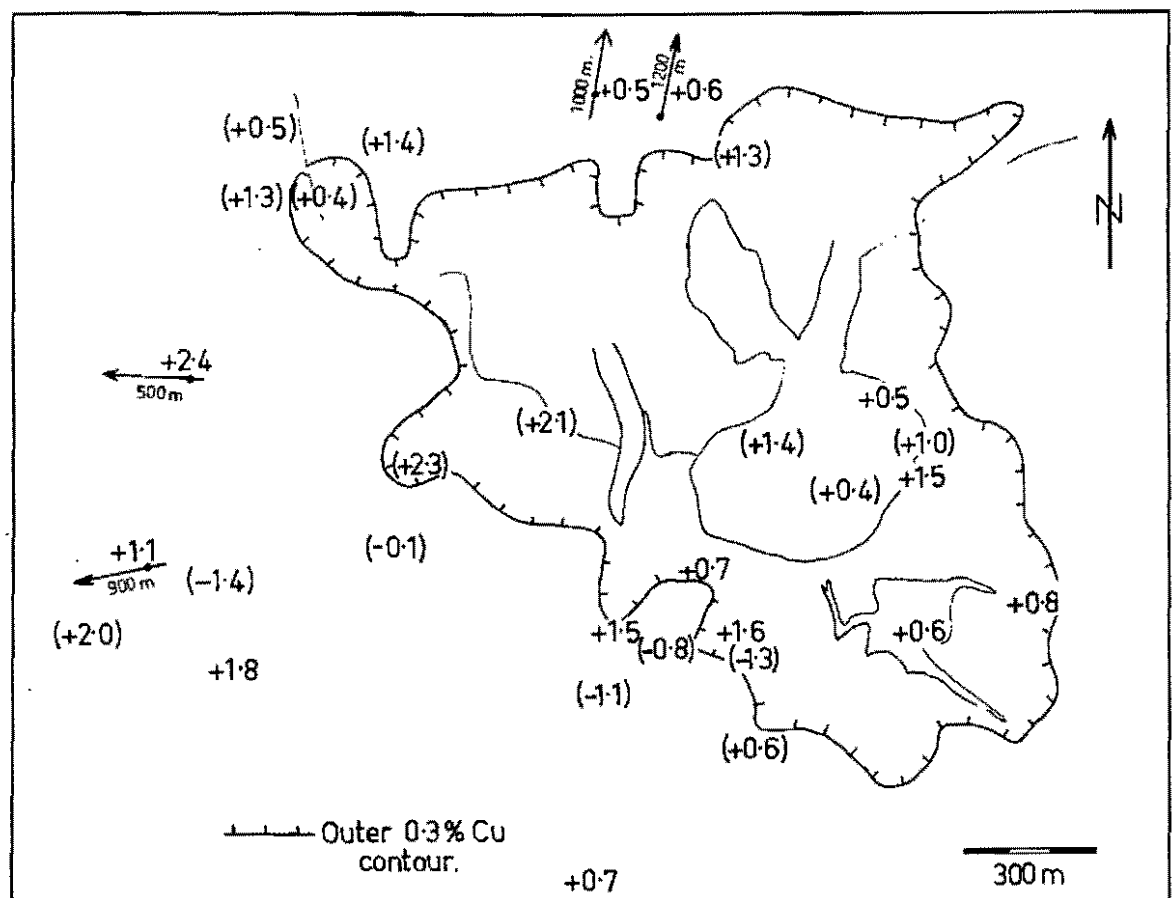


Fig. 11-2 Distribution of $\delta^{34}\text{S}$ of pyrite at Panguna. Data in parentheses from Ayres *et al.* (in press). Geological contacts and outer 0.3% Cu contour as in fig. 2-3.

Table 11-3

SULPHIDE $\delta^{34}\text{S}$ VALUES, CLASSIFIED BY VEIN TYPE (see Table 3-1)

Vein type	This study		Ayres <i>et al.</i>		
	Specimen	$\delta^{34}\text{S}_{\text{py}}$, ‰	Specimen	$\delta^{34}\text{S}_{\text{py}}$, ‰	$\delta^{34}\text{S}_{\text{ccp}}$, ‰
(ii)	103029	+1.6	40961?	0.0	-0.3
			40962?		
			34640		
			34641		
			34644		
			34645		
			34647		
			34648?	+2.0	-0.5
			40963		
			27967		
(iv)	103028	+1.5			
QP assoc.	103017	+1.5			
	103040	+0.7			
external	103479	+0.6			
	103045	+0.5			
	103043	+1.1			
(v)	103470	+0.5			
(vi)	103474	+0.6			
(viii)	103472	+0.8			
(ix/x) sp.	103042	+1.8			
	no sp. 103477	+0.7	30643	+0.8	
				(Listed under ccp by Ayres <i>et al.</i>)	
	see also Table 11-1.				
Other	103478	+2.4	Pyrites associated with biotite alteration:		
			-1.4, +0.4, +0.5, +0.6, +1.3, +1.3, +2.0, +2.1, +2.3		

FURTHER EXAMINATION OF ANHYDRITE-CHALCOPYRITE FRACTIONATION

Field & Gustafson (1976) prepared a plot of $\delta^{34}\text{S}$ of coexisting sulphides and sulphates as a function of Δ , i.e. effectively as a function of temperature. They explained that the data will plot as two straight lines if three conditions are met:-

1. The sulphur reservoir was effectively infinite;
2. The $\delta^{34}\text{S}$ of the sulphur reservoir remained constant;
3. There was a constant ratio of oxidised to reduced sulphur species throughout mineralisation.

Field & Gustafson found this to be so for anhydrite and sulphides at El Salvador. There were two trends, one pair of lines (for anhydrite and Cu,Fe sulphides) converging to $\delta^{34}\text{S} = +1.6\%$ and the other (for anhydrite and pyrite) to $+6.8\%$ at $\Delta = 0.0\%$. For any intercept on the $\Delta = 0$ axis it is possible to calculate a family of lines giving $\delta^{34}\text{S}$ variation in anhydrite and a sulphide as a function of Δ and the ratio of oxidised to reduced sulphur species. This was done for pyrite and anhydrite by those authors (who assumed that oxidised sulphur would be present as sulphate in the liquid, and reduced sulphur as H_2S) for $\delta^{34}\text{S} = 0\%$ at $\Delta = 0\%$. The $\delta^{34}\text{S}$ value to which the lines defined by actual measurements converge gives the isotopic composition of the sulphur reservoir.

A similar diagram has been prepared for the four pairs of data from Panguna. A pair of straight lines is defined, and these give a $\delta^{34}\text{S}$ value near 1% , within the range shown, at the point of convergence (fig. 11-3).

The assumptions of Field & Gustafson warrant further attention. Given the straight line plots, the three numbered assumptions above seem justified. In view of the nature of the hydrothermal system, however,

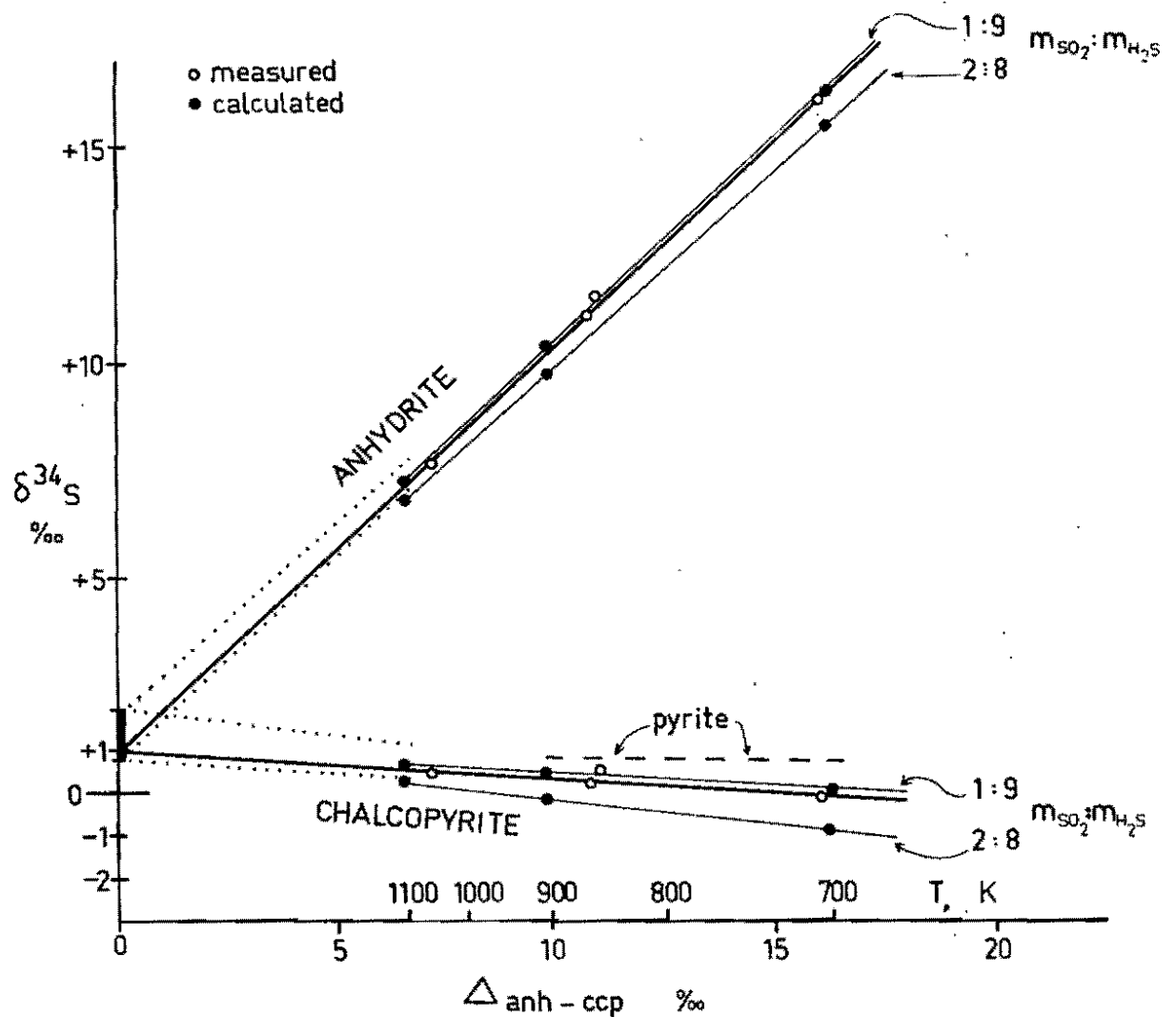


Fig. 11-3 $\delta^{34}\text{S}$ in anhydrite-chalcopyrite pairs as a function of $\Delta(\text{anhydrite-chalcopyrite})$. Open circles and thick black lines are for measurements on Panguna samples. The dotted lines are limits on the position of the thick black lines. The black circles and thin black lines are calculated (see text) for the indicated molar ratios of oxidised to reduced sulphur species in the salt-rich liquid. The dashed line gives the $\delta^{34}\text{S}$ variation of a small amount of pyrite in isotopic equilibrium with the other minerals.

the meaning of the "sulphur reservoir" concept should be re-examined. The $\delta^{34}\text{S}$ value at the convergence of the two straight lines is not an estimate of the isotopic composition of magmatic sulphur. It is only an estimate of the bulk isotopic composition of the initial salt-rich liquid (which precipitates the sulphides and sulphates at lower temperatures). The implied constancy of $\delta^{34}\text{S}$ in the sulphur reservoir (assumption 2) is thus a constancy in the salt-rich liquid, implying a constraint on $\delta^{34}\text{S}$ of the magma in which the salt-rich liquids originated. The infinite supply of sulphur (assumption 1), however, refers to the salt-rich liquid only. Thus assumptions 1 and 2 are independent, and both are necessary. At temperatures below 750 K, the situation will be more complicated because of the possibility of adding sulphur from groundwater, and of depositing pyrite either before or with chalcopyrite. A small amount of pyrite in equilibrium with chalcopyrite would have the $\delta^{34}\text{S}$ values shown in fig. 11-3, with little variation as a function of temperature. Both pyrite and groundwater would affect only a small interval - the lowest temperature part - of the range of Δ being considered, so that ignoring them would not greatly affect the arguments used here. Likewise, deviation from the infinite reservoir hypothesis is most likely in the salt-rich liquid at low temperatures where most of the sulphides were deposited. All of these effects might have to be considered in a study based mainly on lower temperature sulphate-sulphide pairs.

$\delta^{34}\text{S}$ IN THE SULPHIDES, SULPHATES & FLUIDS AS A FUNCTION OF f_{O_2}

Sulphur in the liquid and vapour at temperatures over 673 K is present as SO_2 and H_2S (Barnes & Czamanske, 1967) and not as SO_4^{2-} . The sulphate in anhydrite probably originates from the decomposition of SO_2 ,

which becomes an unimportant species near 673 K under porphyry copper f_{O_2} conditions. The calculation of a family of curves giving $\delta^{34}S$ as a function of $\Delta_{anh-ccp}$ under the conditions at Panguna is based on the following equation:

at temperature T, given values for $\Delta_{SO_2-H_2S}$; Δ_{anh-H_2S} ; Δ_{ccp-H_2S} (≈ 0)
[all fractionation data are from Ohmoto & Rye (in press) ; see
Table 11-4]; $m_{H_2S}:m_{SO_2} = a:1-a$

$$\begin{aligned}\delta^{34}S_{liq} &= a \delta^{34}S_{H_2S} + (1-a)(\delta^{34}S_{H_2S} + \Delta_{SO_2-H_2S}) \\ &= 1 \text{ (value taken from fig. 11-3).}\end{aligned}$$

Whence, $\delta^{34}S_{ccp} = \delta^{34}S_{H_2S}$

and $\delta^{34}S_{anh} = \delta^{34}S_{H_2S} + \Delta_{anh-H_2S}$

Some of the curves are plotted in fig. 11-3. The curves bracket $m_{H_2S}:m_{SO_2}$ between 9:1 and 8:2. The ratio 9:1 will be adopted for the purposes of the following calculations.

Thus, at 1100 K,

$$1 = 0.9(\delta^{34}S_{H_2S}) + 0.1(\delta^{34}S_{H_2S} + 3.4)$$

and $\delta^{34}S_{H_2S} = +0.7\%$.

$\delta^{34}S_{SO_2} = +4.1\%$.

Since the vapour contains effectively only SO_2 (see Chapter 10),

$\delta^{34}S_{vap} = +4.1\%$.

In this relatively simple situation, the $\delta^{34}S$ of the fluids, sulphides and sulphates depends on the oxygen fugacity. The higher the oxygen fugacity, the higher will be $m_{SO_2}:m_{H_2S}$ in the liquid, the steeper the sulphide lines and therefore the larger the difference in $\delta^{34}S$ between the liquid and the sulphides, and the smaller the difference between the liquid and the anhydrite.

Table 11-4

FRACTIONATION AMONG SULPHUR SPECIES

T	$\Delta\text{SO}_2\text{-H}_2\text{S}$	$\Delta\text{HS}^-\text{-H}_2\text{S}^*$	$\Delta_{\text{ccp}}\text{-H}_2\text{S}^*$	$\Delta\text{CaSO}_4\text{-H}_2\text{S}^*$
700	9.1	-0.7	-0.10	16.3
800	6.8	-0.7	-0.08	12.5
900	5.3	-0.7	-0.06	9.9
1000	4.2 \pm 0.5	-0.7 \pm 0.2	-0.05 \pm 0.08	8.0 \pm 1.0
1100	3.4	-0.7	-0.04	6.6

* extrapolated

Data from Ohmoto & Rye (in press). All values in ‰.

Under any conditions at which sulphate and sulphide coexist, the $\delta^{34}\text{S}$ of chalcopyrite will decrease with decreasing temperature. This ought to be reflected as a zonation of $\delta^{34}\text{S}_{\text{ccp}}$ with outward decrease. The smallness of the decrease implied by fig. 11-3 for Panguna must make zonation difficult to detect if there is also scatter in the data. Ayres *et al.* give a $\delta^{34}\text{S}$ range of 3‰ for Panguna chalcopyrite, compared with the predicted decrease of <1‰ in fig. 11-3. However, the prediction corresponds with the isotopic zonation reported by Field (1966) at Bingham, where there is an outward decrease in $\delta^{34}\text{S}$. The apparent contrast between salt-rich liquid ($m_{\text{SO}_2} : m_{\text{H}_2\text{S}} \approx 1:9$) and the vapour ($f_{\text{SO}_2} : f_{\text{H}_2\text{S}} = 10^{3.9}$ at 1000 H, HM) deserves comment. The large difference may be an artefact of thermodynamic assumptions (standard states and activity coefficients), possibly implying that one of the gas species interacts strongly with another chemical species in the liquid. Alternatively, the assumption that SO_2 is the only oxidised sulphur species in the liquid may be at fault.

COMPARISON WITH OTHER DEPOSITS

Coexisting pairs of anhydrite and sulphide have been examined in relatively few porphyry copper deposits. For El Salvador (Field & Gustafson, 1976) and Frieda (Appendix 3), there were sufficient data to plot curves like those in fig. 11-3. Limited fluid inclusion studies of both deposits (Gustafson & Hunt, 1975 and appendix, this study) show that the hydrothermal systems consisted of boiling salt-rich liquid, comparable with the Panguna system. The isotopic data for Frieda and El Salvador both give converging pairs of straight lines, two pairs at El Salvador and possibly two at Frieda. From the discussions above, the slopes of the lines and the intercept on the $\delta^{34}\text{S}$ axis are the most important parameters for comparison.

The $\delta^{34}\text{S}$ lines for anhydrite and chalcopryrite or bornite converge at about +1.6‰ in the case of El Salvador. The ratio of oxidised to reduced sulphur species, using SO_2 as the oxidised species instead of SO_4^{2-} , is recalculated as follows:

$$\delta^{34}\text{S}_{\text{liq}} = 1.6 = \delta^{34}\text{S}_{\text{H}_2\text{S}} \cdot m_{\text{H}_2\text{S}} + \delta^{34}\text{S}_{\text{SO}_2} \cdot m_{\text{SO}_2}$$

(where $m_{\text{H}_2\text{S}} + m_{\text{SO}_2} = 1$). From Field & Gustafson's diagram, at $\Delta = 10.0\%$ ($T = 900 \text{ K}$), $\delta^{34}\text{S}_{\text{ccp}} = -3.0\%$. From Table 11-4, $\Delta_{\text{SO}_2-\text{H}_2\text{S}} = 5.3\%$ and $\Delta_{\text{ccp}-\text{H}_2\text{S}} \approx 0\%$ at 900 K, so that

$$m_{\text{H}_2\text{S}} = 0.13 \quad \text{and} \quad m_{\text{SO}_2}/m_{\text{H}_2\text{S}} = 7:1$$

Thus conditions were more oxidising than at Panguna. As an alternative measure of this, the difference in $\delta^{34}\text{S}$ between the liquid and the Cu,Fe sulphides at El Salvador is 4.6 to 7.6‰, greater than at Panguna.

Anhydrite-pyrite mineralisation at El Salvador gives a very different pair of lines. These converge to +6.8‰, and have slopes indicating high oxygen fugacity. Field & Gustafson concluded that a correction to the pyrite data may be required. A subtraction of 3‰ from $\delta^{34}\text{S}_{\text{py}}$ would correct temperature estimates (see below) and align the pair of lines so as to indicate a single source-composition of sulphur.

The difficulty with pyrite does not seem to arise in the case of Frieda (Appendix 3). In summary, the two pairs of lines (one pair of which, as drawn, coincides exactly with the Panguna curves) may reflect mineralisation from two different centres. If so, the slope of the steeper sulphide line is greater than at Panguna, indicating a higher oxidation state. The pairs of lines both converge near +1‰.

Sulphide data from other selected deposits are listed in Table 11-5. The sulphide from El Salvador is isotopically very light compared with the other deposits. Other deposits with low $\delta^{34}\text{S}$ are known,

Table 11-5

SULPHUR ISOTOPE DATA FOR PORPHYRY-TYPE MINERALISATION
FROM SELECTED DEPOSITS

Deposit	$\delta^{34}\text{S}$ range, ccp ‰	$\delta^{34}\text{S}$ range, py ‰	Reference
Panguna	-1.6 to +1.5	0.5 to +2.4	Ayres <i>et al</i> (in press); this study.
Frieda	-3.5, +0.1	-1.6 to +2.1	this study
Bingham (central)	-2.9 to -0.1	-0.4 to +1.1	Field (1966)
Butte (deep zone)	-3.0 to 0.0	-1.0 to +2.7	Lange & Cheney (1971)
Valley Copper	-3.3 to +1.5	-3.1	Osatenko & Jones (1976)
El Salvador (except peripheral)	-5.3 to -3.1	-5.1 to -0.3	Field & Gustafson (1976)

e.g. Yerington, Nevada (Field, 1966, data for undifferentiated sulphides). Panguna sulphides are a little heavier than the others. The range for pyrite is displaced about 2‰ in the positive direction in each case. If this difference reflects the temperature of formation, then the temperature would be less than 250°C, considerably lower than other estimates. At El Salvador, coexisting pyrite-chalcopyrite pairs have been examined, and they give apparently erroneous temperatures. At Panguna, it is at best uncertain whether chalcopyrite and pyrite were ever in equilibrium; the same may apply to the other deposits.

All information points to Cu,Fe sulphide-anhydrite pairs as the most useful and reliable source of data on porphyry copper mineralisation. In a well-controlled and sufficiently detailed study, pyrite may yield additional insight. The variety of pyrite occurrences at Panguna suggests that very careful sampling would be necessary.

THE ISOTOPIC COMPOSITION OF MAGMATIC SULPHUR

The near-zero $\delta^{34}\text{S}$ values of porphyry copper sulphides have in the past been taken to indicate that magmatic sulphur in these systems also had $\delta^{34}\text{S}$ near 0‰. The fixing of much sulphur as anhydrite (likely even in deposits where it has not been observed because it has been dissolved away), and the removal of large amounts as SO_2 in vapour imply that this approach is greatly oversimplified. Field & Gustafson's suggestion that the point of convergence of curves such as those in fig. 11-3 represents the isotopic composition of magmatic sulphur is also inadequate in any system in which two fluid phases separated from the crystallising magma.

Two extreme cases are to be considered. In the first, the magmatic volatiles separate in isotopic equilibrium with the silicate liquid,

i.e. without depleting the magmatic sulphur reservoir significantly.

H₂S in the salt-rich liquid will therefore be in equilibrium with HS⁻ in the magma (Ohmoto & Rye, in press). At Panguna, $\delta^{34}\text{S}_{\text{H}_2\text{S}} = +0.7\%$ so that $\delta^{34}\text{S}_{\text{HS}^-} = 0.0\%$.

In the second case, the volatiles remove all sulphur from the magma. The $\delta^{34}\text{S}$ of all the volatiles taken together is the same as the magmatic $\delta^{34}\text{S}$. The problem becomes one of knowing the relative proportions of vapour and salt-rich liquid, and the oxidation states of the fluids. The evolution of an early, boiling salt-rich liquid at relatively low oxygen fugacity has been discussed in Chapter 10.

Using the estimates of magmatic volatile content cited in Chapter 10 (viz. for 1 kg magma, 15 g H₂O and 1 g NaCl), and assuming the evolution of salt-rich liquid of 65% NaCl and vapour of 2% NaCl, the molar ratio of vapour and liquid is found (from a calculation similar to those performed in Chapter 10) to be 0.034:0.61 for dimers in the vapour, $\approx 1:18$.

In the vapour evolved during copper mineralisation (1100 K, HM and 800 atm) $P_{\text{SO}_2} > 6 \text{ atm}$ (Chapter 10), i.e. $X_{\text{SO}_2} > 0.01$ and 18 moles of vapour contain more than 0.18 moles S as SO₂.

If one mole of salt-rich liquid contains enough sulphur to form chalcopyrite corresponding to 1900 ppm Cu (Chapter 5), i.e. 1900 ppm S, and 65% NaCl, the mole fraction of S as chalcopyrite is

$$\frac{0.19/32}{65/58.5 + 35/18 + 0.19/32} \approx 1.9 \times 10^{-3}$$

If the molar ratio of SO₂:H₂S in the liquid is 1:9, and if sulphate forms by reaction 10.52, this corresponds with a total sulphur mole fraction of

$$1.9 \times 10^{-3} \left[1 + \left[\frac{1}{9} / \left(9 + \frac{1}{4} \right) \right] \right] \approx 1.9 \times 10^{-3}$$

Doubling the above figure to account (roughly) for sulphur lost by boiling in the ore-zone, the mole fraction of sulphur in the liquid becomes about 4×10^{-3} .

$$\text{Thus, } \frac{\text{moles S in liquid}}{\text{moles S in vapour}} < \frac{4 \times 10^{-3}}{0.18} = \frac{1}{45}$$

SO_2 is also the dominant sulphur species in the vapour down to $\log f_{\text{O}_2} = \text{HM} - 3$ ($k_{10.15}$ from Table 10-6; $\log f_{\text{H}_2\text{O}} = 2.8$). If more sulphur is carried in the vapour than in the liquid under all f_{O_2} conditions, then $\delta^{34}\text{S}_{\text{magma}} = \delta^{34}\text{S}_{\text{SO}_2}$ summed over the whole process of expulsion of volatiles. Late, relatively oxidised fluids must have removed all sulphur remaining in the magma which would therefore have had $\delta^{34}\text{S} = +4.1\%$ at that stage. Early, relatively reduced fluids may have removed sulphur in isotopic equilibrium with magmatic sulphur, before significant depletion of the reservoir. Since this sulphur was removed as SO_2 , the initial $\delta^{34}\text{S}$ of the magmatic sulphur would have been greater than $+4.1\%$. How much greater depends on the amount of sulphur carried in the reduced fluids, and there is no information about this.

Again using the calculation of the number of moles of liquid and vapour expelled by a kilogram of magma, it is possible to estimate the amount of sulphur lost from the magma as volatiles. Considering only the sulphur in the vapour, for which the limits $X_{\text{SO}_2} = 0.01$ to 0.1 were set in Chapter 10, the number of moles of S lost as vapour would be 6.1×10^{-3} to 6.1×10^{-2} , and the weight 0.2 to 2.0 g. The estimates of X_{SO_2} apply only to the relatively oxidised vapours expelled during copper mineralisation. If, say, half of the volatiles were expelled in that condition, then 0.1 to 1.0 g S would leave the magma during copper mineralisation. The more reduced half of the fluids might be expected to carry less SO_2 because of the lower oxygen fugacity, but no estimate is possible. In any case, the amount of S carried in the fluids would be

no less than 0.1 to 1.0 g, a quantity to be compared with the amount of S remaining in unaltered Kaverong Quartz Diorite (0.3 g/kg, analyses from Ford, 1976). Thus isotopic equilibria could well be subject to a depletion effect, even for the minimum quantities estimated here, and the results would approach those of the second case discussed above.

The problem of the isotopic composition of magmatic sulphur is thus a difficult one, dependent for its solution on a complete understanding of the processes by which volatiles are evolved and expelled from the magma. The speculations here are founded on guesses as to the relative quantities of oxidised and reduced fluids, and the amount of sulphur in the reduced fluids.

Comment. Less than 2% of the sulphur expelled from the magma during copper mineralisation is carried in salt-rich liquid (see calculation above). The figure used in the calculation was a minimum estimate of the amount carried away as vapour. Earlier fluids may also have removed significant sulphur, and the mineralising salt-rich liquid itself may not deposit all of the sulphur it contains. Thus the formation of a porphyry copper fixes little, probably much less than 1%, of the sulphur expelled from the magma, and much sulphur may be available for mineralisation higher in the hydrothermal system.

CONCLUSIONS

The sequence of mineralisation at Panguna porphyry copper deposit comprises many types and episodes of veining, including the quartz-Cu,Fe sulphide veins associated with the copper mineralisation. Fluid inclusions in quartz of these veins contain three types of fluid: dense salt-rich liquid, low-density water-rich vapour, and brines of low to moderate salinity unsaturated in NaCl at room temperature. The fluids may be grouped into two systems, one of salt-rich liquid in equilibrium with vapour, the other of low to moderate salinity brine. The two systems were distinct in the ore-zone.

The composition of the salt-rich liquid, in terms of the system NaCl-KCl-H₂O, ranged between 76% and 46% salts by weight in inclusions which had nucleated sylvite. The NaCl content varied from 60% to 30% while the KCl content remained constant at $16 \pm 2\%$. Salt-rich liquids with $T_{\text{gNaCl}} < 320^{\circ}\text{C}$ had not nucleated sylvite, except for one inclusion which had 22% KCl and 27% NaCl. The K/Na ratio of the salt-rich liquids ranged from 0.46 to 0.17 (atomic proportions), increasing as the salinity decreased and, in general, as the temperature decreased. Na, K, Fe and Cl are the predominant ions in leachates of crushed quartz; Ca, SO₄ and minor Mg are also present. Chlorides of Na, K and Ca (minor Mn, Zn), a Cu,Fe sulphide and possibly apatite have been identified among the daughter salts of opened inclusions of salt-rich liquid. Volume measurements on chalcopyrite crystals in fluid inclusions indicate an original copper concentration near 1900 ppm in the salt-rich liquid from a vein formed at temperatures below 550°C . The density of the salt-rich liquids lay in the range 1.2 - 1.5 g/cm³. The temperatures of these liquids varied between 350°C and 700°C or higher.

Salt-rich liquid deposited quartz-Cu,Fe sulphides, anhydrite and iron oxides and was associated with the development of potassic alteration assemblages. They may also have deposited earlier amphibole-magnetite-quartz veins. Some, at least, were of magmatic origin, because primary salt-rich inclusions occur in quartz phenocrysts. The temperature and salinity distributions of the salt-rich liquids, combined with field data, indicate three phases (A, B and C) of quartz-Cu,Fe sulphide mineralisation from different centres. Phase A, the earliest, took place while the Kaverong Quartz Diorite was at near-magmatic temperatures ($>700^{\circ}\text{C}$) to the north of the orebody and was bounded to the south and southwest by a zone at $350^{\circ} - 430^{\circ}\text{C}$. This zone corresponds closely with the 0.3% Cu ore-grade contour and is parallel to a pyritic halo beyond the orebody. T_{SNaCl} values were $450^{\circ} - 490^{\circ}\text{C}$ except along this zone, where they fell below 420°C . Prior to phase A copper mineralisation, a hydrothermal system of similar extent brought about pervasive alteration of the Panguna Andesite to an amphibole-plagioclase-magnetite assemblage. Before this, the Panguna Andesite may have undergone thermal metamorphism to biotite hornfels at the contact of the Kaverong Quartz Diorite.

Two later phases, B and C, occurred after a long period of cooling and may have been partly concurrent. Phase B, which seems to have comprised two stages, was associated with the emplacement of the Leucocratic Quartz Diorite. Temperatures exceeded 600°C at the centre and T_{SNaCl} values varied between 390°C and 490°C . The cell of mineralisation was bounded by a halo of pyrite veins and possibly by another of fluids at or near the critical point. Phase C postdated the Biuro Granodiorite. Temperatures exceeded 580°C and T_{SNaCl} values attained 570°C at the centre. A group of veins with $T_{\text{SNaCl}} < 400^{\circ}\text{C}$ east of the

Biotite Granodiorite may be part of the phase C boundary, which has not otherwise been located.

Brines of low to moderate salinity, in terms of the system $\text{NaCl-H}_2\text{O}$, covered the whole composition range of solutions unsaturated at 25°C . Brines of 0 - 5 wt. % eq. NaCl predominated. Formation temperatures (corrected for pressure) ranged between 160°C and 400°C . The brines deposited quartz-pyrite veins and were associated with some of the phyllic alteration. They also appear to have been associated with the deposition of sphalerite-pyrite and pyrite-clay veins near 300°C . Isotopic evidence (Ford & Green, 1977) combined with fluid inclusion evidence, indicates that these were meteoric waters. No regular temperature or salinity distributions were found for the brines of low to moderate salinity. They were present outside the zones of ore-deposition during phases A, B and probably C, and inundated the orebody between phases A and B, and again after the waning of phases B and C. They were present throughout the cooling of the ore zone from 400°C to below 200°C , and may have been involved in the formation of the post-mineralisation pebble dykes that intersect the hot centres of phases B and C. The opening of large fractures is thought to have carried groundwater into rock hot enough to cause violent boiling.

The fluids near the critical point at 400°C (the QP association of Chapter 6) are thought to represent the boundary of the region of two coexisting fluids from which copper was deposited in each phase of fluid circulation. The critical pressure of the fluids (270 - 280 bars) is a minimum estimate of the pressure at the edge of the system, to be compared with a maximum estimate of 290 bars based on the behaviour of gas-rich inclusions, and an estimate of 200 - 300 bars based on the vapour pressures of saturated salt-rich liquids. Under a hydrostatic pressure regime, this implies a depth of formation of about 3 km.

With the critical pressure of the QP association as a boundary pressure, the phase behaviour of salt-rich liquid in fluid inclusions is found to compare closely with the behaviour predicted in the literature for boiling NaCl-H₂O liquids, provided supersaturation is permitted in the real system in place of saturation, and despite the presence of significant KCl in the real liquids. The evolution of the liquids was as follows: unsaturated, boiling salt-rich liquid was expelled from the magma, and cooled by boiling to saturation and supersaturation at temperatures probably near 500°C. Further cooling was in part due to mixing with cooler, more dilute liquid so that the salt-rich liquids became unsaturated again by about 430°C. During phase C, some liquids were concentrated by boiling to 75% salinity without mixing. Dilution and cooling of the boiling liquids continued from 430°C to 400°C, at which temperature the compositions of the liquid and gas had converged to a single, critical composition.

The compositional variation of the salt-rich liquids, a straight-line trend on the NaCl-KCl-H₂O triangular diagram, is consistent with the mixing of two salt-rich liquids, one of about 65% salts and low K/Na, derived from the magma, and the other containing at most 45% salts and with a higher K/Na, probably derived from groundwater by boiling. Both would have contained the same concentration, about 16% (wt.) of KCl. The K/Na ratios of magmatic salt-rich liquids are consistent with equilibrium between the liquids and the rims of plagioclase phenocrysts in the various stocks. No buffering mechanism can be suggested for salt-rich liquid derived from groundwater.

Salt-rich liquid probably ascended from crystallising magma to the ore-zone by the pumping action of the difference between lithostatic pressure in the magma and hydrostatic pressure in the ore-zone. At a level

probably determined by the presence of groundwater, salt-rich liquid moved horizontally into the country rocks, then descended, because of its density, through the ore-zone.

The critical-point boundary proposed for the region of two fluid phases can continue at most 600 m above present levels of exposure. The nature of the boundary over the two-phase region cannot be inferred. Below the exposed ore-zone, the salinity at the critical-point boundary, if it and groundwater persist to depth, would increase with depth.

At 1000 K, 500 bars and $\log f_{\text{O}_2}$ at the hematite-magnetite boundary, vapour leaving the magma would have had the following chemical parameters:

$\log f_{\text{O}_2} = -8.8$	$\log f_{\text{NaCl}} < -1.8$
$\log f_{\text{S}_2} = -7.1 \pm 2.3$	$\log f_{\text{CuCl}} = -10 \pm 5$
$\log f_{\text{SO}_2} = 0.6 \pm 1.0$	$\log f_{\text{NaFeCl}_3} = -11 \pm 2$
$\log f_{\text{H}_2\text{S}} = -3.3 \pm 1.0$	$\log f_{\text{ZnCl}_2} > -3.7 \pm 1.8^*$
$\log f_{\text{H}_2\text{O}} = 2.6$	$\log f_{\text{MoO}_2(\text{OH})_2} > -3.6 \pm 1.5^*$
$\log f_{\text{HCl}} = 0.1 \pm 0.5$	(* values at 850 K)

when in equilibrium with an assemblage of quartz, anhydrite, rutile, molybdenite, sphalerite and Cu,Fe sulphide, and with $X_{\text{SO}_2} < 0.1$. Values at other conditions are tabulated in the text. Enhanced volatility in mixed halide systems brings about a significant increase in the volatility of iron only, but does not lead to significant vapour transport of iron. The metal-bearing species above are the predominant species for each metal except for Na (NaOH.H₂O predominating) and Mo [Mo₇O₁₈(OH)₆ predominating]. Zinc and molybdenum may separate (in vapour) from iron and copper (in liquid) by virtue of their greater volatility. The formation from magmatic vapour of a salt-rich condensate with the copper concentration observed in fluid inclusions of salt-rich liquid is unlikely unless

$f_{\text{CuCl}} > 10^{-6.8}$. The chemical appraisal of the vapour plume mechanism of Henley & McNabb cannot be improved without better thermochemical data.

Since biotite is the most abundant alteration product associated with copper mineralisation, the acidity of the salt-rich liquid must be dominantly controlled by the formation of biotite from amphibole and plagioclase. The acidity of the salt-rich liquid should show a net increase, driving the liquid towards equilibrium with sericite rather than the observed K-feldspar, or K-feldspar + sericite. The formation of anhydrite and sulphides also produces HCl, so that boiling may be necessary in addition to the precipitation of quartz in order to take up excess HCl and avoid the formation of large quantities of sericite. The alteration reactions also control the activity of FeCl_2 in the liquid, and may therefore control the distribution of bornite and chalcopyrite.

The decomposition of SO_2 may account for the presence of the sulphate fixed as anhydrite but cannot account for the increase in sulphide deposition below 500°C . Reactions such as the reduction of SO_2 by Fe^{2+} may be significant at lower temperatures.

The high oxidation state of the magmatic fluids during copper mineralisation reflects the loss of H_2 in earlier fluids, those responsible for amphibole-magnetite-plagioclase alteration in the Panguna Andesite prior to phase A. There is no evidence of the deposition of copper by the reduced fluids, which appear to have been salt-rich liquid and vapour. The transport of copper may thus be dependent on the oxygen fugacity.

Sulphur isotope data yielded temperatures near 300°C for sphalerite-pyrite veins, and $400 - >800^\circ\text{C}$ for anhydrite-chalcopyrite pairs. No space or time variation of $\delta^{34}\text{S}$ in pyrite or chalcopyrite could be detected in the data available. Pyrite has a $\delta^{34}\text{S}$ range of +0.5 to +3.1‰, chalcopyrite (Ayres *et al.*, in press) -1.6 to +1.5‰ and anhydrite +7.6 to +16.0‰. The salt-rich liquid which deposited anhydrite and sulphides had

$\delta^{34}\text{S} = 1\%$. The $\delta^{34}\text{S}$ values of the liquid and the solid phases should vary as a function of oxygen fugacity and are not simply related to the $\delta^{34}\text{S}$ value of magmatic sulphur.

The evolution of salt-rich liquid from crystallising magma, the condensation of salt-rich liquid from cooling magmatic vapour, the boiling of groundwater and groundwater convection driven by heat from the intrusive centre - all suggestions by other authors regarding the mechanism of porphyry copper formation - may all have contributed to the formation or evolution of the Panguna deposit. The association of salt-rich liquid with copper is definite. The continuity of K/Na ratios between salt-rich liquids in veins and in the magma, along with the improbability of significant copper transport in the vapour under porphyry copper conditions implies that liquid expelled direct from the magma, and not condensate, was responsible for the mineralisation. Some metals and sulphur may have been derived from groundwater.

Further work at Panguna could examine the amphibole-bearing veins and alteration in greater detail, if the quality and quantity of specimens permit. More detailed work on the composition and properties of inclusions (solid and fluid) in quartz phenocrysts may also yield interesting data on processes occurring in the magmas. Any extension of the sulphur isotope study should, at the outset, be limited to anhydrite-chalcopyrite pairs (which are not common) or to chalcopyrite samples with temperature control. Depth was not considered as a spatial variable for the set of samples used in this study, so that ultimately, a new set of samples from the deepened pit may make an interesting comparative study.

REFERENCES

- ANDERSON, G.M., 1967. Specific volumes and fugacities of water. In Barnes, H.L. (ed.). *Geochemistry of Hydrothermal Ore Deposits*, 632-635. Holt, Rinehart & Winston, New York. 670 p.
- AYRES, D.E., BURNS, M.S. & SMITH, J.W., (in press). A sulphur reconnaissance study of the porphyry copper deposits at Panguna and Mt. Fubilan, Papua New Guinea. *Pacific Geology*.
- BALDWIN, J.T., SWAIN, H.D. & CLARK, G.H., 1978. Geology and grade distribution at the Panguna porphyry copper deposit, Bougainville, Papua New Guinea. *Econ. Geol.* 73, 690-702.
- BAMFORD, R.W., 1972. The Mt. Fubilan (Ok Tedi) porphyry copper deposit, Territory of Papua & New Guinea. *Econ. Geol.* 67, 1019-1033.
- BARIN, I. & KNACKE, O., 1973. *Thermochemical properties of inorganic substances*. Springer-Verlag, Berlin, New York. 921 p.
- BARNES, H.L. & CZAMANSKE, G.K., 1967. Solubilities and transport of ore minerals. In Barnes H.L. (ed.). *Geochemistry of hydrothermal ore deposits*. 344-381. Holt, Rinehart & Winston, New York. 670 p.
- BARTON, P.B. & SKINNER, B.J. (in press). Sulphide mineral stabilities, In Barnes, H.L. (ed.) *Geochemistry of hydrothermal ore deposits*. Wiley.
- BAUMER, A. & FRASER, R.B., 1975. Panguna porphyry copper deposit, Bougainville. In *Economic Geology of Australia and Papua New Guinea*. 1. Metals. 855-66. Australas. Inst. Min. Metall., Melbourne. 1126 p.
- BEANE, R.E., 1974. Biotite stability in the porphyry copper environment. *Econ. Geol.* 69, 241-256.
- BINNEWIES, M. & SCHAEFER, H., 1973. Gasfoermige molekelkomplexe $M_xM_yCl_z$. *Z. anorg. allg. Chem.*, 395, 77-81.
- BLAKE, D.H. & MIEZITIS, Y., 1967. *Geology of Bougainville and Buka Islands, New Guinea*. Bureau of Mineral Resources, Geology and Geophysics, Bulletin 93. Canberra, 56 p.
- BLOOM, H., 1967. *The chemistry of molten salts*. Benjamin, New York. 184 p.
- BLOOM, H., O'GRADY, B.V., ANTHONY, R.G. & REINSBOROUGH, V.C., 1970. Mass spectrometric identification of $NaZnCl_3$ and $Na_2Zn_2Cl_6$. *Austral. J. Chem.*, 23, 843-845.

- BRIMHALL, G.H., Jr., 1977. Early fracture-controlled disseminated mineralisation at Butte, Montana. *Econ. Geol.* 72, 37-59.
- BRITTAN, M.I., 1970. Kinetics of copper segregation by the TORCO process. *South African Inst. Mining Metall. J.* 70, 278-289.
- CABRI, L.J. & HALL, S.R., 1972. Mooihoekite and Haycockite, two new copper-iron sulfides, and their relationship to chalcopyrite and talnakhite. *Amer. Mineralogist* 57, 609-708.
- CATHLES, L.M., 1977. An analysis of the cooling of intrusives by groundwater convection which includes boiling. *Econ. Geol.* 72, 804-826.
- CARMICHAEL, I.S.E., TURNER, F.J. & VERHOOGEN, J., 1974. *Igneous petrology*. McGraw-Hill, New York. 739 p.
- CHIVAS, A.R., 1976. Magmatic evolution and porphyry copper mineralization of the Koloula igneous complex, Guadalcanal. Abstracts, 25th Intl Geol. Congress, Sydney. 1, 48.
- CHIVAS, A.R. & WILKINS, R.W.T., 1977. Fluid inclusion studies in relation to hydrothermal alteration and mineralisation at Koloula porphyry copper prospect, Guadalcanal. *Econ. Geol.* 72, 153-169.
- CHOU, I.M. & EUGSTER, H.P., 1977. Solubility of magnetite in supercritical chloride solutions. *Amer. J. Sci.* 277, 1296-1314.
- CLOKE, P.L., KELSER, S.E., JOWETT, R.E. & WILSON, J.W.J., (in press). The halite trend in magmatic-hydrothermal mineralisation. *Geol. Soc. Amer. Abstracts*.
- CORNEC, E. & KROMBACH, H., 1932. Equilibres entre le chlorure de potassium et le chlorure de sodium et l'eau depuis -23° jusqu'à $+190^{\circ}$. *Annales de chimie* 18, 5-31.
- CRERAR, D.A. & BARNES, H.L. (1976). Ore solution chemistry V: Solubilities of chalcopyrite and chalcocite assemblages in hydrothermal solution at 200°C to 350°C . *Econ. Geol.* 71, 772-794.
- CZAMANSKE, G.K. & WONES, D.R., 1973. Oxidation during magmatic differentiation, Finnmarka complex, Oslo area, Norway. Part 2: the mafic silicates. *J. Petrology* 14, 349-80.
- DENBIGH, K., 1971. *The principles of chemical equilibrium*. Cambridge University Press, Cambridge. 494 p.
- DENIS, M., 1974. Altérations et fluides associés dans le porphyre cuprifère de Sierrita (Arizona, Etats-Unis). Comparaison avec d'autres gisements du même type. Thesis (unpublished), Docteur de Spécialité (3^e cycle). CRPG-ENSG-Université de Nancy 1. Nancy, France. 146 p.

- DEWING, E.W., 1970. Gaseous complexes formed between trichlorides (AlCl_3 and FeCl_3) and dichlorides. *Metall. Trans.* 1, 2169-2174.
- EASTOE, C.J., 1978. A fluid inclusion study of the Panguna porphyry copper deposit, Bougainville, Papua New Guinea. *Econ. Geol.* 73, 721-748.
- ESPIE, F.F., 1971. The Bougainville copper project. *Proc. Aust. Inst. Mining & Metall.* 238, 1-10.
- ETMINAN, H., 1977. Le porphyre cuprifère de Sar Cheshmeh (Iran). Rôle des phases fluides dans les mécanismes d'alteration et de minéralisation. Sciences de la Terre, Mémoire no.34, Nancy, France. 249 p.
- EUGSTER, H.P. & WONES, D.R., 1962. Stability relations of the ferruginous biotite, annite. *J. Petrol.* 3, 82-125.
- FIELD, C.W., 1966. Sulfur isotope abundance data, Bingham district, Utah. *Econ. Geol.* 61, 850-871.
- FIELD, C.W. & GUSTAFSON, L.B., 1976. Sulfur isotopes in the porphyry copper deposit at El Salvador, Chile. *Econ. Geol.* 71, 1533-1548.
- FORD, J.H., 1976. A geochemical and stable isotope study of the Panguna porphyry copper deposit, Bougainville. Unpubl. Ph.D. thesis, Univ. of Queensland. 213 p.
- FORD, J.H., 1978. A chemical study of alteration at the Panguna porphyry copper deposit, Bougainville, Papua New Guinea. *Econ. Geol.* 73, 703-720.
- FORD, J.H. & GREEN, D.C., 1977. An oxygen- and hydrogen-isotope study of the Panguna porphyry copper deposit, Bougainville, Papua New Guinea. *J. Geol. Soc. Aust.* 24, 63-80.
- FOUNTAIN, R.J., 1972. Geological relationships in the Panguna porphyry copper deposit, Bougainville, Island, New Guinea. *Econ. Geol.* 67, 1049-1064.
- FOUNTAIN, R.J., 1973. Geology of the Panguna porphyry copper deposit, Bougainville. Unpubl. Ph.D. thesis, University of Sydney.
- FOURNIER, R.O., 1976. Exchange of Na^+ and K^+ between water vapour and feldspar phases at high temperature and low vapour pressure. *Geochim. Cosmochim. Acta* 40, 1553-1561.
- GALITSKIY, N.V., 1968. Pressure and composition of the vapour over FeCl_3 -NaCl and AlCl_3 -NaCl systems. *Russ. J. Inorg. Chem.* 13, 1607-1610.

- GLEMSER, O. & WENDLANDT, H.G., 1963. Gaseous hydroxides: *Advances Inorganic Chemistry Radiochemistry* 5, 215-258.
- GROSS, P. & STUART, M.C., 1971. On the equilibrium pressure of cuprous chloride in the segregation reaction. In Kubaschewski, O., (ed.), *Metallurgical Chemistry Symposium*, London. H.M. Stationery Office, 499-512.
- GUIDO, M., GIGLI, G. & BALDUCCI, G., 1972. Dissociation energy of CuCl and Cu_2Cl_2 gaseous molecules. *J. Chem. Phys.* 57, 3731-3735.
- GUSTAFSON, L.B., 1978. Some major factors of porphyry copper genesis. *Econ. Geol.* 73, 600-607.
- GUSTAFSON, L.B. & HUNT, J.P., 1975. The porphyry copper deposit at El Salvador, Chile. *Econ. Geol.* 70, 857-912.
- HAAS, J.L., Jr. & ROBIE, R.A., 1973. Thermodynamic data for wustite, $\text{Fe}_{0.947}\text{O}$, magnetite, Fe_3O_4 , and hematite, Fe_2O_3 . (Abstract). *Amer. Geophys. Union Trans.* 54, 483.
- HALL, R.J. & SIMPSON, P.G., 1975. The Frieda porphyry copper prospect, Papua New Guinea. *Economic Geology of Australia and Papua New Guinea*, 1. Metals, 836-45. Australas. Inst. Min. Metall., Melbourne. 1126 p.
- HASTIE, J.W., 1975. *High-temperature vapors: science and technology*. Academic Press, New York. 480 p.
- HENLEY, R.W. & McNABB, A., 1978. Magmatic vapor plumes and ground-water interaction in porphyry copper emplacement. *Econ. Geol.* 73, 1-20.
- HOLLAND, H.D., 1965. Some applications of thermochemical data to problems of ore deposits. II. Mineral assemblages and the composition of ore-forming fluids. *Econ. Geol.* 60, 1101-1166.
- HOLLAND, H.D., 1967. Gangue minerals in hydrothermal deposits. Ch. 9, 382-436. In Barnes, H.L. (ed.). *Geochemistry of hydrothermal ore deposits*. Holt, Rinehart & Winston Inc., New York. 670 p.
- HOLLISTER, V.J., 1975. An appraisal of the nature and source of porphyry copper deposits. *Minerals Sci. Engng.* 7, 225-233.
- HORTON, D.J., 1978. Porphyry-type copper-molybdenum mineralisation belts in Eastern Queensland, Australia. *Econ. Geol.* 73, 904-921.
- JANAF, 1971. *Thermochemical tables*. Nat. Stand. Ref. Ser., Nat. Bur. Stand. (U.S.) 37, 1141 p.
- JAMES, A.H., 1971. Hypothetical diagrams of several porphyry copper deposits. *Econ. Geol.* 66, 43-47.

- KEEVIL, N.B., 1942. Vapour pressures of aqueous solutions at high temperatures. *J. Amer. Chem. Soc.* 64, 841-850.
- KESLER, S.E., 1973. Copper, molybdenum and gold abundances in porphyry copper deposits. *Econ. Geol.* 68, 106-112.
- KNIGHT, C.L., FRASER, R.B. & BAUMER, A., 1973. Geology of the Bougainville copper orebody, New Guinea. *Austr. Bur. Min. Res. Bulletin* 141, 123-133.
- KOSAKA, H. & WAKITA, K., 1978. Some geologic features of the Mamut porphyry copper deposit, Sabah, Malaysia. *Econ. Geol.* 73, 618-627.
- KRAUSKOPF, K.B., 1964. The possible role of volatile metal compounds in ore genesis. *Econ. Geol.* 59, 22-45.
- LAGACHE, M. & WEISBROD, A., 1977. The system: two alkali feldspars-KCl-NaCl-H₂O at moderate to high temperatures and low pressures. *Contrib. Mineral. Petrol.* 62, 77-101.
- LANGE, I.M. & CHENEY, E.S., 1971. Sulphur isotopic reconnaissance of Butte, Montana. *Econ. Geol.* 66, 63-74.
- LARSON, L.T., MILLER, J.D., NADEAU, J.E. & ROEDDER, E., 1973. Two sources of error in low temperature inclusion homogenisation determination and corrections on published temperatures for the East Tennessee and Laisvale deposits. *Econ. Geol.* 68, 113-116.
- LAWRENCE, L.J. & SAVAGE, E.N., 1975. Mineralogy of the titaniferous porphyry copper deposits of Melanesia. *Proc. Australas. Inst. Min. Metall.* 256, 1-14.
- LOWELL, J.D. & GUILBERT, J.M., 1970. Lateral and vertical alteration-mineralisation zoning in porphyry ore deposits. *Econ. Geol.* 65, 373-408.
- MacNAMARA, P.M., 1968. Rock types and mineralisation at Panguna porphyry copper deposit, upper Kaverong valley, Bougainville Island. *Proc. Aust. Inst. Min. Metall.* 228, 71-79.
- MARSHALL, W.L. & JONES, E.V., 1974. Liquid-vapor critical temperatures of aqueous electrolyte solutions. *J. Inorg. Nuclear Chem.* 36, 2313-2318.
- MASON, D.R. & McDONALD, J.A., 1978. Intrusive rocks and porphyry copper occurrences of the Papua New Guinea-Solomon Islands region: a reconnaissance study. *Econ. Geol.* 73, 857-877.
- METZGER, J.W., KELLY, W.C., NESBITT, B.E. & ESSENE, E.J., 1977. Scanning electron microscopy of daughter minerals in fluid inclusions. *Econ. Geol.* 72, 141-152.

- MILLS, K.C., 1974. *Thermodynamic data for inorganic sulphides, selenides and tellurides*. Butterworths, London. 845 p.
- MONTOYA, J.W. & HEMLEY, J.J., 1975. Activity relations and stabilities in alkali feldspar and mica alteration reactions. *Econ. Geol.* 70, 577-584.
- MOORE, W.J. & NASH, J.T., 1974. Alteration and fluid inclusion studies of the porphyry copper ore body at Bingham, Utah. *Econ. Geol.* 69, 631-645.
- NASH, J.T., 1976. Fluid inclusion petrology - data from porphyry copper deposits and applications to exploration. *U.S.G.S. prof. paper* 907-D. 16 p.
- NEWTON, R.H., 1935. Activity coefficients of gases. *Ind. Eng. Chem.* 27, 302-306.
- NEY, C.S. & HOLLISTER, V.J., 1976. Geologic setting of porphyry deposits of the Canadian Cordillera. In Sutherland-Brown, A. (ed.), *Porphyry deposits of the Canadian Cordillera*, CIM special volume 15, 21-29.
- NORTON, D., 1978. Sourcelines, sourcereions and pathlines for fluids in hydrothermal systems related to cooling plutons. *Econ. Geol.* 73, 21-28.
- NORTON, D. & KNIGHT, J., 1977. Transport phenomena in hydrothermal systems: Cooling plutons. *Amer. J. Sci.* 277, 937-981.
- OHMOTO, H. & RYE, R.O., (in press). Isotopes of sulphur and carbon. In Barnes, H.L., (ed.), *Geochemistry of hydrothermal ore deposits*, 2nd ed. Wiley.
- ORVILLE, P.M., 1963. Alkali ion exchange between vapor and feldspar phases. *Amer. J. Sci.* 261, 203-237.
- OSATENKO, M.J. & JONES, M.B., 1976. Valley Copper. In Sutherland-Brown, A., (ed.), *Porphyry deposits of the Canadian Cordillera*. CIM special volume 15, 130-143.
- PAGE, R.W. & McDOUGALL, I., 1972. Geochronology of the Panguna porphyry copper deposit, Bougainville Is., New Guinea. *Econ. Geol.* 67, 1065-1074.
- POTTER, R.W., III, 1977. Pressure corrections for fluid inclusion homogenisation temperatures based on the volumetric properties of the system NaCl-H₂O. *U.S.G.S. J. Res.* 5, 603-608.
- POTTER, R.W., & BROWN, D.L., 1977. The volumetric properties of aqueous sodium chloride solutions from 0°C to 500°C at pressures up to 2000 bars based on a regression of available data in the literature. *U.S.G.S. Bulletin* 1421-C.

- POTTER, R.W., III, CLYNNE, M.A. & BROWN, D.L., 1978. Freezing point depression of aqueous sodium chloride solutions. *Econ. Geol.* 73, 284-285.
- POTY, B., LEROY, J. & JACHIMOVICZ, L., 1976. Un nouvel appareil pour la mesure des températures sous le microscope: l'installation de microthermométrie Chaixmecc. *Bull. Soc. fr. Minéral. Cristallogr.* 99, 182-186.
- POTY, B., STALDER, H.A. & WEISBROD, A.M., 1974. Fluid inclusion studies in quartz from fissures of the Western and Central Alps. *Schweiz. Min. Petr. Mitt.* 54, 717-752.
- PRZIBRAM, K. & CAFFYN, J.E., 1956. *Irradiation colours and luminescence: a contribution to mineral physics.* Pergamon, London. 332 p.
- RAFTER, T.A., 1957. Sulphur isotopic variations in nature, part 2: A quantitative study of the reduction of barium sulphate by graphite for recovery of sulphide-sulphur for sulphur isotopic measurements. *N.Z. J. Sci. Tech.* 38, 955-968.
- RAVICH, M.I. & BOROVAYA, F.E., 1949. Fazovyye ravnovesiya v troynnykh vodno-solyevykh sistemakh pri vysokikh tyemperaturakh. (Phase equilibria in ternary water-salt systems at elevated temperatures.) *Akad. Nauk. S.S.S.R., Izvestiya Syektora Fiz.-Khim. Analiza*, 19, 69-81.
- REES, C.E., 1978. Sulphur isotope measurements using SO_2 and SF_6 . *Geochim. Cosmochim. Acta* 42, 383-389.
- REES, C.E., JENKINS, W.J. & MONSTER, J., 1978. The sulphur isotopic composition of ocean water sulphate. *Geochim. Cosmochim. Acta* 42, 377-381.
- ROBIE, R.A. & WALDBAUM, D.R., 1968. Thermodynamic properties of minerals and related substances at 298.15 °K (25.0 °C) and one atmosphere (1.013 bars) pressure and at higher temperatures. *U.S.G.S. Bull.* 1259, 256 p.
- ROEDDER, E., 1967. Fluid inclusions as samples of ore solutions. In Barnes, H.L., (ed.), *Geochemistry of hydrothermal ore deposits*, 515-574. Holt, Rinehart & Winston, New York. 670 p.
- ROEDDER, E., 1970. Application of an improved crushing microscope stage to studies of gases in fluid inclusions. *Schweiz. Miner. Petr. Mitteil.* 50, 41-58.
- ROEDDER, E., 1971. Fluid inclusion studies on the porphyry-type ore deposits of Bingham, Utah, Butte, Montana, and Climax, Colorado. *Econ. Geol.* 66, 98-120.

- ROEDDER, E. & SKINNER, B.J., 1968. Experimental evidence that fluid inclusions do not leak. *Econ. Geol.* 63, 715-730.
- ROSE, A.W., 1970. Zonal relations of wallrock alteration and sulphide distribution at porphyry copper deposits. *Econ. Geol.* 65, 920-936.
- RYABCHIKOV, I.D., 1975. *Termodinamika flyuidnoy fazy granitoidnykh magm.* (Thermodynamics of the fluid phase of granitoid magmas.) Izdatel'stvo "Nauka", Moscow. 231 p.
- RYZHENKO, B.N. & VOLKOV, V.P., 1971. Fugacity coefficients of some gases in a broad range of temperatures and pressures. *Geochem. International* 8, 468-481.
- SAKAI, H. & YAMAMOTO, M., 1966. Fractionation of sulphur isotopes in and preparation of sulphur dioxide - an improved technique for the precision analysis of stable sulphur isotopes. *Geochem. J. (Japan)* 1, 35-42.
- SCHAEFER, H., 1974. Nachweis und Anwendung von Gaskomplexen beim chemischen Transport. *Z. anorg. allg. Chem.* 403, 116-126.
- SCHAEFER, H., 1976. Gaseous chloride complexes with halogen bridges - homo-complexes and hetero-complexes. *Angewandte Chemie* 15, 713-727.
- SERAPHIM, R.H. & HOLLISTER, V.J., 1976. Structural settings, In Sutherland-Brown, A., (ed.), *Porphyry deposits of the Canadian Cordillera*. CIM special volume 15, 30-43.
- SILLITOE, R.H., 1973. The tops and bottoms of porphyry copper deposits. *Econ. Geol.* 68, 799-815.
- SMITH, J.W., DOOLAN, S. & McFARLANE, E.F., 1977. A sulphur isotope geothermometer for the trisulphide system galena-sphalerite-pyrite. *Chem. Geol.* 19, 83-90.
- SOURIRAJAN, S. & KENNEDY, G.C., 1962. The system NaCl-H₂O at elevated temperatures and pressures. *Amer. J. Sci.* 260, 115-141.
- SUTHERLAND-BROWN, A., (ed.), 1976a. *Porphyry deposits of the Canadian Cordillera*. Canadian Inst. Mining Metall. Special Vol. 15, 510 p.
- SUTHERLAND-BROWN, A., 1976b. Morphology and classification, In Sutherland-Brown, A., (ed.), *Porphyry deposits of the Canadian Cordillera*, CIM special volume 15, 44-51.
- TAUSON, V.L. & CHERNYSHEV, L.V., 1977. Phase relationships and structural features of ZnS-CdS mixed crystals. *Geochem. Internat.* 14, 11-22.

- TAYLOR, H.P., 1974. The application of oxygen and hydrogen isotope studies to problems of hydrothermal alteration and ore deposition. *Econ. Geol.* 69, 843-883.
- TAYLOR, S.R., 1969. Trace element chemistry of andesites and associated calc-alkaline rocks, In McBirney, A.R., (ed.), *Proc. Andesite Conference, Dept. Geol. Miner. Res. Oregon Bull.* 65, 43-64.
- THOMPSON, J.E., 1962. The Pumpkuna copper-gold prospect, Bougainville Island, Territory of Papua and New Guinea. *Aust. Bur. Mineral Res. Geol. Geophys. Rec.* 1962/39 (unpub.).
- TITLEY, S.R., 1972. Intrusion, and wall-rock, porphyry copper deposits. *Econ. Geol.* 67, 122-3.
- TITLEY, S.R., 1975. Geological characteristics and environments of some porphyry copper occurrences in the southwestern Pacific. *Econ. Geol.* 70, 499-514.
- TITLEY, S.R. 1978. Copper, molybdenum and gold content of some porphyry copper systems of the southwestern and western Pacific. *Econ. Geol.* 73, 977-981.
- TITLEY, S.R., FLEMING, A.W. & NEALE, T.I., 1978. Tectonic evolution of the porphyry copper system at Yandera, Papua New Guinea. *Econ. Geol.* 73, 810-828.
- TOULMIN, P., III & CLARK, S.P., Jr., 1967. Thermal aspects of ore formation, In Barnes, H.L., (ed.), *Geochemistry of hydrothermal ore deposits*, 437-464. Holt, Rinehart & Winston, New York. 670 p.
- TOURAY, J.C., 1970. Analyse thermo-optique des familles d'inclusions à dépôts salins (principalement halite). *Schweiz. Mineralog. Petrogr. Mitt.* 50, 67-69.
- TURNER, J.S., SHIRTCLIFFE, T.G.L. & BREWER, P.G., 1970. Elemental variations of transport coefficients across density interfaces in multiple-diffusive systems. *Nature* 228, 1083-1084.
- URUSOVA, M.A., 1975. Phase equilibria and thermodynamic characteristics of solutions in the systems NaCl-H₂O at 350-550°C. *Geochem. Internat.* 11, 944-950.
- VEDENEYEV, V.I., GURVICH, L.V. KONDRAT'YEV, V.A., MEDVEDEV, V.A. & FRANKEVICH, Ye.L., 1966. *Bond energies, ionisation potentials and electron affinities*. Edward Arnold, London. 202 p.
- WATERMAN, G.C. & HAMILTON, R.L., 1975. The Sar Cheshmeh porphyry copper deposit. *Econ. Geol.* 70, 568-576.
- WEAST, R.C. (ed.), 1975. *Handbook of chemistry and physics*. CRC Press, Cleveland.

- WOODCOCK, J.R. & HOLLISTER, V.F., 1978. Porphyry molybdenite deposits of the North American Cordillera. *Minerals. Sci. Engng.* 10, 3-18.
- WYLLIE, P.J., 1977. Crustal anatexis: an experimental review. *Tectonophysics* 43, 41-71.
- YERMAKOV, N.P. *et al.*, 1965. *Research on the nature of mineral-forming solutions.* Pergamon, New York. 743 p.
- YUND, R.A. & KULLERUD, G., 1966. Thermal stability of assemblages in the Cu-Fe-S system. *J. Petrol.* 7, 454-488.

Appendix 1

LIST OF SPECIMENS FROM PANGUNAABBREVIATIONS

bD - Biotite Diorite, bG - Biotite Granodiorite, BiG - Biuro Granodiorite, IB - Intrusive Breccia, KqD - Kaverong Quartz Diorite, lqD - Leucocratic Quartz Diorite, PA - Panguna Andesite, qfP - Quartz Feldspar Porphyry.

RL: reduced level in m above sea level. No RL is given for samples from diamond drill core; instead the position in the hole (m from origin) and hole no. (DDH BVP ...) are given.

-
- | | |
|--------|---|
| 102594 | Quartz-bornite vein (minor anhydrite, hematite, rutile, digenite, tennantite, stannite, galena, bravoite) from PA. RL: 625, coords. 61850, 121900 approx. |
| 102609 | Quartz-chalcopryrite-bornite vein (minor anhydrite, hematite) from PA. RL: 625, coords. 61840, 122080. |
| 102612 | Quartz-chalcopryrite-bornite vein (minor anhydrite, hematite) from lqD. RL: 625, coords 61840, 122050. |
| 102619 | Quartz-chalcopryrite-bornite vein (minor anhydrite, molybdenite, pyrite) from lqD. RL: 625, coords. 16840, 121925. |
| 102636 | Quartz-chalcopryrite-pyrite vein (minor hematite, anhydrite, rutile) from PA. RL: 625, coords. 61435, 121830. |
| 102645 | Quartz-chalcopryrite vein from bD. RL: 640, coords. 61250, 121285. |
| 102651 | Quartz-chalcopryrite-pyrite vein (minor hematite, rutile) from PA. RL: 670, coords. 61790, 122560. |
| 102658 | Quartz-chalcopryrite-bornite vein (minor hematite) from PA. RL: 670, coords 61950, 122410. |
| 102661 | Quartz-chalcopryrite-bornite vein (minor digenite, hematite, molybdenite, rutile) from PA. RL: 670, coords. 62000, 122030. |

- 102662 Quartz-chalcopryrite vein (minor anhydrite) from PA. RL: 670, coords. 61980, 121840.
- 102666 Quartz-chalcopryrite-bornite vein (minor anhydrite, hematite) from PA. RL: 670, coords. 61750, 121650.
- 102668 Quartz-chalcopryrite-bornite vein (minor hematite) from PA. RL: 670, coords. 61980, 121775.
- 102673 Quartz-anhydrite-chalcopryrite vein (minor hematite, rutile) from BD. 301 m, DDH BVP 61.
- 102676 Quartz-anhydrite vein (minor chalcopryrite, bornite, hematite) from BD. 476 m, DDH BVP 88.
- 102997 Quartz-chalcopryrite-pyrite vein (minor anhydrite, hematite) oxidised to give covellite ? chalcocite, from BD. From surface coords. 62050, 123320.
- 102998 Quartz-chalcopryrite vein (minor anhydrite, hematite) from KqD. 338 m, DDH BVP 146, coords. 61380, 123150.
- 102999 Quartz-chalcopryrite-pyrite vein (minor anhydrite, rutile) from BD. 67 m, DDH BVP 248, coords. 61700, 122960.
- 103000 Quartz-chalcopryrite-pyrite vein (minor anhydrite) from PA. 33m, DDH BVP 281, coords. 62100, 122770.
- 103001 Quartz-chalcopryrite-pyrite vein (minor anhydrite, hematite) from bG. 233 m, DDH BVP 105, coords. 61370, 122770.
- 103002 Quartz-chalcopryrite-pyrite vein (minor anhydrite, magnetite) from PA. RL: surface, coords. 60150, 123110.
- 103003 Quartz-chalcopryrite vein (minor anhydrite, hematite, molybdenite) from PA. RL: surface, coords. 60380, 122650.
- 103004 Quartz vein (sulphides oxidised) (minor hematite) from BD. RL: 670, coords. 61350, 122600.
- 103005 Quartz vein (sulphides oxidised to chrysocolla) from bG (minor anhydrite, hematite). RL: 670, coords. 61510, 122610.
- 103006 Quartz-pyrite-chalcopryrite vein (minor anhydrite, hematite) from IB. RL: 670, coords. 61670, 122650.
- 103007 Quartz-chalcopryrite-pyrite-hematite vein (minor anhydrite, rutile) from PA. RL: 670, coords. 61750, 122620.
- 103008 Quartz-chalcopryrite vein (minor hematite) from PA. RL: 700, coords. 61850, 122670.
- 103009 Quartz-chalcopryrite-bornite breccia filling (minor anhydrite, hematite, rutile) from IB. RL: 655, coords. 61750, 122480.
- 103010 Quartz-chalcopryrite vein (minor anhydrite, hematite, rutile) from IB. RL: 655, coords. 61750, 122480.

- 103011 Quartz-chalcopryrite-pyrite vein (minor anhydrite, hematite, rutile) from bG. RL: 655, coords. 61540, 122480.
- 103012 Quartz-chalcopryrite vein (minor anhydrite, hematite, rutile) from PA. RL: 640, coords. 61250, 122440.
- 103013 Quartz-chalcopryrite vein (minor anhydrite, hematite, rutile) from BiG. RL: 625, coords. 61170, 122335.
- 103014 Quartz-chalcopryrite-pyrite-sphalerite vein (minor anhydrite, hematite, molybdenite) from BiG. RL: 625, coords. 61180, 122340.
- 103015 Quartz-chalcopryrite vein (minor hematite) with second fracture filling: quartz-pyrite-chlorite vein from bG. RL: 640, coords. 61480, 122270.
- 103016 Quartz-chalcopryrite vein (minor anhydrite, hematite) from bG. RL: 655, coords. 61500, 122400.
- 103017 Quartz-pyrite vein (minor chalcopryrite, sphalerite, marcasite, hematite) from Diorite. RL: 640, coords. 61820, 122310.
- 103018 Quartz-chalcopryrite vein (minor rutile) from Diorite. RL: 640, coords. 61820, 122310.
- 103019 Quartz-bornite-chalcopryrite vein (minor hematite, greenockite) from PA. RL: surface, coords. 62320, 122430.
- 103020 Quartz-pyrite vein from PA. RL: 760, coords. 62290, 122170.
- 103021 Quartz-pyrite-chalcopryrite vein (minor hematite) from qfP. RL: 625, coords. 61650, 122210.
- 103022 Quartz-chalcopryrite vein (minor hematite, rutile) from bG. RL: 610, coords. 61300, 122180.
- 103023 Quartz-chalcopryrite-bornite breccia filling from PA/IB. RL: 610, coords. 61250, 122200.
- 103024 Quartz-pyrite-chalcopryrite vein (minor anhydrite, hematite) from PA. RL: 610, coords. 61055, 122150.
- 103025 Quartz-chalcopryrite vein (minor hematite) from PA. RL: 72, DDH BVP 142, coords. 60875, 122175.
- 103026 Quartz-chalcopryrite vein (minor anhydrite, hematite, rutile) from PA. 128 m, DDH BVP 140, coords. 60880, 122880.
- 103027 Quartz-pyrite-chalcopryrite vein (minor anhydrite, magnetite) from PA. RL: 595, coords. 61100, 122050.
- 103028 Quartz-chalcopryrite vein (minor anhydrite, hematite, rutile) and second fracture filling: quartz-pyrite vein (minor molybdenite) from PA. RL: 595, coords. 61140, 121900.
- 103029 Quartz-pyrite-chalcopryrite vein (minor rutile, pyrrhotite) from PA. RL: 595, coords. 61450, 121900.

- 103030 Quartz-pyrite-chalcopryrite vein from PA. RL: 610, coords. 61430, 121860.
- 103031 Quartz-chalcopryrite vein (minor anhydrite, hematite) from PA. RL: 640, coords. 61920, 121950.
- 103032 Quartz-pyrite vein from PA. RL: 775, coords. 62280, 121880.
- 103033 Quartz-chalcopryrite vein (minor anhydrite, rutile, hematite, magnetite, molybdenite) from PA. RL: 655, coords. 62000, 121800.
- 103034 Quartz-chalcopryrite-pyrite vein (minor sphalerite, rutile) from PA. RL: 715, coords. 62180, 121760.
- 103035 Quartz-chalcopryrite vein (minor sphalerite) from PA. RL: 775, coords. 62250, 121590.
- 103036 Quartz-chalcopryrite-bornite vein from PA. RL: 655, coords 61770, 122700.
- 103037 Quartz-chalcopryrite vein (minor anhydrite, hematite) from PA. RL: 655, coords. 61630, 121710.
- 103038 Quartz-pyrite-chalcopryrite vein from PA. RL: 655, coords. 61440, 121725.
- 103039 Quartz-pyrite vein from PA. RL: surface, coords. 61040, 121550.
- 103040 Quartz-pyrite vein (minor chalcopryrite, molybdenite) from PA. RL: surface, coords. 61085, 121380.
- 103041 Quartz-pyrite vein from PA. RL: surface, coords. 61500, 121350.
- 103042 Quartz-pyrite-clay vein (minor chalcopryrite, sphalerite, galena) from PA. RL: surface, coords. 60260, 121860.
- 103043 Quartz-pyrite vein from PA. RL: surface, coords. 59120, 121900.
- 103044 Quartz-pyrite vein from PA. RL: surface, coords. 59860, 122800.
- 103045 Quartz-pyrite vein (minor chalcopryrite, molybdenite) from KqD. RL: surface, coords. 61290, 124130.
- 103046 Quartz-pyrite vein from PA. RL: 655, coords. 62180, 121930.
- 103047 Quartz-chalcopryrite-bornite-molybdenite vein (minor anhydrite, hematite) from lqD. RL: 610, coords. 61865, 122045.
- 103048 Quartz heeling brecciated sphalerite (minor pyrite) from PA/bD? RL: ? within the quadrilateral of 103004, 103011, 103022, 103013.
- 103049 Amphibole-plagioclase-magnetite vein (minor quartz, sphene) from PA. RL: 625, coords. 61585, 121970.
- 103466 Discontinuous veinlet from PA. RL: 685, coords. 61935, 121590.

- 103467 Discontinuous chalcopyrite-pyrite veinlet from PA. RL: 595, coords. 61100, 122050.
- 103468 Pyrite-clay-quartz vein from PA. RL: 685, coords. 61770, 121570.
- 103469 Vivianite (minor quartz, pyrite) veinlets from bG. RL: 640, coords. 61500, 122300.
- 103470 Thin pyrite vein with a bleached selvage, from qfP. RL: 655, coords. 61750, 122480.
- 103471 Massive sphalerite-pyrite vein (minor quartz, chalcopyrite) from IB. RL: 655, coords. 61750, 122480.
- 103472 Thin pyrite-chalcopyrite vein (minor quartz) from PA. RL: 655, coords. 62040, 122000.
- 103473 Calcite-sphalerite-pyrite vein (minor chalcopyrite, galena) from argillaceous fault-zone in PA. RL: 655, coords. 61950, 121950.
- 103474 Thick, massive pyrite vein (minor chalcopyrite) from PA near lqD contact. RL: 610, coords. 61870, 121920.
- 103475 Sphalerite-pyrite vein from PA. RL: 685, coords. approx. 61950, 121800.
- 103476 Calcite-pyrite (minor chalcopyrite, sphalerite) vein. RL: surface (creek bed), coords. 61370, 121410.
- 103477 Pyrite-clay vein from PA. RL: 595, coords. 61300, 122000.
- 103478 Vein of pyritohedra in a chloritic matrix, from ?bD. RL: surface, coords. 59700, 122550.
- 103479 Pyrite vein from KqD. RL: surface, coords. 61520, 124300.
- 103480 Sphalerite-pyrite vein from PA. RL: 625, coords. approx. 61250, 122300.
- 103481 Sphalerite-pyrite from PA/bD. RL: ? , coords. within quadrilateral of 103004, 103011, 103022 and 103013.

For descriptions of alteration assemblages with certain of these specimens, see Table 3-2.

Appendix 2

FLUID INCLUSION DATA FROM PANGUNA

A. TYPES I, II and IV

Explanation:

Type I Inclusions predominantly of low to moderate salinity aqueous solution.

Type II Gas-rich inclusions.

Type IV Inclusions with visible liquid CO₂.

x - with a small solid phase, insoluble on heating;

a - the gas appears to be divided in two, probably by a plate-like transparent solid.

T_h = temperature of disappearance of the bubble in type I inclusions, °C, or temperature of disappearance of the liquid rim in type II inclusions (and in a few type I inclusions), °C, or temperature of disappearance of the aqueous liquid-gas meniscus, °C.

T_{hCO_2} = temperature of homogenization of CO₂-rich liquid and CO₂-rich gas °C.

Ø = phase remaining immediately following homogenization at T_h . This is indicated only for inclusions belonging to the QP fluid association (see text), in the following manner:

L = liquid

G = gas

* = supercritical fluid

B = gas, after boiling

T_f = temperature of fusion of ice, °C; in a few cases, possibly the decomposition of other solids.

NO.	Type	T_h, θ	T_f	Other	NO.	Type	T_h, θ	T_f	Other
SPECIMEN 102594					17	1	180	0.4	
1	1	316	-5.5		18	1	177		
2	1	340	-15.8		19	1x	315±5	-4.5±.5	
3	1x	348	-15.5		20	1x		-4.5±.5	
4	1	199±5	-1.7		21	1	322±3		
5	1		-0.5±.5		22	1	304	-5.5±.5	
6	1	193	-0.5±.5		23	11		-12.9	
7	1	291	-1.9		24	1	288	-5.5±.5	
8	1	322			25	1	334±2	-4.2	
9	1	313	-4.2		26	11		-4.4±.7	
10	1	321	-4.2		27	1	341	-4.5	
11	1	327	-3.8		SPECIMEN 102609				
12	1x	163	-0.5±.5		1	1x	156	-0.4	
13	1x		-16.7		2	1	159	-0.9	
14	1	278	-0.6±.6		3	1	359	-2.7±.3	
15	1	284			4	1	274	-18.5	
16	1	251	-5.2		5	1	305	-19.7±1.0	
NO.	Type	T_h, θ	T_f	Other	NO.	Type	T_h, θ	T_f	Other
6	1	360±3	-18.5±.5		7	1	199±5		
7	1	374	-18.5±.5		8	1	225±3	-1.0	
8	1	379	-20.7		9	1	199±5	-0.9	
9	1	346±3			10	1x	232	-0.9	
10	1	353±5			SPECIMEN 102619				
11	1x	243±10	-0.6		1	1	272±5	-0.3±.3	
12	1	226±3	-1.7		2	1	286±2	-0.3±.3	
13	1x	223	-1.7		3	1	274	-0.6	
14	1	276	-9.5±.5		4	1	274	-0.6	
15	1	359	-2.5±.5		5	1	291	-0.2	
SPECIMEN 102612					6	1	315±5	-3.7±.3	
1	1x	199±5	-1.5±.5		7	1	312±5	-3.7	
2	1	214			8	1	310	-3.7	
3	1	209±5	-0.9		9	1	312±3	-8.0±.4	
4	1	214	-1.6		10	1	312±3	-8.5±.5	
5	1	219±5	-0.9		11	1	516	-28.0	
6	1	220	-1.0		12	1		-28.0±.5	
NO.	Type	T_h, θ	T_f	Other	NO.	Type	T_h, θ	T_f	Other
13	1		-28.5±.5		SPECIMEN 102676				
SPECIMEN 102636					1	1	298	-1.8	
-					2	1	330	-1.5	
SPECIMEN 102645					3	1	311	-1.5	
-					4	1	347	-11.0	
SPECIMEN 102651					5	1		-11.0	
-					6	1	307		
SPECIMEN 102658					7	1	307		
-					8	1	308		
SPECIMEN 102661					9	1	316		
-					10	1	318		
SPECIMEN 102662					11	1	318		
-					12	1	320		
SPECIMEN 102666					13	1	324		
-					14	1	326		
SPECIMEN 102668					15	1	331		
-					16	1	332		

NO.	Type	$T_h, ^\circ\text{F}$	T_f	Other	NO.	Type	$T_h, ^\circ\text{F}$	T_f	Other
17	1	338			2	1	358		
18	1	345			3	1	350		
19	1	308 \pm 2	-1.6		4	1	347		
20	1	306 \pm 4	-1.5		5	1	338 \pm 3		
21	1	313	-1.3		6	1	335 \pm 3		
22	1	332	-2.1		7	1	335 \pm 3		
23	1	322			8	1	377		
24	1	329			9	1	332		
25	1	326			10	1	340 \pm 3		
26	1	329			11	1	335 \pm 3		
27	1	334			12	1	354		
28	1	339			13	1		-16.9	
29	1	339			14	1		-2.5	
30	1	346			15	1	380	-9.0	
SPECIMEN 102673					16	1	370		
1	1	205			17	1	353		
SPECIMEN 102997					18	1	363		
1	1	356			19	1	362		

NO.	Type	$T_h, ^\circ\text{F}$	T_f	Other	NO.	Type	$T_h, ^\circ\text{F}$	T_f	Other
20	1	282			2	1		-0.3	
21	1	284			3	1		-0.3	
22	1	290 \pm 2			4	1	227		
23	1	295 \pm 4			5	1	220		
24	1		-9.3		6	1	208 \pm 3	-0.3	
25	1		-9.6 \pm .3		7	1	213 \pm 5	-0.3	
26	1	338			8	1	209 \pm 2	-0.3	
27	1	343 \pm 4			9	1	227	-0.3	
28	1	351			10	1	199 \pm 5	-0.4	
29	1	358			11	1		-2.1	
30	1,0	350 \pm 5	-3.8		12	1	224 \pm 4		
31	1,0	330	-1.0		13	1	224 \pm 4		
32	1	331 \pm 3			14	1	224 \pm 4		
33	1	350 \pm 3			15	1	224 \pm 4		
34	1	359			16	1	224 \pm 4		
SPECIMEN 102998					17	1	250		
1	1		-0.3		18	IV	191 \pm 11		$T_h\text{CO}_2 = 27\pm 1$

NO.	Type	$T_h, ^\circ\text{F}$	T_f	Other	NO.	Type	$T_h, ^\circ\text{F}$	T_f	Other
19	IV,x		-10.3	$T_h\text{CO}_2 = 23.9$	15	1	252 \pm 2		
SPECIMEN 102999					16	1	252 \pm 2		
1	1	275	-1.1		17	1	259		
2	1	270	-1.1		18	1	281		
3	1	302			19	1	283		
4	1	330			SPECIMEN 103000				
5	1	271			"				
6	1	269			SPECIMEN 103001				
7	1	283			"				
8	1	283			SPECIMEN 103002				
9	1	214	0.0		1	1	379		
10	1	292	0.0		2	1	372		
11	1	324			3	1	388		
12	1	228			4	1	366	-10.7	
13	1	321 \pm 3			5	1	334		
14	1	250			6	1		+6.6	
					7	1	325 \pm 3	-6.1	

NO.	Type	$T_h, ^\circ\text{F}$	T_g	Other	NO.	Type	$T_h, ^\circ\text{F}$	T_g	Other
8	1	365			SPECIMEN 103003				
9	1	>400	-19.8		SPECIMEN 103004				
10	1	313	-11.7		1	1		-24.9	
11	1	?	-10.0		2	1		-9.1	
12	1	330	-9.8		3	1	219 \pm 5	-1.3	
13	1	333	-11.4		4	1	182 \pm 3	-1.2	
14	1		-8.0		5	1	209 \pm 5	-1.0	
15	1	321	-1.4		6	1	248		
16	1	333			7	1	264		
17	1	283			8	1	247		
18	1	327			9	1	247		
19	1	335			10	1	251		
20	1	354			11	1	252		
21	1	327 \pm 3			12	1	266 \pm 2		
22		382 \pm 3			13	1	269 \pm 2		
23			-7.8		14	1	269 \pm 2		
24			-8.5		SPECIMEN 103005				
SPECIMEN 103005					7	1	251 \pm 3		
1	1	231	-0.4		8	1	251 \pm 3		
2	1	233 \pm 5	-0.4		9	1	274	-1.4 \pm .2	
3	1	289 \pm 5	-23.5 \pm .5		10	1	277	-1.4 \pm .2	
4	1	230 \pm 3			11	1	263 \pm 2	-1.4 \pm .2	
5	1	262			SPECIMEN 103009				
SPECIMEN 103006					1	1	341	-6.5	
SPECIMEN 103007					2	1	355	-3.8	
SPECIMEN 103008					3	1	340 \pm 10	-7.5 \pm .5	
1	1	242	-0.8		4	1		-5.5	
2	1	233	-1.6 \pm .4		5	1		-21.0	
3	1	275	-1.0 \pm 1		6	1	296		
4	1	240	-1.0 \pm 1		7	11	424 \pm 3		
5	1	233			SPECIMEN 103010				
6	1	251 \pm 3			1	11	364		
SPECIMEN 103011					2	11	371 \pm 3		
4	11	370			3	11	380 \pm 10		
5	11	381 \pm 3			SPECIMEN 103012				
6	11	381 \pm 3			1	1	353	-12.3	
7	11	369			2	1	363	-10.7	
8	11	377 \pm 8			3	1		-10.5 \pm .5	
9	11	371 \pm 3			4	1	336	-4.5 \pm .6	
10	11	347 \pm 3			SPECIMEN 103013				
11	1	254			5	1	176	-0.2	
12	1	260 \pm 3			6	1	182	-1.0 \pm 1	
13	11	397 \pm 5			7	1	161	-1.0 \pm 1	
SPECIMEN 103012					8	1	218	-1.0 \pm 1	
1	1	353	-12.3		9	1	200		
2	1	363	-10.7		10	1	224		
3	1		-10.5 \pm .5		11	1	216	-1.5 \pm 1.5	
4	1	336	-4.5 \pm .6		12	1	185	-1.8	
SPECIMEN 103013					13	1	164 \pm 3		
5	1	176	-0.2		14	1	251	-1.9	
6	1	182	-1.0 \pm 1		15	1	183	-0.3 \pm .2	
7	1	161	-1.0 \pm 1		16	1	193	-0.3 \pm .2	
8	1	218	-1.0 \pm 1		17	1	184	-0.3 \pm .2	
9	1	200			18	1	183 \pm 2	-0.3 \pm .2	
10	1	224			19	1	173	-0.3 \pm .2	
11	1	216	-1.5 \pm 1.5		20	1	185 \pm 1	-0.3 \pm .2	
12	1	185	-1.8		21	1	172	-0.3 \pm .2	
13	1	164 \pm 3			SPECIMEN 103014				
14	1	251	-1.9		SPECIMEN 103015				
15	1	183	-0.3 \pm .2		SPECIMEN 103016				
16	1	193	-0.3 \pm .2		SPECIMEN 103017				
17	1	184	-0.3 \pm .2		SPECIMEN 103018				
18	1	183 \pm 2	-0.3 \pm .2		SPECIMEN 103019				
19	1	173	-0.3 \pm .2		SPECIMEN 103020				
20	1	185 \pm 1	-0.3 \pm .2		SPECIMEN 103021				
21	1	172	-0.3 \pm .2		SPECIMEN 103022				

NO.	Type	$T_h, ^\circ$	T_f	Other
22	11	390 \pm 10		
23	11	375 \pm 5		
24	11	355		

SPECIMEN 103013

SPECIMEN 103014

1	1	263		
2	1	237 \pm 2		
3	1	>200	-8.8	
4	1	175		

Specimen 103015, Vein

1	1	200	-1.9 \pm 1.9	
2	1	299	-8.6	
3	1	240		
4	1	246		
5	1	303 \pm 2		
6	1	317		

NO.	Type	$T_h, ^\circ$	T_f	Other
7	1	319		
8	1		-7.5 \pm 2.5	
9	1	305	-7.5 \pm 2.3	

10	1	309		
11	1	323		
12	1	319 \pm 2	-3.3 \pm .3	
13	1	332	-4.0 \pm 1.0	

14	1	317 \pm 5		
15	1	321 \pm 3		
16	1	311	-3	
17	1	246 \pm 4		
18	1	253		
19	1	260 \pm 3		

SPECIMEN 103015, Phenocryst

1	11	353 \pm 3		
---	----	-------------	--	--

SPECIMEN 103016

NO.	Type	$T_h, ^\circ$	T_f	Other
-----	------	---------------	-------	-------

SPECIMEN 103017

1	1	432 L	-12.3	
2	1	440 L	-12.0	
3	1		-5.5	
4	1	395 L	-5.2	
5	1		-6.9	
6	1	482 L	-6.5	
7	1	409 \pm 2 L		
8	1		-11.5	
9	1		-6.5	
10	1	395 L		
11	1	402 \pm 2 L		
12	1	406 \pm 2 L		
13	1	414 *		
14	1	456 L		
15	1	400 *		
16	1	406 \pm 3 L		

NO.	Type	$T_h, ^\circ$	T_f	Other
-----	------	---------------	-------	-------

17	11	424 G		
18	1	376 *		
19	1	482 \pm 3 L	-15.1	
20	1	403 \pm 2 *	-15.1	
21	1	442 L		
22	11	403 G		
23	1	410 \pm 3 L		
24	1	527 L		
25	1	511 \pm 3 L		
26	1	508 L		
27	1	522 L		
28	1	427 L		
29	1	441 L		
30	1	444 L		
31	1	476 L		
32	1	395 *		
33	1	478 *		

NO.	Type	$T_h, ^\circ$	T_f	Other
-----	------	---------------	-------	-------

34	1	439 L		
35	1	422 L		
36	1	415 L		
37	1	410 L		
38	1	438 L	-13.8	
39	1		-15.0	
40	1		-22.7	
41	1		-12.5	
42	1	396 L		
43	1	398 L	-5.0 \pm 1.0	
44	1	439 L	-5.5	
45	1		-6.1	
46	1	437 L		
47	1	448 L		
48	1	460 L		
49	1	454 G		
50	1	459 L	-16.8	

NO.	Type	$T_h, ^\circ$	T_f	Other
-----	------	---------------	-------	-------

51	1	460 L	-16.8	
52	1	448 L	-16.8	
53	1	457 L		
54	1	372 L		
55	1	395 \pm 2 G		
56	1	405 L		
57	1	405 L		
58	1	404 L		
59	1	421 \pm 3 L		
60	1	440 \pm 3 L		
61	1	387 *		
62	1	449 L	-12.0	
63	1	418 L	-16.4	
64	1	434 \pm 3 L	-15.5	
65	1	430 L	-18.2	
66	11	381 G		
67	11	385 G		

NO.	Type	T _h , °	T _f	Other	NO.	Type	T _h , °	T _f	Other
68	11	396 G			8	1	241±2	-0.6±.2	
69	11	403 G			9	1	167±3	-0.6±.2	
70	11	399 G			10	1	241±2	-0.6±.2	
SPECIMEN 103018					SPECIMEN 103020				
1	1	301			1	1		-18.4	
2	1	308			2	1		-23.3	
3	1	>380	-6.6		3	11	436		
4	1	>380	-4.7		SPECIMEN 103021				
5	1	405 L	-3.9		SPECIMEN 103022				
SPECIMEN 103019					1	1	229	-0.4	
1	1	167±2	-0.4		2	1	229		
2	1	300	-0.8±.2		3	1	231		
3	1	302±3			4	1	238		
4	1	262	-1.2		5	1	249		
5	1	236	-2.7		6	1	158	0.0	
6	1	302			7	1	159	0.0	
7	1	241±2	-0.6±.2						
NO.	Type	T _h , °	T _f	Other	NO.	Type	T _h , °	T _f	Other
8	1	175	0.0		25	1	317±2		
9	1	158±3	0.0		26	1	317±2		
10	1	319			27	1	317±2		
11	1	317			28	1	317±2		
12	1	317			29	1	317±2		
13	1	166	-1.0		30	1	320±2		
14	1	323±2	-1.8		31	1	320±2		
15	1	320	-1.8		SPECIMEN 103023				
16	1	166			1	11	325±1		
17	1	166			2	11	344±1		
18	1	170			3	11	335		
19	1	165			4	11	344±1		
20	1	166			SPECIMEN 103024				
21	1	179			1	1	264		
22	1	309			2	1	287±4	-7.3±.3	
23	1	313			3	1		-7.0	
24	1	317±2			4	1	279	-7.8±.2	
NO.	Type	T _h , °	T _f	Other	NO.	Type	T _h , °	T _f	Other
5	1	261	-7.6		22	1		-2.2	
6	1	296	-7.8		23	1	259±3	-2.3	
7	1	282±5	-7.2±.2		24	1	276	-3.0	
8	1	295	-7.9		25	1	230		
9	1	296			26	1	237	-2.8	
10	1	296			27	1	221	-2.2	
11	1	260			28	1	238±2	-4.8	
12	1	263			29	1	238±2	-4.5±.3	
13	1	277	-3.4±.7		30	1	219	-4.5±.3	
14	1	257±5	-3.4±.7		31	1	236±5	-4.0	
15	1	243	-5.1		32	1	235	-4.9	
16	1	247	-5.2		33	1	236	-4.9	
17	1		-3.1		34	1	241	-5.5±.5	
18	1		-3.0		35	1	273	-4.2	
19	1		-2.5±.5		SPECIMEN 103025				
20	1	225	-2.2		SPECIMEN 103026				
21	1	223			1	11	368		

NO.	Type	T_h , #	T_f	Other	NO.	Type	T_h , #	T_f	Other
2	11	384±4			2	1	281	-3.0	
3	11	385±5			3	1	264	-2.5±.5	
4	11	385±5			4	1	286	-2.5±.5	
5	11	385±5			5	1	287	-2.5±.5	
SPECIMEN 103027					6	1	290	-2.3±.3	
1	1	240	-1.6		7	1	282	-2.5	
2	1	256			8	1	18045	-2.5	
3	1	224	-1.7±.2		9	1	290	-2.3±.3	
4	1	231	-1.7±.2		10	1	290	-2.3±.3	
5	1	224	-1.7		11	1	303		
6	1		199		12	1	282		
7	1	221			13	1	298		
8	1	210	-0.7		14	1	289		
9	1	217	-0.7		15	1	300		
10	11	358±10			16	1	157	-1.0	
SPECIMEN 103028					17	1	282	-2.5	
1	1	228	-3.0		18	1	279		
NO.	Type	T_h , #	T_f	Other	NO.	Type	T_h , #	T_f	Other
19	1		-3.1		16	11	396		
SPECIMEN 103039					17	11	393		
1	1	254	-3.3		18	11	395		
2	1	258			19	11	384±4		
3	1	242			20	11	435±5		
4	1	238±5	-4.4		SPECIMEN 103030				
5	1	255			1	11	378		
6	1	258			2	11	350±10		
7	1	257			3	1x	347±3		
8	1	261			4	1	258±2		
9	11	440±5			5	1	255		
10	11	440±5			6	1	257		
11	11	435±10			7	1	261		
12	11	382±5			8	1	262		
13	11	397±10			9	1	261		
14	11	392±5*			10	1	264		
15	11	382			11	1	276		
NO.	Type	T_h , #	T_f	Other	NO.	Type	T_h , #	T_f	Other
12	1	263			29	11	390		
13	1		-5.5		SPECIMEN 103031				
14	1	244	-4.5±.5		NB. SEE "TYPE III INCLUSIONS" FOR INCLUSIONS WITH $T_f < -25^\circ\text{C}$				
15	1	243			1	1	306		
16	1	242			2	1	302	-12.4	
17	1	236			3	1x	302	-10.9	
18	1	303			4	1	215	-18.7	
19	1	308			5	1	311		
20	1	311			6	1	256±10		
21	1	304			7	1	292	-7.5	
22	11	359			8	1	297	-9.4	
23	11	364±5			9	1	297	-14.2	
24	11x	364±5			10	1	299		
25	11	364±5			11	1	305	-14.3	
26	11	366±3			12	1	308	-21.1	
27	11	383±2			13	1	162		
28	11	378			14	1	203±5		

NO.	Type	T_h, β	T_f	Other	NO.	Type	T_h, β	T_f	Other
SPECIMEN 103032									
1	1x		-5.8		17	1	368 L		
2	1		-4.8±1.5		18	11	380±10 G		
3	1		-12.5±.5		19	11	380±10 G		
4	1	433 L			20	11	380±10 G		
5	1		-19.6		21	11	380±10 G		
6	1	362 L			22	11a	393±2 G		
7	1	366 L			SPECIMEN 103033				
8	1	350 L			1	1	267		
9	1	362 L			2	1	267		
10	1	329±5	-0.2		3	1	265		
11	1	326			4	1	284±5		
12	1	329±5	-0.6±.6		5	1	294		
13	1	330			6	1	272±3		
14	1	329±5			7	1	275		
15	1	334			8	1	277		
16	1	396±1*			9	1	283		
NO.	Type	T_h, β	T_f	Other	NO.	Type	T_h, β	T_f	Other
11	1	279			5	1	387±5	-24.1	
12	1	281	-17.9±.5		4	1		-1.5	
13	1		-15.7		5	1		-25.5	
14	1	273	-15.4		6-19	1	365±3	-1.0±.8	
15	1	262±3	-1.4		SPECIMEN 103035				
16	11	403±5			1	1		-9.2	
17	11	403±5			2	1		-9.7	
18	1x	149	+3.7		5	1		-0.5±.5	
19	1		-16.7		4	1	298		
20	1	151±2	-1.0±1.0		5	1	305		
21	1	148	-1.3		6	1	308		
22	1		-1.4		7	1	313		
23	1		-1.1		8	1	314		
24	1x	250	-4.3		9	1	314		
SPECIMEN 103034									
1	1	370	-17.9		10	1	315		
2	1	363	-1.1		11	1	316		
NO.	Type	T_h, β	T_f	Other	NO.	Type	T_h, β	T_f	Other
13	1	376±3			30	1	217		
14	1	347±3			31	1	227		
15	1	419			32	1	220		
16	1	364			33	1	221		
17	1	386			34	1	214±5		
18	1	221	0.0		35	1	208		
19	1	221±4	-0.2		36	1	216		
20	1	221			37	1	234		
21	1	238±5	-4.9		38	1	240		
22	1	261	-1.8		39	1	254		
23	1	225	-0.3		40	1	254±2		
24	1	224	-0.3		41	1	257		
25	1		-2.9		42	1	259±2		
26	1	309	-8.1		43	1	262		
27	1	229	-7.0		44	1	284		
28	1	308	-13.2		45	1	285		
29	1	221			46	1	296		

NO.	Type	$T_h, ^\circ$	T_f	Other	NO.	Type	$T_h, ^\circ$	T_f	Other
47	1	296			10	1		-5.4	
48	1	301			11	1	303	-1.4	
49	1	302			12	1	306±4	-4.9	
50	1	308			13	1	319	-1.0	
51	1	309			14	1	306±4	-6.5±.5	
52	1	310			SPECIMEN 103037				
53	1	244			1	1		-2.5	
SPECIMEN 103036					2	1		-1.0±.5	
1	1	293	-6.3±.3		3	1	340	-15.5	
2	1	289	-6.5		4	1		-18.7±.3	
3	1	247±5	-6.5±.5		5	1		-15.5	
4	1		-7.0±.5		6	1	341		
5	1		-7.0±.5		7	1	343±2		
6	1		-1.4		8	1	329		
7	1	242	-1.4		9	1	372±5	-7.6, -23.1	
8	1	315	-9.4		10	1		-22.5±.5	
9	1	257	-1.6		11	1	366	-22.5±.5	
NO.	Type	$T_h, ^\circ$	T_f	Other	NO.	Type	$T_h, ^\circ$	T_f	Other
12	1x		-22.5±.5		29	1	no bubble	-1.1	
13	1	332	-6.1, -22.5±.5		SPECIMEN 103038				
14	1	348			1	1	313	-2.1	
15	1	328	-23.2		2	1	359 G		
16	1	349	-22.5±.5		3	1	375 L		
17	1	371±5			4	1	355±5 L		
18	1	404			5	1	373 L		
19	1	418±3			6	1x	440 L	-8.3	
20	1	310			7	1	427 L	-8.3	
21	1	395			8	1	408 "	-7.9	
22	1	311			9	1	359±10 G		
23	1	417			10	1	380 "		
24	1	335	-2.9±.5		11	1	433 L		
25	1	343±5	-5.3		12	1	441 "		
26	1	340			13	1	386 L		
27	1	336±4			14	1	378 L		
28	1	337			15	1	397 L		
NO.	Type	$T_h, ^\circ$	T_f	Other	NO.	Type	$T_h, ^\circ$	T_f	Other
16	1	371±2 L			SPECIMEN 103040				
17	1	410 L			1	11	377 G/*		
18	11	403±5 G			2	1	407 L		
19	11	384±5 G			3	1	384 L		
20	11	381±3 G			4	1	380 "		
21	11	379±10 G			5	1	373 "		
22	11	386±3 G			6	1	370 "		
23	11	384±5 G			7	1	377 G/*		
24	11	460±5 G			8	1	370±3 "		
25	11	343 G			9	11	373±5 G		
26	11	347±3 G			10	11	371±3 "		
SPECIMEN 103039					11	1	382 "		
1	1	361±3 L			12	11	388 G		
2	1	371 L			13	1	370.*/L		
3	1	363±5.8			14	11	376±3 "		
4	1	363±5.8			15	1	385 "		
5	1	363±5.8			16	1	408±2 L		

NO.	Type	$T_h, ^\circ$	T_f	Other	NO.	Type	$T_h, ^\circ$	T_f	Other
17	1	400 L			4	11	372 G		
18	1	385 \pm 3 *			5	11	374 G		
19	1	378 *			6	11	378 G		
20	1	393 \pm 2 L			7	11	327 G		
21	11	388 G			8	11	384 \pm 5 G		
22	11	388 G			9	11	398 \pm 10 G		
23	1	413 \pm 2 L			10	11	417 \pm 10 G		
24	1	392 *			SPECIMEN 103042				
25	1	394 L			1	1	267	-1.2 \pm .4, -15	
26	1	402 *	-27 \pm 3		2	1	276		
27	1	409 *	-25 \pm 5		3	1	295 \pm 2	-1.0 \pm .5	
28	1	403 *			4	1	313	-14.8	
29	1	392 *			5	1	300		
SPECIMEN 103041					6	2	307		
1	1	319			7	1	310		
2	1	383			8	1	317		
3	11		-8.1		9	1	322		
NO.	Type	$T_h, ^\circ$	T_f	Other	NO.	Type	$T_h, ^\circ$	T_f	Other
10	1	323	-0.1		27	1	306		
11	1	321			SPECIMEN 103043				
12	1	310			1	1	267		
13	1	302			2	1	267		
14	1	298			3	1	263		
15	1	290			4	1	244		
16	1	295			5	1	244		
17	1	293			6	1	256	0.0	
18	1	303			7	1	184 \pm 3	0.0	
19	1	304			8	1	261		
20	1	313			9	1	249		
21	1	313			10	1	261 \pm 3		
22	1	324			11	1	281 \pm 2		
23	1	313			12	1	256		
24	1	318			13	1	245		
25	1	305			14	1	242		
26	1	299			15	1	194	-0.3	
NO.	Type	$T_h, ^\circ$	T_f	Other	NO.	Type	$T_h, ^\circ$	T_f	Other
16	1	223	-0.3		7	1	272		
17	1		-0.3		8	1	280		
18	1	186	-0.3		9	1	284		
19	1	250			10	1	288		
20	1	249			11	1	296		
21	1	243 \pm 2			12	1	296		
22	1	243 \pm 2			13	1	323 \pm 2		
23	1	246 \pm 2			14	1	306		
24	1	272			15	1	302		
25	1	271			16	1	312	-24.4	
SPECIMEN 103044					17	1	303	-30.5	
1	1	274			18	1	279 \pm 5	-29.4	
2	1	299	-7.9		19	1	376 \pm 5	-32.0	
3	1	234			20	1	281	-25.0	
4	1	260			21	1	287		
5	1	260			22	1		-28.0	
6	1	272			23	1		-22.8	

NO.	Type	T_h , °	T_f	Other	NO.	Type	T_h , °	T_f	Other
24	1		-12.8		2	11	366±7 °/G		
SPECIMEN 103045					SPECIMEN 103047				
1	1	291±2	-1.2		1	1x	377±2		
2	1	295±3	-1.5		2	1x	382		
3	1	300±3	-1.5		3	1	319		
4	1	298	-2.5		4	1	324		
5	1	278±5			5	1x	399	-12.0	
6	1	317			6	1x	396±2	-11.2	
7	1	366	-17.4		7	1x	390		
8	1	373	-20.8		8		394		
9	1	334±3	-18.5		SPECIMEN 103048				
10	1	375			1	1	244±5	-0.5±.5	
11	1	341±5			2	1	226		
12	1	376			3	1	299	-0.8±.5	
13	1	368±2			4	1	259±5		
SPECIMEN 103046					5	1	311		
1	11	374±5 °			6	1	314		
NO.	Type	T_h , °	T_f	Other	NO.	Type	T_h , °	T_f	Other
7	1	303			7	1	338	-0.2±.2	
8	1	303			8	1	339	-0.9±.9	
9	1	304±3							
10	1	249±5	-1.3						
11	1	258±5	-1.3						
12	1	278							
13	1	201							
14	1	203							
15	1	251							
16	1	321							
SPECIMEN 103049									
1	1	323±5	-0.5±.5						
2	1	323±5	-0.7						
3	1	328±1							
4	1	336	-0.5±.5						
5	1	335							
6	1	331	-0.1±.1						

B. TYPE III INCLUSIONS

No. with asterisk : measurement made with a stage built at the
University of Tasmania.

No. without asterisk : measurement made with Chaixmeca equipment.

$T_{s\text{ KCl}}$ = temperature of disappearance of the KCl crystal on heating,
°C.

$T_{s\text{ NaCl}}$ = temperature of disappearance of the NaCl crystal on heating,
°C.

T_h = temperature of disappearance of the bubble on heating, °C.

Other = (a) temperature of disappearance of a salt x on heating
($T > 20^\circ$)

(b) temperature of fusion of (?) hydrate phases, or salts
precipitated by cooling, during warming ($T < 20^\circ\text{C}$)

<h : for T_h , when $T_h < T_{s\text{ NaCl}}$, but not precisely known

>g : for $T_{s\text{ NaCl}}$, when $T_{s\text{ NaCl}} > T_h$, but not precisely known.

TYPE III INCLUSIONS

NO.	T _g KCl	T _g NaCl	T _h	Other	NO.	T _g KCl	T _g NaCl	T _h	Other
SPECIMEN 102997					16	104±5	411	413	
1	119	>g	436±2		17	113			
		446	<h		18	113	434	>h	522
3		470±3	<h		19		389	>h	
4		464			20		473	>>h	
5		481	493		21		450		
6		469	<h	467	22		394±7	<h	481
7			437		23	111	427	384	<80
8		480	492		24		464	<h	
9		457±3	415±5		25		454	<h	
10		460			26		475	316	558
11		455	449		27		466±2	364	
12		464	<h		28		462	524±5	484±2
13		483	<h		29		465±2	>>h	
14	87±2	356	>>h		30		465±2	>>h	
15	106	434	391±5	>450	31		465		
NO.	T _g KCl	T _g NaCl	T _h	Other	NO.	T _g KCl	T _g NaCl	T _h	Other
32		441	412±3		16		439	>>h	
SPECIMEN 102998					17		457	>>h	118
1		422	>>h		18		477	>>h	104
2		433	>>h		19		436	>>h	
3		441	>>h		20		452±8	>>h	116±3
4		441±3	>>h		21		457	>>h	
5		439±5	>580		SPECIMEN 102999				
6		457	>580		1		408	358±5	
7		435	>580		2			364±5	
8		436	>580		3		438	<h	
9		472	>>h	199	4		458	<h	
10		440	>>h	190, 325	5		465	<h	
11	116		>>h		6		444	<h	
12	109±10	458	>>h		7		477±5	<h	
13		458	>>h	198	8		421±5		
14	114±15	462	476	300	9		400±4		
15		443±2	>>h	174±10	10		427	<h	
NO.	T _g KCl	T _g NaCl	T _h	Other	NO.	T _g KCl	T _g NaCl	T _h	Other
11		468	422±3		5		445	454±3	
12		386	>h		6		431		
13		449	<h		7		503		
14		502	<h		8		480	272	
15		461	>>h		9		486	303	
16		485	<h		10		499	363	
17		480±3	<h		11		472±5	317	
18		453±3	<h		12		483±2		
19		513	<h		13		443±5	299±3	
20		524			14			332±5	
21		521			15			388	
22		528±3			16		493	<322	
SPECIMEN 10300					17		486	377	
1		442	<h		18		493±3	326	
2		442	<h		19		491±5	<h	
3		467			20		492	387	
4		431			21		493±3	355±4	

NO.	T _g KCl	T _g NaCl	T _h	Other	NO.	T _g KCl	T _g NaCl	T _h	Other
22		492			6	197	546	484	
23		478±2			7		559	<h	
24		482±3			8		562	<h	
25		501	386		9		571	<h	
26		463	<h		10	191			
27		424	>h		11	174±3	562	<h	
28		418	<h		12	173			
29			372		13		561	<h	
30		449	370±5		14		563	<h	
31		477±2	370±5		15		572	<h	
32		435	370±5		16		563	<h	
SPECIMEN 103001									
1	>166		518±2	210	17		563	<h	
2		566	515		18		567	<h	
3		358	<h		19		566	<h	
4		569	<h	215	20		562	<h	
5		370	<h	207±2	21		565±3	<h	
NO.	T _g KCl	T _g NaCl	T _h	Other	NO.	T _g KCl	T _g NaCl	T _h	Other
23		569			2		524	<h	
SPECIMEN 103001, Phenocryst 1									
1		474±4	>583	>583	3		461	>h	
2	146	492	>583		4		561	>583	
3		322	>583		5		545±3	>583	
4		504	>583		6		536	>583	
5		519±4	>583		7		525	>583	
6		507	>583		8		533	>583	
7		538	>583		9		536±3	>583	
8		540	>583		SPECIMEN 103001, Phenocryst 3				
9		527	>583		1		532±7	>583	
10		550±3	>583		2	173	532	>583	
11		514	>583		3	153±1	562	>583	
12		526	>583		4		478	>583	
13		532	>583		5		514±2	>583	
SPECIMEN 103001, Phenocryst 2									
1		327	<h		6		517±2	>583	
NO.	T _g KCl	T _g NaCl	T _h	Other	NO.	T _g KCl	T _g NaCl	T _h	Other
9		536	>583		12		470	>580	
10		537	>583		13	134	492	>580	
11		540	>583		14		473	>580	485±4
12		545	>583		15	123±2	474	>580	
13		548	>583		16		473	>580	
SPECIMEN 102676									
1			>580	>580	17		452±3	>580	
2			>580	>580	18		472	>580	
3		409	359		19		464	>580	
4		449	>580		20		474	>580	
5		454±5	>580		21		483	>580	
		466			22		488	>580	
7		469±5	>580		23		526	>580	
8		489	>580		24		439±4		
9		475	>580		25		436		
10		476±2	>580		26		447±2		
11		450	450		27	124±2	457	>580	
					28		475	>580	

NO.	T ₂ KCl	T ₂ NaCl	T _h	Other	NO.	T ₂ KCl	T ₂ NaCl	T _h	Other	Other
29		478	>580		6		506	<h		
30		475	>580		7		538	<h		
31		484±2	>580		8		513			
32		492	>580		9		500	<h		
33		480±2	>580		10		494±4	>>h		
34		507			11		462±5	>>h		
35		503			12		479±3	>>h		
36		492			13		462±5	>>h	467	
37		487	>580		14		485	501±8		
38		492	>580		15		494	430	492±2	
39		496	>580		16		523±2			
		SPECIMEN 102673			17		523	<h		
1		346±5			18		490	460		
2		427±2	537		19		485	>583		
3		338±5	>h		20		466	>583		
4		458	<h		21		476±2	>583		
5		596±2	<h		22		503±7	<h		
NO.	T ₂ KCl	T ₂ NaCl	T _h	Other	NO.	T ₂ KCl	T ₂ NaCl	T _h	Other	Other
23		501	>>h		10		398	<h		
24		473	480±4		11		288	523		
25		429			12		510±3	525		
26		476	537±1		13		519	561		
27*		461			14		530±5	501		
28*		475	281±5		15		519±2	505		
29*		442	281±3		16	116	>388	516±5	94, 329	
		SPECIMEN 103002			17		403±5	<h		
1		203±10	591	-26	18		435	436		
2		206	511		19		360	519	104	
3		340	542±3		20	115	471	>h	107	
4		297	531		21	122	455	555±15	96, 275±25	
5		516±5	527		22		420	570±10		
6		557±4	<h		23		441±5	564±4		
7		557±4	<h		24		415	<h	523	
8		519	<h		25		345	567		
9		556	299		26		419	<h		
NO.	T ₂ KCl	T ₂ NaCl	T _h	Other	NO.	T ₂ KCl	T ₂ NaCl	T _h	Other	Other
		SPECIMEN 103003			17	98±10	518±15	585	593	
1		266±3	433	584	18		539±2			
2		269±5	413		19		550	571	543	
3		271±2	415		20		529	599		
4		269±5	444		21			415±2		
5		287±4			22			417		
6		293	417		23		527±5	>h		
7		320	400		24		580	414		
8		264	598		25		577	578	105, 578	
9	89	528	>>h		26		558	583		
10		527±3	575		27		504			
11		501	>>h		28		560	592±4	540	
12		288	557±15		29		556±5	414		
13	99	541	420				SPECIMEN 103004			
14		500	571		1		529	>580		
15		536	404±4		2		535	>580		
16		518	566		3		516±5	>580		

NO.	T ₃ KCl	T ₃ NaCl	T _h	Other	NO.	T ₃ KCl	T ₃ NaCl	T _h	Other
4		531±2			21	165	518	>580	
5		155	330		22		516		
6		543	<h		23		323		
7		338±3	<h		24		520±2	>h	
8		546			25		545±3	458	
9		538	>580		26		530±2	462	
10		552	<h		27		528	<h	
11		543±2			28		525	488±5	
12		536	>h		29		519	>580	
13		547	>580		30		517	>580	486±3
14		544	>580		31		522±2	>580	
15		536	>580		32		580	<h	
16		535	>580		33		563		
17		531	<h		34		536	>580	
18		532±2	<h		35		539	<h	
19		527	<h		36		515±3	509	
20	167	521	>580		37		538±3	>580	
NO.	T ₃ KCl	T ₃ NaCl	T _h	Other	NO.	T ₃ KCl	T ₃ NaCl	T _h	Other
38		554±3	<h		14		396	>580	
39		539	>580		15		351±3	>580	
40		551	532±5		16		439	>580	
		SPECIMEN	103005		17		473	>580	
1	117	387			18		465±2	>580	
2		474	451		19		467	>580	
3		318	>>h		20		543	482	
4		542	408		21		537	472	
5		513	451		22		532	506	
6		458			23		518	466	
7		497	446±4		24		502	452	
8		463	>580		25		537	503	
9		460±2	498		26		520	470	
10		451	>580		27		534	<h	
11		486	455±3		28	139	509	>580	
12		425	>580		29		494	>580	
13		452	>580		30		518	538	
NO.	T ₃ KCl	T ₃ NaCl	T _h	Other	NO.	T ₃ KCl	T ₃ NaCl	T _h	Other
31		502	>580		3		516	<h	
32		542	447±3		4		497	<h	477
33		502	>580		5	124	?		
34		508	<h		6	122	490	<h	474
35		501	>580		7	93±3	407		447
36		474	250	437	8	123			
37		461	279		9		491	<h	
38		448	<h		10		504	<h	
39				457	11		504	<h	
40	117	471	299		12	139±1	501	489	
41		492	539±5		13	131	484	471	
42		479	430±5		14	109	430	456	
43		457			15	129	476	484	
44		499±3			16		521	447	
		SPECIMEN	103006		17		511	447	
1		481	<h		18	140	510	<h	
2	120	474	<h	474	19	146	523	<h	

NO.	T _s KCl	T _s NaCl	T _h	Other	NO.	T _s KCl	T _s NaCl	T _h	Other
20	96±2	401	435		2	114	469	481	
21		524±1	<h		3		467	>h	
22	140±2	509	483		4		475	452	
23		492	<h		5		516±2	408	
24		494±2	<h		6		468±1		
25		502	<h		7		470	440	
26		544±1	<h		8		516±2	<h	
27		529			Phenocryst 2				
28	111	441			1	141±3	501	>583	
29	96±3	444	406±2		2		512	489	
30	105±3	434	<h		3		520		
31		442	405		4		513	<h	
32		448			5		514	409	
33		436	383		6		480		
34		423±5			SPECIMEN 103007				
Phenocryst 1					1	106	?		
1	136	495	493		2	117	?		
NO.	T _s KCl	T _s NaCl	T _h	Other	NO.	T _s KCl	T _s NaCl	T _h	Other
3		453	<h		20		440		
4		471	<h	>h	21	120±2	429	<h	312±7
5		418	354		22		435±2	287	
6		418	344±10	334	23		438±3	<h	
7		228			24		436	<h	
8		217	535		25		460±5	<h	
9		233	514		26		458	298±6	
10		230±5			27	114	426	<h	
11		244			28	123	433±5	<h	
12		229±4			29	120	432	<h	
13		249			30		422±4	<h	
14		233			31		443	<h	
15		215			32		448	<h	
16		242			SPECIMEN 103008				
17	<h		541		1		349	375±5	
18		416	<h		2		297	375±5	
19		421			3		464	<h	
NO.	T _s KCl	T _s NaCl	T _h	Other	NO.	T _s KCl	T _s NaCl	T _h	Other
4		342±3	>h		4		411	377±8	
5		307±3	363		5		410±5	377±8	
6		271	>h		6		404	377±8	
7		310±3			7		419	377±8	
8		283	<h		8		403±5	<h	316±5
9		487	383±5		9		383	320±10	260±20
SPECIMEN 102651					10				258±5
1*		289	485±10		11		442	<h	
2*		301±7	485±10		12		461±5	<h	
3*		409	363		13		494	<h	
4*		451	395		14		459±3	454	
5*		451			15		504	<h	
6*		455	327		16		443	<h	
SPECIMEN 103009					17		482±5	<h	
1	121±3	433	377±8		18		484	<h	
2	124	424	377±8		19		494	<h	
3	118	403	377±8		20		476		

NO.	T _g KCl	T _g NaCl	T _h	Other	NO.	T _g KCl	T _g NaCl	T _h	Other
21		469±5			38		482	310±20	
22		407	<h		39		476	328	
23		423±3	<h		40		403±5	403±5	
24		436	<h		41			388	
25		444	<h				SPECIMEN	103110	
26		450	<h		1		258±5	>h	
27		468	<h		2		326±5	360±10	
28		480	<h		3		326±5	<h	
29		485	340	182	4		407	<h	
30		485	311±10		5		456	<h	
31		523	311±10	189	6		464	<h	
32		453±3	339		7		371	360±10	
33		451	311±10	189	8		356	305	
34		450	301		9			278±15	
35		448	299		10		362	>h	
36		469	337±8		11		395±3	442	
37		433	358						
NO.	T _g KCl	T _g NaCl	T _h	Other	NO.	T _g KCl	T _g NaCl	T _h	Other
		SPECIMEN	103011		17		389±8		
1		466	456±5	126±8	18		462	445	
2	114±5	480	434	134, 327, >584	19		466		196, >583
3	110	501±2	<h		20	119	501		
4	114±4	482	462		21		463±2	456	
5		534	<h	462±5	22		460	>583	175±4
6		563	<h		23		472	>583	181±9
7		481	>583		24		460		
8		491±5			25		472		
9		575	<h		26		>583	<h	247
10		450	<h		27		578	<h	
11		433±5	>h		28		517	<h	
12		474	475		29		572	<h	134±3
13		460	<h		30		509		
14		478					SPECIMEN	103012	
15		475			1		493±5	>580	>580
16		438	371±11		2	171	493	>580	547
NO.	T _g KCl	T _g NaCl	T _h	Other	NO.	T _g KCl	T _g NaCl	T _h	Other
3		500±3	>580		20		469	<h	
4	169	501	>580		21		514	451	
5		501	>580		22	142	459	522	
6	178	504	>580		23		537	>580	
7		485±3	>580	551±5	24		464		
8		489	>580	>580	25		486		
9		508	<h				SPECIMEN	103013	
10		476	<h		1		517	<h	>560
11		538			2		516		>560
12		517±5			3		489±5	432±15	>560
13		533±3	428±7		4		529	393±3	>560
14		519±3			5		531±2	<h	>560
15		520±2	<h		6		544	423	>560
16		537	<h		7		503	<h	>560
17		542			8		501	>560	
18		479	<h		9		496	391	
19		454	<h		10		499		

NO.	T _g KCl	T _g NaCl	T _h	Others	NO.	T _g KCl	T _g NaCl	T _h	Other
11		501	<h		2		520	<h	>583
12		505	<h		3		506±3	<h	
13		509	<h		4	148	515	<h	>583
14	123±5	489	>580		5		516±1	<h	>583
15	133	490	>h		6		520	<h	>583
16		490±5	>h		7		500±4	<h	>583
17		498	>580		8		515	<h	>583
18		500	>580		9		517±3	<h	>583
19		504	>580		10		499	<h	
20		300	>580		11		519	<h	
21		495	>580	>540	12		520	<h	
22		476	340±10		13		508±3	<h	
23		510	340±10	519±5	14		507	<h	
24		491	<h	526	15		515	<h	
25		519±5	340±10	539	16		509	<h	
		SPECIMEN 103014			17		533	<h	
1		497	<h	>583	18		539	<h	

NO.	T _g KCl	T _g NaCl	T _h	Other	NO.	T _g KCl	T _g NaCl	T _h	Other
19		541	<h		5	123±5			
20		544	<h		6		466	>580	
21		532	<h				SPECIMEN 103015, Phenocryst 1		
22		535	<h		1		441	>580	304
23		538	<h		2		425	>580	
24		539	<h		3	106			
25		543	<h		4	95			113, 291
26		559±5	<h		5		403	>580	
		SPECIMEN 102645			6		401±3	>580	
1*		437	259±4				SPECIMEN 103016, Vein		
2*		433	280±6		1		414	>h	
3*		433±5	280±6		2	117	449	>583	>583
		SPECIMEN 103015, Vein			3		569	>583	
1	122±2	502	>580		4		262	240±5	
2	136				5		235	244±5	
5		469±2	>580		6		429		
4		470	>580		7		401		

NO.	T _g KCl	T _g NaCl	T _h	Other	NO.	T _g KCl	T _g NaCl	T _h	Other
8		416			2		489	434	199
9	117	450	>580		3		487		220, 307±15
10	114	457	>580		4		438		207
11		457	>580		5		445		210
12		480	<h		6		471	>h	
13		486	<h		7		467	>h	
14		474	>h		8		481	<h	
15	117	482	423±5		9		430±2		
16		465	<h		10		474	>h	
17		430	438		11		456	<h	
18		422			12		449	>>h	
19		476	<h		13		470	>>h	
20		454±3	401±6				SPECIMEN 103016, Phenocryst 2		
21		468	<h		1	160	521		>583
22		462	<h		2		505		193
		SPECIMEN 103016, Phenocryst 1			3		397		137±5
1		444							

NO.	T _s KCl	T _s NaCl	T _h	Other	NO.	T _s KCl	T _s NaCl	T _h	Other
		SPECIMEN	103017		17		362	427	
1		391±2	343±2		18		370	412±4	
2		391±2	357		19		365±3	375±3	
3		<g	379		20		290	257	
4		390	339		21		372	391±2	
5			343±2		22		335±5	384	
6		387	<h		23		503		
7		373±3	340		24		514	388	
8		284	273±10		25		513	<h	
9		312±4	296±4		26		529	<h	
10		278±3	371		27		495	<h	
11		374±4	<h		28		470±5	490±5	
12		413	<h		29		300	335	
13		350	380		30		283	333	
14		331	>h		31		287±5	331	
15		330	<h		32		290±3	349	
16		<g	428		33		274	349	
NO.	T _s KCl	T _s NaCl	T _h	Other	NO.	T _s KCl	T _s NaCl	T _h	Other
34		292	350±5		6		470	<h	
35		<g	330		7		443	<h	
36		290	335±4		8		329	370	
37		317±5	346		9		393±3	<h	
38			336		10		408	395±3	
39			336		11		436	347±8	
40			349		12		423	>h	
41		298±3			13		458	<h	
42			331		14		447	321±3	
43			332		15		455	321±3	
44			336		16		433	<h	
		SPECIMEN	103018		17		395±3	<h	
1		462	337±3		18		212	>h	3±1
2		432	336		19	105	384	449	
3		433±3	340		20		460	>h	>h
4			335		21		422±12		
5		376	<h		22		382±3		
NO.	T _s KCl	T _s NaCl	T _h	Other	NO.	T _s KCl	T _s NaCl	T _h	Other
23		450	436±10		2	108	460	423	
24		414	393±5		3		427	>h	
25		440±3	<h		4	103	420	>>h	
26		434	421±4		5		403	>>h	
27		548	<h		6		458	<h	
28		540	<h		7		440	>580	
29		460	<h		8		462	486±5	
30				2	9		382±5	>580	
		SPECIMEN	102658		10		474	<h	
1*		424	30±x2		11		415±2	>580	
2*		423	296±3		12		481	>h	
3*		422	304±5		13		508	>h	
4*		363	361±4		14		469	441	
5*		439	308±3		15		474	<h	
6*		442	308±3		16		483	<h	
		SPECIMEN	103019		17		506	<h	
1	123	486	373		18		431	<h	

NO.	T _s KCl	T _s NaCl	T _h	Other	NO.	T _s KCl	T _s NaCl	T _h	Other
19		408±3	>>h		36		451	<h	
20		406	>>h		37		466±2	<h	
21		421±5	<h		38		459	>>h	
22		473	<h		39		475		
23		474	<h		40		462	<h	
24		460	<h		41		515		
25	132	522	460±5				SPECIMEN 102661		
26	134±2	490	483		1		435	<h	
27		461±3	422		2		457	<h	
28		462	421±5		3	118	437	415	
29		472	474±2		4	116	458	415	
30		461±3	456		5		459	<h	
31		461±3	432		6		459	<h	
32		482±2	<h		7		460	<h	
33		526	<h		8		460	<h	
34		475	<h		9		461	<h	
35		477	<h		10		461	<h	
NO.	T _s KCl	T _s NaCl	T _h	Other	NO.	T _s KCl	T _s NaCl	T _h	Other
11		462	<h		28		364		
12		462	<h		29		393±2	437±2	
13		463	419		30		405	<h	
14		464	<h		31		451±2	416	
15		464	<h				SPECIMEN 103021, Vein		
16		465	<h		1		358	478	
17		465	<h		2		357	445	
18		465	<h		3		360	315	
19		465	<h		4		352±4	418	
20		465	<h		5		302	>>h	
21		467	<h		6		273±10	>>h	
22		468	<h		7		386	447	
23		469	<h		8		321	525	
24		469	<h		9		457	>583	
25		470	<h		10		563	>583	
26		471	<h		11		569	>583	
27		475	<h		12		358±3	486	
NO.	T _s KCl	T _s NaCl	T _h	Other	NO.	T _s KCl	T _s NaCl	T _h	Other
13		380			2		411	<h	
14			540		3		543	<h	
15		365±5			4		521	>580	
		SPECIMEN 103021, Phenocryst			5		524		
1		412	355±4		6		539	<h	
2		468	<h		7		540	<h	
3		401	386		8		550	>580	
4		410	383		9		569	531	
5		388±4			10		556	487±5	
6		371			11		568	<h	
7		344	<h		12		>572	448	
8		474			13		571	471	
9		421	470		14		557	466	578
10		482	397		15		>>580	<h	
11		471±4			16		558	465±4	
		SPECIMEN 103022			17		552±2	<h	
1	170	543	546	515	18		530	<h	

NO.	T _g KCl	T _g NaCl	T _h	Other	NO.	T _g KCl	T _g NaCl	T _h	Other
19		548	<h		2		432	>>h	
20		538	465±4		3		435±3	>h	
21		549	<h		4		430±3	429	
22		544	472		5		437		
23		562±2	<h		6		446		
24	192±2	538	<h		7		429±5	427	
25	193	558	<h		8		431		
26	183	568	<h		9		409		
27	182±7	>572	485	521	10		463	>591	>591
28	185	548	472	534	11		452		
29	148±3				12		444±5		
30	168	542	486	517	13		425±2	>591	>591
31	177				14		481		>591
32	140				15		457	>591	
33		545	<h	538	16		461±2	>591	
		SPECIMEN	103023				SPECIMEN	103024	
1	131						>g	440±5	

NO.	T _g KCl	T _g NaCl	T _h	Other	NO.	T _g KCl	T _g NaCl	T _h	Other
2		349±5	>580		18		418±2	<h	
3		344	537				SPECIMEN	103025	
4		347±4	537±5		1		381	569	
5		356±4	>580		2		381	>583	
6		335	>h		3		377	>583	
7		356±5	434		4		339	>583	
8		352	416		5			514±3	
9		369			6		415	495±8	
10		408±8	<h		7			483	
11		398	387		8		397	>583	
12		418±2	<h		9		394	>583	
13		407±4	<h		10		381±2	>583	
14		373±5	>580		11		367	568±2	
15		403	484±4		12		368	501	
16		399	<h		13		375	>h	
17		418±2	>h		14		388	>583	
18		374	<h						

NO.	T _g KCl	T _g NaCl	T _h	Other	NO.	T _g KCl	T _g NaCl	T _h	Other
		SPECIMEN	103026		17		211	>583	
1		237	443		18		247	496±5	
2		324±3	393		19		238	555	
3		342	404		20		227	>583	
4		<g	434		21		263	416	
5		282	437		22		269±2	447	
6			355±4		23		216	>583	
7		341			24		233	525	
8		297	382		25		<g	538	
9		320	430±3				SPECIMEN	103027	
10		288±5	407		1		521	426	
11		416	380		2		474		
12		335	>h		3		462	332	
13		292			4		485		
14		302			5		230		
15		251	394		6		492	415	>543
16		265	409		7		492	414	

NO.	T _s KCl	T _s NaCl	T _h	Other	NO.	T _s KCl	T _s NaCl	T _h	Other
8		490±2			4		281±2	>h	
9		486			5		305	413±3	
10		501			6		329	>h	
11		507	465		7		294	>h	
12		517			8		304	>h	
13		491	434		9		383±2	>h	
14		482	411±3		10		394	<h	
15		474±2	416±3		11		317	>h	
16		473	416		12		342±2	374	
17		476			13		366		
18		469	<h		14		308	420±4	
19		489	<h		15		286±5	376	
20		491	<h		16		314±5		
		SPECIMEN	103028		17		329	<h	
1		364			18		265		
2		299	403		19		300	396	
3		281±2	>h		20		284±3		
NO.	T _s KCl	T _s NaCl	T _h	Other	NO.	T _s KCl	T _s NaCl	T _h	Other
21		270			9		491±5	368	
22		247±5	>>h		10		486		
23		310	>h		11	78	449	382±5	
24		534±5	360±2		12		484	<h	
25		288±3	<h		13		505±2	<h	
26		287	249		14		505±2	<h	
27		289	230±3		15		439	<h	
28		302±2	306		16		372	<h	
		SPECIMEN	103029		17		444±5		
1		359	>580		18		384	<h	
2			436		19		361±3		
3		345	473		20		370±2	>h	
4		325	>580		21		313	386	
5	85±3	463	386	>>h	22		338±5	376	
6	93±5	448	<h	>>h	23		317±4		
7		494±6	<h		24		292	399	
8		510±3			25		370	>h	
NO.	T _s KCl	T _s NaCl	T _h	Other	NO.	T _s KCl	T _s NaCl	T _h	Other
26		405	>h		9		490		
27		293±3	450		10		491		
28		416			11		493		
29		392	>h		12		498		
30		467±4	>h		13		500±2		
31		445	>h		14		483		
		SPECIMEN	103030		15		488	>583	
		SPECIMEN	102636		16		491±5	>583	
1	114±5	493	495±2	210, 423	17		505	>583	
2	109	475	>h		18		501±5	>583	
3		506	<h		19		501±5	>583	
4		509	<h		20		507±3	>583	
5		499			21		507±3	>583	
6		470	<h		22		507±3	>583	
7		472	444		23		512	>583	
8		501			24		483		
					25		487		

NO.	T _g KCl	T _g NaCl	T _h	Other	NO.	T _g KCl	T _g NaCl	T _h	Other
26		477					SPECIMEN 1025W4		
27		483			1	81			
28		481			2	89			
29		441			3	88	410	465	
30		464			4		398±3	>h	536
31		479			5		449	423±5	
32		489			6		466	485±2	
33		462±1			7		410	>h	
34		475±3			8		412	458	
35		489			9		451	428	
36		460			10		495		
37		479			11		394		
38		464			12		390	453	
39		471			13		398±3	486	
40		446			14		463±4	424	
41		464			15		409	496±3	
42		468			16		458±4		
NO.	T _g KCl	T _g NaCl	T _h	Other	NO.	T _g KCl	T _g NaCl	T _h	Other
17		469±5			34		418±3	395	
18		369	>h		35		337±8	>h	
19		500	502		36		380	>h	
20		398±3	461		37		372±3	390	
21	101	385			38		437	421	
22	93	407			39		439	>>h	
23		463±3	376±10		40		465	<h	
24		395					SPECIMEN 102609		
25		472			1		152		
26		468	376		2		433	>>h	
27		468			3		440±5	>h	
28		390±3	449±2		4		404	>h	
29		405	>>h		5		470	<h	
30		495	361		6		432	>h	
31		459±4	<h		7		426±4	510±3	
32	106	433	400±3		8		444	>h	
33	101	423	405±3		9		376	>h	
NO.	T _g KCl	T _g NaCl	T _h	Other	NO.	T _g KCl	T _g NaCl	T _h	Other
10		403	398±6		27		467±4		
11		392	>h		28		466	422	
12		418	<h		29		457		
13		381	<h		30		454		
14		433±3	313±4		31		454		
15		397			32		393	<h	
16	118	436	388±7		33		479	428±2	
17		446	<h		34		439	<h	
18		469	371		35		459	<h	
19		381	>>h		36		457±2	<h	
20		476	<h		37		452	<h	
21		448±2	346		38		451	<h	
22		411	>>h		39		322	>h	
23		432	>h		40		425	357	
24		393	469±3				SPECIMEN 102612		
25		436±5	<h		1		419	>h	
26		424±2			2		448	>h	

NO.	T _s KCl	T _s NaCl	T _h	Other	NO.	T _s KCl	T _s NaCl	T _h	Other
68		-	350	-44	85		117	346	-42
69		-		-44	86			346	-42
70		-	346	-42, -0	87			346	-29
71		-	346	-42	88			346	-40
72		95	346	-35	89		245	>h	-7.8
73			346	-43			SPECIMEN 103032		
74		115	345	-34	1		253	344±5	
75			348	-31	2		294±3	361	
76			333	-41	3		355	368	
77			348	-37	4		280±3	355±5	
78			350	-41	5		239±5	>h	
79			347	-37	6		277	357	
80			347	-40	7		277	346±5	
81				-30, 13±2	8		262	358	
82		139	303	-42	9		232±3	363	
83		117	335	-30, 3±3	10		269±5	>h	
84		95	346	-42	11		280±3	362±2	
NO.	T _s KCl	T _s NaCl	T _h	Other	NO.	T _s KCl	T _s NaCl	T _h	Other
1-25*		SPECIMEN 102662			15		411±5	345±5	
		426±10	320±15		16		442	<h	
		SPECIMEN 103033			17		404±3	385	
1	130	435	408±5		18		388±5	468±3	
2		457	410±10	329	19	115	431	392±3	268
3	115	426	388±2	295±3	20	104	393	424	
4		398	458		21	102±3	380	384	
5		449	<h		22	97	368	>h	
6		422	386		23	115	432		319
7		341	435		24	111	453	390	335
8		403	384±5		25		435	<h	
9		357	>h		26		384±5	390±3	
10		414±3	<h		27		413±5	<h	
11		408	407		28		437	350	
12	130	418±2	366		29		461		
13			372		30		435	429±3	
14			380		31		453±3		
NO.	T _s KCl	T _s NaCl	T _h	Other	NO.	T _s KCl	T _s NaCl	T _h	Other
32		461					SPECIMEN 103035		
33		372	374		1	67±2	380	429	
34		362	364		2	94	367	373±6	
35		330	393		3		429		
36			378		4		397		
37		306±8	383		5		391±3		414±5
		SPECIMEN 102668			6		405	412	
1*		418			7		382	>>h	
2*		418	330±2		8		417	<h	
5*		425	357±5		9		396	<h	
		SPECIMEN 103034			10		397	<h	
1		295±5			11		396	<h	
2		279±5	372		12		406	<h	
3		268±5	401		13		387	345±5	
4		255			14		312	<h	
5		438	286±3		15		370	>h	
6		394±3	<h		16		369	>h	

NO.	T _s KCl	T _s NaCl	T _h	Other	NO.	T _s KCl	T _s NaCl	T _h	Other
17		384	337±3		2*		354	369	
18		393	391±2		3*		433	488	
19		385	412		4*		406	398±5	
20		383	430		5*		404	398±5	
21		382±3	424		6*		432	398±5	
22		412±5	429		7*		433	396±5	
23		417	422		8*		411		
24		413							
25		419	405						
26		397±2	412±5						
27			456						
28		412	431						
29		381	<h						
30		403	412±5						
31		414							
			SPECIMEN 102666						
1*		393	419						

NO.	T _s KCl	T _s NaCl	T _h	Other	NO.	T _s KCl	T _s NaCl	T _h	Other
10		191	>h		8	108	425±4	367	
11		165	>h		9		358	373	
12		167±3	442		10		371±3	>>h	
13		262	>>h		11	121±4	480	<h	
14		387±3	<h		12		410		
15		390			13		389	359	
16		395	360±5		14		432±2	338	
17		411±2	<h		15		385	368	
18		340	411±2		16		429	339	
			SPECIMEN 103057		17		410	398	
1	91	354	293		18		170	329	-9.8±.2
2		353	296		19		164	327	-1±1
3		418	<h		20	89	388	433	
4		356	305±10		21	75	404	436±2	
5		348	391		22			388	
6		367	>>h		23		396	<h	
7		387	<h		24		435	<h	

NO.	T _s KCl	T _s NaCl	T _h	Other	NO.	T _s KCl	T _s NaCl	T _h	Other
25		366±3	370						
26		424	372						
27		381	<h						
28		408	454						
29		412	>h						
30		388	401±5						
31		392	>h						
32		362	408						
33		372	>>h						
34		415	410	163					
35		389	436						
36		375	>>h						
37		341							
38		351							
39		445							
40		449							
41		300	453						

NO.	T _g KCl	T _g NaCl	T _h	Other	NO.	T _g KCl	T _g NaCl	T _h	Other
		SPECIMEN 103042			7		507	<h	
					8	128	506	438	
		SPECIMEN 103043			9	120±2	294	314	
					10		358		
		SPECIMEN 103044			11		363	298	
					12		334	381	
		SPECIMEN 103045			13		374	316	
					14		335	<h	
		SPECIMEN 103046			15		499	>580	
					16		496	>580	
		SPECIMEN 103047			17		486	<h	
1	155	490	>580	477	18		483	365	498
2	149	510	>580		19		507	375±5	>h
3		498±4	>580		20		476	<h	
4			>580		21		475	<h	
5	124±3	495	>580		22		472±5	365	
6	130±1	487	>580		23		506	<h	500

NO.	T _g KCl	T _g NaCl	T _h	Other	NO.	T _g KCl	T _g NaCl	T _h	Other
24		492±6	<h		10		328±5	<h	
25		497±3	<h		11		415	321	
26	105	451			12		399±10	247	
27	105	428	<h	433±5	13		427±5	298	
28		423±5							

SPECIMEN 103048

SPECIMEN 103049

1		>g	286	
2		366	296±3	
3		387	320	
4		>g	320	
5		356±9	550	
6			322	
7			335	
8		249±5	270	
9		34~	276	

High T_h values of type III inclusions, measured on a Leitz 1350° stage. (Many of the same inclusions were studied on a Chaimeca stage, and accurate salinity results typical of the same groups of inclusions are given earlier in the table).

SPECIMEN 102998

a		?	610±23	
b		?	745±25	
c		?	795	
d		?	675±5	
e		?	675±5	
f		?	800	

SPECIMEN 102676

a		695±15	767±3	
---	--	--------	-------	--

NO.	T _g KCl	T _g NaCl	T _h	Other	NO.	T _g KCl	T _g NaCl	T _h	Other
b			767±3		s			690	
c			792±3		t			730	
d			710±5		u			712±3	
e		695±15	752±3		v		452±13	745±5	
f			750±3		w			715±5	
g			717±3		x			595	
h			793±12		y			750	
i			787±3		z			630	
j			645		aa			675	
k		460±30	630±5		B		475±25	705±5	
l			672±5		Y			700	
m			723±8		d		<g	670	
n			647±3						
c		?	742±3						
p			682±8						
q			745±5						
r			750						

SPECIMEN 103051

a			692±8	
b			635±5	
c		<500°C	685±10	
d			730±5	

NO.	T_g KCl	T_g NaCl	T_h	Other
e			690±5	
f			617±8	
g		<500°C	625±5	
h			622±3	
i			610	
j			692±8	

Appendix 3

A RECONNAISSANCE FLUID INCLUSION AND SULPHUR ISOTOPE STUDY OF THE
FRIEDA PORPHYRY COPPER PROSPECT, PAPUA NEW GUINEA

INTRODUCTION

The Frieda prospect is in the West Sepik Province of Papua New Guinea, about 50 km NNE of Telefomin at Latitude $4^{\circ}41'S$, Longitude $141^{\circ}45'E$ (fig. A1). Access is by company aircraft from Madang, approximately 300 km east. The prospect is in the densely forested, sparsely populated and rugged ranges south of the Sepik trough. Despite the physical obstacles, an intensive programme of mapping and some preliminary diamond drilling were carried out before 1974 by the Carpentaria Exploration Company. The work continues under the auspices of Frieda Exploration Pty Ltd, a consortium of Japanese companies and Carpentaria Exploration.

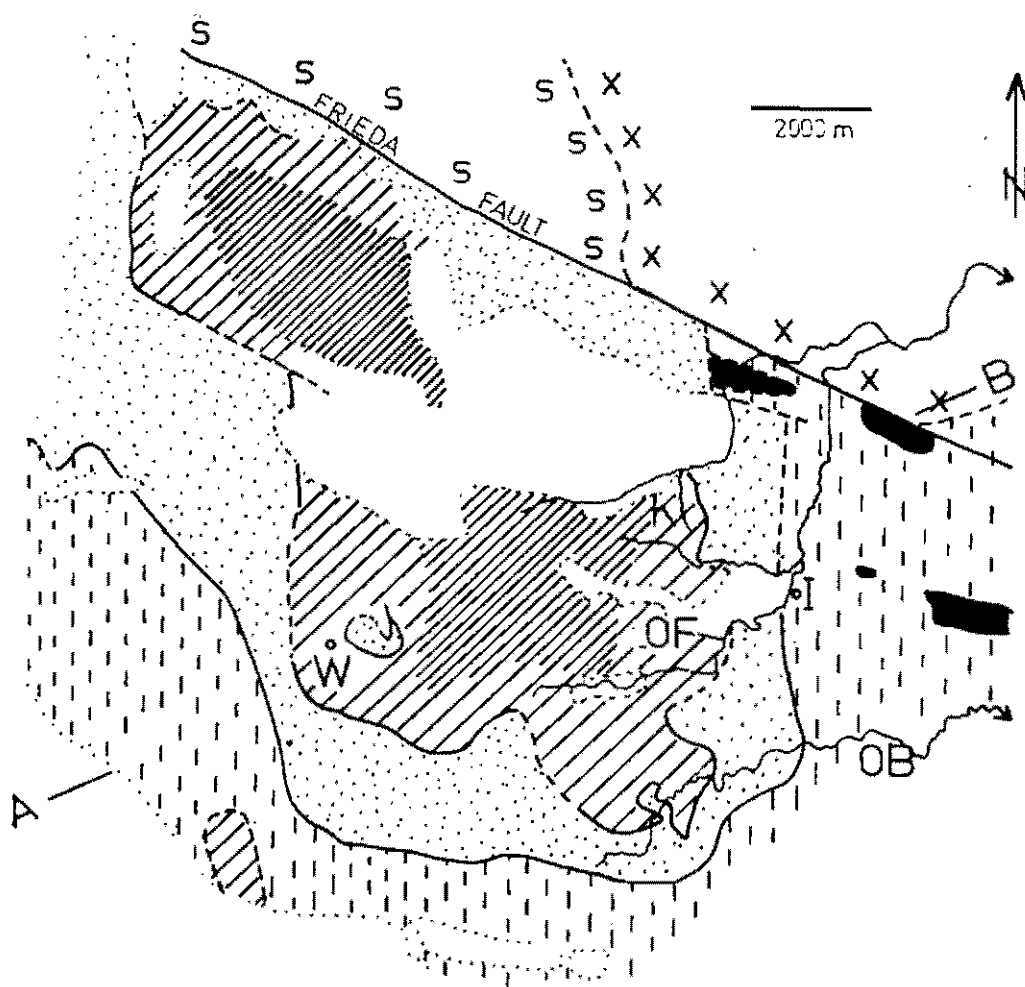
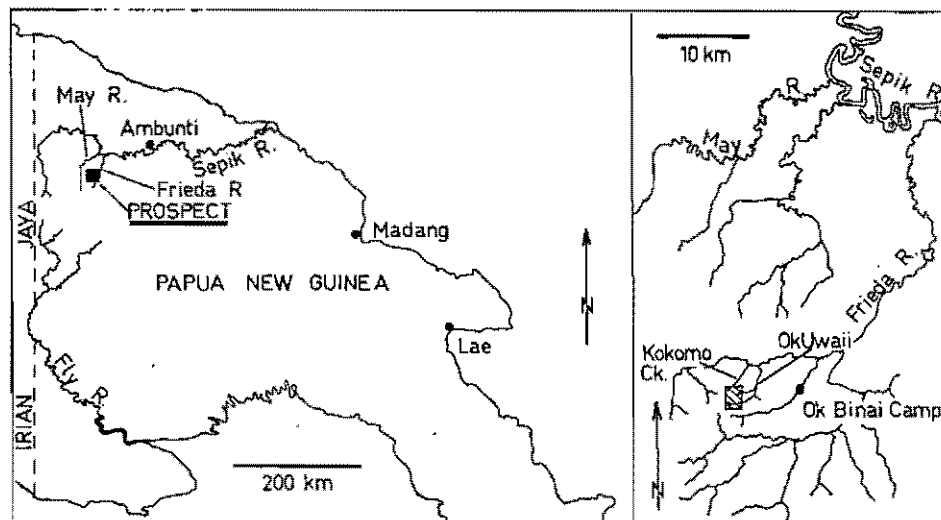
Scope of the study. The author visited the prospect in December 1974 and collected samples for fluid inclusion, sulphur isotope and general geological study. The samples were taken mostly from diamond drill core, and a few were obtained from outcrop or from float in stream beds. A study using these methods, (those employed at Panguna) could not rise above the level of a reconnaissance, given the difficulty of sampling and lack of exposure at Frieda. Alone, the study would have been of much less value than the Panguna study. Much is added to the Frieda study, however, by comparing the findings with analogous results from Panguna where a broader understanding was possible. It is recommended that the reader do so in order to make the most of the few data presented here.

Fig. A-1 Locality maps.

Fig. A-2 Geological map and section of the Frieda Intrusive Complex.
(mapping by company geologists). The letters signify the
following:

A-B	cross section
I	Iwaitaman (Top Camp)
K	Koki Creek
OB	Ok Binai
OF	Ok Flintem
W	Wisliadebom

Blank areas in the Frieda Intrusive Complex are obscured by
recent deposits.



- | | |
|--------------------|---|
| [X] Nena Diorite | [Heavy Hatching] Frieda Intrusive Complex * |
| [S] Ambunti metam. | [Dotted] Wogamush Beds |
| [I] Salumei metam. | [Solid Black] April Ultramafics |

* heavy hatching = alunitic alteration

Acknowledgements. During the visit to the prospect, the author was helped generously in many ways by Frieda Exploration Pty Ltd. He wishes to thank the regional manager, Mr. George Hirata, and the Chief Geologist of the Carpentaria Exploration Company, Mr. Keith Holmes, for their assistance. In particular, the author is most grateful to Mr. Peter Simpson, a Carpentaria Geologist, who introduced him to the geology of the prospect, shared a wealth of interesting information on the local people and geography and provided a very warm welcome in Madang.

A note on geographic nomenclature. The name of the prospect derives from its proximity to the Frieda River, presumably a name of German origin. Current usage for the immediate area of the prospect reflects the various present cultural influences, e.g. Koki, Kumul and Kokomo Creeks from Melanesian Pidgin; Horse, Storm and Peeache (pH) Creeks from English (scientific and otherwise), and many original names from the language of the Telefomin people on whose land the prospect is situated. In the last case, "Ok" means water or stream (as Ok Flimtem) and "Debom" mountain (as Wisliadebom). In 1974, Japanese influence was making an appearance among the names of helicopter landing pads.

REGIONAL GEOLOGY

Sedimentation and igneous activity in the Mesozoic and Tertiary have resulted in the following major units. The descriptions are summarised from Hall & Simpson (1975); see fig. A-2.

The Salumei Formation. This is known in the Frieda area as the Salumei Metamorphics. Slate, phyllite, sericite schist, marble, altered mafic and intermediate volcanics, feldspathic sandstones and greywackes make up the formation, which has been strongly deformed, and

no bedding has been observed. Intrusions have not affected the trend of the regional foliation.

The Wogamush Beds. This sequence of sandstones and subgreywackes is younger than the Salumei Metamorphics, and is represented in the immediate vicinity of the prospect by a hornfelsed shale.

The April Ultramafics. These are rare in the vicinity of the prospect, but more common near Ok Binai. They consist of variably serpentinitised peridotites, pyroxenites and dunites.

The Frieda Complex. This is a fault-truncated, elliptical body of intrusive and extrusive calc-alkaline rocks, 18 km by 4 km. The complex has a concentric structure, the centre consisting of volcanic hornblende andesite which has been subjected to strong alunite-pyrite alteration, possibly as a result of permeation by sulphurous volcanic emanations. The margins of the complex consist of intrusive diorites and andesites of which thirteen varieties have been mapped. The intrusives enclose remnants of metasediments and volcanics. The precise form of the intrusions has not been established; Lacy (pers. comm. to C.E.C.) has suggested three possibilities - a ring dyke, a cone sheet or a central stock with a system of sills. The intrusive rocks have been dated at 13-15 m.y. (Page & McDougall, 1972). The whole complex suggests a volcanic centre, subsequently intruded. Small plutons, separate from the complex, intrude the Salumei Metamorphics to the east near the Ok Binai camp.

Structure. The dominant feature is the Frieda Fault, one of a series of major transcurrent faults running parallel to the axis of New Guinea. The disposition of the April Ultramafics and other intrusive complexes appears to be controlled by the Frieda Fault. Near the prospect, faulting of a lesser magnitude has juxtaposed the Wogamush Beds and the Salumei Metamorphics.

INTRUSIVE ROCKS

The division into thirteen species, on the basis of mapping, may to a certain extent be geographical. This is indicated by similarities in the appearance of some of the porphyries. Figs. A-3 and A-5 are detailed geological maps of the intrusive rocks in the main mineralised areas.

In general, the intrusive rocks are plagioclase porphyries. (Despite the "quartz" appellations in some cases, quartz is not nearly as evident as plagioclase in hand specimens.) The plagioclase phenocrysts are commonly several mm across, and show spectacular oscillatory zoning (e.g. 47610). Hornblende is, or was, the major ferromagnesian mineral, but is commonly replaced by biotite. Primary hornblende occurs in the Leucocratic Quartz Andesite (47601), the Porphyritic Hornblende Quartz Andesite (47607) and the Koki Quartz Andesite Porphyry (47602). Biotite phenocrysts may have been present in the Leucocratic Quartz Andesite (47601). In the Porphyritic Hornblende Quartz Andesite (47607) there are prominent xenoliths of quartz and quartz diorite. Apatite, zircon and opaques are minor phenocryst species. The groundmasses of the porphyries are commonly altered to such an extent that the original mineralogy is obscured.

The porphyry (47605) which intrudes the Salumei Metamorphics near Ok Binai differs from those of the complex in having a higher phenocryst to groundmass ratio and in being richer in quartz.

The sequence of intrusion, as deduced by company geologists for the Koki Creek and Ok Flintem areas, is summarised below. No correlation between the two areas is offered.

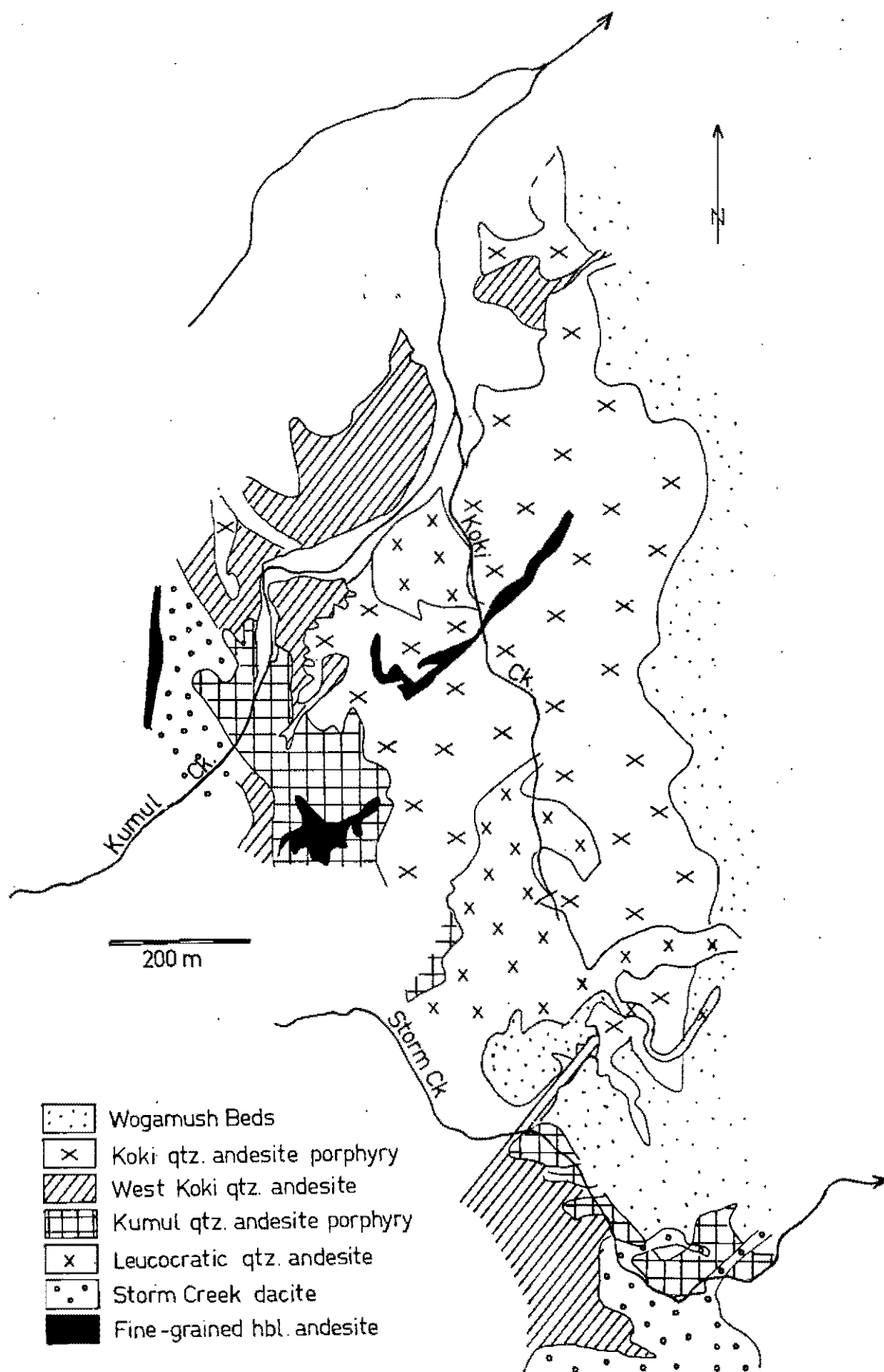


Fig. A-3 Koki Creek mineralised area: geology (mapping by company geologists).

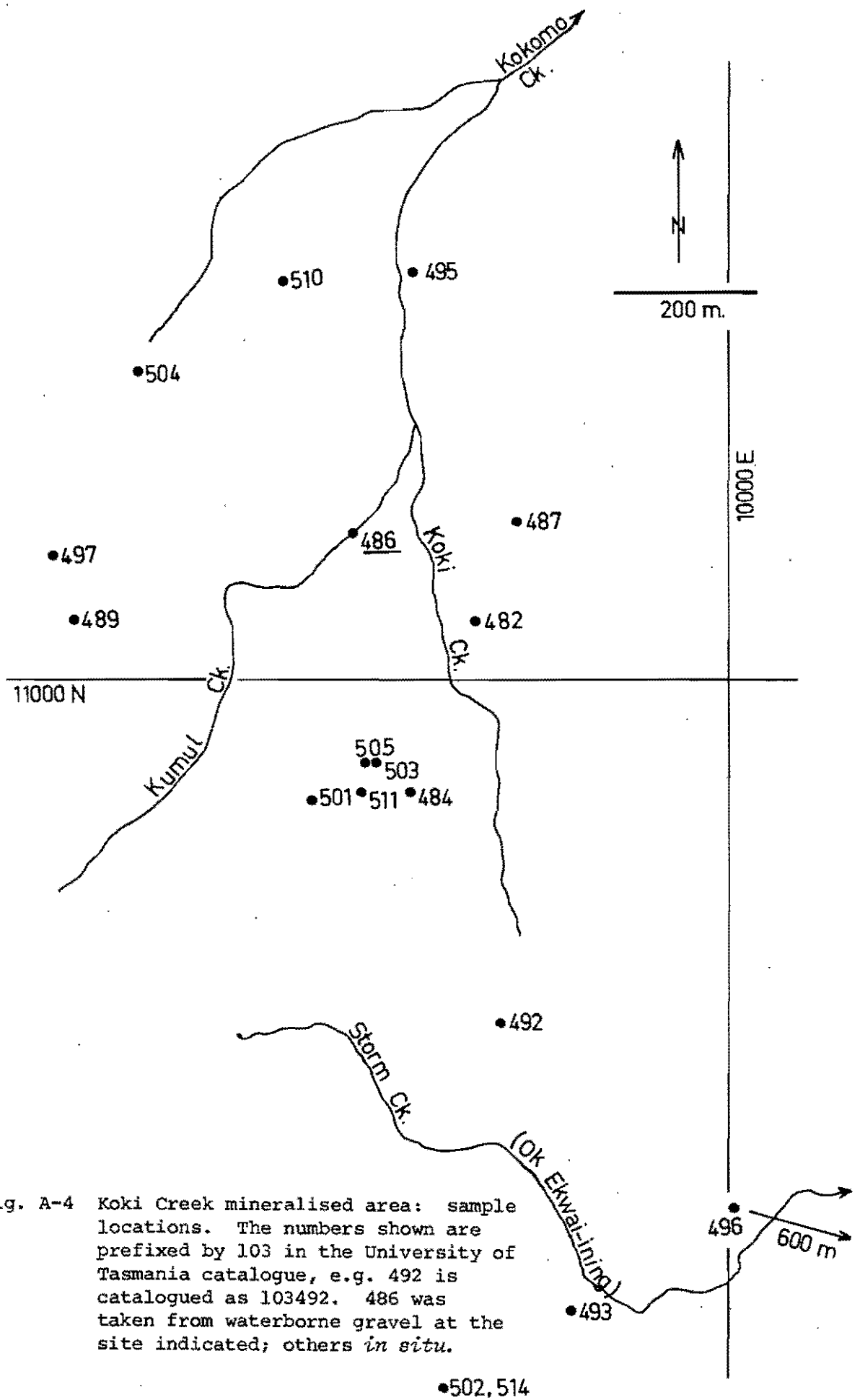


Fig. A-4 Koki Creek mineralised area: sample locations. The numbers shown are prefixed by 103 in the University of Tasmania catalogue, e.g. 492 is catalogued as 103492. 486 was taken from waterborne gravel at the site indicated; others *in situ*.

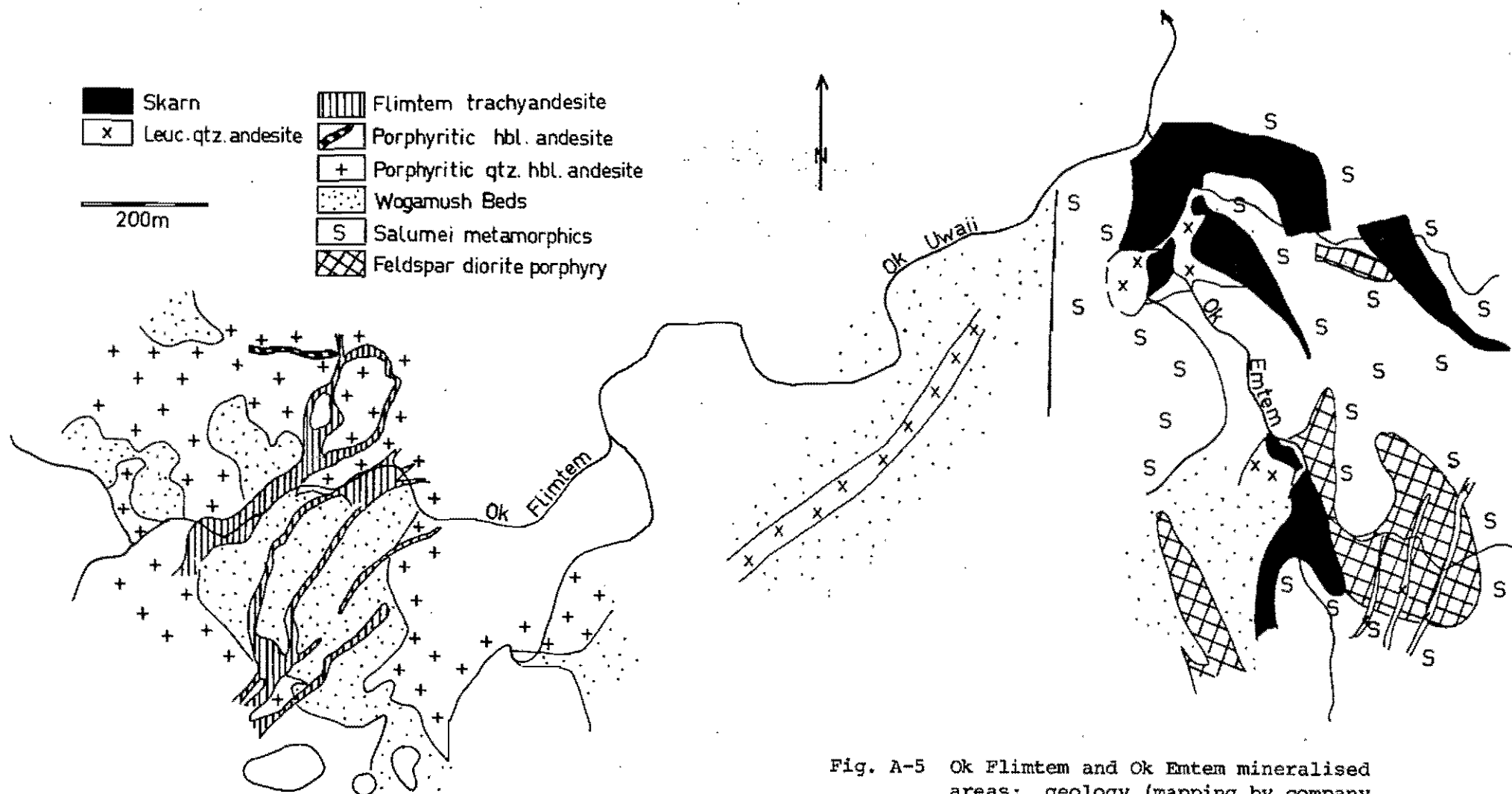


Fig. A-5 Ok Flintem and Ok Entem mineralised areas: geology (mapping by company geologists).

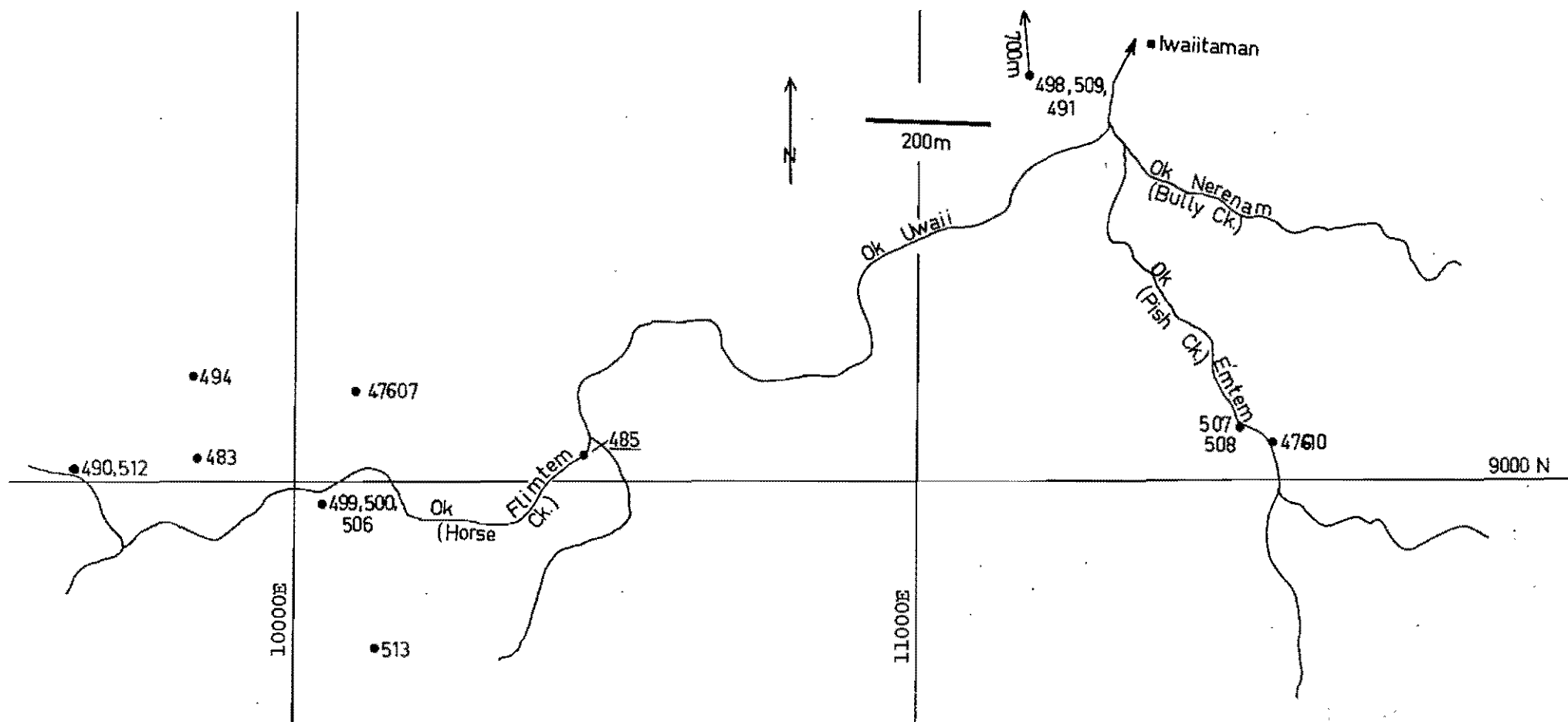


Fig. A-6 Ok Flimtem and Ok Emtem mineralised areas: sample locations. The three-digit numbers shown are prefixed by 103 in the University of Tasmania catalogue, e.g. 483 is catalogued as 103483. 485 was taken from water-borne gravel at the site indicated; others *in situ*.

Intrusive Sequence in the Frieda Prospect

KOKI CREEK	OK FLIMTEM
<i>Youngest</i>	
Leucocratic Quartz Andesite	Flimtem Trachyandesite
Storm Creek Dacite	
Kumul Quartz Andesite Porphyry	Porphyritic Hornblende Quartz Andesite
Koki Quartz Andesite Porphyry	
Wogamush Beds	Wogamush Beds
<i>Oldest</i>	

ALTERATION

The patterns of alteration are far from clear. A detailed study is at present being undertaken by R. Britten.

Potassic alteration. As mentioned above, secondary biotite commonly pseudomorphs primary hornblende (e.g. 47609), and may replace other elements of the porphyries to a lesser extent. K-feldspar occurs as thin selvages along veinlets (Hall & Simpson, 1975), and a 1 cm vein of massive K-feldspar was observed in the bed of Koki Creek. Thus the potassic alteration at Frieda is typical of the pattern in the Southwest Pacific: abundant biotite and less important feldspar (Gustafson, 1978). The most extreme example of potassic alteration seen in the suite of rocks is in 47600, the so-called Thermally Altered Hornblende Diorite, an altered porphyry from the southern part of the Ok Flimtem area. Aggregations of opaque crystals are associated with coarse biotite, anhydrite, secondary quartz and a little rutile.

Phyllic alteration. Hall & Simpson (1975) report that secondary quartz and variable sericitisation of feldspars are found in association with potassic alteration. The presence of sericitic vein selvages cutting

potassic alteration suggests some of the sericitic alteration is later than the potassic.

Propylitic alteration. Chlorite-epidote-sericite-calcite-anhydrite alteration has been observed around the peripheries of both mineralised areas (Hall & Simpson, 1975). This author has observed epidote alteration of plagioclase near small pyrite-bearing veins in the Feldspar Diorite Porphyry at Ok Emtem (47610).

Other notes. (a) Simpson (pers. comm. 1974) recognised a central unaltered zone in the Koki Creek area. (b) During this study, it was noted that there seemed to be an upper limit to the occurrence of anhydrite and gypsum in the drill cores examined. Above this limit, there were calcite veins. A similar phenomenon occurs at Panguna (Baumer & Fraser, 1975), where it appears to be related to the topography.

MINERALISATION

The eastern side of the Frieda Complex includes a broad area of weak copper mineralisation, and a further area, detached from the Complex, is situated in a stock of porphyry near Ok Binai. In 1974, exploration had revealed two concentrations of mineralisation worthy of interest, those around Koki Creek and Ok Flimtem. They do not appear to be connected, and their geology differs in certain respects, e.g. the presence of an unaltered centre at Koki Creek. Lacy (pers. comm. to C.E.C.) suggested that the Koki Creek mineralisation was the deeper-seated of the two.

Disseminated mineralisation and veins account for equal proportions of the copper in the intrusions (Hall & Simpson, 1975). At Koki Creek, the mineralisation seems to be closely associated with the Koki Quartz Andesite Porphyry, and at Ok Flimtem, with the Porphyritic Hornblende

Quartz Andesite. There is no zone of supergene enrichment. The ridges are oxidised to a depth of 75 m, and watercourses intersect hypogene sulphide.

The following styles of mineralisation and veining were observed in the diamond drill core remaining after assaying.

Disseminated sulphides: both pyrite and chalcopyrite as crystals, irregular blebs or replacing ferromagnesian minerals.

Sulphide-only veins: pyrite veins with bleached, sericitic margins, and pyrite or chalcopyrite in continuous or discontinuous veinlets with no obvious selvages.

Quartz veins: barren, massive quartz; quartz with a central seam of sulphide (commonly pyrite); quartz with disseminated sulphide (pyrite, chalcopyrite, bornite and minor molybdenite and pyrrhotite), magnetite and rutile also occur ; and quartz-pyrite veins with characteristic milky quartz from the Salumei Metamorphics.

Anhydrite veins: purple anhydrite in veins up to 2 cm thick, of coarse tabular or finer, equant crystals; commonly containing pyrite; and white anhydrite in veins up to 2 cm thick or as breccia matrix, consisting of coarse tabular crystals and commonly containing chalcopyrite. The white and purple cannot be clearly distinguished according to their sulphides; minor pyrite has been observed in the white, and minor chalcopyrite and molybdenite in the purple.

Calcite veins: white, opaque veins up to 3 cm thick, occasionally containing pyrite. A few veins contain both calcite and anhydrite, but as noted above, the two minerals characteristically occur in different zones at Frieda.

Hematite veins: veins of red, flaky hematite up to 1 cm thick, some associated with pyrite; borders to the clasts of a breccia with a white anhydrite and pyrite matrix.

Gypsum veins: thin, transparent veinlets, and selvages to anhydrite veins.

Skarns: these replace calcareous members of the Salumei Metamorphics. Marble is common among the boulders of Ok Emtem where most of the skarn outcrops are to be found; there they may be associated with the Feldspar Diorite Porphyry. Magnetite-, hematite- and pyrrhotite-rich outcrops were observed, but the hematite may be a surface alteration product. Pyrite in lustrous crystals bands magnetite and pyrrhotite in 103509, and there are bands of epidote, amphibole and garnet with the ores in 103507 and 103508.

An attempt was made to establish a sequence of mineralisation events. The very small number of relevant observations suggested the following:

<i>Oldest</i>	Quartz	cannot differentiate ages of various types of quartz veins.	
	Pyrite (bleached margins)	alteration as evidence (see text)	} order?
	Purple anhydrite	based on one observation	
	White anhydrite		
	Discontinuous sulphide		
<i>Youngest</i>	Gypsum		

Since anhydrite is easily remobilised, the relationship of quartz and anhydrite is also unclear.

FLUID INCLUSION STUDIES IN QUARTZ VEINS

Only three of the many prepared samples contained sufficient fluid inclusions to be of interest. Two of these came from float in creek-beds. Some quartz veins had been deformed and retained few inclusions; others were optically unsuitable. In this respect, the study was disappointing, but it nonetheless indicates the types of fluid that were present. The fluid inclusions are classified as follows:

- Type I Inclusions of low to moderate salinity, not saturated in NaCl at room temperature.
- Type II Gas-rich inclusions with small liquid rims. Some contain daughter minerals.
- Type III Salt-rich inclusions containing halite, sylvite and commonly birefringent salts, opaque crystals (some chalcopyrite) and hematite as daughter minerals.

No inclusions bearing CO₂ were seen, and the formation of CO₂ hydrate was not observed in any run. The crushing of quartz released only minor CO₂, if any. No definite primary inclusions were identified. In addition to the fluid inclusions, solid inclusions of hematite, and others similar to those identified as anhydrite at Panguna were noted.

Inclusions of types I and III were heated, and type I inclusions were frozen, on the Chaixmeca equipment described in Chapter 4. The inclusions at Frieda are generally small (<20 μ across) so that all measurements, and particularly T_f measurements in type I inclusions, are difficult. The data are listed in Table A-1.

Type I inclusions. T_f measurements ranged between -38 and 0°C (salinities of 0 - 25% eq. NaCl, or greater), and homogenisations between 50 and 515°C. Apart from a small group of type I inclusions with T_h in the range 500 - 515°C, the T_h readings were below 410°C and most were in

the range $270 \pm 50^{\circ}\text{C}$. The data are presented as histograms in fig. A-7 B and C. In fig. A-9, the seven available T_h, T_f pairs are plotted on a T_h vs. T_f diagram. No salinities were determined for the inclusions with $T_h = 500 - 515^{\circ}\text{C}$, but from a consideration of critical compositions in the $\text{NaCl-H}_2\text{O}$ system, these must contain more than 10% eq. NaCl (Sourirajan & Kennedy, 1962). Pressure corrections are presumably necessary for the type I inclusion data, because there is no evidence that these fluids boiled. The only indication of what the fluid pressure might have been at Frieda is the vapour pressure of the salt-rich liquids (see below). If the pressure was similar to that at Panguna, the correction would be $25 \pm 10^{\circ}\text{C}$.

Type III inclusions. These occur in association with type II inclusions in all three specimens. Although no other evidence is available at Frieda, this presumably indicates that the salt-rich liquids were boiling, as is thought at Panguna (see Chapter 4). Also by analogy with Panguna, the composition of the salt-rich inclusions suggests a close association between salt-rich liquid and copper deposition at Frieda. Examples of a type II and a type III inclusion are shown in fig. A-10.

$T_s\text{NaCl}$ and T_h data are presented as histograms in fig. A-7 A. Measurements on type III inclusions were subject to the same difficulties encountered at Panguna, i.e. heterogeneity at trapping, the reversal of homogenisation order and the metastability effect described in Chapter 5. The three specimens 103482, 103483 and 103486 from which sufficient data were obtained are distinguishable from each other by their T_h and $T_s\text{NaCl}$ distributions, and this suggests that with a better suite of samples, a study of similar nature to the Panguna study would have been possible.

$T_s\text{NaCl}$ data cover the entire range $300 - >580^{\circ}\text{C}$ in 103486 alone, but modal $T_s\text{NaCl}$ values are defined in each of the specimens. Both $T_s\text{NaCl}$ and $T_s\text{KCl}$ were measured in four inclusions. These data have

Fig. A-7 Histograms of fluid inclusion data.

- A. T_h (white) and T_{gNaCl} (black) for type III inclusions from quartz veins. Specimen numbers indicated at top left. The symbol "9<" means that nine T_h values were less than T_{gNaCl} in the respective inclusions, but were not determined precisely. The temperature scale breaks at 580°C ; to the right, $T > 580^{\circ}\text{C}$.
- B. T_h for type I inclusions from quartz and anhydrite veins. Black indicates readings from purple anhydrite, and white from white anhydrite.
- C. T_f for type I inclusions from quartz and anhydrite veins. Black indicates readings from purple anhydrite, and white from white anhydrite.

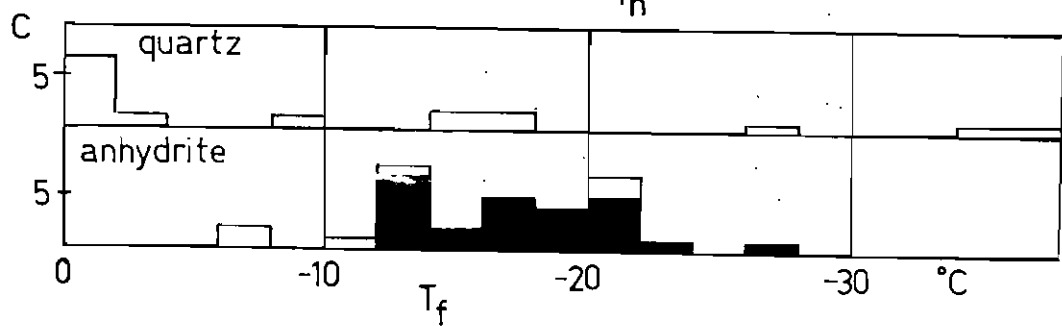
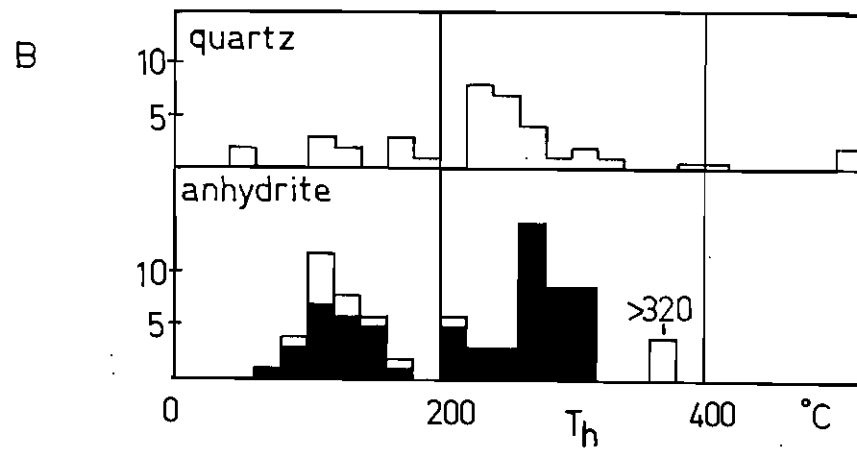
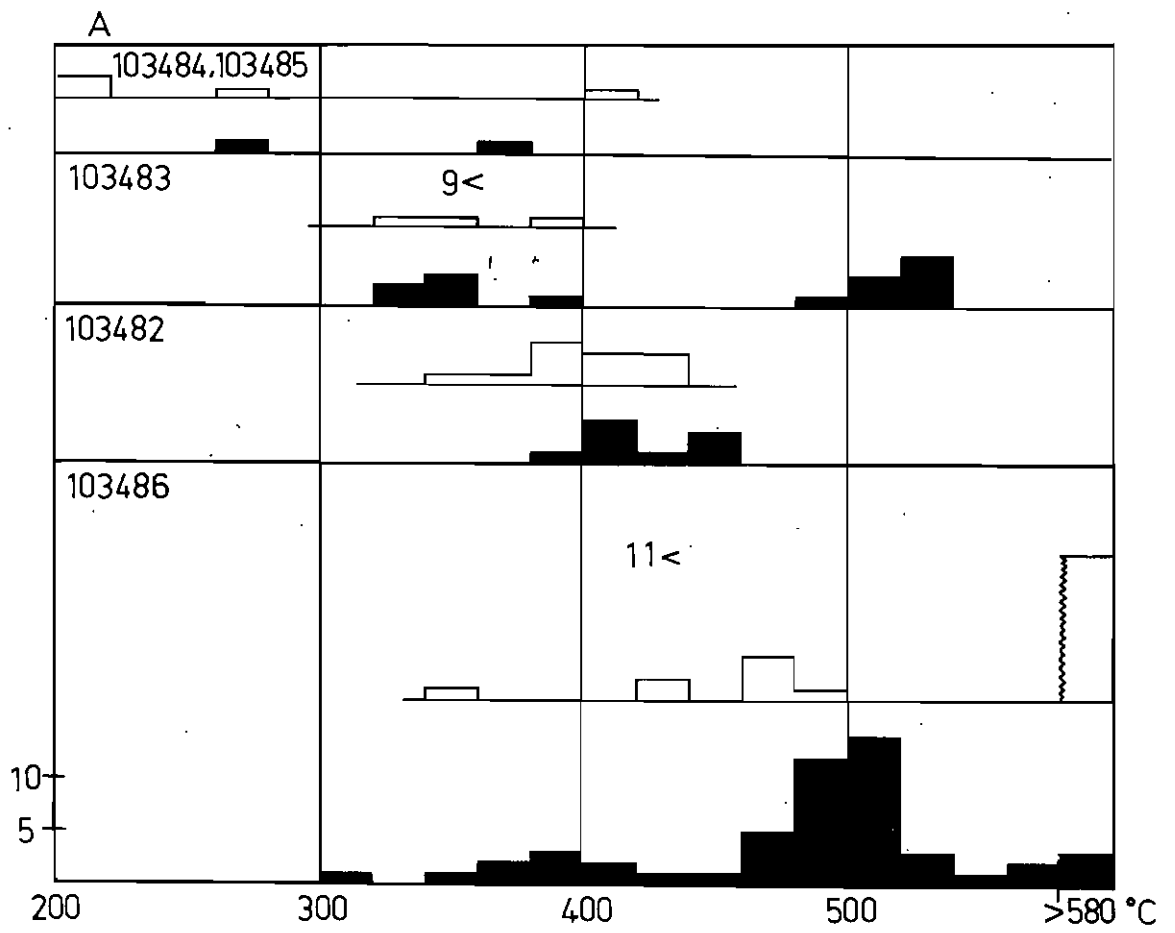


Fig. A-8 T_h vs. T_{SNaCl} for type III inclusions from quartz veins.
Data for which only an upper limit was fixed are
indicated by a point with a bar on the $T_{SNaCl} = T_h$ line.

Fig. A-9 T_f vs. T_h for type I inclusions from quartz and
anhydrite veins.

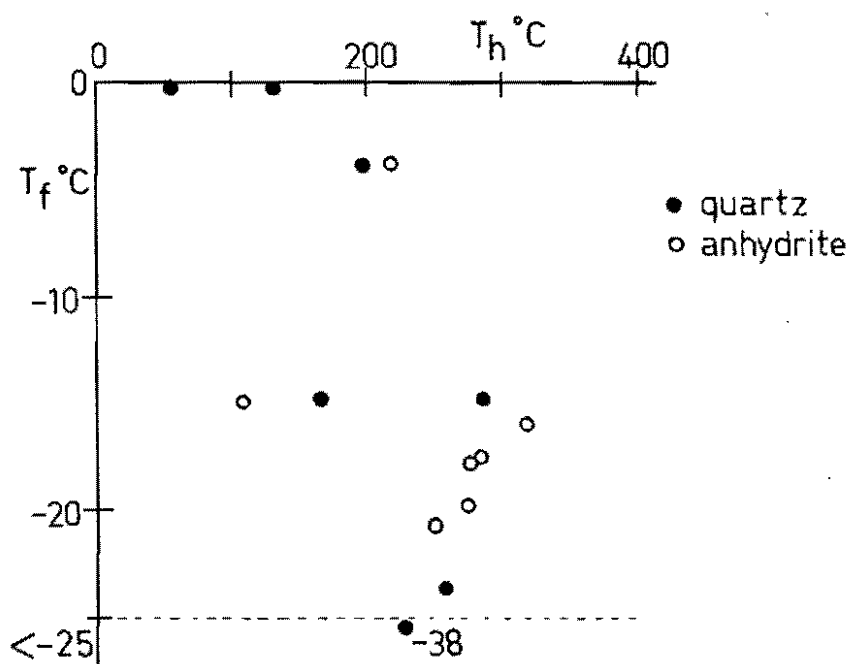
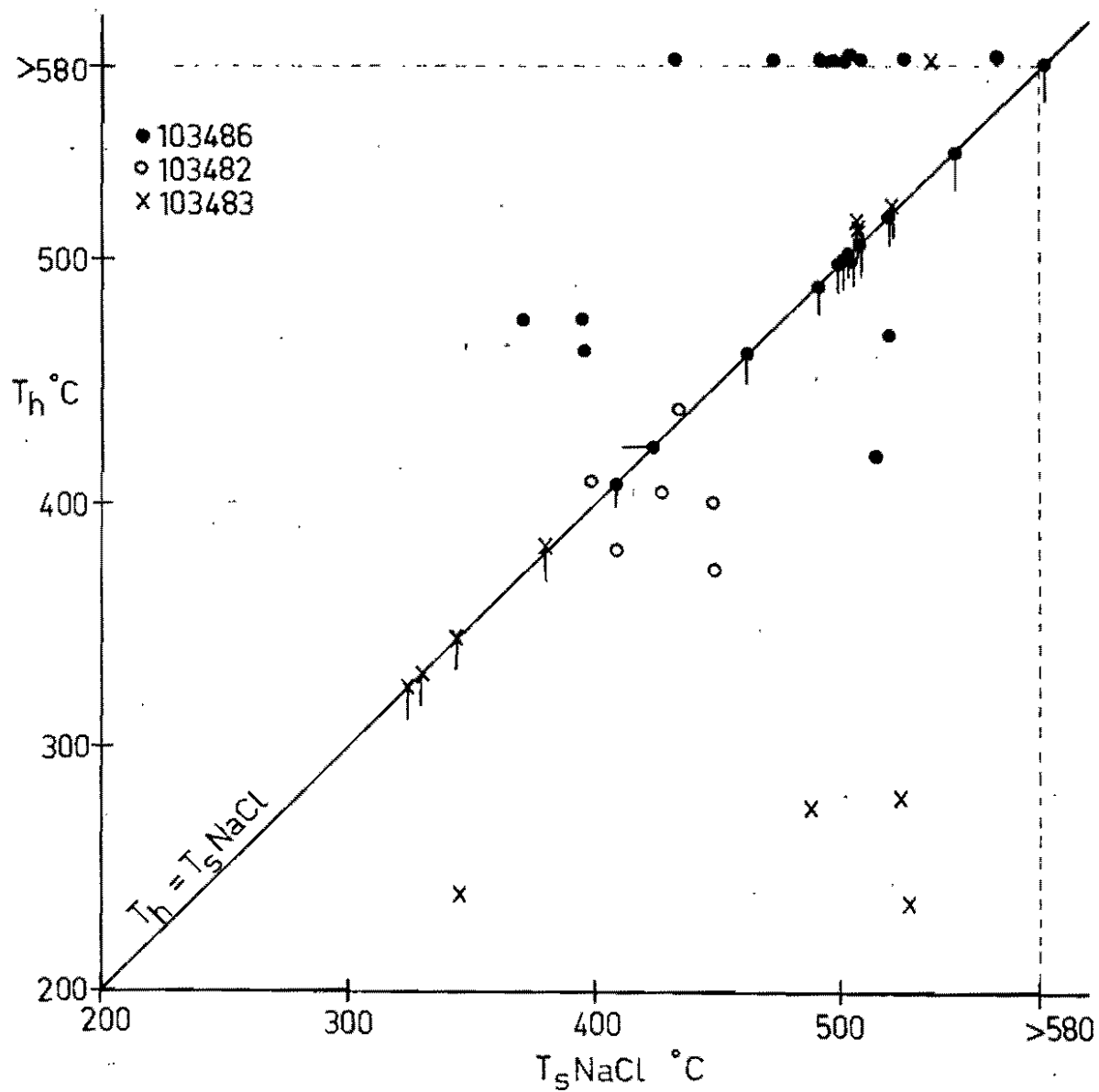
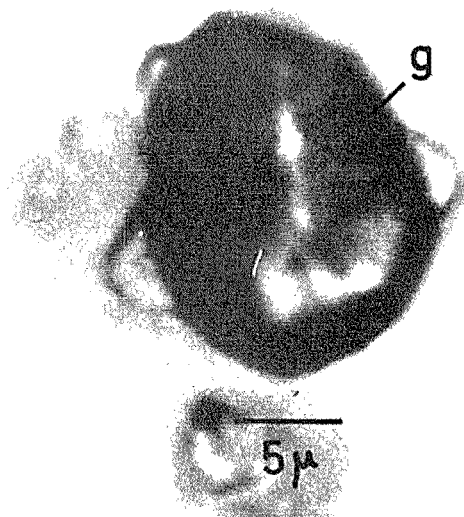


Fig. A-10 A. a type II inclusion from 103486. g = gas.

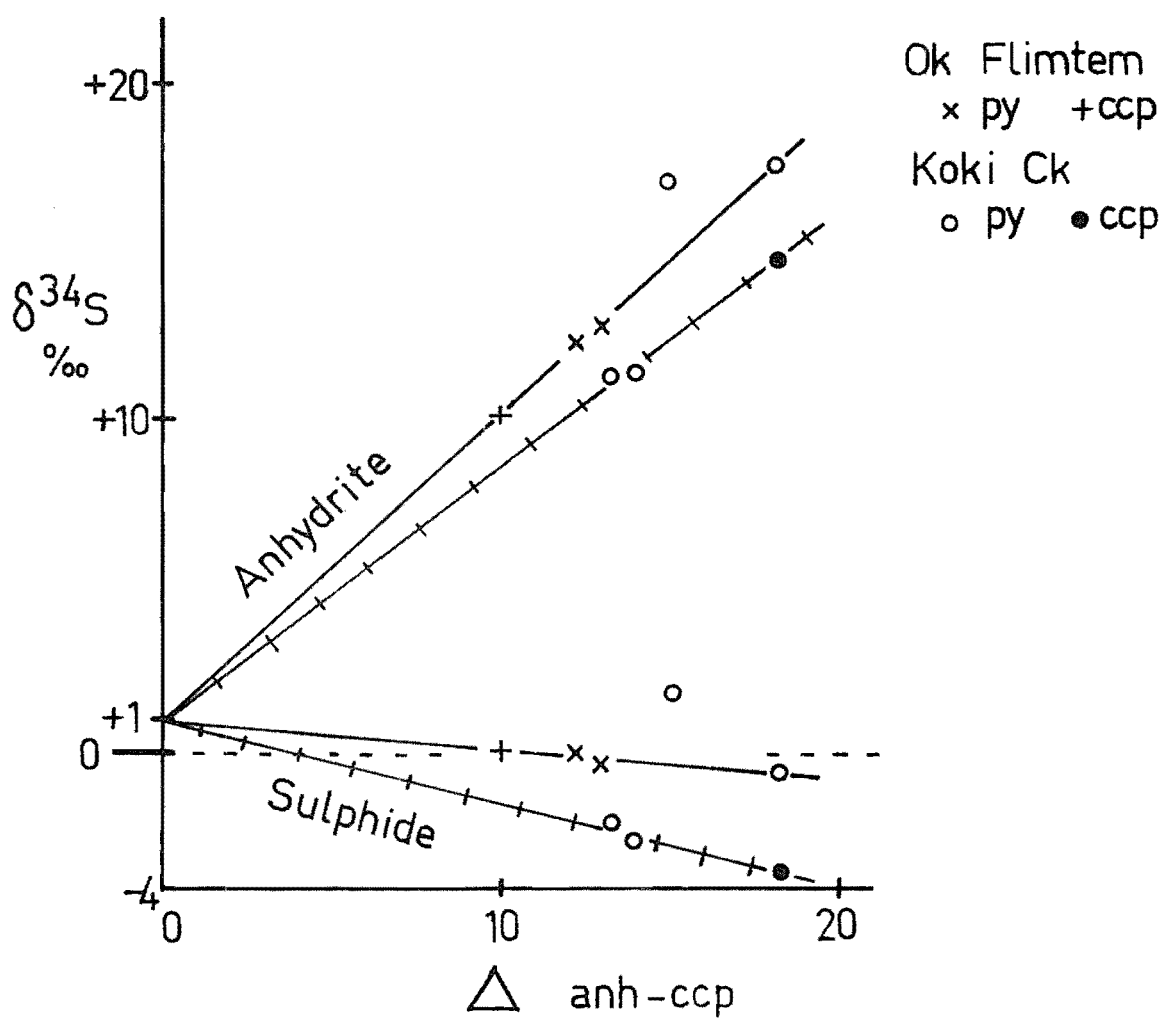
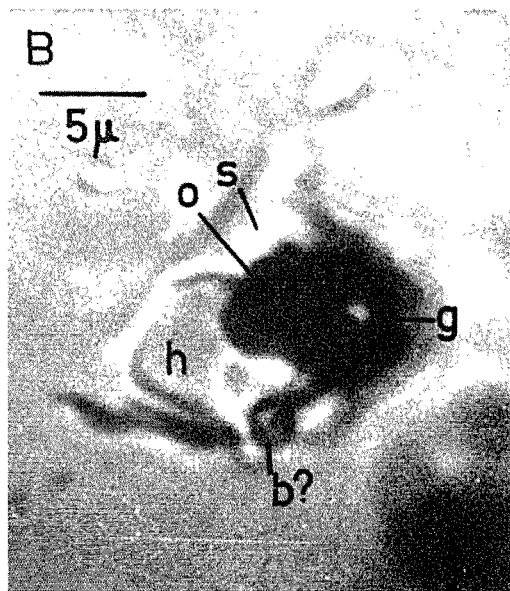
B. a type III inclusion from 103486. o = opaque,
g = gas, h = halite, s = sylvite, b? = possible
birefringent salt.

Fig. A-11 $\delta^{34}\text{S}$ for anhydrite, pyrite and chalcopyrite as a
function of Δ anhydrite-sulphide.

A



B



already been considered in Chapter 10 where they were compared with the trend established by the Panguna data. They fit the trend approximately, but are not numerous enough to confirm a trend for Frieda. The salinities of these four inclusions range between 55% total salts (15% KCl + 40% NaCl) and 66% total salts (18% KCl + 48% NaCl) according to the data of Ravich & Borovaya (1949). The whole salinity range is broader, particularly in the direction of lower salinities.

$T_S\text{NaCl}$ and T_h data together indicate the range of phase behaviour found in the salt-rich liquids. In fig. A-8, T_h is plotted against $T_S\text{NaCl}$ and the following types of salt-rich liquid are indicated:

- (i) Unsaturated liquid at high temperatures ($>580^\circ\text{C}$), for $T_S\text{NaCl} \approx 500^\circ\text{C}$, mainly in 103486.
- (ii) Near-saturated liquid at $T_h = T_S\text{NaCl} \approx 420^\circ\text{C}$, in 103482.
- (iii) Unsaturated liquid at $T_h \approx 480^\circ\text{C}$, $T_S\text{NaCl} \approx 400^\circ\text{C}$, in 103486.
- (iv) Supersaturated liquids at $T_S\text{NaCl} \approx 500^\circ\text{C}$, $T_h \approx 450^\circ\text{C}$, and at higher and lower $T_S\text{NaCl}$ in 103486; at $T_S\text{NaCl} \approx 500^\circ\text{C}$, $T_h \approx 270^\circ\text{C}$, and $T_S\text{NaCl} \approx 340^\circ\text{C}$, $T_h \approx (?)230^\circ\text{C}$ in 103483.

The importance of each type of phase-behaviour, quantitatively and spatially, cannot be assessed without a more comprehensive set of specimens. The varieties of salt-rich liquid noted at Panguna are present with the exception of the lower-temperature unsaturated liquids. Frieda also differs from Panguna in that there appears to be unsaturated liquid at 480°C and supersaturation continues to $T_S\text{NaCl}$ below 430°C . The very high degree of supersaturation in 103483 is not matched at Panguna, nor are the inclusions with $T_S\text{NaCl} > 580^\circ\text{C}$ (although these are so few and so scattered in 103486 that they may well be spurious, the result of necking down). The evolution of salt-rich liquid at Frieda may thus be different from, and possibly more complex than, what has been deduced at Panguna.

The maximum temperature at which salt-rich liquid was present was $>580^{\circ}\text{C}$. A minimum temperature is difficult to fix. The T_h values indicated for supersaturated fluids (minimum 240°C in 103483) may not be reliable, as is suspected for some of the supersaturated liquids at Panguna (Chapter 5). The T_h measurements for 103482 indicate a temperature of $400 - 430^{\circ}\text{C}$ for the near-saturated liquid in that specimen. This liquid would have had a vapour pressure of 200 - 300 bars like similar liquids at Panguna (Ravich & Borovaya, 1949). The apparent high degree of supersaturation in certain fluids at Frieda could indicate lower pressures, however, and there is no indication of the geometry of the distribution of homogenisation phenomena. A knowledge of the distribution at Panguna was important to the understanding and interpretation of the vapour pressures of salt-rich liquids. Thus the formation pressure at Frieda is uncertain. If the Frieda Intrusive Complex does indeed represent an ancient intruded volcanic edifice, pressures comparable with or lower than those at Panguna are very likely.

FLUID INCLUSION STUDIES IN ANHYDRITE VEINS

Type I inclusions, generally of secondary habit, are the most abundant fluid inclusions found in anhydrite veins from Frieda. Several contain opaque crystals. Rare type II inclusions, and rare inclusions with phase ratios between those of types I and II were also observed, but because of their relative rarity, and because anhydrite cleaves easily, permitting the escape of fluid, these may be spurious. One inclusion, number 39 in 103512, appeared from its phase properties at temperatures less than 20°C to contain a fluid other than water. Rare solid inclusions of hematite were noted.

The inclusions are small, commonly less than $10\ \mu$ long, and rectangular in shape. Because of small size and metastability, T_f measurements

could not be made on most. Homogenisation temperatures were also difficult to measure in the usual way. It was possible to measure T_h in very small inclusions by using the rapid and easily-visible Brownian motion of the bubbles in these inclusions when they were cooled at temperatures just below T_h . (The bubble remains stationary as the temperature rises.) A sample was heated 5°C , cooled 2.5°C , heated 5°C , cooled 2.5°C and so on. Finally, Brownian motion was not observed during a cooling period, so that homogenisation must have occurred within the preceding 5°C rise in temperature.

The data, presented as histograms in figs. A-7 B and C, are distinguished according to the colour of the anhydrite. They are chiefly of interest in comparison with the data from type I inclusions from quartz veins. T_f values define a broad range, -12 to -28°C in purple anhydrite and -6 to -22°C in white anhydrite. The lowest salinities found in type I inclusions from quartz veins were not noted in anhydrite; this may be because the inclusions in anhydrite are saturated in calcium sulphate. Many type I inclusions initially without bubbles nucleated them during freezing runs. T_h measurements covered the range $60 - 320^{\circ}\text{C}$ for all veins, and for purple anhydrite alone. White anhydrite gave a range of $80 - 220^{\circ}\text{C}$. (Higher T_h values, not actually determined, are thought to be spurious and due to leakage.) These temperatures should be subject to the same pressure corrections as T_h measurements from quartz veins, and therefore the secondary, low to moderate salinity fluids in both vein sets appear to be similar. The same conclusion can be drawn from the T_h vs. T_f plot, fig. A-9.

SULPHUR ISOTOPES

Twelve samples of pyrite (not including pyrite-anhydrite veins) were prepared and analysed in the same way as specimens from Panguna (see Chapter 11). They were chosen to represent a broad selection of the types of pyrite at Frieda, including vein and disseminated pyrite, specimens from the Ok Flimtem and Koki Creek areas and others from Ok Binai, the skarns and the Salumei Metamorphics. The results are listed in Table A-2. The $\delta^{34}\text{S}$ values fall in the range -1.6 to +2.1‰ (without anhydrite vein data) or -2.6 to +2.1‰ (all data). They show no regularities as a function of mineralisation-type or of location.

Eight anhydrite-sulphide pairs were analysed, and the $\delta^{34}\text{S}$ measurements and temperatures are listed in Table A-2. For anhydrite, the $\delta^{34}\text{S}$ range is +10.1 to +17.6‰, and the two samples of chalcopyrite gave -3.5 and +0.1‰. Data for individual pairs were converted to temperatures with calibration equations from Ohmoto & Rye (in press). The temperature ranges are 356 - 677°C for all, and for white anhydrite, and 414 - 524°C for purple anhydrite. Thus the temperatures of formation do not seem to correlate with colour in these anhydrites. The isotopic temperatures certainly do not agree with the temperatures given by type I inclusions in the anhydrite (these inclusions were presumed to be secondary), but they do correspond with the temperatures from type III inclusions in quartz. A plot of $\delta^{34}\text{S}$ vs. Δ (fig. A-11) was drawn up from the anhydrite-sulphide data. The construction and uses of this type of plot have been discussed in Chapter 11. The data do not define a single pair of straight lines unless there is considerable scatter, but they appear (with the exception of one data pair) to fit two pairs of lines, representing two different states of oxidation. One state is identical (according to the slopes of the lines) with that at Panguna; the other

is more oxidising. The pair of lines indicating the lower oxidation state is defined by data from the Koki Creek area, and the other by data from Ok Flimtem and one specimen from south of Koki Creek. Thus the distinction may correspond with different centres and episodes of mineralisation. As shown in fig. 11-3, the fractionation to be expected between pyrite and chalcopyrite is "not great enough at these temperatures to account for much isotopic difference between the two, so that both minerals would be expected to plot on nearly-similar lines.

Both pairs of lines converge to +1‰ at $\Delta = 0$, implying that the salt-rich liquid had $\delta^{34}\text{S} = +1\%$ throughout mineralisation, independent of the oxidation state. The isotopic composition of magmatic sulphur cannot be determined at Frieda with any certainty because of the difficulties discussed in the context of Panguna in Chapter 11. No explicit evidence for early fluids at relatively low oxidation states has been uncovered in this study, but the evolution of such fluids is implicit in the high oxidation state during copper mineralisation (according to the presence of hematite, and the comparison of S-isotopes with Panguna). The salt-rich liquids in both deposits had $\delta^{34}\text{S} = +1\%$; this suggests that the processes leading to the expulsion of salt-rich liquid from the magmas had much in common in both deposits. An explanation of the regulation of the isotopic composition of the salt-rich liquids will be an important factor in an improved understanding of the magmatic-hydrothermal processes in porphyry copper deposits.

CONCLUSIONS

Salt-rich liquid, apparently boiling, was present at temperatures from a possible minimum of 240°C to greater than 580°C. Salinities of 55 - 66% total salts have been measured. Observations of fluid inclusion homogenisation behaviour in three specimens indicate the presence of

high-temperature ($>580^{\circ}\text{C}$) unsaturated liquids, supersaturated liquids and near-saturated liquids (at $400 - 430^{\circ}\text{C}$). Secondary fluids in inclusions from quartz and anhydrite contained 0 - ~25% eq. NaCl, and most were present at $200 - 350^{\circ}\text{C}$ (assuming only a small pressure correction). Although lacking in detail, the fluid inclusion work at Frieda indicates that fluid phenomena similar to those inferred at Panguna took place at Frieda, and that the evolution of fluid compositions may have been more complicated at Frieda.

Temperature determinations based on sulphur isotope fractionation between anhydrite and sulphides gave a range of $356 - 677^{\circ}\text{C}$, which agrees with the range of temperatures from type III inclusions. The isotope data may indicate two different states of oxidation during copper mineralisation, one similar to that at Panguna, the other higher. Both data trends indicate that the salt-rich liquids had $\delta^{34}\text{S} = 1\%$.

REFERENCES

- BAUMER, A. & FRASER, R.B., 1975. Panguna porphyry copper deposit, Bougainville. In *Economic Geology of Australia and Papua New Guinea*. 1. Metals. 855-66. Australas. Inst. Min. Metall., Melbourne. 1126 p.
- GUSTAFSON, L.B., 1978. Some major factors of porphyry copper genesis. *Econ. Geol.* 73, 600-607.
- HALL, R.J. & SIMPSON, P.G., 1975. The Frieda porphyry copper prospect, Papua New Guinea. In *Economic Geology of Australia and Papua New Guinea*. 1 Metals. 836-45. Australas. Inst. Min. Metall., Melbourne. 1126 p.
- OHMOTO, H. & RYE, R.O., (in press). Isotopes of sulphur and carbon. In Barnes, H.L. (ed.), *Geochemistry of hydrothermal ore deposits*. 2nd ed. Wiley.

- PAGE, R.W. & McDOUGALL, I., 1972. Ages of mineralisation of gold and porphyry copper deposits in the New Guinea Highlands.
Econ. Geol. 67, 1034-1048.
- RAVICH, M.I. & BOROVAYA, F.E., 1949. Fazovyye ravnovyesiya v troynykh vodno-solyevykh sistemakh pri vysokikh tyemperaturakh.
(Phase equilibria in ternary water-salt systems at elevated temperatures.) *Akad. Nauk. S.S.S.R., Izvestiya Syektora Fiz.- Khim. Analiza*, 19, 69-81.
- SOURIRAJAN, S. & KENNEDY, G.C., 1962. The system NaCl-H₂O at elevated temperatures and pressures. *Amer. J. Sci.* 260, 115-141.

Table A-1

FLUID INCLUSION DATA, FRIEDA

1. Quartz veins, Type I inclusions

Number	T _f	T _h	Number	T _f	T _h
103482			103486		
1	-33.6		1	0.0	130±10
2	-38	227	2	-1.0±1.0	
3		254	3	-3.5	
4		250	4	-0.1	
5		222	5	0.0	55±5
6		246±3	6	-1.2	
7		244±2	7		>580
8	-14.7	287	8	-16.3	>380
9	-16.6	no bubble	9		64±2
10	-14.9	165	10		102±2
11		515±2	11		139
12		515±2	12		102±2
13		>506	13	-0.8	
14		225	14		102±2
15		246	15	-7.9	197
16		225	16		310±4
17		262	17		173
			18		278
103483			19		270±3
1	-26.8	259	20		222
2		222±5	21		228
3	0.0		22		306
			23		237
103484			24		264
1		386	25		243±3
2		334±5			
3		404			
103485					
-					

2. Quartz veins, type III inclusions.

Number	T _g KCl	T _g NaCl	T _h	Number	T _g KCl	T _g NaCl	T _h
103482				cont.			
1	118	409	381±4	6		498	>580
2	115	448	401±10	7		501±5	<h
3		449±2	374	8		504	>580
4		448	<h	9	172	487±5	
5		>g	352±10	10	164		343
6		404±2	>h	11		500±3	<h
7		401	.	12		494	>580
8		416	407	13		434±5	>580
9			396±5	14			>580
10			396±5	15		514±8	
11			394	16		498	<h
12		399	409	17	116	493	
13		435	439	18		532±2	
103483				19		525	>554
1		537	>h	20		490	<250
2		488	275	21		506	493±4
3		528	236	22		390	
4		326	<h	23		396	463
5		352	<h	24		409±4	<h
6		330	<h	25		519	469±6
7		524	280±5	26		518	<h
8		520±5	<h	27		545	<h
9		509±3	<h	28		372±10	476±9
10		509±3	<h	29		462	<300
11		509±3	<h	30		453	
12		381	<h	31		487	
13		346±3	240	32		507	
14		346±3	<h	33		508	<370
103484				34		>580	
1		276	185	35		473±5	
103485				36		>580	<280
1			261	37		573	
2			207±10	38		503±3	>580
3			207±10	39		563±3	>580
4		371		40		517	
103486				41		487	
1		501±5	>580	42		529±4	
2		473±5	>580	43			>580
3		507	>580	44		484±5	>h
4		514	420	45		495±4	>h
5		492±5	<h	46		487±5	
				47		>580	
				48		317±3	>h
				49		473±5	
				50		405±4	
				51		365±3	
				52		367±5	

Table A-1 cont.

3. Anhydrite veins, type I inclusions.

Number	T _f	T _h	Number	T _f	T _h
103502	white		cont.		
1	-6.4	no bubble	10	-19.8	274
2	-10.6		11	-16.6	320
3	-21.0		12	-21.4	251
4	-7.3	217	13	-19.1	
5	-19±1	92±3	14	-19.4	
6		114±2	15	-15.5	
7		116±2	16	-12.7	
8		1.8	17	-16.0	
103503	purple		18	-15.5	
1		154±5	19	-11.8	
2		160±3	20	-15.8	
3		209±3	21	-17.9	276
4		202±5	22	-14.8	109
			23		313
			24		270±3
			25		274±2
103504	purple		26	-15.3	
1		109	27		141
2		111	28	-17.4	
3		95	29		218
4		65	30	-11.8	
5		100±5	31		206
6		91±3	32		151
7		111	33		212
			34		221
			35		223
103505	white		36		237
1		110	37		308
2		106	38		315
			39		10.6
103511	white		* opaque phase fused -7°C, bubble changed shape +3°C.		
1		115±5			
103512	purple		103513	white	
1	-13.0		1	-12.3	no bubble
2	-20.8		2		>311
3	-26.6		3		>311
4	-12.5		4		>350
5	-19.6		5		176
6	-19.6		6		148
7	-13.4		7		132±3
8	-12.4		8		>350
9	-18.4				

Table A-2

SULPHUR ISOTOPE DATA, FRIEDA

Sulphate-Sulphide

Number	Area	Anhydrite Colour	$\delta^{34}\text{S} \%$	Sulphide $\delta^{34}\text{S} \%$	$\Delta \%$	T °C *
103499	Flintem	white	+12.2	0.0 py	12.2	519 ± 32
103500	Flintem	white	+10.1	+0.1 ccp	10.0	631 ± 46
103501	Koki	purple	+11.3	-2.0 py	13.3	485 ± 28
103502	sth Koki	white	+17.6	-0.6 py	18.2	374 ± 18
103503	Koki	purple	+11.4	-2.6 py	14.0	466 ± 27
103504	Koki	purple	+17.0	+1.9 py	15.1	438 ± 24
103505	Koki	white	+14.8	-3.5 ccp	18.3	393 ± 19
103506	Flintem	purple	+12.7	-0.3 py	13.0	494 ± 30

* data from Ohmoto and Rye (in press).

Pyrite

Number	Area	Type	$\delta^{34}\text{S}_{\text{py}} \%$
103487	Koki	pyrite vein	+0.4
103488	Ok Binal	pyrite vein from porphyry	+1.2
103489	Koki	quartz-pyrite vein	+2.1
103490	Flintem	quartz-pyrite vein	-1.2
103491	Storm Ck	quartz-pyrite (from Salumai Metamorphics)	-1.6
103492	S. Koki	quartz-pyrite vein	-0.7
103493	Storm Ck	quartz-pyrite (molybdenite)	-0.4
103494	Flintem	quartz-pyrite vein	-0.9
103495	Koki	pyrite with quartz selvage	-1.2
103496	Storm Ck	quartz-pyrite vein	-0.9
103497	Koki	pyrite disseminated in chalky altered rock	+1.3
103498	Storm Ck	skarn	-0.1

Table A-3

LIST OF SPECIMENS FROM FRIEDA

- 47600 "Thermally Altered Hornblende Diorite" - porphyry altered to a biotite-quartz-anhydrite-pyrite assemblage. Ok Flimtem area, exact coordinates not known.
- 47601 Leucocratic Quartz Andesite - a fresh porphyry with plagioclase & hornblende phenocrysts in a groundmass of plagioclase, hornblende quartz and opaques. Kumul Ck, Koki Ck area, exact coordinates not known.
- 47602 Koki Quartz Andesite Porphyry. Heavily altered porphyry with plagioclase, hornblende and minor apatite phenocrysts in a quartz-biotite-chlorite-opaques groundmass. Koki Ck, Koki Ck area. Exact coordinates not known.
- 47603 Flimtem Trachyandesite. A porphyry with plagioclase and hornblende phenocrysts and xenoliths in an (?) altered feldspathic groundmass. Ok Flimtem, Ok Flimtem area. Exact coordinates not known.
- 47604 Wogamush Beds. Veined, hornfelsed shale. Koki Ck, Koki Ck area. Exact coordinates not known.
- 47605 Ok Binai Porphyry. Plagioclase and biotite phenocrysts in a quartz-plagioclase-biotite-chlorite-opaques (accessory apatite, zircon) groundmass. From a small tributary of Ok Binai SE of Ok Binai Camp. Exact coordinates not known.
- 47606 Kumul Quartz Andesite Porphyry. Very altered porphyry with plagioclase and ferromagnesian phenocrysts altered to biotite, in a groundmass largely of secondary biotite, quartz and opaques. Koki Ck, Koki Ck area. Exact coordinates not known.
- 47607 Porphyritic Hornblende Quartz Andesite. Fresh porphyry with plagioclase, hornblende, apatite, quartz and opaque phenocrysts in a quartz-plagioclase groundmass with secondary chlorite, calcite, anhydrite and biotite. Plentiful xenoliths. From Ok Flimtem area, DDH 48, 287.8 m. Coords. 10100E, 9145N.
- 47608 Storm Creek Diorite. An altered porphyry with phenocrysts of plagioclase, quartz and hornblende (altered, except the quartz, to biotite, chlorite and sericite) in a fine-grained, extremely altered quartz-biotite-chlorite-? sericite groundmass. From Koki Ck area. Exact coordinates not known.
- 47609 West Koki Quartz Andesite. An altered porphyry of plagioclase and quartz phenocrysts set in a very altered groundmass of quartz, biotite, chlorite, sericite and opaques. From Storm Ck, S. Koki Ck area. Exact coordinates not known.

- 47610 Feldspar Diorite Porphyry. An altered porphyry of plagioclase phenocrysts (altered to epidote) and micro-phenocrysts of hornblende and apatite in a quartz-sericite-opaques groundmass. Ok Emtm. Coords. 11570E, 9060N.
- 103482 Quartz vein with chalcopryite, from DDH 8, 80 m. Coords. 9645E, 11080N.
- 103483 Quartz vein with chalcopryite, from surface. Coords. 9845E, 9060N.
- 103484 Quartz vein with minor ? pyrite, from DDH 50, 293 m. Coords. 9550E, 10890N.
- 103485 Quartz vein with chalcopryite (oxidised to covellite), from float in Ok Flimtem. Collected at coords. 10460E, 9040N.
- 103486 Quartz vein, from float in Kumul Ck, collected at coords. 9475E, 11205N.
- 103487 Pyrite vein, from DDH 11, 233 m. Coords. 9700E, 11225N.
- 103488 Pyrite vein from Ok Binai porphyry, exact coordinates not known. The porphyry is SE of the Ok Binai camp, fig. A-2.
- 103489 Pyrite vein from DDH 62, 60 m. Coords. 9080E, 11065N.
- 103490 Quartz-pyrite vein from DDH 30, 451 m. Coords. 9650E, 9025N.
- 103491 Quartz-pyrite vein from DDH 53, 120 m. Coords. 11120E, 10260N.
- 103492 Quartz-pyrite vein from DDH 25, 7 m. Coords. 9680E, 10505N.
- 103493 Quartz-pyrite vein with minor molybdenite, from DDH 32, 168 m. Coords. 9780E, 10105N.
- 103494 Quartz-pyrite vein, from DDH 18, 229 m. Coords. 9840E, 9170N.
- 103495 Pyrite vein from DDH 28, 127 m. Coords. 9555E, 11555N.
- 103496 Quartz-pyrite vein, from DDH 37, 104 m. Coords. 10475E, 10100N.
- 103497 Pyrite vein from DDH 65, 45 m. Coords. 9700E, 11225N.
- 103498 Pyrite-bearing skarn from DDH 53, 90 m. Coords. 11120E, 10260N.
- 103499 White anhydrite vein with pyrite from DDH 40, 314 m. Coords. 10045E, 8965N.
- 103500 White anhydrite vein with chalcopryite from DDH 41, 345 m. Coords. 10045E, 8965N.
- 103501 Purple anhydrite vein with pyrite from DDH 51, 372 m. Coords. 9415E, 10880N.

- 103502 Breccia with matrix of white anhydrite, hematite and pyrite from DDH 35, 556 m. Coords. 91600E, 9995N.
- 103503 Purple anhydrite vein with pyrite from DDH 50, 287 m. Coords. 9505E, 10885N.
- 103504 Purple anhydrite vein with pyrite from DDH 61, 341 m. Coords. 9120E, 11485N.
- 103505 White anhydrite vein with chalcopyrite from DDH 50, 311 m. Coords. 9490E, 10885N.
- 103506 Purple anhydrite vein with pyrite from DDH 41, 335 m. Coords. 10045E, 8965N.
- 103507 Magnetite-garnet skarn from Ok Emtem. Coords. 11520E, 9075N.
- 103508 Magnetite skarn from Ok Emtem. Coords. 11520E, 9075N.
- 103509 Pyrite-magnetite skarn from DDH 53. Coords. 11120E, 10260N.
- 103510 Breccia with white anhydrite and calcite matrix from DDH 26, 249 m. Coords. 9375E, 11565N.
- 103511 White anhydrite vein with chalcopyrite from DDH 51, 413 m. Coords. 9485E, 10840N.
- 103512 Purple anhydrite vein with pyrite from DDH 30, 597 m. Coords. 9650E, 9025N.
- 103513 White anhydrite vein with pyrite from DDH 46, 253 m. Coords. 10130E, 8735N.
- 103514 Purple anhydrite vein from DDH 35, 519 m. Coords. 9600E, 9995N.